The biomineralization of ferritin and haemosiderin

Wade, Vanessa J.

Award date:
1991

Awarding institution:
University of Bath

The Biomineralization of Ferritin and Haemosiderin

THE UNIVERSITY OF BATH

submitted by Vanessa J. Wade

for the degree of Doctor of Philosophy

of the University of Bath

1991

ProQuest LLC
789 East Eisenhower Parkway
P.O. Box 1346
Ann Arbor, MI 48106-1346

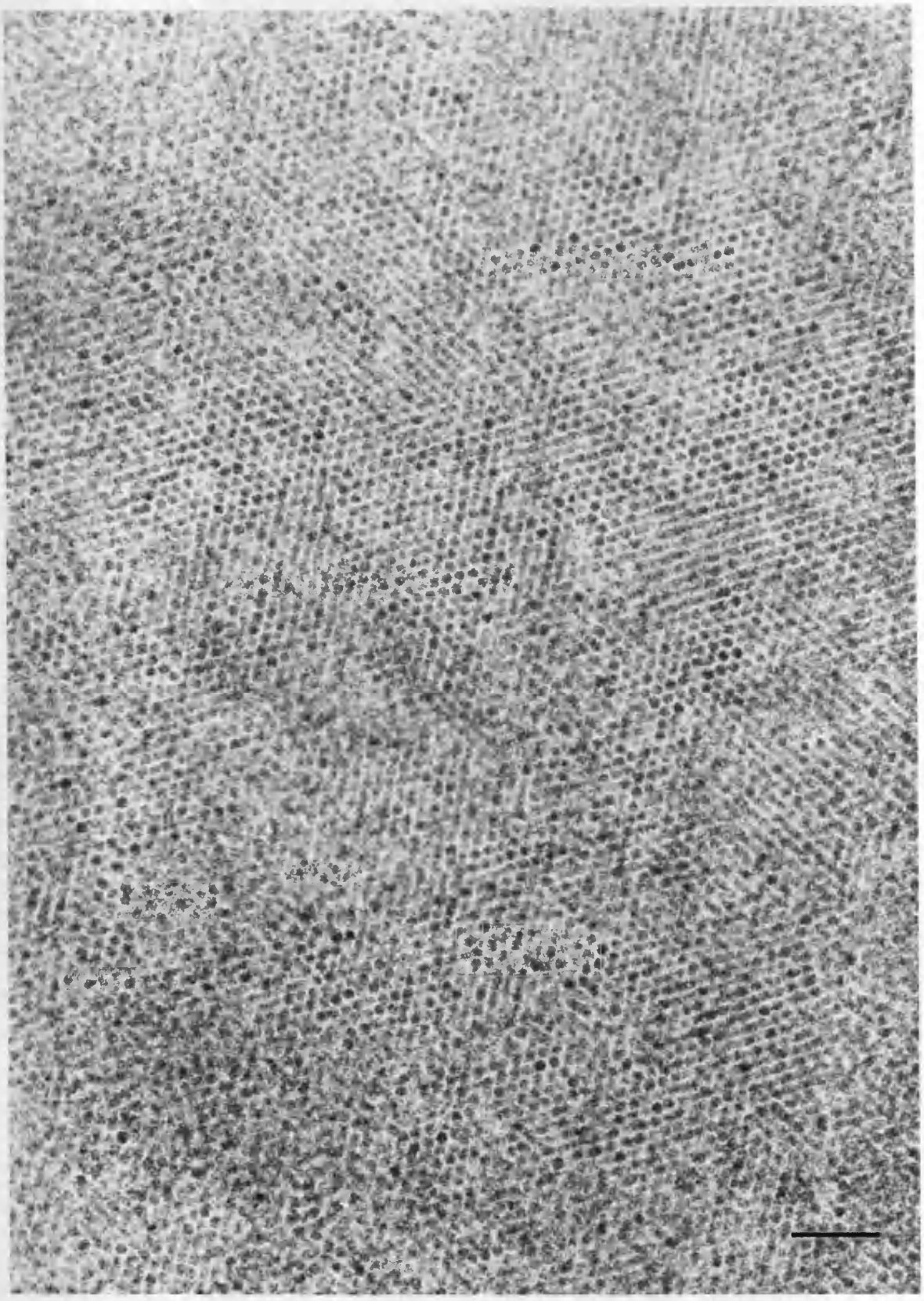

Transmission electron micrograph of unstained native human liver ferritin. The electron dense ferritin cores are seen closely packed, covering the nitrocellulose and carbon coated electron microscopy grid. The bar marker represents 50nm.

The Biomineralization of Ferritin and Haemosiderin

submitted by Vanessa J. Wade

for the degree of Doctor of Philosophy

of the University of Bath

1991

Abstract

The structure, size and morphology of iron cores from a number of native ferritins, haemosiderins and reconstituted ferritins have been investigated by analytical transmission electron microscopy.

Native mammalian ferritins (human spleen, liver, brain and horse spleen) and haemosiderins (spleen of an iron-balanced human subject, horse spleen, reindeer liver and spleen) contained cores of ferrihydrite ($5Fe_2O_3.9H_2O$). By contrast, human haemosiderin cores from β-thalassemic spleen were goethite-like, and those from idiopathic haemochromatosis liver were poorly crystalline ferrihydrite or amorphous. Native pea seed ferritin cores were amorphous, but reconstitution at pH 7 produced crystalline ferrihydrite cores. Reconstituted *E. coli* bacterioferritin (pH 7) also had ferrihydrite cores.

The reconstitution of horse spleen apoferritin with iron, or iron and zinc (Fe:Zn ratio 10:1) at pH 6.5 was assayed by monitoring the reaction spectrophotometrically at 420nm. Apoferritin catalysed the oxidation of iron, and mediated the formation of discrete ferrihydrite cores at all loadings (200, 875 & 3500 Fe atoms/molecule). Reconstitution with iron in the presence of Zn^{2+} ions reduced the rate of uptake/oxidation compared to control experiments. Analyses of protein-free controls revealed that zinc inhibited nucleation of the oxidation product. The nucleation cluster inside each protein cavity was estimated to be ~220 Fe atoms/molecule, by incremental reconstitution in the presence of Zn^{2+}.

The reconstituted cores of human H- and L-subunit homopolymers and heteropolymers were all ferrihydrite of similar crystallinity, but a significant decrease in core size with increasing proportion of H-subunit in the molecule was observed. Reconstituted H-subunit

homopolymers modified at the ferroxidase centre (Glu 62, His 65 → Lys, Gly) resembled reconstituted L-subunit homopolymers. H-subunit variants modified in the 3- or 4-fold channels were not significantly different to unmodified H-subunit ferritins. Modification of H-subunit at a putative nucleation site (Glu 61, 64, 67 → Ala) produced cores of wider size distribution, while modification of both ferroxidase and "nucleation" residues completely inhibited iron uptake and deposition.

Discrete, amorphous manganese oxide cores were formed following reconstitution of horse spleen apoferritin with Mn^{2+} at pH 7.5, 8.0 and 9.2. At pH 8.0 the reaction was catalysed by apoferritin.

To my parents and to Andy.

Acknowledgements

My thanks are due first of all to my supervisor Professor Stephen Mann for giving me the opportunity to carry out research in the exciting area of bio-inorganic chemistry and for his guidance and support throughout the studentship.

Secondly, I wish to thank Dr. Nick Sparks for teaching me on the transmission electron microscopes and for his encouragement and support in the early days. My thanks also go to the staff of the Electron Optics Unit for their help on many occasions.

I acknowledge the help and support of members of Prof. Mann's research group and other members of the Inorganic Chemistry department throughout the period of research and writing-up. Particular thanks are due to Fiona Meldrum for allowing me to use a couple of her micrographs in this thesis and for reading, with a critical eye, two of the chapters contained herein. Thanks too, to Justin Walker for proof reading two chapters. I also wish to thank Alan Carver for running Atomic Absorption and X-ray Diffraction analyses for me.

I thank Prof. Ron Board for his encouragement, support and friendship throughout my time at Bath University.

Thanks are due to Dr. R. Ewan of Bristol Polytechnic for carrying out X-ray Photoelectron Spectroscopy on samples of native ferritin and ferritin reconstituted with manganese.

My thanks go to those with whom I was involved in collaborative research: Prof. P.M. Harrison, Dr. A. Treffry, Dr. P. Arosio, Prof. T.J. Peters, Dr. R.J. Ward and Dr. D.P.E. Dickson. The funding of my studentship by the Science and Engineering Research Council is gratefully acknowledged.

Special thanks go to my husband Andy for his constant support, encouragement and tolerance during this period of work and for his help with the final production of this thesis. Also, special thanks to my parents for their continued support, encouragement and understanding.

Contents

Chapter 1

INTRODUCTION

The work presented in this thesis was undertaken in order to a) broaden our understanding of the nature and extent of influence that the protein shell of the iron storage protein, ferritin, has on the structure of the iron oxide formed within its cavity following *in vitro* reconstitution,
b) determine the structural characteristics of the iron cores of ferritin and the other major storage form of iron, haemosiderin, formed *in vivo* in normal and some pathological states of mammalian iron metabolism,
c) demonstrate if apoferritin could assimilate, in a way similar to iron, another transition metal, manganese,
d) study, for the first time by transmission electron microscopy and electron diffraction, the native iron cores of some recently isolated ferritins and to see the effect of *in vitro* reconstitution on the structure of their cores.

The *in vitro* reconstitution studies were conducted using two approaches: i) studying the structure of the cores by transmission electron microscopy and electron diffraction at different iron loadings and ii) monitoring the kinetics of the reconstitution reaction as it proceeded. These results were compared with those from the concomitant study of the oxidation of Fe(II) in the absence of apoferritin. Such comparisons were very valuable and enlightening.

Furthermore, structural and kinetic studies of Fe(II) oxidation in both the presence and absence of apoferritin, together with Zn^{2+} ions, a known inhibitor of iron uptake by apoferritin, increased our insight into the role of the protein and the nature of the mineralization process.

Structural studies were also carried out on the reconstituted cores of a range of ferritins of differing subunit composition and homopolymers of genetically engineered ferritins. The results were most useful in extending our knowledge of the role of key features of the protein shell, and of the protein shell as a whole, in iron uptake and deposition.

The structural studies of the ferritin and haemosiderin iron cores formed *in vivo* have given us a better understanding of the nature of the haemosiderins formed in different diseased states. They have also posed new questions about the relationship between ferritin and haemosiderin and the role of the protein in any such relationship.

The background of these studies lies in the role of iron in biology, the chemistry of iron, iron biomineralization and the already extensive literature concerning ferritin: the protein shell, the iron core, ion binding and iron uptake, and iron release. Each of these topics is considered in turn below.

1.1 The biological importance of iron

Iron is an essential element for nearly all forms of life, where it is used, for example, to transport and store oxygen, in redox reactions and as a structural component. In order to fulfil its roles

to transport and store oxygen and to participate in redox reactions iron is bound to a variety of proteins in a number of ways. Table 1.1 shows some examples of the two main types of iron containing proteins that occur in nature: the haemproteins and the iron-sulphur proteins. It also shows a few other types of protein that bind iron in different forms in order to function. Another major form of iron in biology is iron oxide. As such it may play a structural role, it may be present in a form in which iron is transported or stored, or it can be used by the organism for magnetoreception. The types of iron oxides known to occur in nature are listed in table 1.2.

The element iron has two particular features which give rise to its importance to biological systems: i) its ability to undergo valency change from Fe(II) to Fe(III) and ii) its tendency to form chelate complexes. The chemical nature of iron, however, also presents problems to biological systems. For although iron is the second most abundant metal in the earth's crust, present at about 4% in a typical soil, iron minerals are relatively insoluble and so the element is not readily available to organisms. Furthermore, at pH values above 6 Fe(II) is readily oxidised to Fe(III) by molecular oxygen and in the neutral pH range hydrated ferric ions rapidly hydrolyse and polymerise into an insoluble form. Nature has overcome these problems; uptake is achieved by chelation and iron is transferred inter- and intracellularly via organic ligands.

Primary uptake of iron from the physical environment is achieved by microorganisms and plants. Many bacteria produce siderophores (hydroxamate and catechol-based compounds, illustrated in figure 1.1) which chelate iron (III) in the environment, the chelate complex is then assimilated into the cells via receptor proteins located in the cell membrane. There is some evidence that reduction of iron and its

Table 1.1 Some types of proteins which contain iron

group/ protein	form of iron	function	occurrence
haemproteins			
haemoglobin	haem	oxygen transport	mammals, invertebrates
myoglobin	haem	oxygen transport and storage	mammals, invertebrates
cytochromes	haem	electron transport, respiration	widely distributed in aerobic cells
hydroperoxidases	haem	H_2O_2 reduction	mammals, plants, aerobic micro-organisms
iron-sulphur proteins			
rubredoxin	Fe4cys	electron transport	bacteria
ferredoxin	2Fe2S or 4Fe4S	redox mediators, electron acceptors nitrogen fixation	mitochondria, chloroplasts, photosynthetic bacteria nitrogen fixing bacteria
flavoproteins	eg. $2Fe_2S_2$, Mo	oxidation and de-hydrogenation reactions	widely distributed in nature
aconitase	Fe_4S_4 type	dehydration of citric acid in TCA cycle	widely distributed in aerobic cells

continued overleaf

Table 1.1 continued

others			
haemerythrin	2Fe(II) per monomer	oxygen transport	marine invertebrates
prokaryotic dioxygenases	require Fe^{2+}	O_2 incorporation	prokaryotes
ribonucleotide reductase	2Fe(III)	DNA synthesis	prokaryotes and eukaryotes

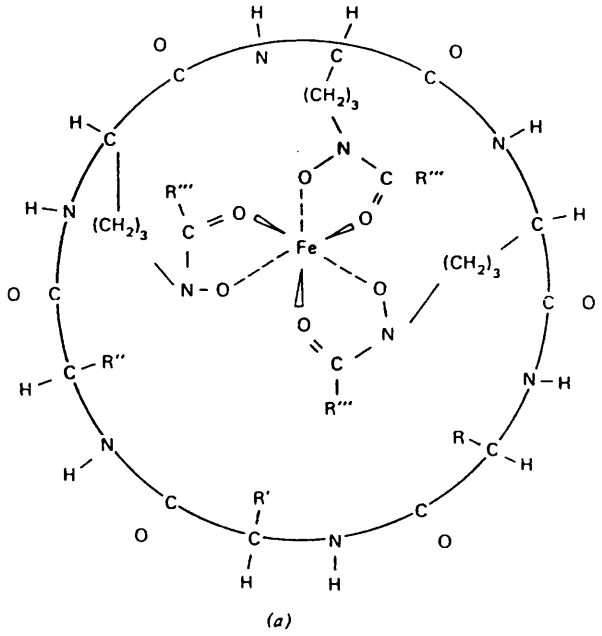

(a)

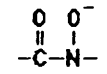

hydroxamate moiety

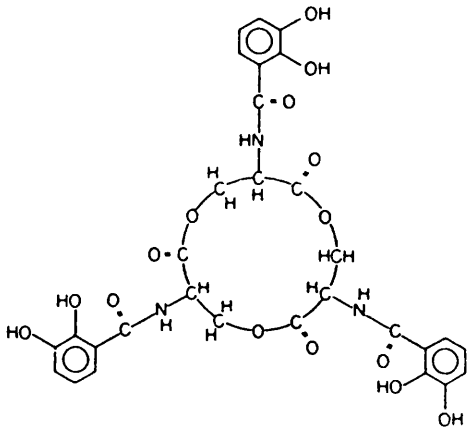

(b)

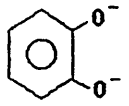

catecholate moiety

Figure 1.1 Two examples of siderophores. *(a)* shows an iron ferrichrome complex. The ferrichrome is a cyclic hexapeptide in which three successive amino acid residues have side chains ending in hydroxamate groups. *(b)* is an enterobactin, the formation constant for the complex of this molecule with Fe(III) has been estimated at $>10^{45}$, but it is kinetically labile.

Table 1.2 Iron oxides formed in biological systems

Mineral	Occurrence	Function
Magnetite (Fe_3O_4)	Bacteria	Magnetoreception
	Mollusc (chiton)	Teeth
	Arthropods (honey bee)	Magnetoreception?
	Chordates (tuna fish, pigeon head)	Magnetoreception?
Ferrihydrite ($5Fe_2O_3.9H_2O$)	Bacteria	Iron storage and transport
	Fungi	
	Mollusca	
	Animalia	
Goethite (α-FeOOH)	Mollusca (limpet)	Teeth
Lepidocrocite (γ-FeOOH)	Mollusca (chiton)	Teeth
	Porifera (sponges)	Unknown
Amorphous ferric oxides	Bacteria	Unknown
	Protozoa	
	Annelida	
	Mollusca	

reproduced from Mann (1987), with permission.

uptake from minerals is enhanced when bacterial cells are attached to the mineral surface (Jones, 1986). Absorption of iron by plant roots appears to be dependent on the reduction of Fe(III) to Fe(II) before absorption. This is probably mediated at the outer plasmalemma by electron transfer from cytochrome or flavin compounds. Iron is not readily moved between plant organs, therefore growing tissue is dependent on a continuous supply of iron in the xylem, where it is transported mainly in the form of ferric citrate (Mengel & Kirkby, 1978).

In mammals and birds iron is taken up from the diet if it is required and in a bio-available form, (not, for example, complexed with vegetable polyphenols, Torrance *et al.*, 1982). In small mammals iron is absorbed primarily in the duodenum and it appears that

specific uptake mechanisms exist for both haem and non-haem iron, although the details of these mechanisms are not yet clear. Both iron (II) and (III) can be assimilated, but iron (II) forms are probably more readily absorbed, (Simpson, 1990). Since, in mammals, there is no mechanism for its excretion, iron homeostasis must be maintained by regulation of uptake. Again, the details of such regulation are not yet apparent.

In mammals and birds the proteins transferrin and albumin transport iron (III) intercellularly and lower molecular weight compounds are implicated in its intracellular translocation. Two likely candidates for the intracellular translocation of iron (III) are ascorbic acid (Jacobs, 1980) and citric acid (Romslo, 1980). Once acquired iron must be conserved and since iron containing proteins are turned over and cellular needs for iron fluctuate, storage is essential.

1.2 Biologically relevant solution chemistry of iron

Fe(II) and Fe(III) exist in acidic aqueous solution as the hydrated ions $[Fe(H_2O)_6]^{2+}$ and $[Fe(H_2O)_6]^{3+}$, respectively. In the neutral pH range, Fe(II) is readily oxidised to Fe(III) under aerobic conditions. The reaction may be formally described by equation (1):

(1) $$4Fe^{2+}(aq) + O_2 + 4H^+ \rightarrow 4Fe^{3+}(aq) + 2H_2O$$

This overall reaction is the product of the two half-cell reactions:

(2) $$4H^+ + O_2 + 4e^- \rightarrow 2H_2O \qquad E^\circ = +1.229\ V$$

and (3) $$4Fe^{2+} - 4e^- \rightarrow 4Fe^{3+} \qquad E^\circ = -0.770\ V$$

which gives an overall $E^\circ = +0.459$ V. Although equation (1) suggests that the forward reaction is favoured by low pH, at neutral pH the oxidation is favoured due to the removal of $Fe^{3+}(aq)$ from solution by

hydrolysis, polymerisation and subsequent precipitation. Both the Fe(II) and Fe(III) aqua ions readily hydrolyse and polymerise, the solubility of $[Fe(H_2O)_6]^{3+}$ is very low, 10^{-17} M at pH 7 and that of $[Fe(H_2O)_6]^{2+}$ is 10^{-1} M at pH 7, (May & Williams, 1980). The processes of hydrolysis and polymerisation for $[Fe(H_2O)_6]^{3+}$ are illustrated here:

$$[Fe(H_2O)_6]^{3+} \rightleftharpoons [Fe(H_2O)_5(OH)]^{2+} + H^+ \rightleftharpoons [Fe(H_2O)_4(OH)_2]^{+} + H^+$$

$$2[Fe(H_2O)_5(OH)]^{2+} \rightleftharpoons [(H_2O)_4Fe(OH)_2Fe(H_2O)_4]^{4+} + 2H_2O \rightleftharpoons [(H_2O)_4Fe(O)(OH)Fe(H_2O)_4]^{3+} + H^+$$

As shown, hydrolysis involves the loss of protons from the aqua metal ions and polymerisation is a condensation reaction, resulting in the loss of water molecules and of further protons. This process results in the formation of oxo-bridges, where oxygen atoms bridge two iron centres.

Studies of the oxidation of Fe(II) to Fe(III) in aqueous solution have shown that the rate of oxidation of Fe(II) at concentrations of less than 0.5 mM and at pH $\geq$ 5.5 is first order with respect to the concentrations of both Fe(II) and O_2 and second order with respect to the OH^- ion. The kinetics follow the rate law

$$\frac{-d\,[Fe(II)]}{dt} = k\,[Fe(II)][OH^-]^2\,p_{O_2}$$

and k = 8.0 (±2.5) x 10^{13} min^{-1} atm^{-1} $mole^{-2}$ at 20°C. At constant pH an activation energy of 23 kcal (96.232 kJ) $mole^{-1}$ was calculated, (Stumm & Morgan, 1970). It follows that the reaction rate is strongly pH dependent and that a 100-fold increase in rate occurs for a one unit increase in pH.

In a biological fluid such as plasma, the potential necessary to reduce Fe(III) to Fe(II) can vary from 0.77 to 0.36 V depending on the ligands complexed to the metal ions, (May & Williams, 1980). The stabilisation of Fe(II) and Fe(III) by a variety of ligands (biological and non-biological) is illustrated in figure 1.2. Column I gives an idea of the range of values exhibited and reveals that complexes containing anionic ligands occur towards the bottom, since anions tend to stabilise Fe^{3+} more than Fe^{2+} on simple electrostatic grounds. Conversely, ligands such as 2,2'-bypyridyl and 1,10-phenanthroline stabilise Fe^{2+} more than Fe^{3+}, since there is greater π-electron transfer from the 2+ (d^6) ion, than the 3+ (d^5) ion. Column II illustrates the possibility of fine-tuning the redox potentials, for example, by substitutions on the rings of 1,10-phenanthroline. The other columns give some biological examples. Stabilisation by complex formation can afford control over the redox chemistry and hydrolysis of iron. Hydrolysis and therefore polymerisation, is suppressed when ligands occupy all six coordination positions on each ion and mononuclear complexes can exist at physiological pH. Such species are formed by polydentate chelating agents, for example the siderophores illustrated above in figure 1.1.

The compatibility of a metal ion and any ligand ultimately depends on the strength of the chemical bond that can be formed between them. The Hard/Soft, Acid/Base concept is useful in describing which ligands will coordinate with which metals. Using the Lewis definition, a base is defined as a species which can donate a pair of electrons to form a coordinate bond and an acid is defined as a species which can accept this pair of electrons. A metal ion is a hard acid if it has a high positive charge, is small in size and has

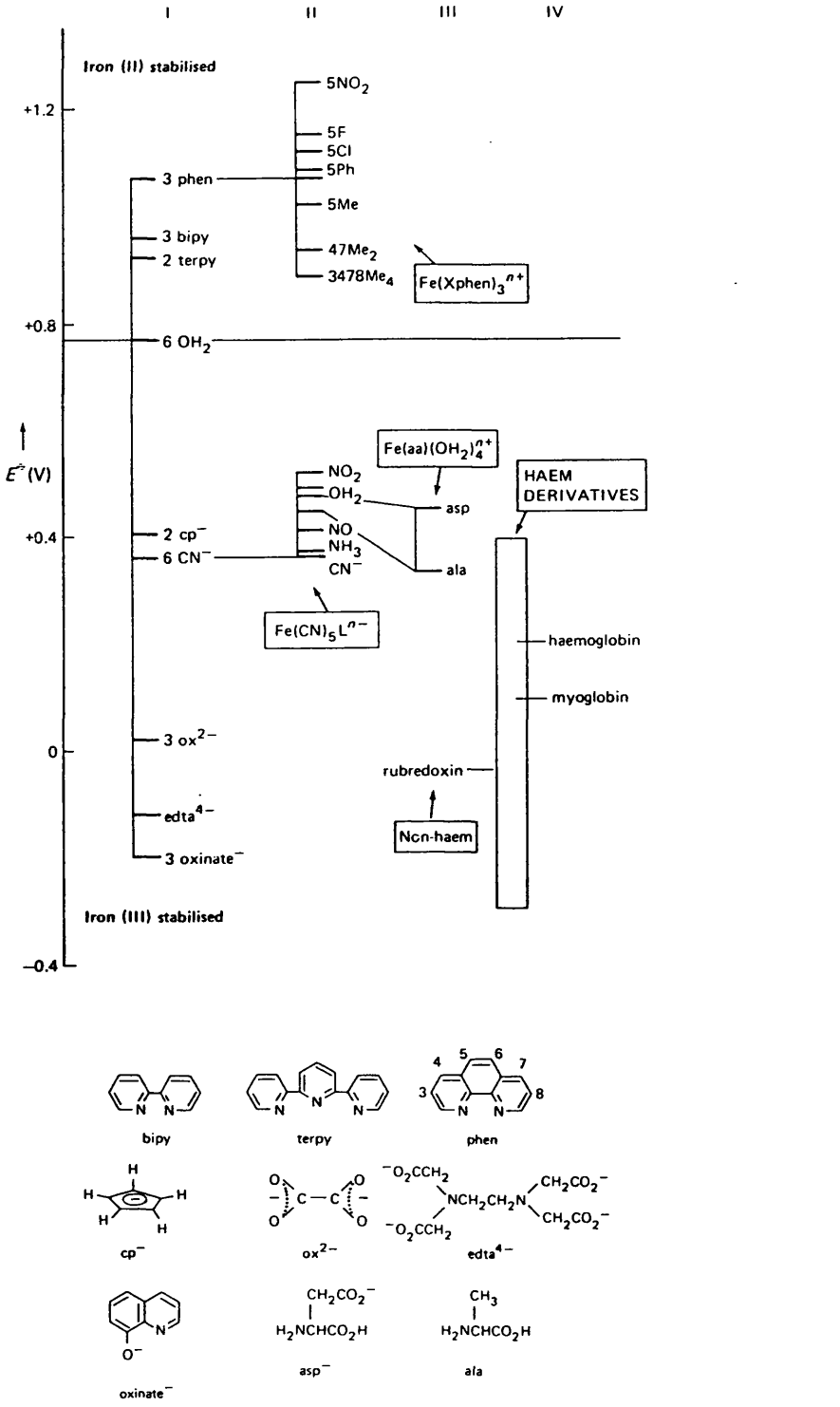

Figure 1.2 The effect of complex formation on the iron/iron couple, in all cases in aqueous solution. See text for details. After Burgess (1988).

no easily excitable outer electrons. A ligand is a hard base if it has a donor atom of low polarisability, high electronegativity, having vacant orbitals only of high energy and is therefore hard to oxidise. Conversely, a metal ion is a soft acid if it is of low charge density, large size and has easily excited outer electrons. A soft base has a donor atom of high polarisability, having empty, low energy orbitals, this atom is of low electronegativity and is easily oxidised. Hard acids form strong bonds with hard bases, whereas soft acids form stable complexes with soft bases. Much less stable complexes are formed between hard acids and soft bases or soft acids and hard bases.

Fe^{3+} is considered to be a hard acid and as such has a preference for ligands which are hard bases; particularly those which contain oxygen, for example hydroxyl and carboxyl groups, (see figure 1.2 above). Fe^{2+} is intermediate between a hard and a soft acid and so can accommodate both hard oxygen based ligands and intermediate or soft ones such as those containing nitrogen, nitrogen with oxygen donors, or sulphur, for example NH_3, NO_2^- and RS^-. These characteristics dictate the behaviour of Fe (II) and (III) regarding their interactions with biological ligands such as amino acid side chains. It also means that a hard donor will favour Fe^{3+} over Fe^{2+} in a redox system and the higher oxidation state will be preferred in an aqueous as opposed to a non-aqueous environment. Increasing the pH of a system will have the same kind of effect, since OH^- is a hard base. Hydroxyl ions are much more powerful electron donors than water molecules, so high pH will favour metal ion hydrolysis over complex formation with many other ligands. Also, it is worth noting that the proton behaves as a very hard acid.

1.3 Iron oxide structures and phase transformations

There are several crystalline forms of iron oxide and oxyhydroxide. These include the ferrimagnetic, mixed valence oxide magnetite (Fe_3O_4), the Fe_2O_3 polymorphs: hematite (αFe_2O_3) which is the most important iron ore and maghemite (γFe_2O_3) which is ferrimagnetic, ferrihydrite which is a non-stoichiometric "hydrous ferric oxide" phase with the general formula $5Fe_2O_3.9H_2O$ and the oxyhydroxides (FeOOH) which are also polymorphic: goethite (α-FeOOH), lepidocrocite (γ-FeOOH) and akaganeite (β-FeOOH). The oxide and oxyhydroxides that are relevant to this thesis are ferrihydrite, goethite and lepidocrocite. The structures of these, their formation in simple aqueous systems and the possibilities of phase transformations between them, under mild conditions and with "biologically relevant" species, will be discussed here.

Table 1.3 Some iron oxide structures

oxide/ hydroxide	crystal system	oxide substructure
ferrihydrite	hexagonal	hcp
goethite	orthorhombic	hcp
lepidocrocite	orthorhombic	ccp
hematite	rhombohedral	hcp
maghemite	tetragonal	ccp

hcp = hexagonal close packed

ccp = cubic close packed, also known as face centred cubic (fcc).

1.3.1 Ferrihydrite

As can be seen from table 1.3, ferrihydrite belongs to the hexagonal crystal system, having an hcp oxide substructure. The most widely accepted model of ferrihydrite structure is that of Towe & Bradley (1967). This proposes a hexagonal unit cell in which a = 0.508 nm and c = 0.94 nm. The iron atoms are located in octahedral sites, in layers between the close packed oxygens, as shown in figure 1.3. The occupancy of the iron sites is variable and some oxygen positions are filled with OH^- ions and water molecules.

Ferrihydrite is readily formed when an Fe(II) solution at around neutral pH is allowed to oxidise rapidly. The initial rate of ferrihydrite (FH) formation is proportional to the rate of Fe(II) oxidation and so it can be described by an equation similar to that given for Fe(II) oxidation above:

$$\text{initial rate FH formation} = k\,[Fe(II)][OH^-]^2\,p_{O_2}$$

After the nucleation of ferrihydrite has occurred the reaction is autocatalytic and the ferrihydrite surface provides an increasing number of active sites. The rate is thus dependent on the concentration of ferrihydrite present and the equation becomes:

$$\text{rate FH formation} = k\,[Fe(II)][OH^-]^2\,p_{O_2}\,[FH]$$

Ferrihydrite can also be made by the addition of some NaOH solution to a solution of an iron (III) salt. The precipitated ferrihydrite is usually poorly crystalline but the crystallinity can be improved by heating the precipitate together with the supernatant for a number of hours at about 70°C.

Synthetic ferrihydrite made under the conditions outlined above forms small particles of nanometre dimensions, with a granular appearance (author's own observations & Mackenzie *et al.*, 1971).

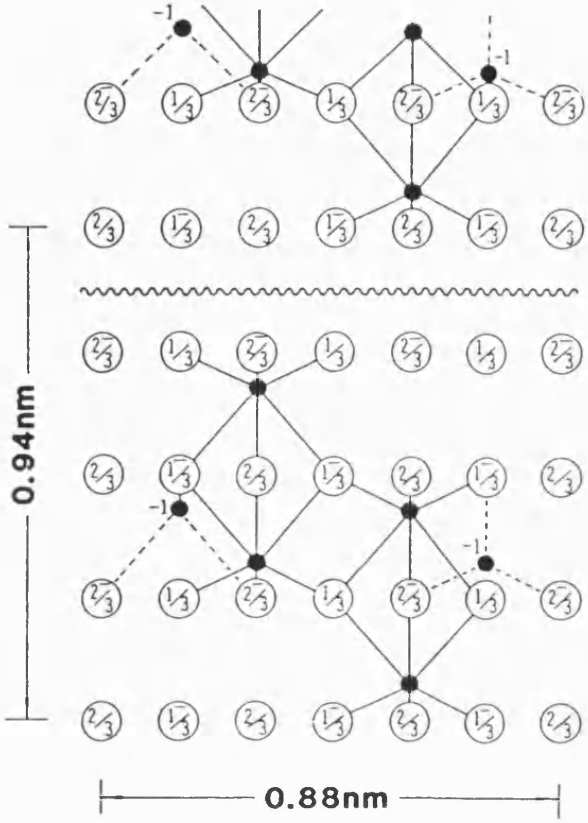

Figure 1.3 A model for ferrihydrite, after Towe & Bradley (1967). The figure shows an idealised detail of four Fe octahedra with fragments of adjacent units, as viewed down the *a* axis. (●) Fe in $(11\bar{2}0)$ and one level below. (○) oxygens above and below $(11\bar{2}0)$ as indicated. The wavy line indicates a level at which lateral displacements are optional. This level accommodates additional Fe^{3+} or H^{+}. The *c*-period consists of only four oxygen levels.

1.3.2 Goethite

Goethite is orthorhombic and has an hcp oxide lattice (table 1.3). The structure of goethite is built of double chains of edge-shared $Fe(O,OH)_6$ octahedra, as illustrated in figure 1.4. From 1.4a it can be seen that, viewed from the [001], the structure resembles a "network". The octahedra share vertices between the layers. The double chains of octahedra are illustrated, in a more 3D view, from the [100], in figure 1.4b. The dimensions of the unit cell are: a = 0.464 nm, b = 0.998 nm, c = 0.303 nm, (Flynn, 1984).

Taylor & Schwertmann (1978) studied the oxidation products formed in Fe(II) solutions containing either carbonate, chloride or sulphate counterions. They found that the largest amounts of goethite were formed in the carbonate system under conditions of low aeration and/or high iron concentration. The pH of these solutions was between 5.9 and 6.4. Lepidocrocite could be formed in this system if the aeration rate was increased and/or the iron concentration decreased. Ferrihydrite was formed at very high aeration rates, when the pH was increased to around 7.0. The formation of goethite from $FeCl_2$ solutions in the presence of CO_2 has been reported by Schwertmann & Thalmann (1976).

Synthetic goethite crystals are invariably acicular and they generally have a considerable length: cross section ratio (Mackenzie *et al.*, 1971).

1.3.3 Lepidocrocite

From table 1.3, it can be seen that lepidocrocite also has an orthorhombic structure, but that the oxide lattice is ccp. Lepidocrocite is built of edge-shared $Fe(O,OH)_6$ octahedra, but, as can be seen from the view of the [001] in figure 1.4c, it has a

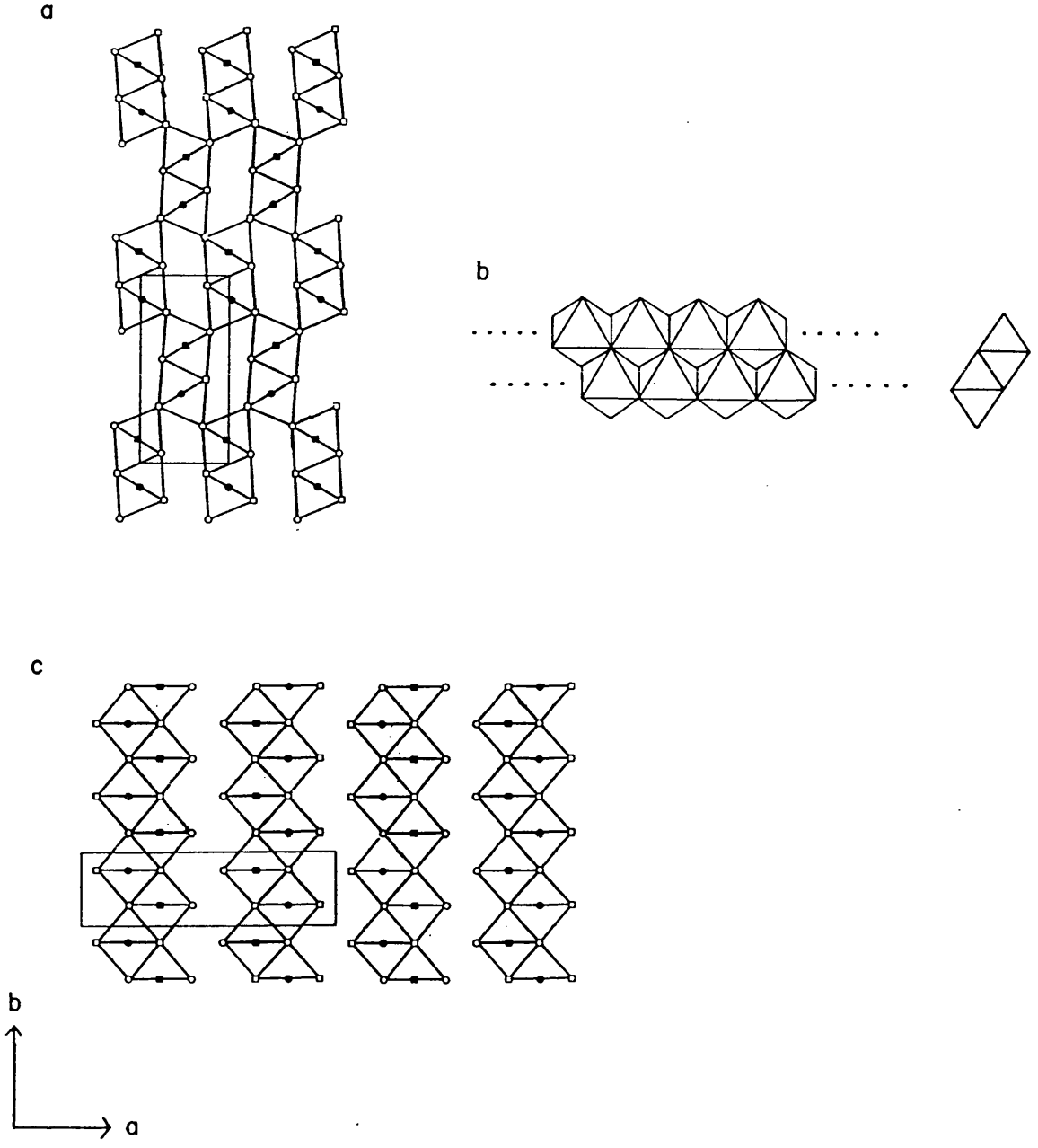

Figure 1.4 Schematic diagrams of the crystal structures of goethite and lepidocrocite. *a* Goethite (α-FeOOH), projection along [001], (●) Fe at z = ¼, (■) Fe at z = ¾, (○) O at z = ¼, (□) O at z = ¾. *b* More 3D view of the chains of octahedra as viewed from the [100] of both goethite and lepidocrocite. *c* Lepidocrocite (γ-FeOOH), projection along [001], (●) Fe at z = 0, (■) Fe at z = ½, (○) O at z = 0, (□) O at z = ½. After Flynn (1984).

lamella structure, in which the layers are held together by H bonds. Figure 1.4b corresponds to the [100] of lepidocrocite. The dimensions of the unit cell are: a = 1.253 nm, b = 0.388 nm, c = 0.307 nm, (Flynn, 1984).

Taylor & Schwertmanns' studies (1978) showed that lepidocrocite was the major oxidation product formed in Fe(II) chloride solutions (pH 5.5) at high aeration rates, (with decreased aeration the major product was maghemite). In the sulphate system (pH 5.5) lepidocrocite was again the major product at the aeration rate used. These authors noted that although lepidocrocite is thermodynamically less stable than goethite, it is kinetically favoured. Therefore, in an Fe(II) system, goethite will only be formed instead of lepidocrocite if there is some factor which slows the formation of Fe(III) species. The synthesis of lepidocrocite from $FeCl_2$ solutions at pH values between 5 and 7, by bubbling of CO_2-free oxygen has been reported (Schwertmann & Thalmann, 1976).

Lepidocrocite, prepared synthetically, exhibits two morphologies: acicular and lamellar. The acicular crystals usually have a smaller length:cross section ratio than those of goethite, and they may appear more lath-like. The lamellar morphology is consistent with lepidocrocite's lamellar crystal structure and with the tabular habit observed macroscopically (Mackenzie *et al.*, 1971).

1.3.4 Phase transformations

In a long-term experiment conducted by Schwertmann & Murad (1983), freshly prepared ferrihydrite was stored as aqueous suspensions at 24°C and pH 2.5 - 12.0 for almost three years. The range of pH values for the different samples was achieved by the addition of HNO_3 or NaOH. The products of phase transformation were

goethite and hematite; maximum goethite was formed at pH 4 and 12 and maximum hematite was formed between pH 7 and 8. From table 1.3 above it can be seen that all three oxides have a hcp oxide lattice and that they all belong to different crystal systems. However, the structures of ferrihydrite (hexagonal) and hematite (rhombohedral) are closely related and "topotactic" transformation between the two can occur, (ie. since there is a definite relationship between the two structures, transformation can occur by the simple rearrangement of atoms, with no major crystallochemical changes). The structures of ferrihydrite and goethite (orthorhombic) are not closely related and transformation would have to occur via a dissolution-reprecipitation pathway. Schwertmann & Murad (1983) concluded that two transformation processes were in competition in their experiment: hematite was formed by internal rearrangement and dehydration, while goethite was formed via solution, preferably from monovalent Fe(III) ions ($[Fe(OH)_2]^+$ and $[Fe(OH)_4]^-$). They related the proportions of hematite and goethite formed to the activity of the Fe(III) ion species in solution; this implied that conditions favourable for the formation of hematite were unfavourable for that of goethite and *vice versa*.

Ford *et al.* (1984) reported that ferrihydrite ages to hematite on heating to 40°C for 10 - 14 days or to goethite in 0.02 M $FeSO_4$ at pH 6 or in 1 M KOH.

The more recent work of Cornell & Schneider (1989) has shown that ferrihydrite will transform into goethite in the pH range 7.5 - 9 and at temperatures between 25 and 70°C, in the presence of L-cysteine. This was the first organic ligand found to promote the transformation to goethite. Others, such as carboxylic acids and simple sugars, had stabilised the ferrihydrite or promoted hematite formation. Adsorption of the cysteine, via its sulphedral group, onto

the ferrihydrite surface was the first step in the reaction. The cysteine then reduced some of the surface Fe(III) sites rendering them more labile. This appeared to facilitate the transformation to goethite, possibly by promoting the dissolution of ferrihydrite. Cystine was formed in the supernatant. The transformation may be summarised as:

ferrihydrite + RSH →

$Fe(II)_x Fe(III)_y$hydroxide + ½ RSSH + ½ H^+ → goethite

The ferrihydrite could be stabilised against transformation to goethite, by the presence of phosphate and silicate species.

The pathways of phase transformation between the iron oxides mentioned are summarised schematically in figure 1.5.

1.4 Iron biomineralization

"*Biomineralization* refers to the processes by which organisms form minerals" (Lowenstam & Weiner, 1989). Much work has been done on the biomineralization of calcium salts and silicates as well as iron oxides and, very recently, iron sulphides. The process of ferritin iron uptake is one of biomineralization, with the deposition of the iron oxide being directed by the protein so that the iron is sequestered inside the protein cavity and the ultimate size of the particle is limited. The protein also has some influence on the structure of the oxide formed, since the rapid oxidation of Fe(II) to Fe(III), promoted by the protein, leads to the formation of ferrihydrite, rather than the more thermodynamically stable oxides such as lepidocrocite and goethite.

It is apparent that ferritin and ferrihydrite are important in other iron biomineralization processes. Table 1.2 above, shows the

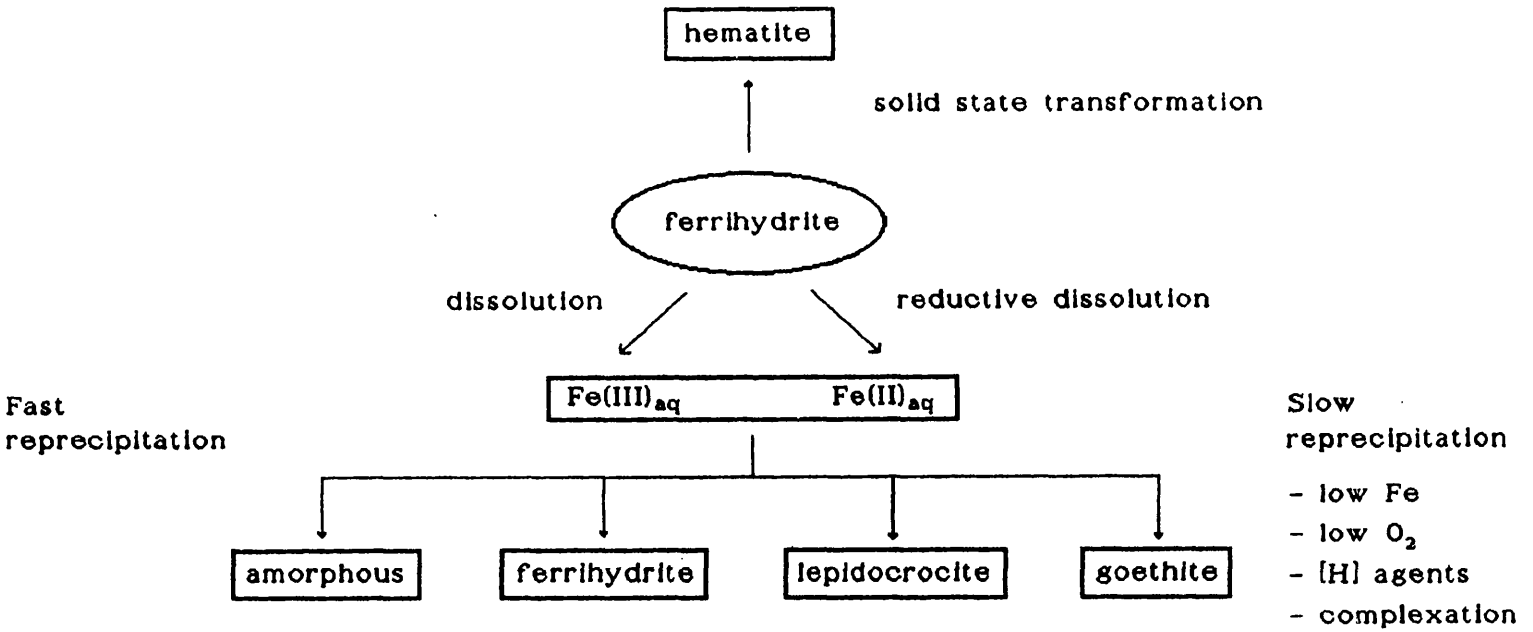

Figure 1.5 Schematic representation of some pathways of phase transformation between iron oxides.

occurrence and types of iron oxide biominerals present in nature. Ferritin is the source of iron for the mineralization of chiton teeth (Kim *et al.*, 1989) and probably for those of the limpet also (see below). Ferrihydrite, or a similar phase, seems to be a precursor in the formation of magnetite particles in the magnetotactic bacteria (Frankel *et al.*, 1983, Mann *et al.*, 1987a).

Ferritin has been shown to accumulate in the cells adjacent to chiton teeth just before the onset of mineralization. The iron is believed to be mobilised and delivered to the mineralizing teeth as Fe(II), where some ferrihydrite is reformed as the precursor of the other iron oxides found in mature chiton teeth. The ferrihydrite is replaced by goethite, lepidocrocite and/or magnetite, as mineralization proceeds. These phase transformations appear to be due to competition between the different reactions leading to the different phases (see equations i) and ii)) and this competition may arise from the generation of differential redox potentials within the tooth cusp (Kim *et al.*, 1989).

i) Fe(II) + Fe(III) (ferrihydrite) → α-FeOOH

this reaction is slow and requires the oxidation of the Fe(II).

ii) Fe(II) + Fe(III) (ferrihydrite) → Fe_3O_4

the formation of magnetite requires some Fe(II) to remain unoxidised, since this is a mixed valence oxide, formally written as $Fe(II)Fe(III)_2O_4$.

The mineralization processes occurring in limpet teeth are related to those in chiton teeth (Kim *et al.*, 1989). Ferritin from the limpet *Patella vulgata* has been isolated and studied (Mann *et al.*, 1986a). It is probable that ferritin would be the source of iron for the mineralization of limpet teeth, although the presence of

ferritin in the cells adjacent to the mineralizing teeth has not been demonstrated (Mann *et al.*, 1986b). There is some circumstantial evidence for the presence of an iron oxide phase akin to ferritin cores in the Mössbauer spectra from early and mature teeth (St. Pierre *et al.*, 1986c) but there is no deposition of a ferrihydrite precursor (Mann *et al.*, 1986b).

1.5 Ferritin occurrence and distribution in nature

The non-specific intracellular deposition of an iron (III) oxide would be toxic and its iron difficult to mobilise. The iron storage proteins, ferritin and haemosiderin, provide elegant solutions to these problems. Ferritin, the main topic of this thesis, is discussed and described at length here. Haemosiderin is considered in chapter 5.

Ferritins are very widely distributed in nature. They are found in mammals, amphibians, fish, molluscs and birds, and similar molecules have been isolated from flowering plants, fungi and bacteria. The ferritin molecule provides an iron storage facility into which iron in excess of immediate requirements can be deposited, and from which iron can be mobilised in times of need. Body iron may accumulate when iron in the diet is readily available, thus stores can be built up. However, should dietary iron become inadequate or iron be lost from the body, for example, due to injury, the iron stores can be drawn upon. Ferritin provides a high capacity iron store which is itself soluble, the iron is kept in a non-toxic form and can be readily mobilised. A summary of the iron containing compounds in man, together with the approximate amount of iron in each, is given in table 1.4.

Table 1.4 Iron containing compounds in man

		mg in a 75kg male (approximate)
Functional compounds	haemoglobin	2300
	myoglobin	320
	haem enzymes	80
	non-haem enzymes	100
		2800
Storage complexes	ferritin	700
	haemosiderin	300
		1000
	Total	3800

After Bothwell *et al.* (1979).

1.6 Some general aspects of mammalian cellular iron metabolism and the role of ferritin

In mammalian systems iron is carried around the body largely by transferrin. The transferrins are a class of Fe^{3+}-binding glycoproteins widely distributed in extracellular fluid. They are characterised by the following properties: i) single polypeptide chain structures, ii) two similar, but probably not identical, iron binding sites, one in the N-terminal and one in the C-terminal half of the molecule, iii) iron-binding strong enough to resist hydrolysis

in the circulation, yet reversible under conditions pertaining in certain intracellular compartments, iv) binding of iron dependent on binding of carbonate or bicarbonate which serve as bridging ligands between the protein and the metal. (The bridging anion, by depriving water of a coordination site on the metal, may serve to inhibit hydrolysis while locking the metal ion in its place on the protein.) (Chasteen, 1983.)

The iron bound to transferrin is thus the major form of iron available to cells. The exact mechanism of iron uptake by cells from transferrin is still a matter for debate, however, figure 1.6 illustrates a widely accepted model. Iron requiring cells have transferrin receptors, iron-laden transferrin is bound by the receptors at the cell surface and then both the transferrin and receptor are internalised. The transferrin-receptor complex enters an endocytotic vesicle which has an internal pH of 5.5 and here the iron is released. It seems probable that the low pH alone is insufficient to release the iron at the rates observed and small acceptor molecules are envisaged to have a role. Low molecular weight polyphosphates and particularly pyrophosphate have been implicated (Romslo *et al.*, 1982). The reduction of the iron may also be required. The transferrin is then returned to extracellular space and the receptor to the cell membrane. Most of the studies that have lead to the formulation of this model were carried out with immature erythrocytes, since such cells have the highest requirement for iron and they are robust and easily prepared in quantity. Nevertheless, iron uptake by non-erythroid cells is believed to occur by the same mechanism.

Other means of iron uptake from transferrin that have been proposed involve other methods of receptor-mediated uptake and

receptor-independent mechanisms.

Non-transferrin bound iron can be taken up by cells *in vivo*, from the circulation, when transferrin is saturated with iron, as in acute or chronic iron overload, or in congenital atransferrinemia. It has been observed that when transferrin is saturated, iron is taken up by the liver, rather than the bone marrow, which would usually serve as the principal depot for circulating iron. In chronic iron overload (eg. transfusion-dependent thalassemia and haemochromatosis) non-transferrin iron may accumulate in the plasma. Such iron is more reactive in its susceptibility to reduction and chelation than transferrin-bound iron and so may be more toxic. The generalised iron overload seen in atransferrinemic subjects, (who paradoxically also suffer from severe iron deficiency anemia,) clearly shows that cells can take up non-transferrin bound iron, but this iron appears to follow different intracellular routes to that acquired from transferrin, (Theil & Aisen, 1987).

1.6.1 The role of ferritin

Most ferritins function in the intracellular storage of iron. The physiological function of serum ferritin is unclear; the amount of iron involved is small, but it may be a useful parameter in the diagnosis and monitoring of certain diseases. However, the correlation between serum ferritin and for example, the level of iron overload, is not always clear cut, (Worwood, 1980). All mammalian cells appear to have the capacity to synthesise ferritin and synthesis is stimulated by cellular iron uptake in excess of immediate requirements, (Jacobs, 1980). In animal cells endogenous ferritin is accumulated in membrane bound cytoplasmic organelles that contain lysosomal enzymes. When such organelles are packed with

ferritin, they are termed "siderosomes" and these bodies are found in diverse cell types. Under conditions of iron overload, the number and size of the siderosomes is greatly increased. The mechanism by which the ferritin is concentrated into the siderosomes is not known, nor is the extent to which siderosomal iron is re-incorporated into newly synthesised ferritin, (Richter, 1982). Three particular cell types have a major role in iron metabolism in the mammal, some features of their iron metabolism and the role of ferritin in each cell type are outlined below.

1 The hepatocyte

This parenchymal cell of the liver is the principal site of iron storage in the normal organism and is susceptible to overload when body iron increases. Iron uptake by the cell is probably largely determined by the concentration and saturation of the circulating transferrin, and possibly by the expression of transferrin receptors. *In vitro* studies of hepatocytes have shown that iron release from the cells is temperature dependent, that it is facilitated by a number of chelators, ionophores and by apotransferrin and that it probably involves energy metabolism. Desferrioxamine, a clinically important iron chelator at pharmacologically attainable concentrations, also promotes the release of iron from hepatocytes with about the same effectiveness as apotransferrin, (Theil & Aisen, 1987). *In vitro* studies with rat liver mitochondria have shown that mobilisation of iron from ferritin, by dihydroflavin mononucleotide ($FMNH_2$, new systematic name: reduced riboflavin 5'-phosphate), is preceded by saturable binding of ferritin to the mitochondria, (Ulvik, 1982). The half-life of the protein of rat liver ferritin, has been shown to vary with the iron content of the molecules. It varies upwards from

about 50 hours and is longest for heavily loaded molecules, (Richter, 1982).

2 The reticulocyte

In the reticulocyte, iron released from ferritin appears in the haemoglobin of the same cell and presumably in the other iron requiring proteins, if it could be measured in these. It has also been shown that ferritin stores iron from transferrin in this cell type, (Theil & Aisen, 1987). Ferritin can donate its iron to mitochondria (the site of haem synthesis); riboflavin 5'-phosphate (FMN) can mobilise ferritin iron and this flavin coenzyme has been implicated, along with flavin adenine dinucleotide (FAD) and succinate in this process of donation to the mitochondria, in the *in vitro* studies of Egyed (1982). A possible mechanism is shown here:

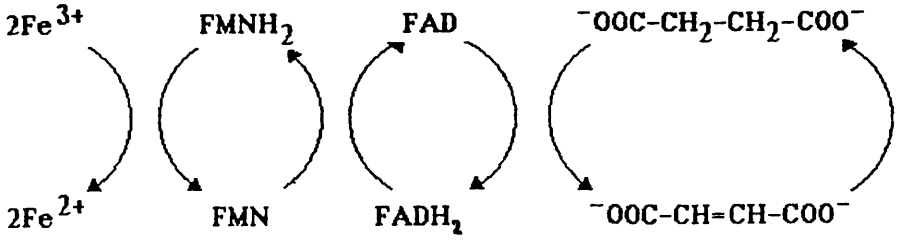

Reticulocyte iron consumption is extremely rapid during maximal haem synthesis, for example, rabbit reticulocytes take up 9 x 10^9 iron atoms in 24 hours. Some of this iron is derived from the ferritin present in the cells and the rest is donated directly from transferrin, (Theil & Aisen, 1987).

3 The reticuloendothelial system (RES)

The cells of the RES are by far the most important in the return of iron to transferrin; the RES handles the breakdown and recovery of iron from effete or damaged erythrocytes. About 85% of iron turned

over in the plasma passes through the RES, (Jacobs, 1980), but little is known of the processes involved. Evidence from *in vivo* experiments suggests that the processing of haemoglobin by the RES is relatively rapid; in humans, labelled iron from damaged erythrocytes appeared bound to circulating transferrin within 30 minutes of injection and 20% of the labelled iron was bound to transferrin within 2 hours. Ordinarily, it would seem that the iron from haemoglobin is promptly released to transferrin without passing through ferritin. There is evidence from studies with rats that during iron loading, haemoglobin iron is not released from the RE cells, but is deposited in intracellular ferritin, (Bothwell *et al.*, 1979).

Isolated macrophages have been used in the *in vitro* study of RES iron metabolism. Macrophages competent to process and release ingested iron may be isolated from the lungs, peritoneal cavities and livers (Kupffer cells) of experimental animals and from circulating human blood. These macrophages may be loaded with iron from damaged erythrocytes or by exposure to complexes of iron loaded transferrin. The bulk of the iron, taken up in any form, is excreted by the cells within 24 hours. Approximately half of the iron released and much of the intracellular iron is in the form of ferritin, when the macrophages are loaded with erythrocytes. However, only a small fraction of the iron delivered via transferrin is recovered in ferritin. When apotransferrin is available to the cells, it rapidly accumulates up to half of the excreted iron, but iron release is largely independent of the presence of apotransferrin in the culture medium. Desferrioxamine enhances iron excretion and increases the size of the low molecular weight iron pool in erythrophagocytosing macrophages. This observation has been taken to suggest that the chelator removes iron from the intracellular transit pool. (Theil &

Aisen, 1987.)

A schematic diagram of the exchange of iron between different body compartments is shown in figure 1.7.

1.6.2 Ferritin iron uptake *in vivo*

In vivo studies have shown that apoferritin shells are fully assembled before iron is associated with them, (reviewed in Harrison *et al.*, 1974). However, the source of intracellular iron for ferritin core deposition is unknown. Also, it has yet to be established if Fe(II) or Fe(III) is required for core formation *in vivo*. Theil & Aisen (1987) state that in reticulocytes the iron released from transferrin passes to both haem and ferritin. The donation of transferrin iron directly to ferritin does not seem to occur; there is evidence from studies with rat hepatocytes *in vitro*, that the iron passes from intracellular transferrin via the small molecular weight chelate system to ferritin (Morley *et al.*, 1982). Theil & Aisen (1987) go on to propose that if the iron is released from transferrin as Fe(III), ligands such as citrate, ATP or hexoses could stabilise the Fe(III) as mono-nuclear species if the ratio of ligand to Fe(III) was high. They continue, that alternatively, Fe(II) could be stabilised as the hydrated cation in regions of low oxygen tension, or by complexation with S or N ligands. So both Fe(II) and Fe(III) species could serve as iron donors to ferritin. Schneider (1988) however, comes to the conclusion that mono-nuclear $Fe(OH)_3$ is the most likely candidate due to thermodynamic and kinetic considerations of the chemistry pertaining in the cell. He suggests that it is unlikely that the biological pathway would involve the generation of so many electrons and protons (1 electron and ~2.5 H^+ per Fe^{2+} added)

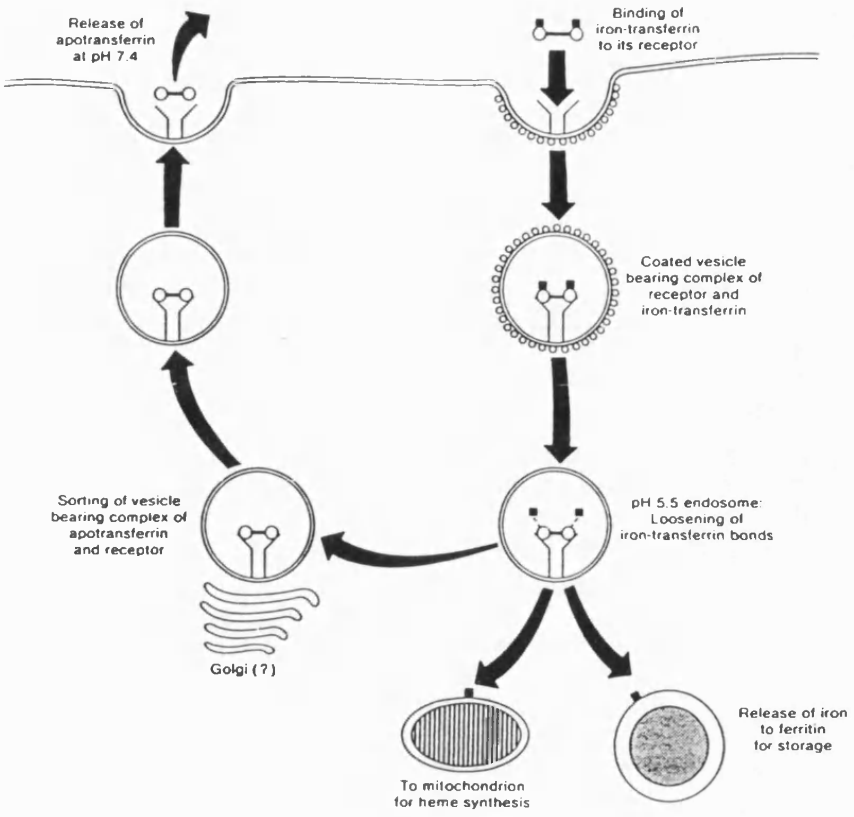

Figure 1.6 Schematic diagram of receptor-mediated transferrin iron uptake by an iron requiring cell. After Theil & Aisen (1987).

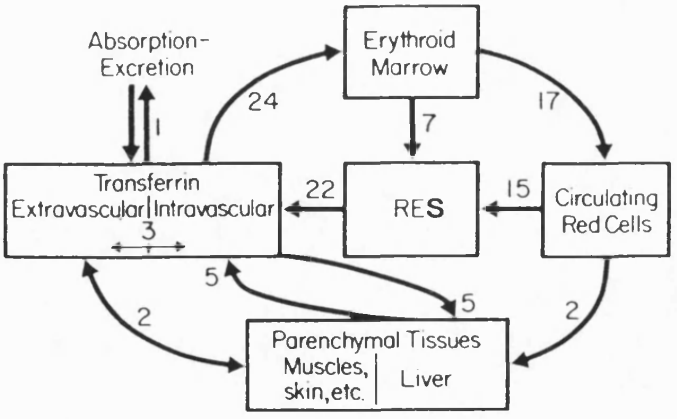

Figure 1.7 The amounts of iron (mg/day) exchanging between different body compartments in a 70 kg subject. After Bothwell *et al.* (1979).

during the deposition of each core, which would be the case if the source of the iron was Fe(II).

1.6.3 Proposed minor roles for ferritin

Ferritin has been implicated in the detoxification of metal ions other than iron. Price & Joshi (1982) proposed that ferritin may act in the first line of defence against zinc toxicity, binding excess Zn^{2+} at concentrations below that required to stimulate the synthesis of metallothionein. They also suggested that ferritin may function in handling transient fluctuations in Zn^{2+}, and possibly Cu^{2+}, concentrations and act as a donor of these ions to the apoenzymes requiring them. Holo- and apoferritin have also been shown to bind Be(II) and Cd(II) in *in vivo* studies with rats, (Joshi *et al.*, 1985).

Aluminium toxicity is a much publicised topic at present and similarities between the chemistries of Fe^{3+} and Al^{3+} might suggest that ferritin would have a role in Al biochemistry. Holoferritin has been shown to bind 20-30 Al ions per molecule *in vitro* and 120 per molecule if the aluminium is present during *in vitro* reconstitution. However, in Alzheimer's and renal dialysis patients, where brain aluminium levels are elevated, no preferential binding of aluminium to brain ferritin was observed (Dedman *et al.*, 1990).

1.7 Ferritin

Ferritins comprise a roughly spherical protein shell, encapsulating an iron oxide core. The bacterioferritins also have haem centres associated with the protein shell (Stiefel & Watt, 1979, Yariv *et al.*, 1981 and Moore *et al.*, 1986). The mammalian protein, isolated typically from spleen or liver, can contain up to 30% iron

by weight, that is about 4500 iron atoms. In such native ferritin samples iron loading varies greatly but it often averages around 2000 iron atoms per molecule. Of all the ferritins, horse spleen ferritin is the best characterised and its three-dimensional structure has been determined and refined at 0.26 nm resolution (Ford *et al.*, 1984 and Harrison *et al.*, 1987). All other ferritins and bacterioferritins isolated so far are believed to have similar quaternary structures to that of horse spleen ferritin. Current knowledge of ferritin is described in four sections below: the protein, the iron core, reconstitution and iron release.

1.7.1. The protein

Apoferritin is made up of 24 subunits arranged, as shown by X-ray diffraction, in approximately cubic 432 symmetry (Harrison *et al.*, 1974). There are two main classes of subunit: H and L, with a minor M class present in tadpoles (Harrison *et al.*, 1989). The L subunit of horse spleen ferritin contains 174 amino acids (Heuterspreute & Crichton, 1981), while the H and L subunits of human liver ferritin contain 182 and 174, respectively (Boyd *et al.*, 1985). The molecular weights of the human H and L subunits are 21,000 Da and 19,000 Da, respectively (Arosio *et al.*, 1978). The subunits contain a high proportion of hydrophobic amino-acids and adopt a tertiary conformation composed of five α-helices (A, B, C, D & E) and an extended loop (L) (figure 1.8, lower right). The subunits readily form dimers and the quaternary structure of apoferritin is attained by further self-assembly of the dimers in the absence of any iron (Ford *et al.*, 1984). Most tissue ferritins are heteropolymers of both H and L subunits. The overall diameter of horse spleen ferritin (15% H, 85% L) is 13 nm, with the diameter of the cavity being

approximately 7.4 nm and a shell thickness of about 2.8 nm, (Harrison *et al.*, 1987). The molecular weight of the horse spleen protein is approximately 480,000 Da (Harrison *et al.*, 1989).

Fourteen well-defined channels exist between the dimers; eight channels with 3-fold symmetry are lined by hydrophilic amino acids and six channels with 4-fold symmetry are lined by hydrophobic amino acids, see figure 1.8, upper right and lower left. These channels allow access to the inner cavity. The 3-fold channels, lined by residues towards the C-terminus of the C helix and the N-terminus of the D helix, are funnel shaped, narrowing to around 0.34 nm for about 0.6 nm leading into the cavity (Harrison *et al.*, 1989). The 4-fold channels, lined by the short E helices, are "hour-glass" shaped, about 1.2 nm long and narrow to 0.3 - 0.4 nm across (Harrison *et al.*, 1980, 1987, 1989). The width of the channels may vary with dynamic fluctuations of the protein since molecules with diameters of about 1 nm have been reported to pass into the cavity (Harrison *et al.*, 1980).

Lawson *et al.* (1989) have located the "ferroxidase centre" of ferritin which is present only on the H subunits. Using recombinant DNA techniques and site-directed mutagenesis, they have shown that substitution of Glu 62 and His 65 for Lys and Gly respectively (as in the L subunit), abolishes the H subunit's superior catalytic activity. With their detailed knowledge of the 3-dimensional structure of ferritin they have proposed how the side chains of the amino acids are arranged and how the Fe(II) is coordinated (figure 1.9). Thus, the ferroxidase centre lies at a site with 2-fold symmetry within the 4-helix bundle of the subunit, about 7-10 Å from

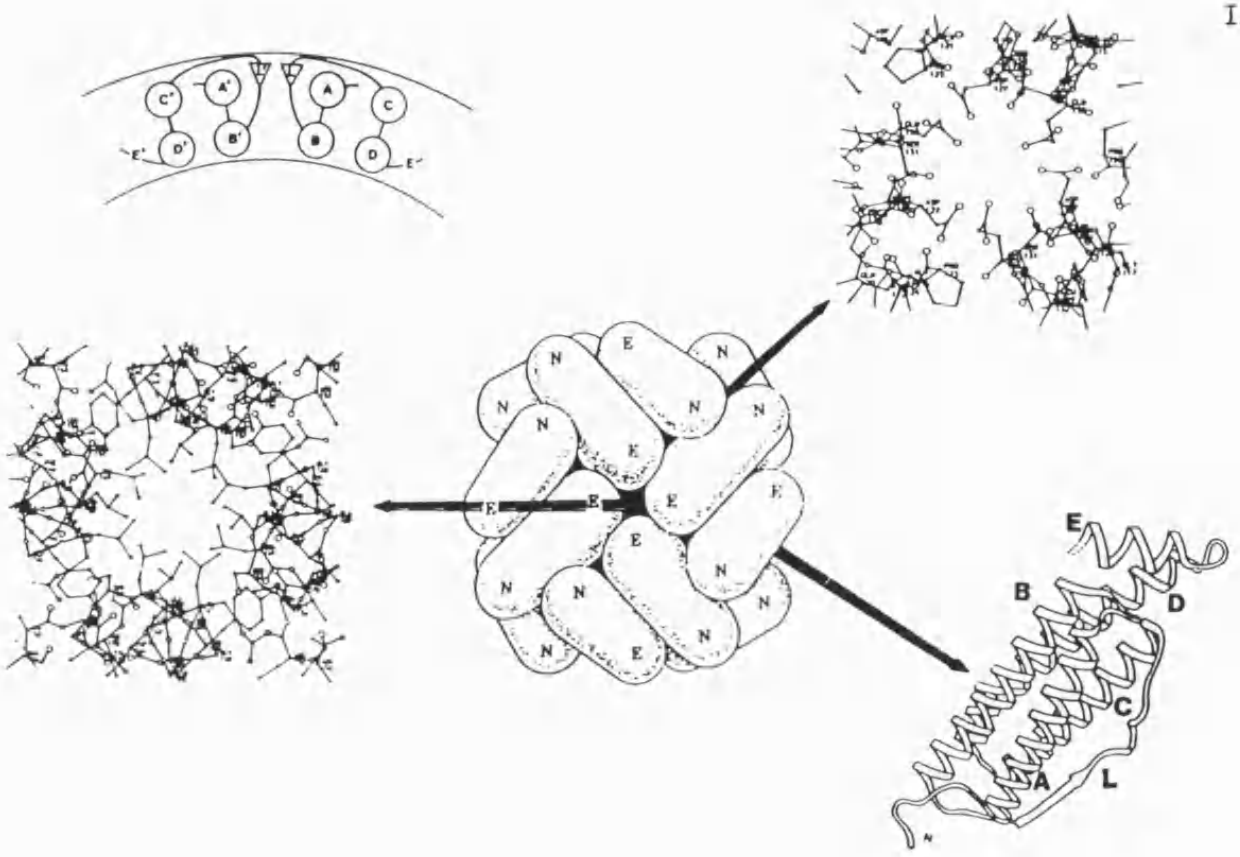

Figure 1.8 Structural features of the apoferritin molecule. The central figure is the symmetrical quaternary structure composed of twenty-four equivalent subunits. Details shown are: lower right, ribbon diagram of a subunit; upper right, region near 3-fold axis, the channel is lined with aspartic acid and glutamic acid residues; lower left, region near 4-fold axis, the channel is lined with leucine residues; upper left, end-on view of interface between 2-fold axis related subunit pairs. Reproduced from Harrison *et al.* (1987), with permission.

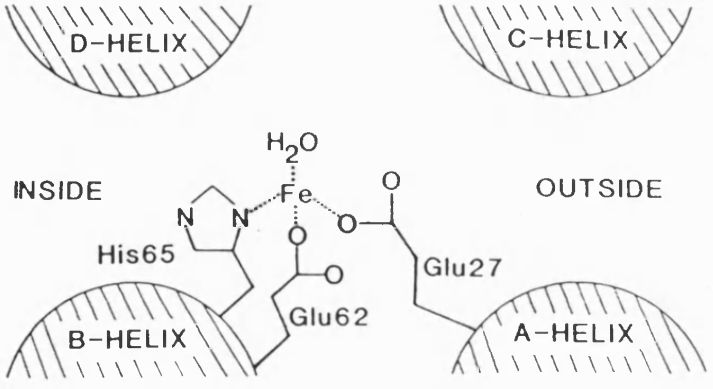

Figure 1.9 Schematic drawing of the ferroxidase centre in recombinant H-subunit ferritin. Reproduced from Lawson *et al.* (1989), with permission.

the internal surface. Narrow channels through the protein may allow access from the outside and the cavity.

Helices B and D form the lining of the cavity and between the symmetry related BB' helices in the dimers there is a "groove" or "pocket", because these two helices are held apart by the interaction of the two loops (LL') which form a β-pleated sheet between the two A helices (AA'), see figure 1.8, upper left. These "pockets" have long been thought to be the most probable sites for core nucleation and initial growth (eg. Ford *et al.*, 1984, Theil & Aisen, 1987, Yang *et al.*, 1987).

Dr. Arosio has proposed a location for the "nucleation centre" (pers. comm.) common to both H and L subunits involving three glutamic acid residues at positions 61, 64 and 67 (H subunit numbering), see figure 1.10. If the positions of tne side chains in the diagram are correct, then presumably Glu 61 is involved in moving the oxidised iron from the ferroxidase centre of H subunit to the "nucleation site" at Glu's 64 and 67. Two positions for Glu 61, one directed towards the ferroxidase centre and one towards the cavity have been demonstrated in the X-ray diffraction studies of a Tb^{3+} derivative of human recombinant H subunit ferritin (Lawson *et al.*, 1991). In the former position Tb^{3+} is coordinated by Glu 61, Glu 62 and Glu 107 (from helix C). In the second position Glu 61 and Glu 64 coordinate a Tb^{3+} ion. Such a Tb^{3+} site is also found in horse spleen apoferritin, which is 85% L subunit (Harrison *et al.*, 1989). As well as indicating the importance of Glu 61 in ferroxidase activity, these findings may suggest that Glu 64 is a key residue in nucleation and that the nucleation site is located in the "pocket".

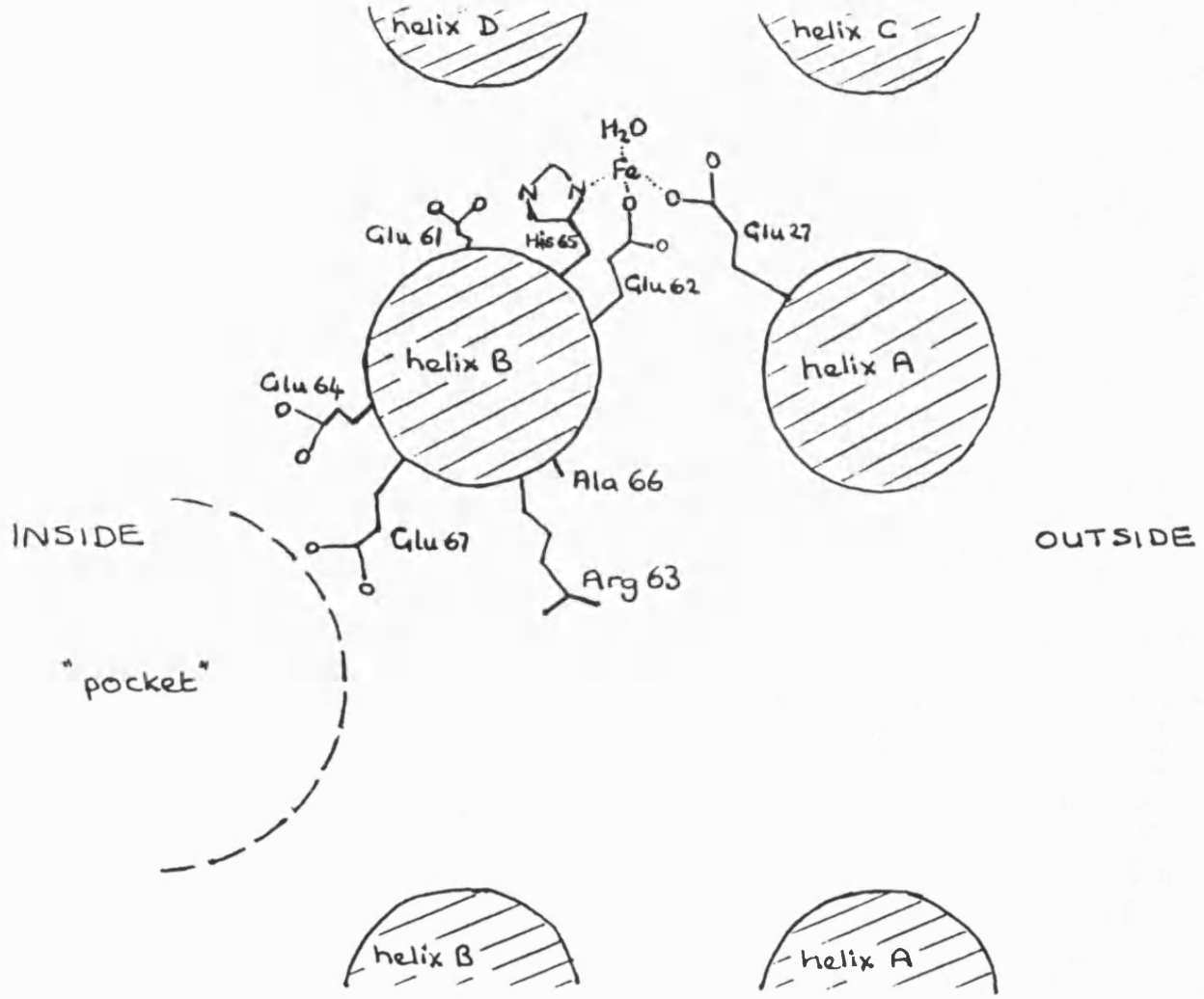

Figure 1.10 Schematic drawing of the proposed nucleation centre, shown in relation to the ferroxidase centre of H-subunits. This drawing is based on that of the ferroxidase centre in Lawson *et al.* (1989) with additional amino acid side chains drawn assuming 3.61 amino acids per turn of α-helix and after careful study of published drawings of the positions of the amino acid side chains at the dimer interface (Rice *et al.*, 1983).

The location of the ferroxidase centre on the H subunits has clarified the apparent functional differences between H- and L-rich heteropolymers. The H-rich heteropolymers, found typically in heart and brain tissue, take up and release iron more rapidly, while the L-rich heteropolymers, from liver and spleen, accumulate more iron. The enhanced ferroxidase activity of the H-rich heteropolymers would facilitate rapid iron uptake and this, in turn, seems to enable rapid release (see chapter 4). Whereas, the accumulation of iron in L-rich heteropolymers, which are subject to slower metabolic turnover, is of importance under conditions of iron loading (Bomford *et al.*, 1981).

1.7.2 The iron core

Iron is stored in mammalian ferritin cores as the mineral ferrihydrite, which was discussed in section 1.3.1. There is usually some phosphate associated with the native cores, either at the core surface or in discontinuities in the core, but this is not a requisite for core development, at least not *in vitro* (Treffry & Harrison, 1978). Molluscan and bacterial ferritins contain higher amounts of phosphate and the composition of the core may be more accurately described as $(FeOOH)_8(FeO.OPO_3H_2)$. The ferrihydrite (or "ferric oxy-phosphate") can be crystalline or amorphous depending on the source of the sample, and this is often correlated to the amount of phosphate in the cores (Treffry *et al.*, 1987). A gradation of ferrihydrite structures may exist, ranging from the well-ordered in which the iron atoms are regularly distributed within the anion sublattice, to disordered materials possessing extensive lattice defects and structural discontinuities. Also, the nature of the sublattice may alter in terms of the relative number and distribution of O^{2-}, OH^- and OH_2 groups and the incorporation of PO_4^{3-} (St. Pierre

et al., 1989). The ratio of iron to phosphate in native ferritins varies from 1:21 or "phosphate not significant" in mammalian samples, to 1:1.5 or 1:1.7 in the bacterioferritins of *Azotobacter vinelandii* and *Pseudomonas aeruginosa*, and in most cases the higher the amount of phosphate the less crystalline the iron cores (Treffry *et al.*, 1987, Mann, 1989).

There is evidence that the Fe(III) in horse spleen ferritin is located in octahedral sites, as suggested by the model of ferrihydrite proposed by Towe & Bradley (1967). Extended X-ray absorption fine structure (EXAFS) measurements (Heald *et al.*, 1979) suggest a distorted octahedral arrangement of oxygens, each iron atom being surrounded by 6 ±0.6 oxygens at a distance of 0.195 ±0.002 nm. Also, each iron atom has 7 ±1 iron neighbours at an average distance of 0.329 ±0.005 nm. This data, together with stoichiometry and density measurements, was used to propose a layered structure with the iron in the interstices between two nearly close packed oxygen layers. It was suggested that the O-Fe-O layers were weakly bound together and that phosphorus was located at the edges of the layers. Data from Mössbauer and electronic absorption spectroscopies (Webb & Gray, 1974) also suggest that the iron is octahedral Fe(III).

X-ray diffraction studies on horse spleen ferritin (Fischbach *et al.*, 1969) and a reconstituted bacterioferritin (Smith *et al.*, 1991) indicate that there is no preferred orientation of the iron cores with respect to the protein shell. These observations rule out the possibility of the protein providing a structural template for the growth of the mineral core.

The iron cores of ferritin can easily be viewed in the transmission electron microscope without the use of staining (plate 1.1a), if a negative stain is applied the core and the surrounding protein

shell can be seen, (plate 1.1b). Transmission electron microscopy (TEM) and electron diffraction, conducted in the transmission electron microscope, require only a very small amount of sample and enable the study of a population of cores. From the electron micrographs the size distribution of the cores and their morphology in 2 dimensions, can be determined. The powder electron diffraction patterns give information on the crystallinity of the sample. Plate 1.1c shows a powder electron diffraction pattern of well crystalline horse spleen ferritin cores and table 1.5 lists the d-spacings measured from it and the standard lines of ferrihydrite from the X-ray diffraction file. In high resolution TEM single cores can be studied and their size, morphology and crystallinity determined. (See Appendix I.)

An early study of horse spleen ferritin by TEM was conducted by Farrant in 1954. He noted that the cores appeared as discrete, angular, electron dense micelles, up to 55Å in diameter. At this time the question as to whether the iron associated with ferritin was located on or inside the protein had not been resolved. Farrant used uranium shadowing of the ferritin to reveal the apoferritin shell around the micelles and proposed that this was further evidence to support the idea that the iron was located inside the protein. In 1965 Haggis published a TEM and electron diffraction study of horse spleen ferritin. He described a wide variety of core shapes, both regular and irregular and noted that some cores appeared to be of uniform electron density, while others had two or more electron dense regions separated by narrow, less dense areas. Powder electron diffraction patterns were readily obtained, exhibiting broadened diffraction lines, (compared with X-ray diffraction file data). Haggis concluded that the ferritin cores contained a crystalline

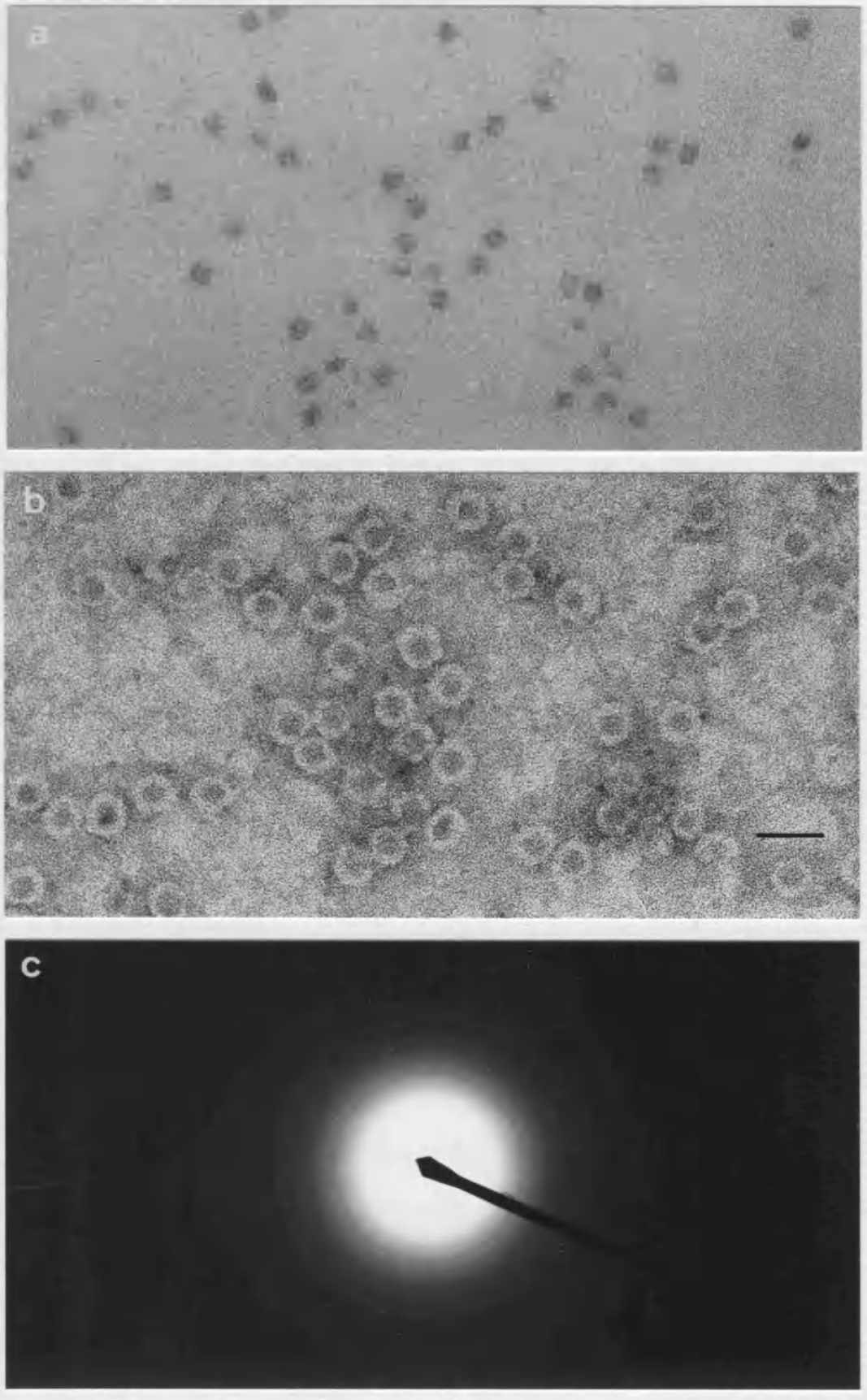

Plate 1.1 Electron micrographs and diffraction pattern of native horse spleen ferritin. *a* unstained, *b* negatively stained with 1% uranyl acetate solution (courtesy of Miss F. Meldrum), bar marker 20nm for both *a* & *b*, *c* powder diffraction pattern, camera length 126cm.

Table 1.5 Electron diffraction data from horse spleen ferritin shown with the ferrihydrite standard.

horse spleen ferritin		ferrihydrite standard		
d(Å)	I	d(Å)	I	hkl
2.49	S	2.50	100	110
2.23	S	2.21	80	200
1.99	M	1.96	80	113
1.72	W	1.72	50	114
1.52	W	1.51	70	115
1.46	S	1.48	80	106

I = intensity of line, for the ferritin sample this was judged by eye:- S = strong, M = medium, W = weak.
Ferrihydrite standard from the Powder X-ray Diffraction Data File compiled by JCPDS-International Centre for Diffraction Data, file number 29-712.

material and that some molecules contained one crystallite per cavity.

A high resolution, dark field TEM study of horse spleen ferritin was published by Massover & Cowley in 1973. These workers reported that the iron cores comprised either a single crystal or several smaller crystallites. Lattice imaging showed that some cores had both ordered and disordered regions, some fringes were not strictly parallel or straight and some cores had other lattice imperfections resembling stacking faults. They noted that some cores that showed no crystallinity may have been in the wrong orientation, with respect to the electron beam, to diffract and that some small crystallites were

quite elongated.

In recent years, ferritins from more diverse sources have been studied, in their native and reconstituted forms, by TEM. Also haemosiderin has come to be studied in this way. Human spleen ferritin and haemosiderin (thalassemic), limpet ferritin and *Pseudomonas aeruginosa* bacterioferritin were studied by Mann *et al.* (1986a). At low magnifications the ferritin cores from all samples appeared as discrete, approximately spherical, electron dense particles. The haemosiderin cores had a more irregular morphology and were more aggregated on the electron microscopy grid. The human spleen ferritin had a modal particle diameter of 70 - 75Å, while that of the haemosiderin was smaller at 60 - 65Å. By electron diffraction both samples were of similar crystallinity, exhibiting 4 or 5 lines on the patterns, which corresponded to ferrihydrite. By high resolution TEM the cores of the ferritin and the haemosiderin were predominantly single domain crystals. In the ferritin sample the lattice fringes were often discontinuous in the centre of the cores, some two dimensional fringes and some elongated particles were observed. In the haemosiderin no multidomain particles were observed. The particle size distribution for the limpet ferritin, with a modal value of 70 - 75Å, suggested that this ferritin may have a larger cavity size than the human and bacterial proteins. Electron diffraction patterns revealed no distinct diffraction lines, but a faint line correlating to hexagonal close packing of the oxygens in a ferrihydrite-like structure, was occasionally resolved. Although very few cores showed coherent lattice fringes, there were some crystalline domains of ~ 30 - 50Å dimensions, but no evidence of long range crystallographic order. The bacterioferritin modal core size was 60 - 65Å, despite a much lower iron content compared with the

human ferritin (8.7% compared with 29% w/w Fe). Again there was no evidence for long range crystallographic order; electron diffraction patterns revealed no diffraction lines and high resolution TEM revealed very few lattice images of cores. Where lattice images were obtained they were of two types: i) convoluted fringes running across particles, indicative of a lamella-type structure, ii) incoherent images showing very short range order, ~ 10 - 20Å. These authors pointed out, as Massover & Cowley (1973) had, that some areas of apparent disorder in the cores may have been due to mis-alignment of the particle with respect to the electron beam.

A TEM study of the native and reconstituted cores of horse spleen ferritin, *Azotobacter vinelandii* and *Ps. aeruginosa* (Mann *et al.*, 1987b) further illustrates the usefulness of this technique in ferritin research. The iron cores of the native horse spleen ferritin were discrete, generally spherical and they had a modal diameter of 5 - 6nm. Microscopy of a fractionated preparation of the protein containing 3000 Fe/molecule (by sucrose density gradient centrifugation) showed a greatly enhanced homogeneity of the particle size distribution. Reconstitution appeared to have introduced more angular core morphologies and more aggregation of the cores on the electron microscopy grids. Also, the reconstituted cores were less well crystalline than the native ones, as shown by fewer lines on the diffraction patterns and fewer cores giving well defined lattice images. The native *Az. vinelandii* sample (approx. 2000 Fe/mol) had discrete, spherical cores with a modal diameter of 5 - 6nm, which were amorphous by electron diffraction. Reconstitution (to 2700 Fe/molecule) resulted in more angular and crystalline (ferrihydrite) cores, which had a smaller modal size (4 - 5nm). A few of these cores gave lattice images with regular, continuous fringes indicative of

single crystal domains in the particles. Reconstitution of the *Ps. aeruginosa* protein (to 2700 Fe/molecule) again resulted in more angular and crystalline cores, which were smaller in size than the native cores despite their higher iron loading. These TEM observations of native and reconstituted bacterioferritins, together with Mössbauer spectroscopy data (St. Pierre *et al.*, 1986), indicate that the core structures of the native samples, especially those of *Ps. aeruginosa*, must be less dense and more hydrated than those of mammalian ferritins; this is probably related to the amount of phosphate in the cores, as discussed above.

Mössbauer spectroscopy has been used to study the iron cores of many ferritins, bacterioferritins and haemosiderins (see chapter 5 for discussion of the latter and Appendix II for relevant theoretical details of this technique). Studies of mammalian ferritin samples from thalassemic human spleen (Bell *et al.*, 1984), native (St. Pierre *et al.*, 1989) and reconstituted (Mann *et al.*, 1987) horse spleen and iron-loaded rat liver (Williams *et al.*, 1986) have revealed a pattern in their Mössbauer spectra with all samples having similar hyperfine interaction parameters, all exhibiting superparamagnetic behaviour and having mean blocking temperatures between 35 and 40 K. The molluscan ferritins exhibit similar hyperfine parameters at 4.2 and 78 K to the mammalian ferritins, but their superparamagnetic behaviour is different; the mean blocking temperatures are lower, being between 25 and 30 K, and the spectra are characteristic of a solid passing from a magnetically ordered to a paramagnetic phase as the temperature is raised (St. Pierre *et al.*, 1986a&b, 1989). Mössbauer spectroscopy of plant ferritins has been limited, but some studies show that these too have lower blocking temperatures than the

mammalian ferritins (Goodman & DeKock, 1982, Prof. P.M. Harrison, pers. comm.).

The Mössbauer spectra from the bacterioferritins of *Escherichia coli* (Bauminger *et al.*, 1980) and *Pseudomonas aeruginosa* (St. Pierre *et al.*, 1986a) are very similar to each other but, unlike those described above, they do not exhibit superparamagnetic behaviour. At 1.3 K the spectrum is a sextet, but by 4.2 K this has collapsed into a broadened doublet and the spectra indicate magnetic ordering temperatures of about 3 K. This is much lower than the magnetic ordering temperatures for all other ferritins which are above 20 K (St. Pierre *et al.*, 1989). The Mössbauer spectra of the *Azotobacter vinelandii* bacterioferritin (Watt *et al.*, 1986) are different from those of the other bacterioferritins described; they show superparamagnetic behaviour with a mean blocking temperature of about 20 K.

St. Pierre *et al.*, (1989) show that the Mössbauer data of all the ferritins and the bacterioferritins of *E. coli* and *Ps. aeruginosa* correlate well with the other structural data on the iron cores (TEM, high resolution TEM and phosphate content) discussed above. In the case of the *A. vinelandii* bacterioferritin they propose that the seemingly anomalous Mössbauer data may be explained if the iron environment in the cores was more akin to that of ferrihydrite (as in mammalian ferritin) than a hydrated Fe(III) phosphate (as in the other bacterioferritins). They suggest that this might arise, despite the high phosphate content of the cores, if the cores had an open and irregular structure with the phosphate bound only at surface sites.

1.7.3 Reconstitution

The removal of the iron core of native horse spleen ferritin can be readily achieved by the reduction and chelation of the iron by agents such as thioglycollic acid. The fully assembled apoferritin shells can be recovered intact and the iron re-introduced to form a core in reconstitution experiments. Reconstitution is achieved most successfully when Fe^{2+} is supplied to the protein with an oxidant at a pH of 6.5 - 7.0. Both molecular oxygen (eg. Levi *et al.*, 1988 & Treffry *et al.*, 1989) and $KIO_3/Na_2S_2O_3$ (eg. Macara *et al.*, 1972 & 1973a) can be used as oxidants; however, while O_2 is more effective for the early stages of core formation, both oxidants are equally effective when a core has started to form (Treffry *et al.*, 1979). Ferritin will only take up Fe^{3+} once a small core, formed from Fe^{2+}, has been established (Treffry & Harrison, 1979).

Many studies of the reconstitution process in horse spleen apoferritin have been undertaken, utilising a variety of techniques. Ion binding has been studied by Electron Paramagnetic Resonance (EPR) and X-ray absorption techniques, investigating the binding of both Fe(II) and Fe(III) and using other metal ions such as Mn(II), Cd(II) and VO(IV) as probes. The early stages of core formation have been studied by Mössbauer spectroscopy which can distinguish several types of Fe(II) and Fe(III). The kinetics of core formation have been studied by uv/visible spectrophotometry, where the red/brown appearance of the developing core can be monitored.

An EPR study, utilising VO^{2+} as a probe, by Chasteen & Theil (1982) revealed that apoferritin binds Fe^{2+}, and that Fe^{3+} remains bound to the protein following *in situ* oxidation by O_2. Also the protein binding sites are saturated with iron at a ratio of 0.5 per subunit, which is 12 per molecule, and the migration of some iron

from its initial binding sites after oxidation was implied, since some of those initial sites became vacant. Furthermore, binding of iron by carboxylate groups, contributed by the protein, was also suggested. These results were confirmed by Sayers *et al.* (1983) using X-ray absorption spectroscopy.

These studies were extended by Yang *et al.* (1987) using new EXAFS (extended X-ray absorption fine structure) techniques and Mössbauer spectroscopy. They showed that Fe(III), at a ratio of 9.6/molecule, was located in an environment different from that in ferritin cores. The Fe(III) was clustered and each Fe(III) atom had both carboxylate-like ligands, presumably from apoferritin, and oxo-bridges to the other iron atoms. Their studies also indicated the migration of Fe atoms during oxidation and that nucleation of core crystallites occurred on the protein; the authors suggested that this might occur at the dimer interface.

Other EPR studies, using Mn(II), VO(IV) and Cd(II) as probe ions (Wardeska *et al.*, 1986), have also shown that oxidation of bound Fe(II) causes the regeneration of some initial binding sites, suggesting migration of iron from these sites. These studies indicated metal ion binding at ratios of 1 and 2 metal ions per 3 subunits, which may imply 1 or 2 sites within each hydrophilic channel. The authors suggested that Fe(II) may bind and be oxidised at the outermost of the two sites in the 3-fold channel, the Fe(III) then being bound to the inner site. The Fe(III) would then be displaced from this site by "incoming" Fe(II)/(III) and migrate to the protein interior to join the forming core.

A Mössbauer spectroscopy study of the early stages of core formation (Bauminger *et al.*, 1989) identified four different Fe(III) species in samples reconstituted with 4 - 480 Fe/molecule. These were

solitary Fe(III), oxo-bridged dimers, small Fe(III) clusters and larger antiferromagnetically coupled Fe(III) clusters. The solitary Fe(III) and dimeric species diminished with time, which suggested that they were intermediates of core formation. Divalent iron was observed in samples reconstituted at pH ≤ 6.25 (4 Fe/molecule, frozen after 3 or 17 minutes) and pH 6.4 (480 Fe/molecule, frozen after 3 minutes or 2 hours). In the samples reconstituted to 480 Fe/molecule two kinds of Fe(II) could be distinguished. It was proposed that these corresponded to Fe(II) bound to either the protein or core surface and Fe(II) free in solution, either inside or outside the protein cavity.

There is some evidence from X-ray absorption near edge structure (XANES) studies (Rohrer *et al.*, 1987, 1989) that the Fe^{2+} added to apoferritin (480 Fe atoms/molecule, pH 7) is not all rapidly oxidised, but is taken up by the protein and stabilised as Fe^{2+} for several hours. No Fe^{3+} was observed after 2 hours by XANES and at 16 hours 10% remained as Fe^{2+} (Rohrer *et al.*, 1987). It is not clear how such observations fit in with the more widely accepted view that the oxidation of Fe(II) by ferritin is a rapid process. For example, it is interesting to note that in the Mössbauer studies of Bauminger *et al.* (1989), mentioned above, for the same iron loading, but at pH 6.4, only 42% of the iron was present as Fe(II) after 2 hours.

A number of kinetic studies of iron uptake by apoferritin have been conducted by Macara *et al.* (1972, 1973a, b, c). They used horse spleen apoferritin, ferrous ammonium sulphate as the source of Fe^{2+}, $KIO_3/Na_2S_2O_3$ as oxidant and uv/vis. spectrophotometry at 420 nm or 310 nm (for lower iron concentrations) to follow the formation of the core. Their paper published in 1972 reported sigmoidal uptake curves for iron added in one aliquot to give loadings of 170, 440, 540 and

590 Fe atoms/molecule. Where iron was added in two or more increments of 58 or 170 Fe/molecule, the uptake curves were hyperbolic for the second and subsequent increments. Also the rate of reaction was shown to be pH dependent, increasing with pH over the range 6.2 - 7.4, which was expected since protons are released during core formation. From this work it was proposed that ferritin core formation involved two stages: i) nucleation and ii) crystal growth, and that the protein catalysed the first (nucleation) stage.

These results were confirmed by Macara *et al.* (1973a) where the transition of the uptake curves from hyperbolic to sigmoidal in shape was found to occur between loadings (by one increment) of about 90 - 150 Fe/molecule. The results also upheld the two stage model proposed before.

Other kinetic studies by this group included observations of the effect of Zn^{2+} ions on ferritin iron uptake (Macara *et al.*, 1973b,c). Zinc is known to inhibit ferritin iron uptake *in vivo* (Coleman & Matrone, 1969). Macara *et al.* showed that Zn^{2+} acted as a competitive inhibitor of iron uptake *in vitro* and that it inhibited both the nucleation and growth phases of the process. That it acted as a competitive inhibitor implied that binding of Fe^{2+} to the protein was essential.

A preliminary kinetic study of iron uptake by *Azotobacter vinelandii* bacterioferritin has been reported (Mann *et al.*, 1987b). Under the conditions used, the bacterioferritin exhibited initial uptake rates some 30% faster than those of horse spleen ferritin. The uptake curves were sigmoidal when more than 500 Fe atoms/molecule were added and the presence of Zn^{2+} ions (~24/mol added before the Fe^{2+}) reduced the initial rate of Fe(III) complex formation with the protein by 78%.

1.7.4 Iron release

The mediators of ferritin iron release which have been studied *in vitro* (although some may act *in vivo* also,) are of three types (reviewed in Harrison *et al.*, 1980):

i) reductants eg. dithionite, thioglycollate, $FMNH_2$ and $FADH_2$,

ii) chelators with a high affinity for Fe(III), eg. transferrin, desferrioxamine and citrate,

iii) chelators with a high affinity for Fe(II) eg. 1,10-phenanthroline and 2,2'-bipyridyl. With these, a fast photoreduction step probably follows removal of Fe(III) from ferritin.

These reductants and chelators have a range of sizes; dithionite is about 5Å in diameter, $FMNH_2$, $FADH_2$ and desferrioxamine are all approximately 13Å across and transferrin is about 50Å in diameter (Harrison *et al.*, 1980, Harris, 1978). It is probable that all the reagents listed above, apart from transferrin, can enter the ferritin molecule. The initial rate of iron release for a number of different mediators has been shown to be maximised for ferritin molecules that are one third to one half full. This pattern indicates direct interaction of the mediator with the iron core surface, except for transferrin where mediation by small molecules occurs, eg. buffer salts (Harrison *et al.*, 1980). Mediation of the reaction with transferrin by citrate has been demonstrated, the rate of reaction was faster in the presence of citrate than in buffer (Tris-HCl) alone (Harris, 1978). In a study of the reductive mobilisation of horse spleen ferritin iron by a number of reducing agents including dithionite, thioglycollate and $FMNH_2$, Funk *et al.* (1985) concluded that the kinetics of mobilisation were linked to the nature and stability of the complexes formed at the surface of the iron core.

Mobilisation of iron by a series of thiols of different size and coordinative properties confirmed the importance of surface complex formation.

Watt *et al.* (1988) however, argue that direct interaction of redox mediators with the core is not necessary. They have demonstrated redox reactions with Fe^{2+} and Fe^{3+} in the protein cavities of horse spleen ferritin and *Azotobacter vinelandii* bacterioferritin with oxidants and reductants too large to penetrate the protein shell. For example, the flavoprotein and ferredoxin I of *A. vinelandii* both reduced the iron cores of the mammalian and bacterio- ferritins. These authors did not discuss the possibility of mediation by buffer salts suggested by Harrison *et al.* (1980), but proposed that electron transfer between the core and the reductant may occur by electron tunnelling through the protein shell.

1.8 A brief outline of the subsequent chapters

Chapter 2 contains details of materials and experimental procedures pertaining to the whole thesis; methods of direct relevance to individual chapters are given within those chapters. Chapter 3 describes reconstitution experiments with horse spleen apoferritin; this is the best characterised and most readily available ferritin. The first reconstitutions were carried out with Fe(II) alone. Then they were performed with Fe(II) in the presence of Zn^{2+} ions, added together with, or before, the iron. The approach adopted is represented schematically in figure 1.11. Comparisons are made in the work between the kinetics and products of these reactions with those performed in the absence of apoferritin. The next chapter, chapter 4, further explores the influence of the protein shell on the

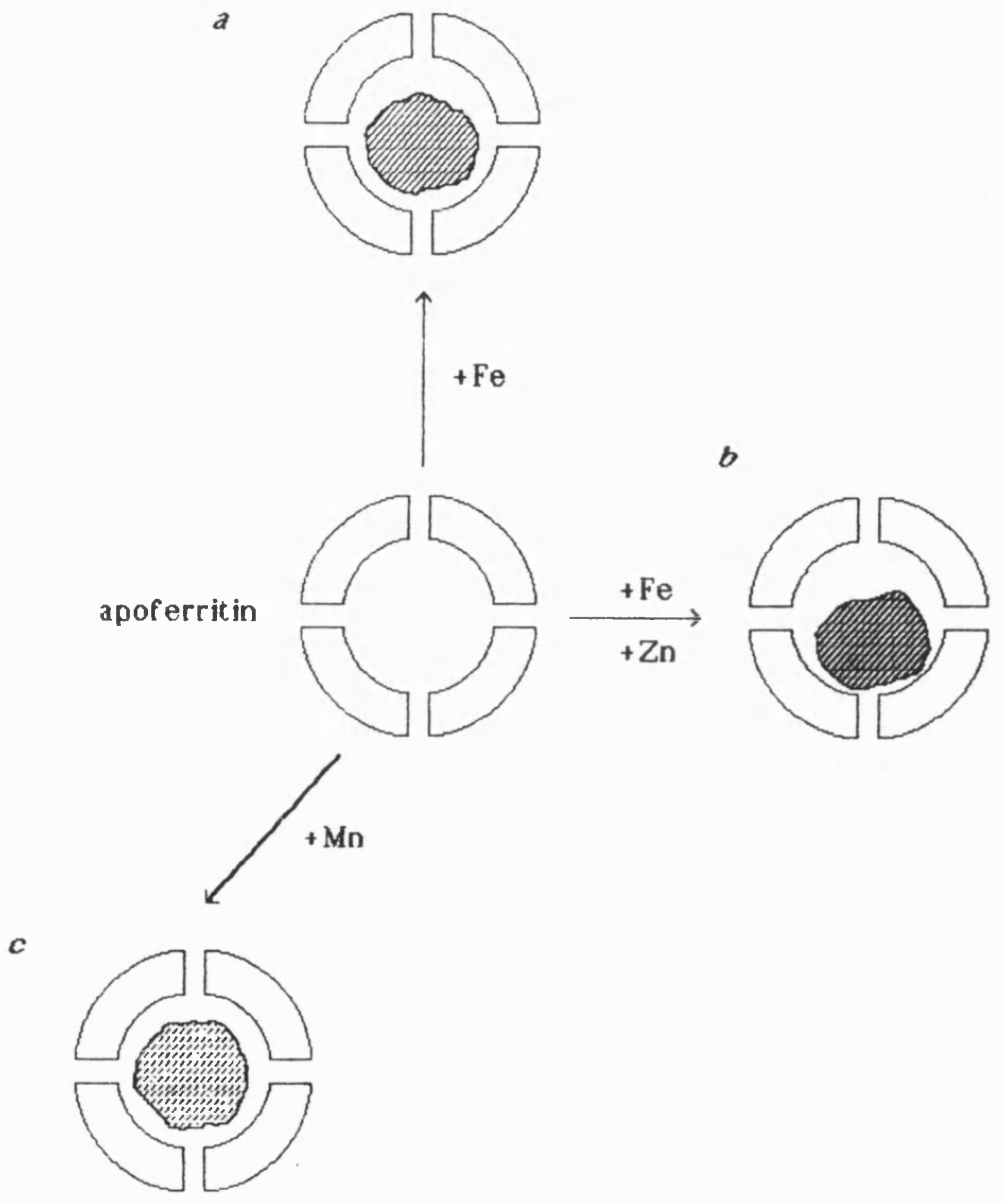

Figure 1.11 Schematic representation of the types of experiments performed with horse spleen apoferritin. *a* reconstitution with iron at high and low loadings, *b* reconstitution with iron and zinc, *c* reconstitution with manganese. For all types of experiment the kinetics of the reconstitution and the structure of the cores formed were studied.

nature of the iron core formed during reconstitution, by changing the protein shell. This was done by examining the iron cores formed within homopolymers and heteropolymers of human H and L subunits and homopolymers of variants of the human H subunit, see figure 1.12. Chapter 5 stays with the theme of the structure of iron cores but includes, along with ferritin, those of haemosiderin. The chapter looks in detail at the iron cores of both forms of storage complex deposited *in vivo*, in horse and reindeer and in human patients in iron balance and two conditions of iron overload: β-thalassemia and idiopathic haemochromatosis.

The work presented in chapter 6 looks at a broader aspect of the nature of the reaction between ferritin and metal ions by focussing not on iron reconstitution, but on manganese - one step to the left in the Periodic Table. This work has begun to open up the possibility of using the ferritin protein cage as a small reaction volume, in which to perform reactions other than just the formation of ferrihydrite, see figure 1.11c. Chapter 7 returns to the iron theme and the function for which ferritin was designed, and describes the characterisation by TEM of some newly isolated ferritins of mammalian, plant and bacterial origin. The final chapter, chapter 8, seeks to summarise and draw together the themes of the previous chapters and to suggest directions for future work.

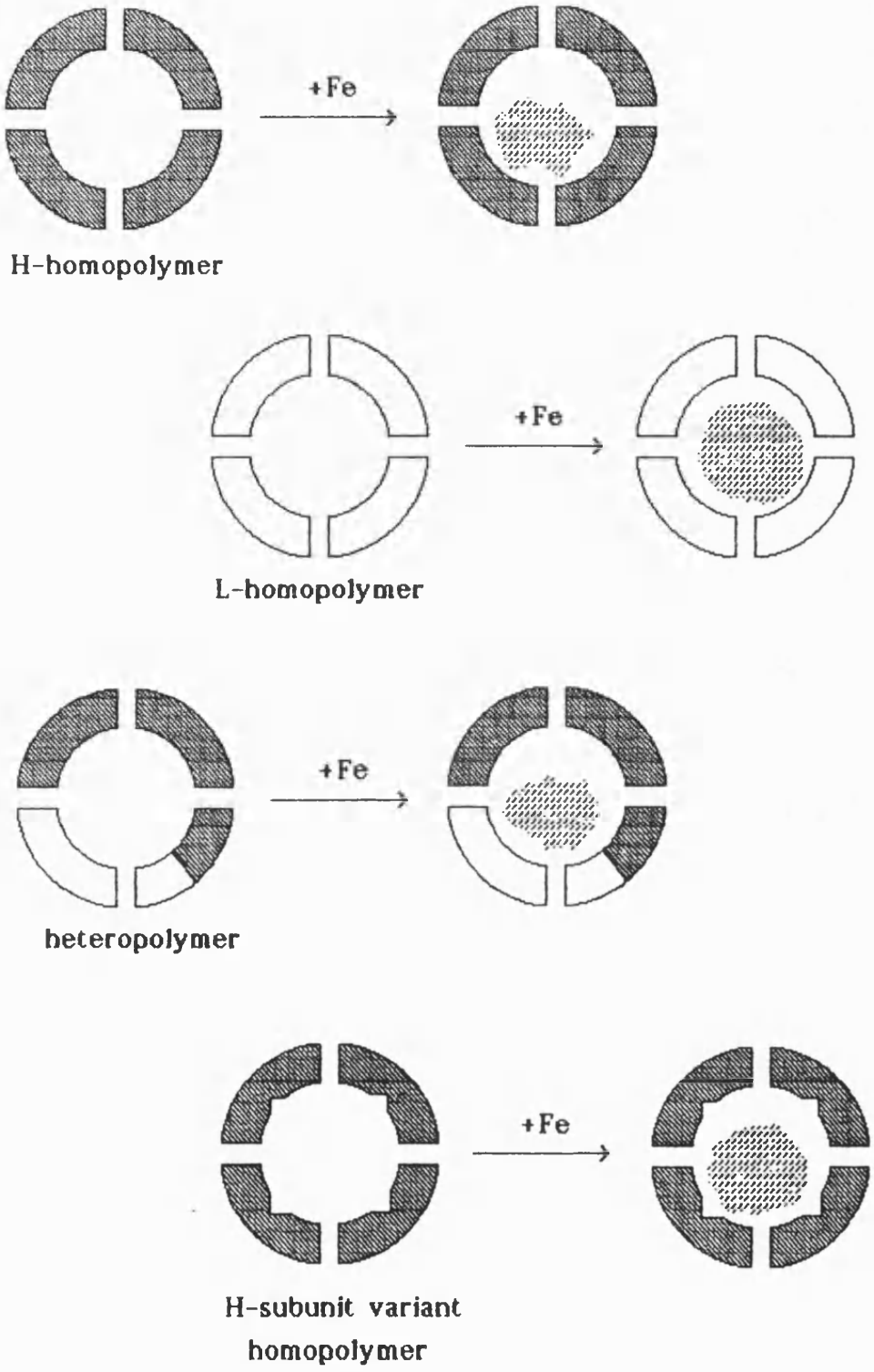

Figure 1.12 Schematic representation of the experiments performed with the H- and L-homopolymers and heteropolymers. In each type of experiment the size, morphology and structure of the cores were studied.

Chapter 2

MATERIALS AND METHODS

2.1 Apoferritin Preparation

Approximately 20 ml horse spleen ferritin (2.8μM, Boehringer Mannheim) was dialysed against two 250ml volumes of 0.1M sodium acetate buffer, pH 4.5 (Analytical grade, Fisons) containing 0.1M thioglycollate (Sigma) over two hours at room temperature, with slow bubbling of N_2. The dialysis tubing containing the protein was washed with a small volume of saline (0.15M, Analytical grade, Fisons) and then dialysed exhaustively against more saline with slow bubbling of N_2 for part of the time. Dissolution of the iron cores was deemed complete when the solution in the dialysis tubing appeared colourless. This criterion was validated by atomic absorption analysis of a number of preparations which demonstrated a residual iron content of less than 4 iron atoms per molecule.

In early preparations 2,2'-bypiridyl (0.06M, Aldrich Chemical Co. Ltd.) was added to the reaction mixture to act as an additional chelating agent but its presence did not seem to enhance the dissolution of the iron cores so its use was discontinued. Also, initially, a colourimetric test was performed on the dialysate to see if all the thioglycollate had been removed (NH_3 + $FeCl_3$ in the presence of thioglycollate gives a dark red/violet colour), but once the regime of dialysis was shown to be effective this too was discontinued.

Total protein estimations were carried out on all preparations. After comparing two methods experimentally; Lowry (using BSA as standard, Lowry *et al.*, 1951) and photometric (A_{280}) estimations, and having considered different "conversion factors" for each, it was decided to use the A_{280} method, converting absorbance units to mg/ml by dividing by 0.96. This method was convenient and did not appear any less accurate than the Lowry method.

2.2 Reconstitution Methods

Horse spleen apoferritin was reconstituted in buffered solution with iron (chapter 3), iron and zinc (chapter 3), or manganese (chapter 6). Details of the methods used are given in the appropriate chapters.

For the kinetics experiments the continual change in absorbance of the test solution with the addition of each volume of ion solution was recorded on a flat-bed chart recorder linked to a Cecil CE 595 double beam UV/visible spectrophotometer. The chart recorder was used on its most sensitive setting where possible and controls were performed to check for drift in the instrumentation.

All procedures were carried out at room temperature, the temperature attained in the spectrophotometer during the long kinetics experiments varied between 22 and 27°C. When all the required ions had been added and oxidation was complete (as judged by the spectrophotometer trace), the preparation was dialysed exhaustively against 0.15M saline at 4°C. Atomic absorption analysis was carried out on all reconstitutions to ascertain final ion loadings and the preparations were stored at 4°C. The clarity of the reconstituted ferritin solutions demonstrated the specificity of the

reaction of apoferritin with Fe^{2+}.

Protein-free controls were also carried out for each type of preparation, method exactly as for reconstitution, substituting 0.15M saline for the protein solution.

Each type of experiment was repeated at least three times.

2.3 Transmission Electron Microscopy (TEM)

The transmission electron microscope used was a JEOL 2000FX operated at 100 or 200KeV. At 200KeV this instrument was capable of a point-to-point resolution of 0.28 nm. A condenser aperture of 120 μm diameter was used routinely. An objective aperture was rarely used, but one of 80 μm was employed occasionally.

As TEM was used extensively in the work presented in this thesis the general principles of the transmission electron microscope, image formation and electron diffraction are outlined in Appendix I.

2.3.1 Sample preparation

Small drops of solutions/suspensions of material to be examined were air dried down onto nitrocellulose and lightly carbon-coated copper electron microscope grids.

2.3.2 Routine alignment of the TEM

Before commencing work on the TEM, on each occasion, the microscope was carefully aligned in order to maximise its performance. Also, to reduce contamination of the specimen and column, which would reduce the microscope's performance, the anti-contamination device was cooled with liquid nitrogen before the alignment procedure and kept cool throughout the period of work. The

amount of unexposed film in the camera was also checked and more loaded if necessary.

Having established that the column vacuum and cooling water supplies were in good order, with the filament current control turned fully down, the HT supply was turned on and set to the required level. With the microscope in Bright Tilt mode and at a magnification of 30K, the filament current was then turned up slowly until a point just below that of filament saturation was reached, a stop on the control was set at this level. The area of illumination was centralised using the gun shift and alignment shift controls for spot sizes 1 and 4. The filament image was then made symmetrical by desaturating the filament further and using the gun tilt controls. With the filament current turned up again, the area of illumination was made symmetrical by using the condenser stigmators and centring the required condenser aperture. When these were properly aligned, the illumination diverged and converged concentrically when the condenser lens current was varied through the cross-over point. The filament current was then turned right down again while the specimen was introduced.

The specimen, loaded into the specimen holder, was inserted into the specimen chamber and this chamber evacuated. When a sufficient vacuum had been attained the specimen was introduced into the column. The filament current was then turned back up to the position set earlier. The grid to be viewed was centred in the beam at low magnification (<10K) by centring the specimen shift controls and selecting the centre of position 1 or 2 with the knurled ring on the specimen selector. The magnification was then increased to 20K and a small but recognisable feature on the grid was selected and positioned in the centre of the screen in order to set the specimen

in the eucentric position. This was done by tilting the goniometer by 10° and repositioning the feature in the centre using the height control on the goniometer. The goniometer was then returned to 0° and the feature repositioned using the specimen shift controls. The feature was refocused when necessary and the procedure repeated until the feature did not move appreciably on tilting the goniometer.

The magnification was then increased to 30K and a suitable feature on the grid centred and focused. Using the objective wobbler and the bright tilt deflectors the current centre was set by minimising the movement of the feature about the centre of the screen. At 100K magnification the voltage centre was set in the same way, using the HT wobbler. Ensuring that the voltage centre was set correctly was particularly important for high resolution work, since this alignment minimises chromatic aberration for axial image points. The final stage of the alignment was to correct any objective astigmatism. This was done at magnifications above 200K by focusing on the carbon substrate on the grid and correcting any asymmetry in the image of the carbon grains at focus positions on either side of absolute (gaussian) focus. Objective astigmatism required correction throughout the period of work and it was particularly important that it was corrected continually during high resolution work and before images were photographed.

2.3.3 Normal imaging

Samples were routinely examined with the microscope operating at 100KeV and at magnifications between 30K and 250K. This accelerating voltage was used in preference to higher voltages, because of the improved contrast in the images that it affords. Images for size measurements were taken at 100K and this magnification was also used

for the electron diffraction patterns.

Measurements of the core diameters were made with callipers from electron micrographs (total magnification ~ 500K - 550K times). The cores chosen for measurement were those that appeared to be roughly isometric (in the xy direction), 50 cores were measured for each histogram. The arithmetical mean diameter and standard deviation (S.D.), were calculated. The histograms drawn from these data are not suitable for rigorous statistical analysis or detailed comparisons; 50 is too small a number and the measurement of the core diameters is difficult and prone to large errors because many cores have irregular shapes and their edges are not always well defined. The resulting data can therefore only be used for identifying broad trends.

2.3.4 High Resolution imaging

For HR imaging the microscope was operated at 200KeV and images were taken at 300K or 400K at various defocus conditions. All areas of sample for which HR images were required were photographed 3 - 5 times in a series of images from gaussian focus to underfocus in steps of 21.6 nm. It was important that the microscope was not subject to any vibration during the recording of HR images.

2.3.5 Image artefacts in the TEM

All work involving TEM is susceptible to the presence of image artefacts. These may arise from the method of specimen preparation; be it just drying down onto the microscopy grid or the more elaborate and lengthy processes of embedding and sectioning. They may also arise from the nature of the conditions inside the microscope. For example radiation damage, caused by inelastic interactions of electrons with the specimen, may disrupt crystalline structures or

cause molecules to polymerise. Also, heating of a specimen of poor thermal conductivity by the electron beam, may cause extensive disruption of the material under investigation. Such damage is more of a problem with biological specimens than with inorganic ones.

Fortunately, the iron storage proteins ferritin and haemosiderin are remarkably stable in the TEM, so for these and the wholly inorganic metal oxides also studied, beam damage was not a problem so long as reasonable care was taken to minimise beam exposure.

The same technique of loading samples onto grids was used for all the work, so although sample aggregation was sometimes apparent this was deemed as largely intrinsic to the sample.

Another form of image artefact, particularly relevant to the microscopy of particles of nanometre dimensions, is that of apparent particle substructure arising at different focus positions. Thus, if genuine substructure was suspected its appearance in a through-focus or gaussian to underfocus series of images was required for its verification. Careful objective astigmatism correction was also a necessity. (Massover, 1985a.)

The micrographs included in this thesis are believed to be largely free of any of the artefacts discussed above.

2.3.6 Selected area electron diffraction

Electron diffraction patterns were obtained by switching the microscope to selected area magnification mode, adjusting the focus and then introducing and centring the required selected area aperture. (Any objective aperture in use had to be withdrawn from the column at this point.) The microscope was then switched to selected area diffraction mode and the condenser and diffraction focus controls adjusted to give a faint but sharp pattern.

Electron diffraction patterns were taken from areas of the grid which were densely covered with material in order to obtain strong diffraction lines. The area of interest was positioned within the 20 μm selected area aperture and the diffraction patterns photographed in the manual mode using a long exposure time in order to record the weakest features of the powder patterns. A calibrated camera length of 80cm was used. An image of the area from which the pattern was taken was also recorded, so that correlation could be made between the two.

Relative crystallinity - comparing electron diffraction patterns. If it was desirable to assess the crystallinity of samples relative to one another then care was taken to compare only those diffraction patterns taken from areas of sample of similar density of coverage on the electron microscopy grid and of similar exposure, as judged by the intensity of the diffuse carbon diffraction rings.

2.3.7 Energy Dispersive X-ray Analysis (EDXA)

This technique was used on selected samples to confirm the presence, or absence, of certain elements. The technique relies on the detection of the characteristic X-rays emitted from the elements present, when they are bombarded by the electron beam. The equipment used was a Link Analytical windowless, Li-drifted, silicon detector, set at 30° to the sample area. Spectra were accumulated and processed by the Link AN 10000 X-ray microanalysis system. For this work the microscope was operated at 200KeV.

2.4 Other Techniques

Atomic Absorption Spectroscopy

Courtesy of Mr. A. Carver, University of Bath, using a Varian AA 275, calibrated by using the appropriate standards at suitable dilutions.

Powder X-ray Diffraction

Courtesy of Mr. A. Carver, University of Bath, using a Philips PW 1130/90 fitted with a Debye Scherrer camera of 114.6 mm diameter. This technique was used for characterising the manganese oxide standards used for XPS. Iron Kα radiation, λ 1.9373Å and copper Kα radiation, λ 1.5405Å were used, the iron Kα radiation gave rise to clearer diffraction lines on the X-ray films.

The d-spacings of the materials under investigation were calculated from:

$$n\lambda = 2d \sin \theta$$

where n = 1, only first order diffraction is observed

λ = wavelength of X-rays used

d = crystal plane spacing

θ = diffraction angle

4θ is given by the distance (mm) between corresponding arcs on the X-ray film.

Mn_3O_4 and Mn_2O_3 were obtained from Strem Chemicals Inc., Newburyport, MA., USA and MnO_2 was from the Analysed Samples for Students series, no. 18, Bureau of Analysed samples Ltd., Middlesbrough, UK. The Mn_3O_4 was confirmed as hausmannite by XRD, the Mn_2O_3 was a synthetic Mn(III) oxide and the MnO_2 was pyrolusite (β-MnO_2).

X-ray Photoelectron Spectroscopy (XPS)

Courtesy of Dr. R. Ewen, Bristol Polytechnic, using a VG Scientific Escalab Mk II, with associated software: VGS 1000 Data System. Aluminium anode Kα radiation and a low energy electron flood gun.

Freeze-drying

When it was necessary for samples to be freeze-dried for XPS this was performed using a SAVANT SpeedVac Concentrator SVC 200H linked to an Edwards Freeze Drier Modulo. Samples of little more than 1ml in volume could be freeze-dried in Eppendorf tubes in less than 6 hours.

Photographic Processing

1. TEM cut film negatives (Agfa-Gevaert Scientia Film 8.3 x 10.2 cm, Belgium) were processed by the author or the staff of the EM suite.
2. Black and white prints of electron micrographs were produced on Kodak or Ilford F2 or F4 glossy paper by the author.

Chapter 3

RECONSTITUTION WITH IRON AND ZINC

3.0 INTRODUCTION

This chapter describes the results of reconstitution experiments using horse spleen apoferritin. It has been proposed that this protein catalyses the oxidation of Fe(II) to Fe(III), *in vitro* (Macara *et al.*, 1972 & 1973a). However, in aqueous solution of around neutral pH and in the presence of dissolved oxygen, Fe(II) is readily oxidised to Fe(III), in the absence of ferritin. The aims of the work presented in the first part of this chapter were: a) by reconstitution with iron, to demonstrate that apoferritin catalyses the oxidation of Fe^{2+} to Fe^{3+} under the conditions used, at a faster rate than that achieved in the absence of ferritin and b) to determine the structure of the mineral products formed in ferritin at low (~200 iron atoms/molecule), intermediate (~875), and high (~3500) iron loadings.

In the later sections, reconstitution experiments with iron and zinc at a ratio of 10:1 are described. Zn^{2+} ions have been shown to inhibit iron uptake by horse spleen apoferritin (Macara *et al.*, 1973 b&c) and the work presented here was carried out in order to find out more about the nature of this inhibition and its effect on core structure.

3.1 EXPERIMENTAL

3.1.1 Reconstitution methods

1 Iron reconstitution

Ten small volumes of de-aerated Fe^{2+} solution (aqueous $(NH_4)_2Fe(SO_4)_2.4H_2O$, Analytical reagent, Fisons) were added sequentially to a buffered apoferritin solution (0.5 μM in 0.1M MOPS buffer, BDH Biochemical, pH 6.5) at intervals of between 20 and 30 minutes. The protein solution was kept in a stoppered bottle or cuvette tightly covered with Nescofilm or Parafilm, in order to restrict its exposure to air. The number of iron atoms per volume varied depending on the final iron loading required, see example calculation given below. The final iron concentrations were; for ~200 iron atoms/molecule: 0.11 mM, for ~875 iron atoms/molecule: 0.44 mM and for ~3500 iron atoms/molecule: 1.77 mM.

The Fe^{2+} was air oxidised to Fe^{3+} and this process could be followed in a UV/visible spectrophotometer (Cecil CE 595 double beam) set at 420nm (Macara *et al.*, 1972). At this wavelength the increasing absorbance of the solution is due to the formation of oxo- and hydroxo-bridged Fe(III) clusters and therefore the rate of appearance of the oxidation product gives a measure of the rate of oxidation. The reference cuvette contained either just buffered saline or a control solution, the exact composition of which depended on the experiment in hand.

Protein-free control experiments were also undertaken. The method was exactly as for reconstitution, substituting 0.15M saline for the protein solution.

Where bovine serum albumin (BSA) was used as a control protein it was present at equivalent concentration to the apoferritin and experimental procedure was as for apoferritin reconstitution.

Example calculation

To reconstitute 1ml of a 1μM apoferritin solution to 3500 iron atoms per molecule. (The Mr for apoferritin used was 445,000).

1 nmole protein requires 3.5 μmoles Fe^{2+}

1ml of the solution given contains 1 nmole

The iron is added in ten 50μl volumes, therefore the 3.5 μmoles Fe^{2+} must be contained in 0.5ml:

ie. 7 μmoles in 1ml

7 mmoles in 1l

Concentration of Fe^{2+} solution required is:

0.007 × 392.14 g/l

= 2.74 g/l.

2 Iron and zinc reconstitution

Method as for iron reconstitution with Zn^{2+} ions being added in a 10:1 Fe:Zn ratio in solution (aqueous, $ZnSO_4.7H_2O$, Analytical reagent, Fisons) either:

a) in the same solution as the Fe^{2+} or

b) in a separate solution 5 - 10 minutes before the Fe^{2+}.

The final protein, iron and zinc concentrations were; for a) 0.5 or 1 μM protein, 0.44 or 0.86 mM iron and 0.044 or 0.086 mM zinc and for b) 1 μM protein, 0.95 mM iron and 0.095 mM zinc. The calculated iron loading was approximately 875 iron atoms/molecule in each case.

The process of iron oxidation was followed in the spectrophotometer as for the iron reconstitutions. The time interval between increments varied for the different types of experiment. It was 20-40 minutes for the experiments where the iron and zinc were added together and between 1 and 4 hours for the experiments where zinc was added before the iron. For both types of experiment it was important

that the next increment of ions was not added until a steady-state in solution was re-established in both the test (Fe & Zn) and reference (Fe) cuvettes. This was judged by the trace on the spectrophotometer chart paper becoming level or regaining its original position.

Protein-free control experiments were also undertaken.

3.1.2 Kinetics methods

In order to monitor the progress of the experiments two types of trace were recorded for each set of experiments; a) an "absolute" trace, reading the test solution against a blank to which no reagents were being added, b) a "difference" trace, where the test solution was read against a control solution which had all the components of the test solution except the one being studied. For example, in order to monitor the effect of the protein on the rate of oxidation of Fe^{2+}, the Fe^{2+} solution was added to both test and reference cuvettes but the protein was only present in the test cuvette, the difference between the rates of reaction in both cuvettes was recorded. It follows that if the rate in the test cuvette (+ apoferritin) is greater than that in the reference cuvette (- apoferritin) then the trace will be positive, ie. move up on the chart paper. Conversely, if the rate in the reference cuvette is greater than that in the test cuvette, then the trace will be negative. If the rates in the two cuvettes are equal, then the trace will be level.

For the iron and zinc reconstitutions where the difference between the test and reference cuvettes was the addition of zinc ions to the test cuvette, the effect of the zinc on the oxidation of each iron increment was again apparent from the level of the difference trace. The extent of the effect was assessed by measuring: i) the

maximum drop of the trace below its starting point (ie. the level of the initial reading between the two cuvettes before any ion solutions were added,) this measurement was designated ΔA_{420} max, ii) the time taken to reach ΔA_{420} max, designated t_{max} and iii) the time taken for the trace to regain its original level, (t_r).

Initial rates of oxidation could be estimated from "absolute" traces by calculating the gradient of the trace over a 120 second period after the addition of an increment.

Abbreviation used:

MOPS 3-(*N*-Morpholino) propane-sulphonic acid

3.2 RESULTS OF THE IRON RECONSTITUTIONS

3.2.1 Kinetic Studies

In order to demonstrate whether or not apoferritin catalysed the oxidation of Fe^{2+} two types of experiment were performed. Firstly, the rate of oxidation of Fe^{2+} (measured as Fe-O-Fe formation by absorbance at 420 nm), in buffered solutions containing either a saline solution of apoferritin, or just saline were recorded. Very low iron concentrations (0.11 mM final conc.), leading to a small average core size (200 iron atoms/molecule), had to be used to avoid the problem of precipitation in the cuvette without apoferritin. For the experiments in the presence of apoferritin the uptake curves were hyperbolic after each iron addition, (see figure 3.1 for data taken from a typical trace). At the low iron concentrations used no oxidation could be detected, by the method in use, in the absence of apoferritin for the first four increments; by the eighth and subsequent additions flocculation of the product began to occur

causing a disproportionate rise in the absorbance of the solution due to light scattering. For increments five to ten, in the protein-free controls, the rate curves were approximately linear. Data taken from a typical trace are shown in figure 3.1. Comparison of the lines for the experiments in the presence and absence of apoferritin, shows the catalytic effect of the protein.

Secondly, a trace of the difference in rate of oxidation between two buffered Fe^{2+} solutions; one containing a saline solution of apoferritin and the other just saline, was recorded. The "difference" trace was positive for each of the first six increments. It was positive and then levelled off for the seventh increment, for the eighth and ninth increments it was slightly positive and then became negative and for the last increment it was level and then became negative. Figure 3.2 shows the progress of a typical difference trace. Again, the catalytic effect of the protein was clearly demonstrated.

Apoferritin was replaced in an experiment similar to the first ones, by Bovine Serum Albumin (BSA) to see if this "non-specific" protein would have a similar catalytic effect. BSA did not promote the formation of the red/brown oxidation product as apoferritin had; an increase in the absorbance at A_{420} only began to occur after 23 hours, (see figure 3.1). It did appear however, that the BSA was acting as a "protective colloid" since no precipitate was observed during the following 11 days.

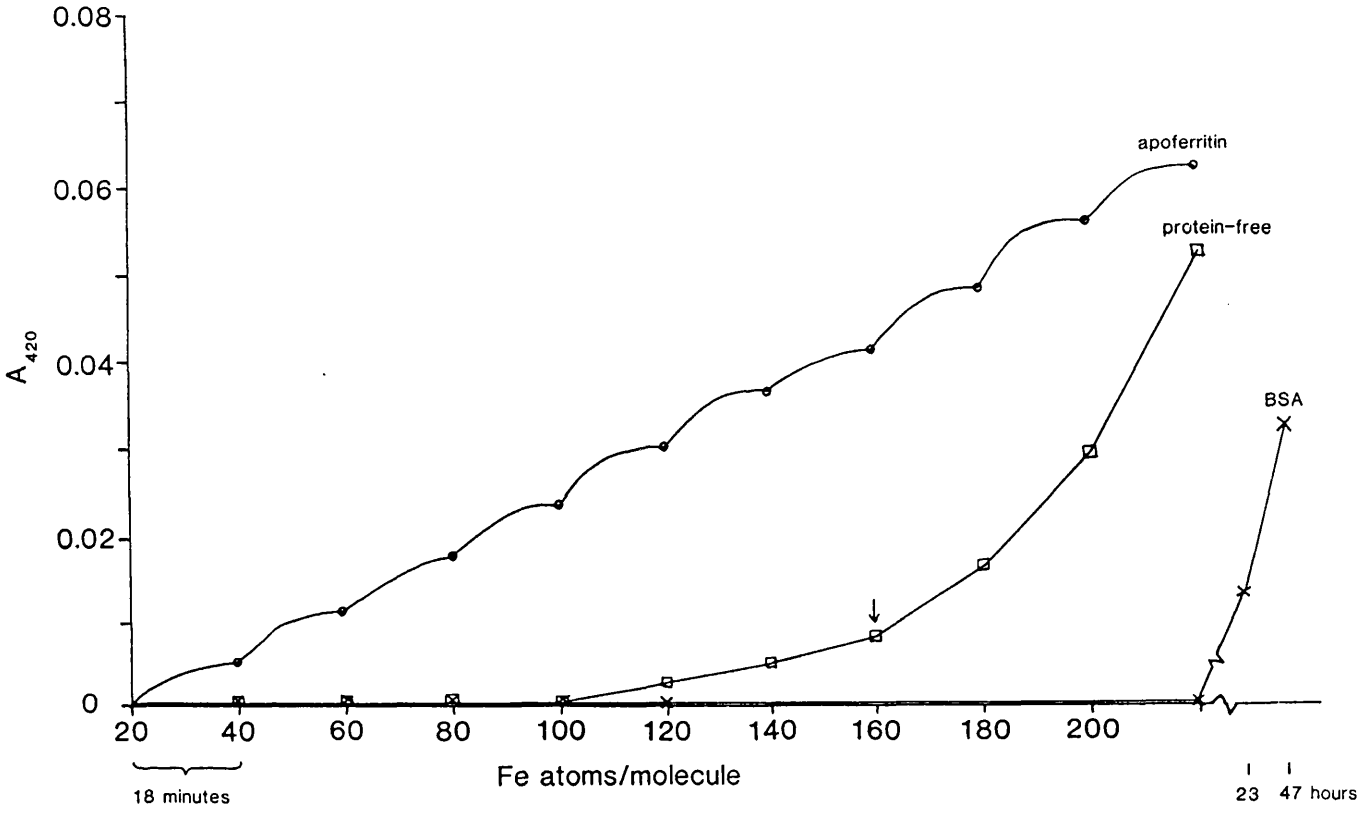

Figure 3.1 . Progress curves for iron oxidation in the presence and absence of apoferritin, and in the presence of BSA. Iron oxidation was measured as the increase in absorbance at 420nm and this value is plotted against the approximate number of Fe atoms/molecule of apoferritin. (↓) precipitation occurring in the protein-free control.

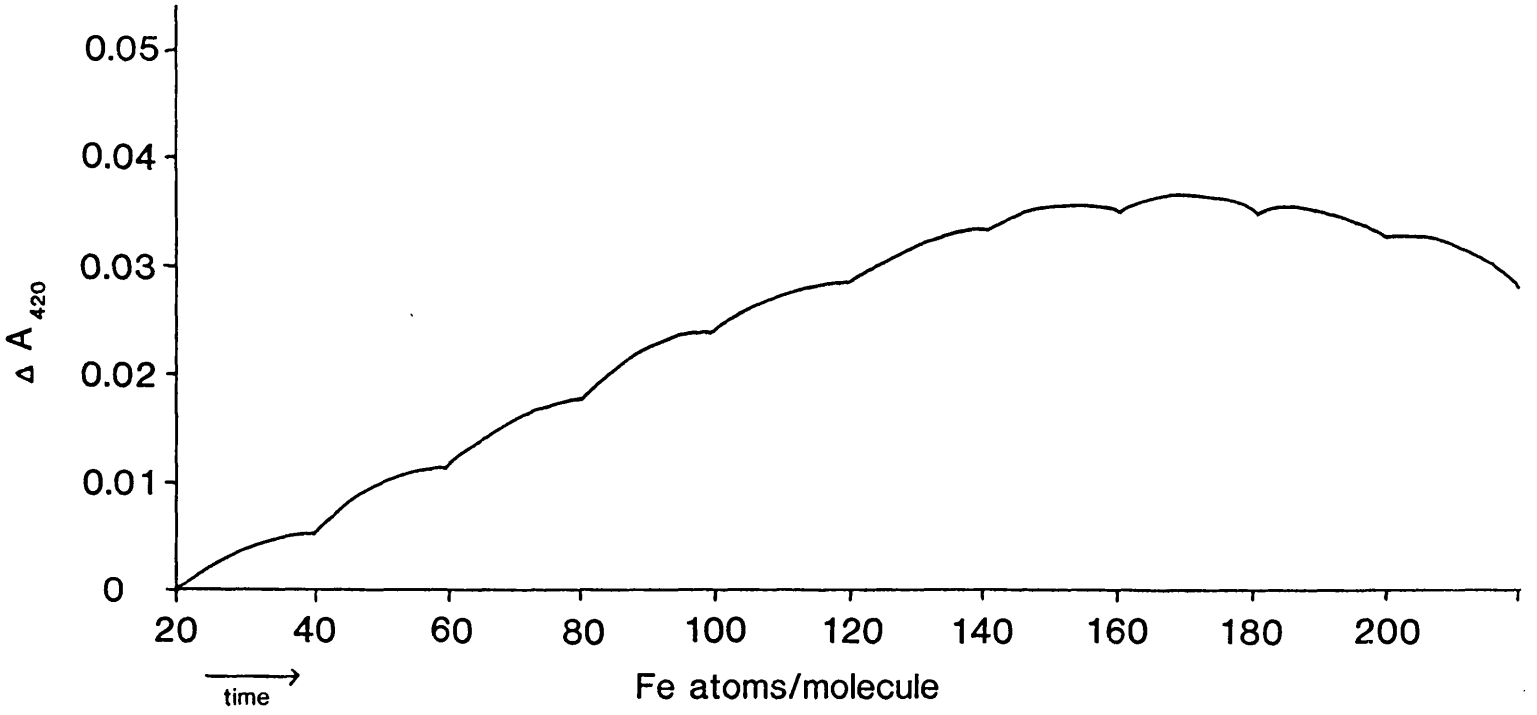

Figure 3.2 "Difference" trace for iron oxidation in the presence and absence of apoferritin. Difference in A_{420} of two solutions, one with and one without apoferritin, plotted against approximate number Fe atoms/molecule.

3.2.2 Structural Studies

1 Reconstitution to an average of ~200 iron atoms per molecule

Atomic absorption analysis of a typical sample from this set of experiments gave a final average iron loading of 227 iron atoms per molecule. The ferritin cores at this loading were discrete, particulate, irregular in shape and heterogeneous in size, as can be seen in plate 3.1a & figure 3.3a. The mean value for the core diameter was 3.26 nm with a standard deviation of 0.54 nm.

The electron diffraction patterns from these small cores were weak, with only two lines at 2.50Å and 1.51Å. This indicated that poorly ordered, partially crystalline ferrihydrite had been formed, (table 3.1).

2 Reconstitution to an average of ~875 iron atoms per molecule

At this level of iron loading the ferritin cores again exhibited irregular shapes and a range of sizes, see plate 3.1b & figure 3.3b. Samples assayed by atomic absorption analysis had average loadings of between 765 and 858 iron atoms per molecule. The cores were more clearly defined than those of the samples reconstituted to 200 iron atoms per molecule. The mean core diameter was 4.97 nm, with a standard deviation of 0.69 nm. This mean core diameter was greater than that at the lower loading.

The electron diffraction patterns at this iron loading were more intense than those of the 200 Fe atoms per molecule samples. Again, they revealed partially crystalline ferrihydrite cores, but these cores exhibited better crystallinity than those with an average of 200 Fe atoms/molecule (see table 3.1).

3 Reconstitution to an average of ~3500 iron atoms per molecule

Reconstitution to this higher iron loading (3352 iron atoms per molecule by atomic absorption analysis) resulted in larger cores of more regular shape. As can be seen in plate 3.1c the cores are more well-defined than those at the lower loadings and they have a variety of shapes; some rounded, oval, four- and five-sided. The mean core diameter was 6.14 nm, with a standard deviation of 0.65 nm and a particle size distribution is shown in figure 3.3c.

Electron diffraction revealed that these cores were of more crystalline ferrihydrite than those at 200 and 875 iron atoms per molecule (table 3.1).

The expected diameter of any spherical particle of ferrihydrite containing a known number of iron atoms can be calculated from the unit cell dimensions and cell content of ferrihydrite. These are a = 5.08Å, c = 9.4Å and $Fe_5HO_8.4H_2O$, (Towe & Bradley 1967 and see appendix III). Such calculations can be applied to ferritin cores if the number of iron atoms per molecule is known and it is assumed that the core is spherical in shape. For the two lower iron loadings used here the mean core diameter was greater than that expected from the calculations. They were for the sample with 227 Fe/molecule: 2.63 nm, (observed 3.26 nm), and for 765 Fe/molecule: 3.94 nm (observed 4.97 nm). These larger core diameters may be explained by the observations that the material formed in these reconstitutions was only partially crystalline ferrihydrite, also, it was probably more hydrated than the formula given and, from the electron micrographs, the cores were not generally spherical.

At the highest iron loading used the observed mean core diameter (6.14 nm) was a little lower than that expected from the calculation;

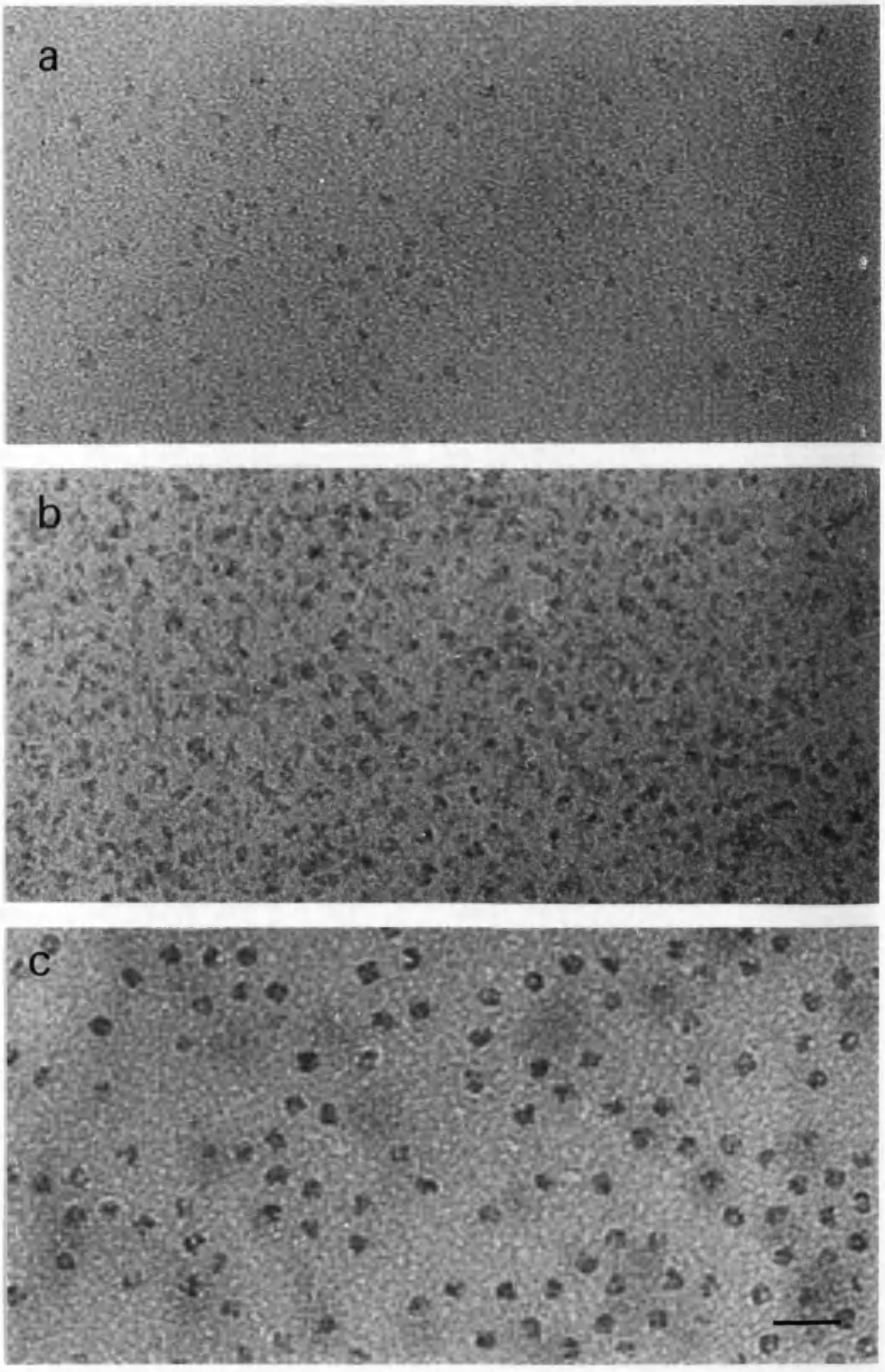

Plate 3.1 Electron micrographs of unstained reconstituted ferritin. *a* ~200 Fe atoms/molecule, *b* ~875 Fe atoms/molecule, *c* ~3500 Fe atoms/molecule. Bar marker 20nm for all micrographs.

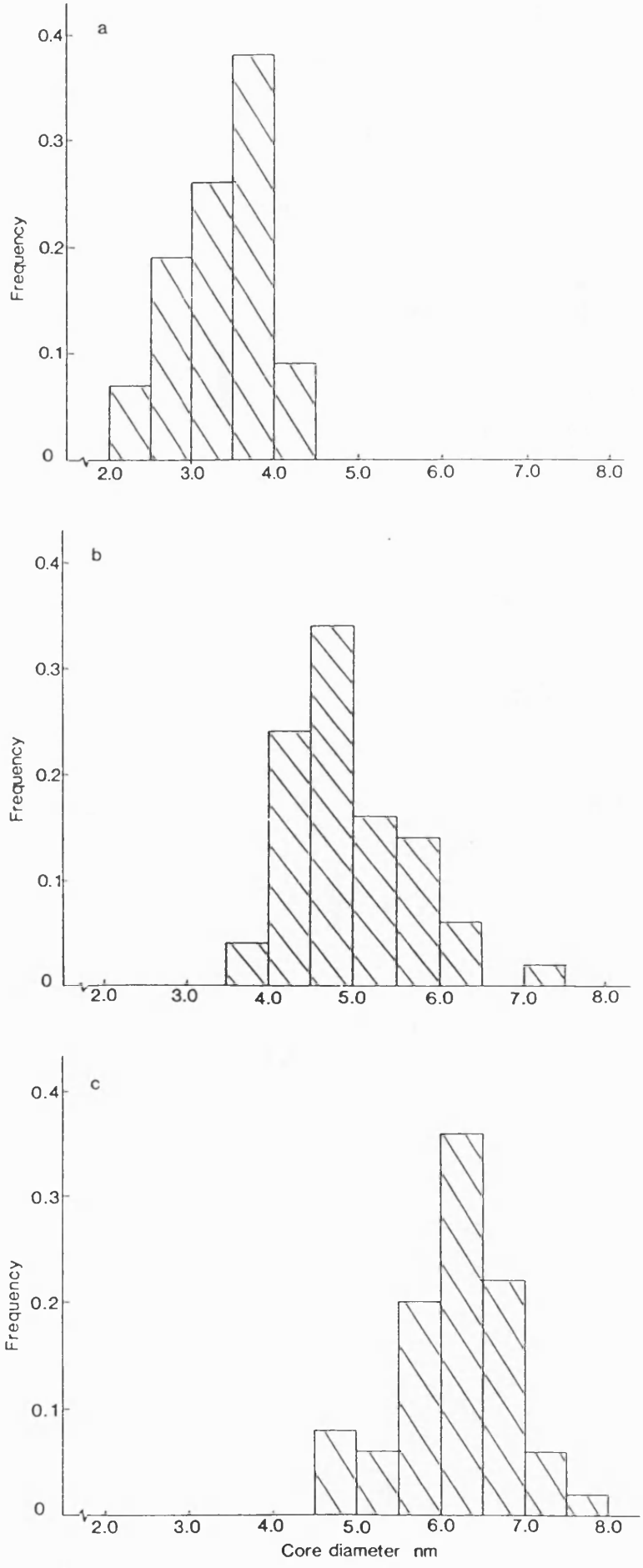

Figure 3.3 Particle size distributions for iron reconstituted ferritin. *a* ~200 Fe atoms/molecule, *b* ~875 Fe atoms/molecule, *c* ~3500 Fe atoms/molecule.

for 3352 Fe/molecule the value was 6.46 nm. This change in the trend could be explained by the improved crystallinity in this sample, and since the growing ferrihydrite particle would be influenced more, at this loading, by the size constraint of the protein cavity, the degree of hydration could have been reduced. Also, as seen on the electron micrographs, the cores were often angular as well as rounded.

4 Protein-free control for 0.44mM final iron concentration

The product formed from the oxidation of Fe^{2+} in the absence of protein appeared in the electron micrographs as small (mean particle diameter: 4.96 nm, S.D. 1.04 nm) aggregated grains of a mixture of lepidocrocite (γ-FeOOH) and ferrihydrite (plate 3.2a). A particle size histogram is shown in figure 3.4. The mean particle diameter was very similar to the mean core diameter measured for the ferritin sample reconstituted at this iron concentration (4.97 nm), but there was a much broader range of particle sizes in the protein-free sample. The mixture of oxides formed was more crystalline than the ferrihydrite formed in the presence of apoferritin, see table 3.2.

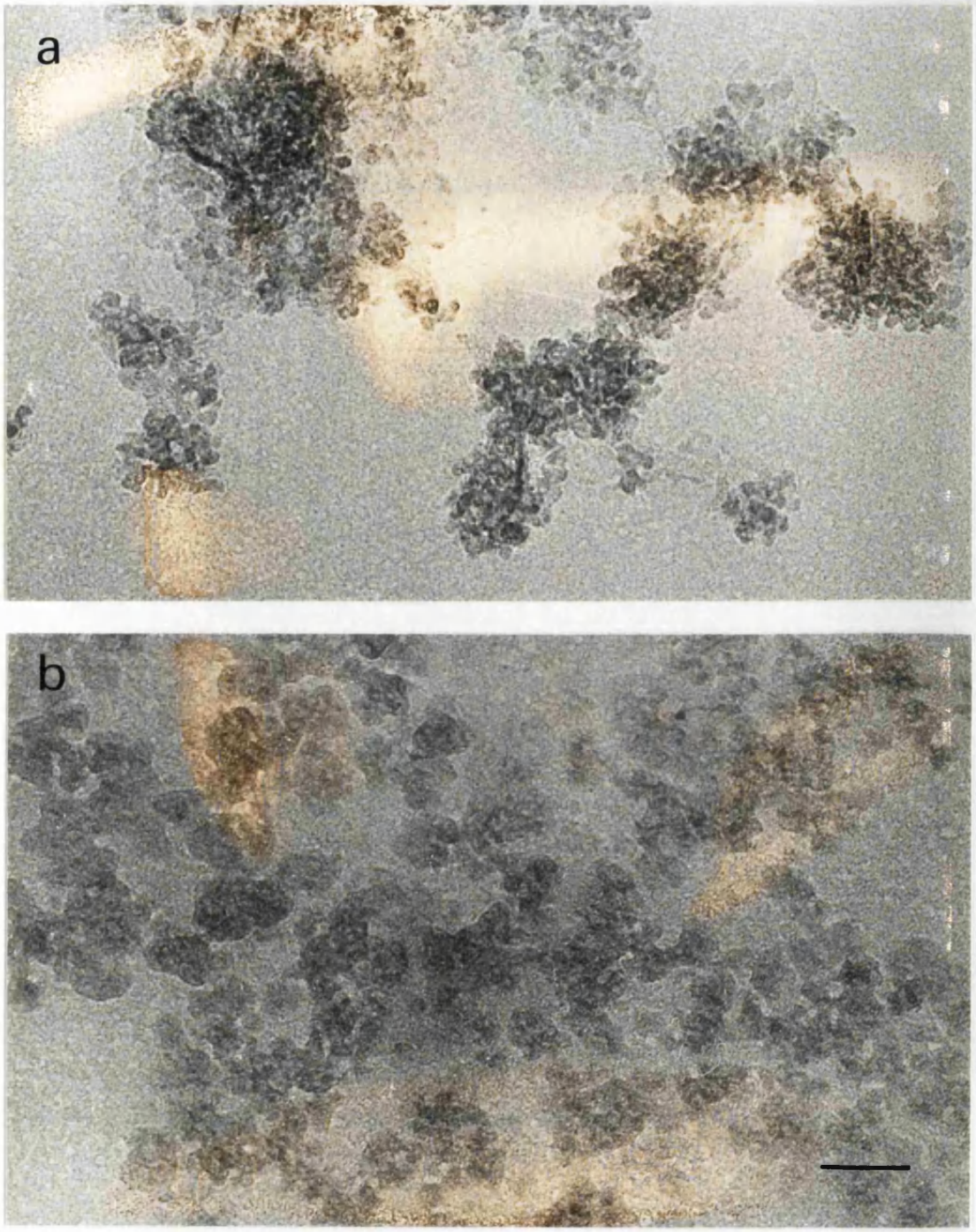

Plate 3.2 Electron micrographs of the granular lepidocrocite/ ferrihydrite oxidation product formed in the protein-free controls. *a* -Zn, *b* +Zn, the zinc being added with the iron. Bar marker 25nm for both micrographs.

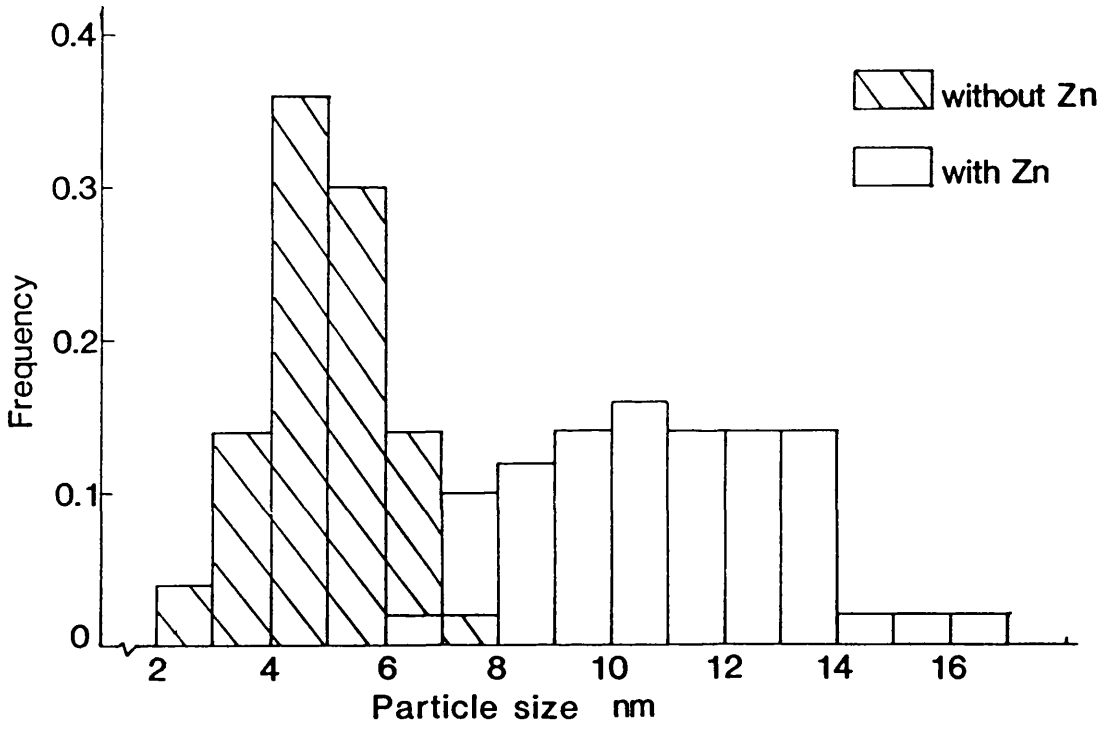

Figure 3.4 Particle size distributions for the oxidation product formed in the protein-free controls, in the presence and absence of Zn^{2+} ions. For the +Zn sample the zinc was added with the iron.

Table 3.1 Electron diffraction data for ferritins reconstituted to approximately 200, 875 and 3500 iron atoms per molecule.

I = intensity of line judged by eye:- S = strong, M = medium, W = weak, B = broadened, BB = broad band.

200		875		3500	
d(Å)	I	d(Å)	I	d(Å)	I
2.50	S	2.48	S	2.47	S
		2.34	SBB	2.26	M
		1.98		1.96	M
		1.54	W	1.52	W
1.51	SB	1.50	S	1.45	S

Table 3.2 Electron diffraction analysis of the product formed in the protein-free controls.

I as judged in Table 3.1

F = ferrihydrite, L = lepidocrocite.

d(Å)	I	assignment
3.30	W	L
2.49	S	F/L
2.21	S	F
1.98	M	F/L
1.73	M	F/L
1.51	S	F/L
1.45	S	F
1.22	W	L
1.04	W	L
0.85	W	L

3.3 RESULTS OF THE IRON AND ZINC RECONSTITUTIONS

Table 3.3 Table relating the approximate number of iron atoms per molecule to the iron concentration in solution for each of the ten increments in the experiments reported in section 3.3 of this chapter.

increment number	approx. no. Fe atoms/ molecule	iron concentration after each increment for the final concentrations (mM): 0.44	0.86	0.95
1	88	0.05	0.10	0.12
2	175	0.10	0.20	0.24
3	263	0.15	0.29	0.35
4	350	0.19	0.38	0.45
5	438	0.24	0.47	0.54
6	525	0.28	0.55	0.64
7	613	0.32	0.63	0.72
8	700	0.36	0.71	0.80
9	788	0.40	0.79	0.88
10	875	0.44	0.86	0.95

3.3.1 Kinetic Studies

1 Reconstitution adding iron and zinc simultaneously

The progress of iron oxidation in these reconstitution experiments in the presence and absence of zinc at a ratio of 10:1 Fe:Zn is illustrated first in figures 3.5 and 3.6, where the absorbance of the solutions at 420 nm (used again as a measure of iron oxidation) is plotted against the calculated number of Fe atoms added per molecule. Figure 3.5 shows the shape of the reaction curves

for 20 minutes following each increment of iron alone or iron and zinc together, for the reconstitutions performed at a protein concentration of 0.5 μM, (final iron concentration 0.44 mM). After each ion addition the curve was hyperbolic in shape, this being more pronounced for the reconstitution in the absence of zinc and for the early increments. As can be seen from the figure, the final absorbance of the apoferritin solution to which iron and zinc were added fell slightly behind that of the solution without zinc. When the final A_{420} of such solutions was monitored over an 18 hour period following the experiments, the absorbance of the solution with zinc would attain a similar level (within experimental error) to that without zinc. This slower oxidation of iron and the flatter reaction curves for each increment in the presence of zinc, suggested that the zinc ions were inhibiting iron uptake by apoferritin.

Figure 3.6 shows the increase in the absorbance of the apoferritin solutions after each increment of iron had been allowed to oxidise fully, for experiments performed at 1 μM protein concentration, (final iron concentration 0.86 mM). The results shown here were from experiments carried out simultaneously, using the same Fe^{2+} stock solution, hence the very close agreement of the readings for the solution with and that without zinc.

The initial rates of oxidation for the first 7 increments in the reconstitutions at 0.5 μM protein concentration were calculated over a 120 second period and are shown in table 3.4 and figure 3.7. Also shown in the table and figure are the initial rates of oxidation for the reconstitutions at 1 μM protein where zinc was added before the iron, (see section 3 below). It is interesting to compare here the results for the two protein concentrations where no zinc was added; for both protein concentrations the initial rate of oxidation

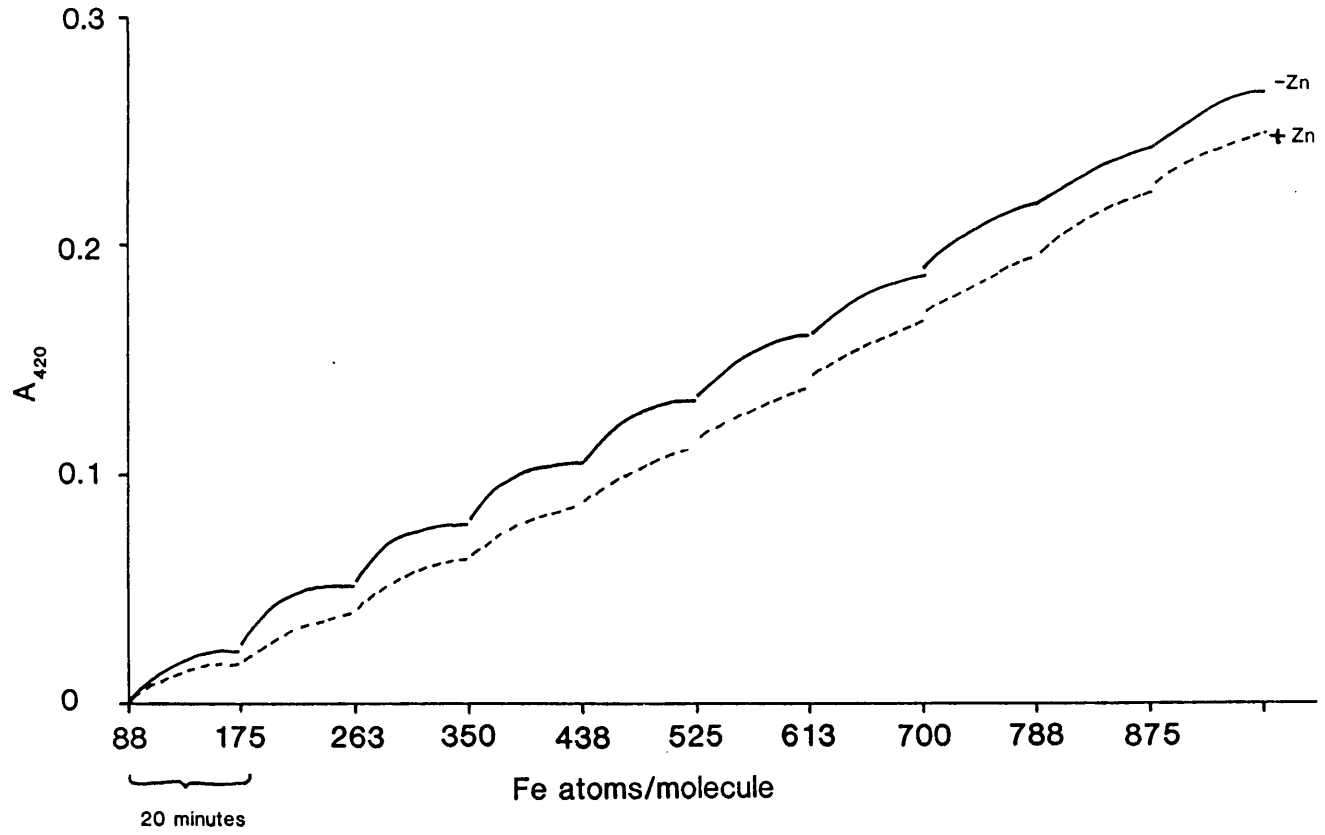

Figure 3.5 Zinc-with-Iron Graph showing the progress of reconstitution in the presence and absence of zinc for experiments at 0.5μM protein concentration, 0.44mM final iron concentration. The figure shows the shape of the reaction curves for 20 minutes following the addition of each increment of ions.

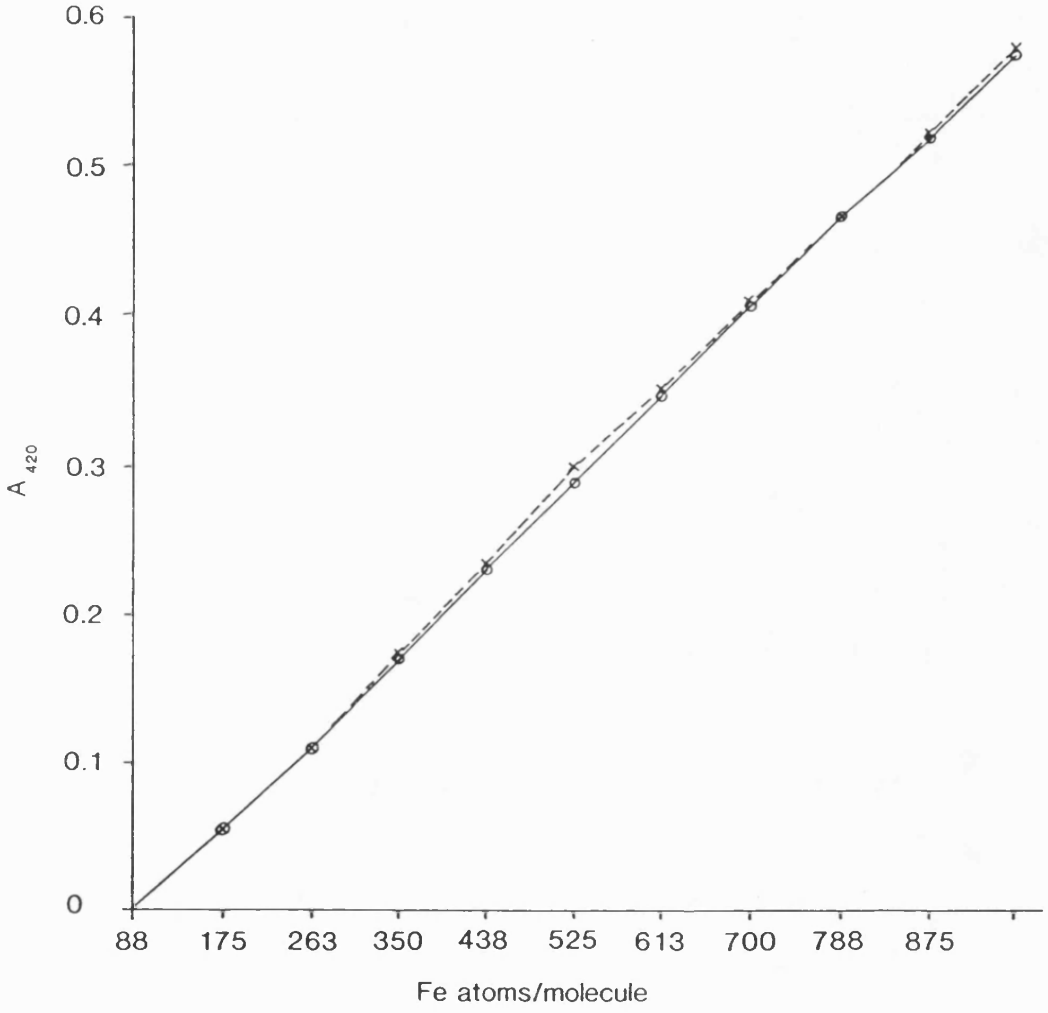

Figure 3.6 Zinc-with-Iron Graph showing the progress of reconstitution in the presence and absence of zinc for experiments at 1μM protein concentration, 0.86mM final iron concentration. The figure shows the increase in A_{420} of the solutions after each increment of iron had been allowed to oxidise fully. x--x +Zn, o—o -Zn.

approximately doubled for the second increment of iron and those for the higher protein concentration were approximately twice those for the lower protein concentration. The initial rates were reduced for increments 4-7. However, in the presence of zinc, (0.5 μM protein concentration), the rate did not double on addition of the second increment and it remained approximately the same for all increments. Also, the initial rates were consistently lower than those where zinc was not being added. These observations of initial rates again suggested that zinc inhibited iron uptake by apoferritin.

Further evidence that the kinetics of iron uptake by apoferritin were diminished by the presence of Zn^{2+} was obtained by recording directly, the difference between the rates of oxidation of Fe^{2+} in two solutions of apoferritin where to one, zinc was added with the iron. The "difference traces" obtained for the experiments at both 0.5 and 1 μM apoferritin concentration were of the pattern shown in figure 3.8 which shows the difference in absorbance (A_{420}) between the two solutions with time, for each increment of iron and zinc. The traces were negative after each increment, and they showed that the extent of the inhibition varied during the course of the reconstitution. The important features of the inhibition by zinc were measured from these complex traces and these results are illustrated in figures 3.9 and 3.10. In figure 3.9 the maximum drop of the trace below its original level (ΔA_{420} max.) is plotted against the number of Fe atoms added per molecule. The zinc had a marginal effect on the rate of oxidation for the first increment (0-88 iron atoms/molecule). On addition of the second increment (175 iron atoms/molecule), a rapid rise in the inhibition by zinc was noted. The effect was maximised for the third increment (263 iron atoms/molecule) and then

Table 3.4 Initial rates of oxidation after each increment, measured as increase in absorbance units per second (x 10^{-5}).

increment number	0.5 µM protein		1.0 µM protein	
	-Zn	+Zn with Fe	-Zn	+Zn before Fe
1	4.2	2.9	7.1	4.2
2	6.7	2.9	14.2	6.3
3	7.1	2.9	12.9	5.0
4			13.8	
scale reduced				
4	5.0	2.5		1.7
5	4.2	2.5	12.5	1.7
6	3.3	2.5	12.5	nd
7	4.2	2.5	12.5	nd

Calculated from "absolute" traces, the scale of pen deflection had to be reduced (where indicated) in order to continue following the reaction so the later figures are less accurate.

---

slowly diminished for further additions. As can be seen in the figure, this pattern of inhibition was apparent in the reconstitutions at both protein concentrations (0.5 & 1.0 µM), suggesting that it was an effect of loading rather than of absolute concentration of any of the reactants.

Figure 3.10 shows the values of t_{max} for each increment. For the experiments at 0.5 µM protein concentration there was no consistent trend in the size of t_{max}, but in the 1 µM protein concentration experiments, t_{max} tended to increase after the third or fourth increments. These results, together with those in figure 3.9,

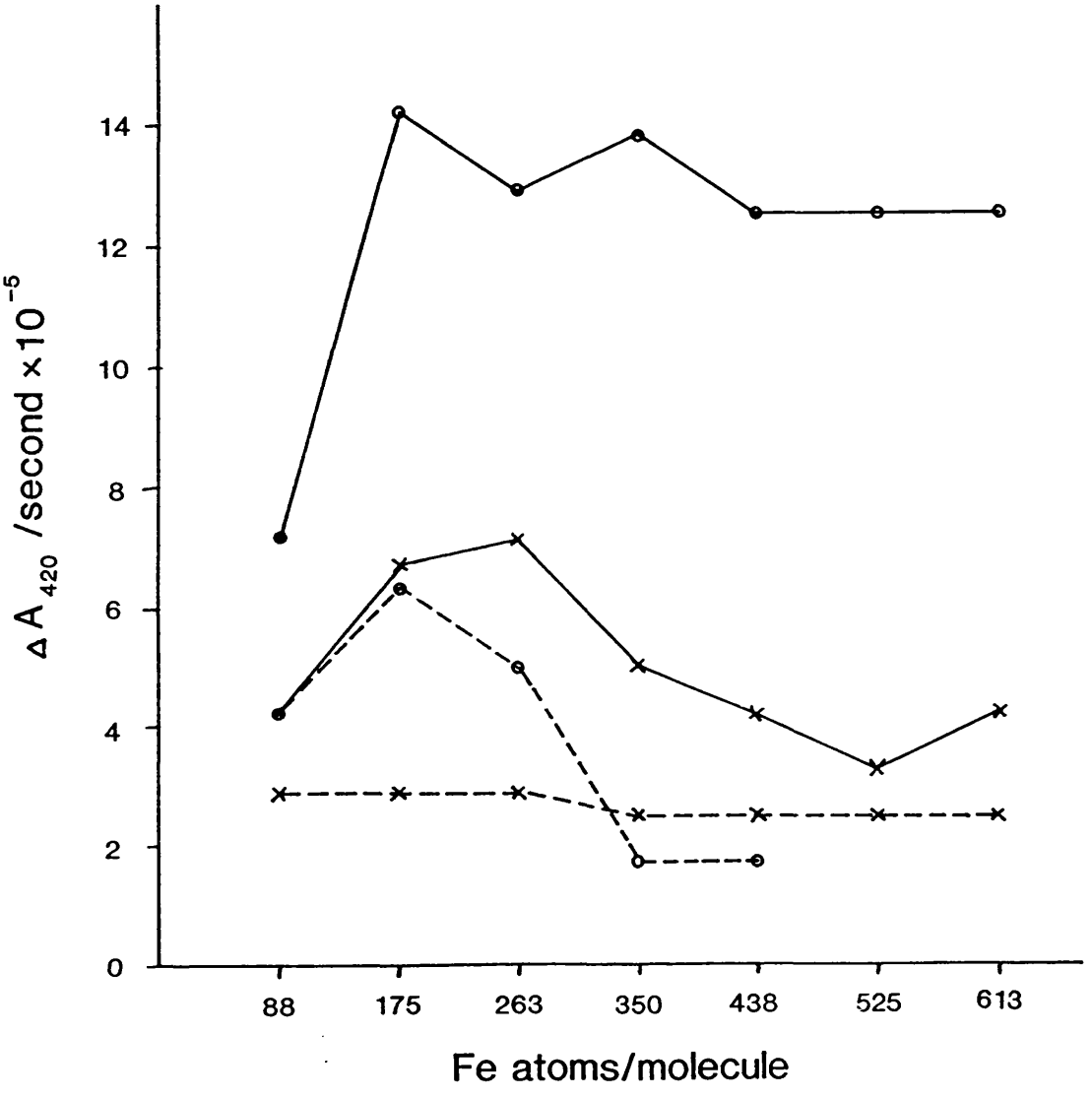

Figure 3.7 Initial rate of oxidation (measured as ΔA_{420}/second) of increments 1-7 in the presence and absence of zinc. For the experiments at 0.5μM protein concentration the zinc was added with the iron and for those at 1μM protein concentration the zinc was added before the iron.

x--x 0.5μM +Zn, x—x 0.5μM -Zn, o--o 1μM +Zn, o—o 1μM -Zn.

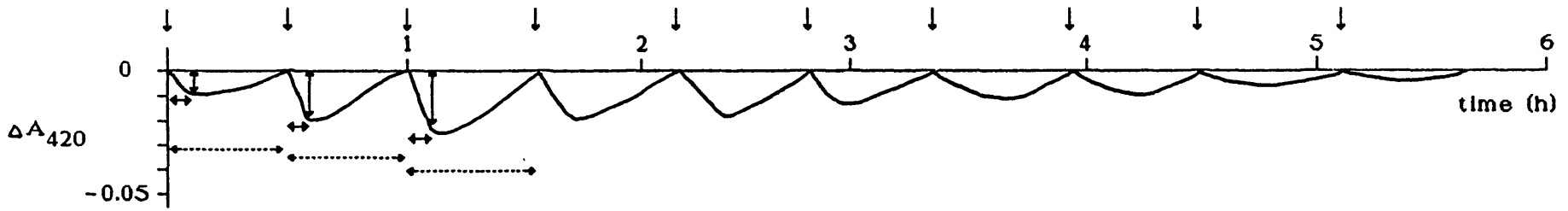

Key:- ↓ increment Fe + Zn added

↕ ΔA_{420} max

↔ time taken to reach ΔA_{420} max, t_{max}

←·····→ time taken to regain original level, t_r

Figure 3.8 Zinc-with-Iron "Difference" trace for reconstitutions in the presence and absence of zinc. The graph shown was reproduced from a typical trace of an experiment at 1μM protein concentration, those from experiments at 0.5μM protein concentration were of the same pattern.

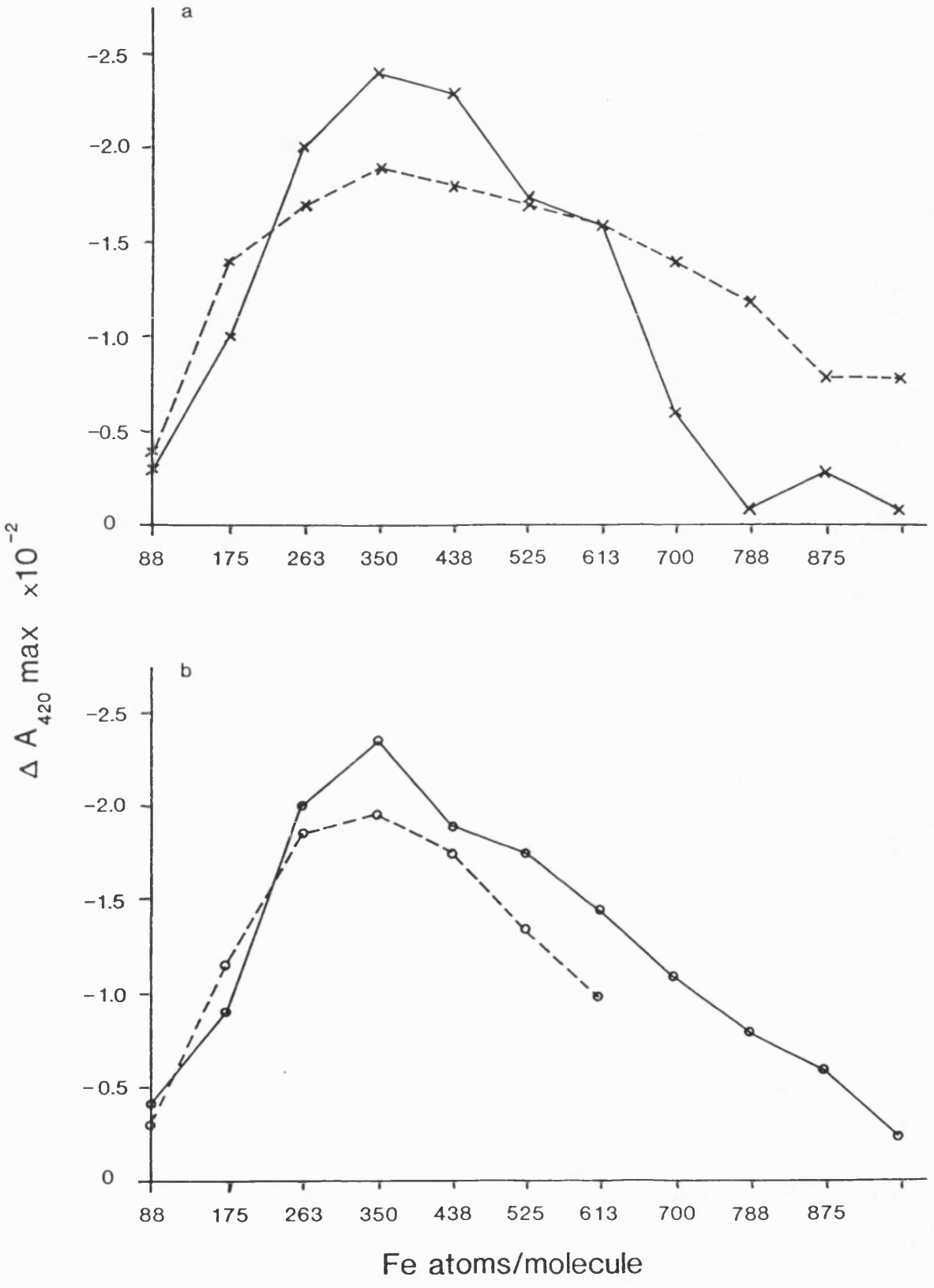

Figure 3.9 Zinc-with-Iron Graphs showing the maximum drop of the "difference" traces below their original level (ΔA_{420} max.) with each increment of ions. Data are shown from two experiments at each protein concentration: *a* 0.5μM, *b* 1μM.

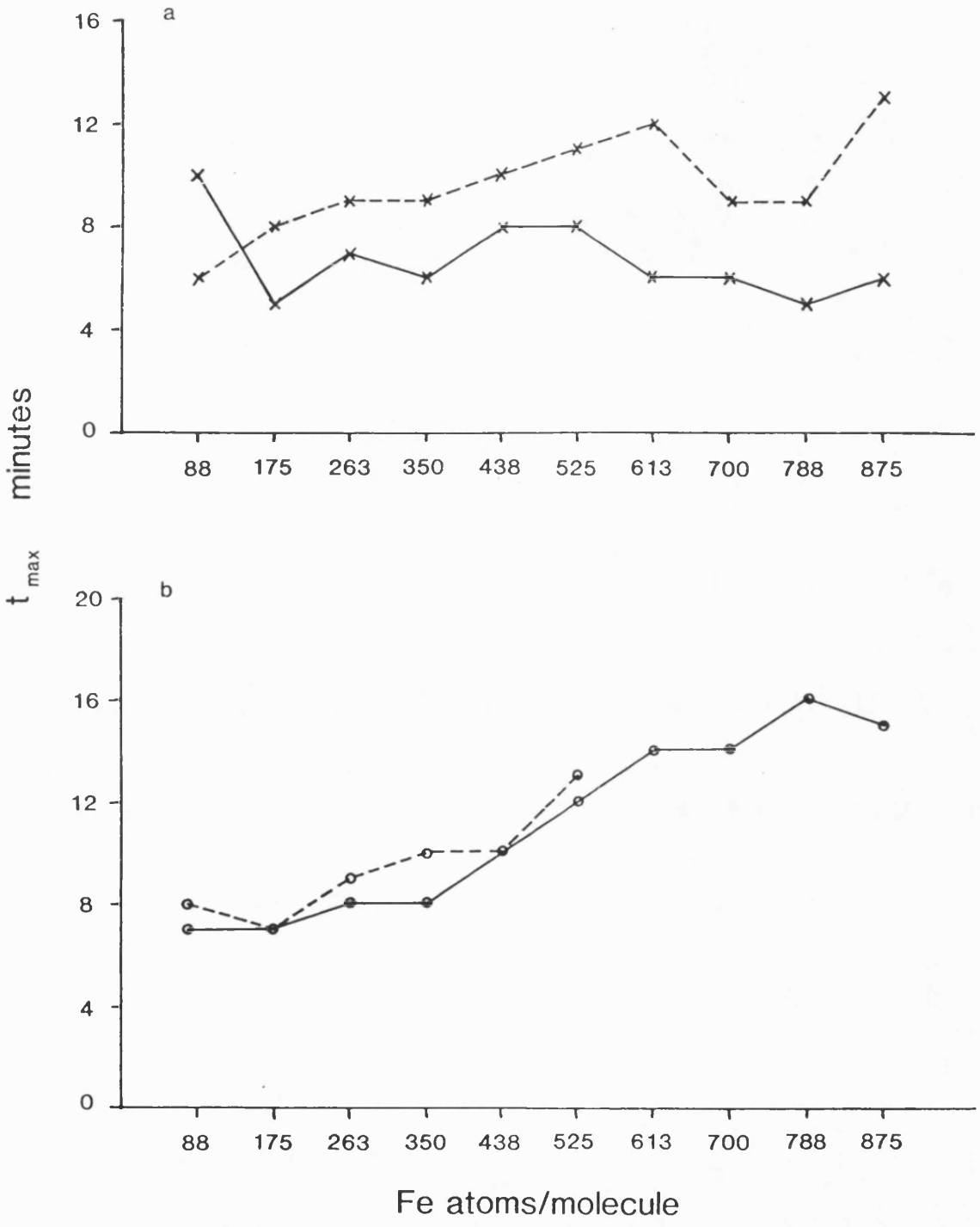

Figure 3.10 Zinc-with-Iron Graphs showing the time taken to reach ΔA_{420} max. (t_{max}) after the addition of each increment of ions. Data are shown from two experiments at each protein concentration: *a* 0.5μM, *b* 1μM.

suggested that the effect of zinc was not as great in the later stages of the reconstitution, because the value of ΔA_{420} max. decreased and the time taken for ΔA_{420} max. to be achieved (t_{max}) increased.

2 Protein-free control adding iron and zinc simultaneously

Oxidation of Fe^{2+} occurred in the protein-free controls and was detectable by the increase in absorbance at 420 nm at iron concentrations greater than 0.05 mM, in both the presence and absence of Zn^{2+} ions. This is shown in figure 3.11, where the absorbance of the solutions at 30 or 40 minutes after the addition of each of the first three increments is plotted against iron concentration. The graphs are representative of the two iron concentrations used for the two protein concentrations in the reconstitution experiments.

The effect of zinc on the rate of oxidation of Fe^{2+} in the protein free systems is illustrated in figure 3.12 where the progress of typical difference traces (reading the absorbance of a buffered iron (II) solution with zinc against one without zinc, ΔA_{420} vs. time) are plotted.

At the lower ion concentrations used (final iron concentration 0.44 mM, plot a) the trace remained level during increments 1, 2 and 3 (0.05 - 0.15 mM iron concentration), suggesting that zinc had no effect on the rate of Fe^{2+} oxidation at this stage of the experiment. The trace began to fall after 15 minutes from the addition of the 4th increment (0.19 mM), so the zinc appeared to be reducing the rate of reaction in the test cuvette. During increment 5 (0.24 mM) the trace continued to fall steeply. Then, during increment 6 (0.28 mM) the trace levelled out but remained below its original position on the chart paper. That the trace levelled out may suggest that the effect

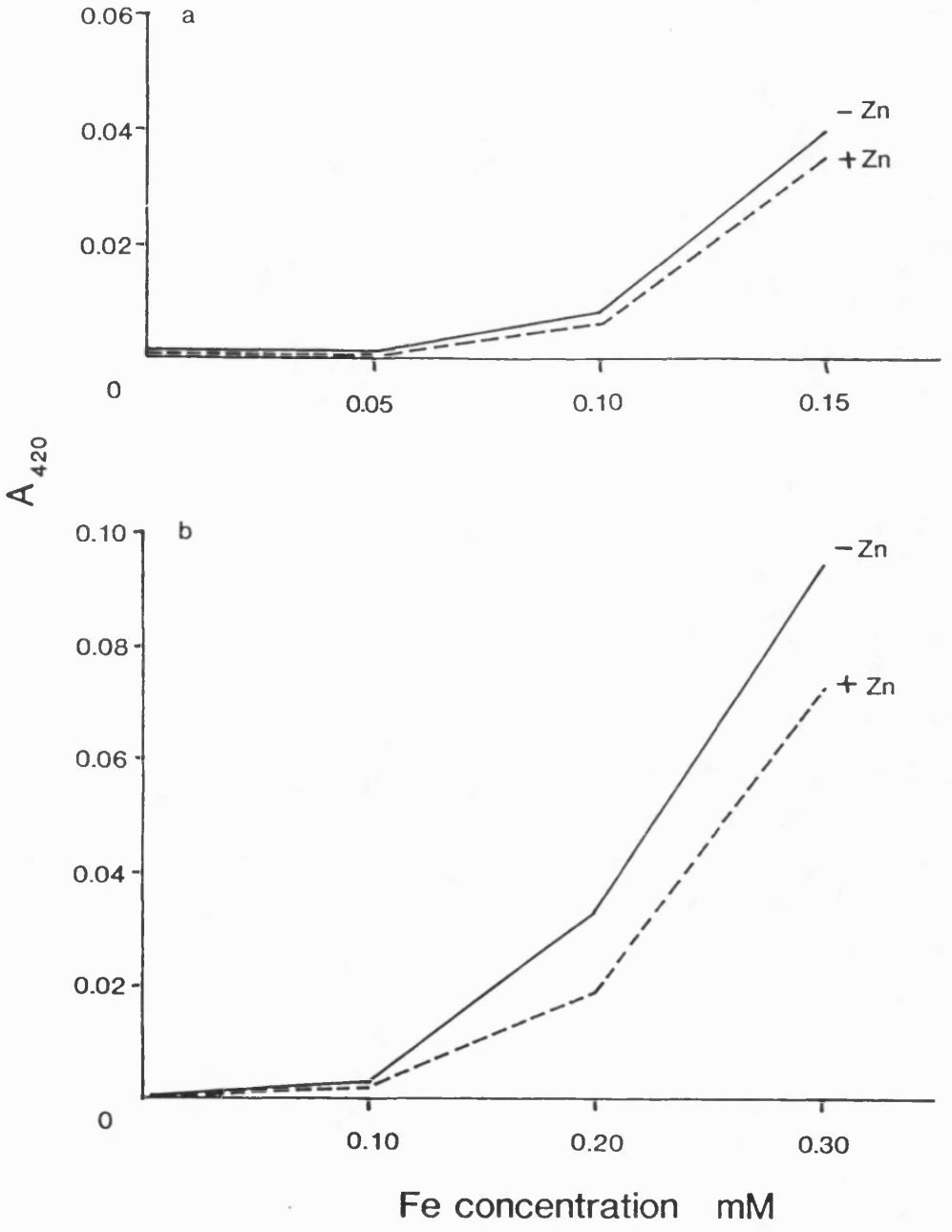

Figure 3.11 Zinc-with-Iron Evidence for iron oxidation in the early stages of the protein-free controls in the presence and absence of zinc. *a* experiments at the final iron concentration of 0.44mM, A_{420} read at 30 minutes after the addition of each increment. *b* experiments at the final iron concentration of 0.86mM, A_{420} read at 40 minutes after the addition of each increment.

of zinc was diminishing. After the addition of increment 7 (0.32 mM) the trace became slightly positive, but still remained below the original level, here the effect of zinc may have been further diminished. Flocculation of the oxidation products in the cuvettes at concentrations above 0.36 mM iron precluded further assessment of the effect of zinc, (the trace became unstable and unreliable since precipitation was starting to occur).

At the higher ion concentrations used (final iron concentration 0.86 mM, plot b) the trace began to fall after about 20 minutes following the addition of the first increment (0.1 mM iron), so zinc appeared to have a slight effect on the rate of oxidation at a lower concentration in these experiments. During the second increment (0.19 mM) the trace continued to fall steadily. After the addition of the third increment (0.29 mM) the trace fell more steeply, levelled out briefly and then began to rise, it remained however, below its original position on the chart. It appeared therefore, that the zinc had its maximum effect on the reaction during this third increment. By the fourth increment (0.38 mM) flocculation in the cuvettes at these higher concentrations was becoming too great to follow the reaction further in the spectrophotometer.

Unlike the difference traces for the experiments with protein, the traces for these experiments did not regain their original level or level-off after each increment. Therefore, a steady-state was not necessary attained in either of the cuvettes, so with each increment, ions were probably added to solutions at different stages of the reaction. That the traces moved down on the chart paper demonstrated that the total absorbance in the reference cuvette (-Zn) was higher than that in the test cuvette (+Zn), this was also borne out by

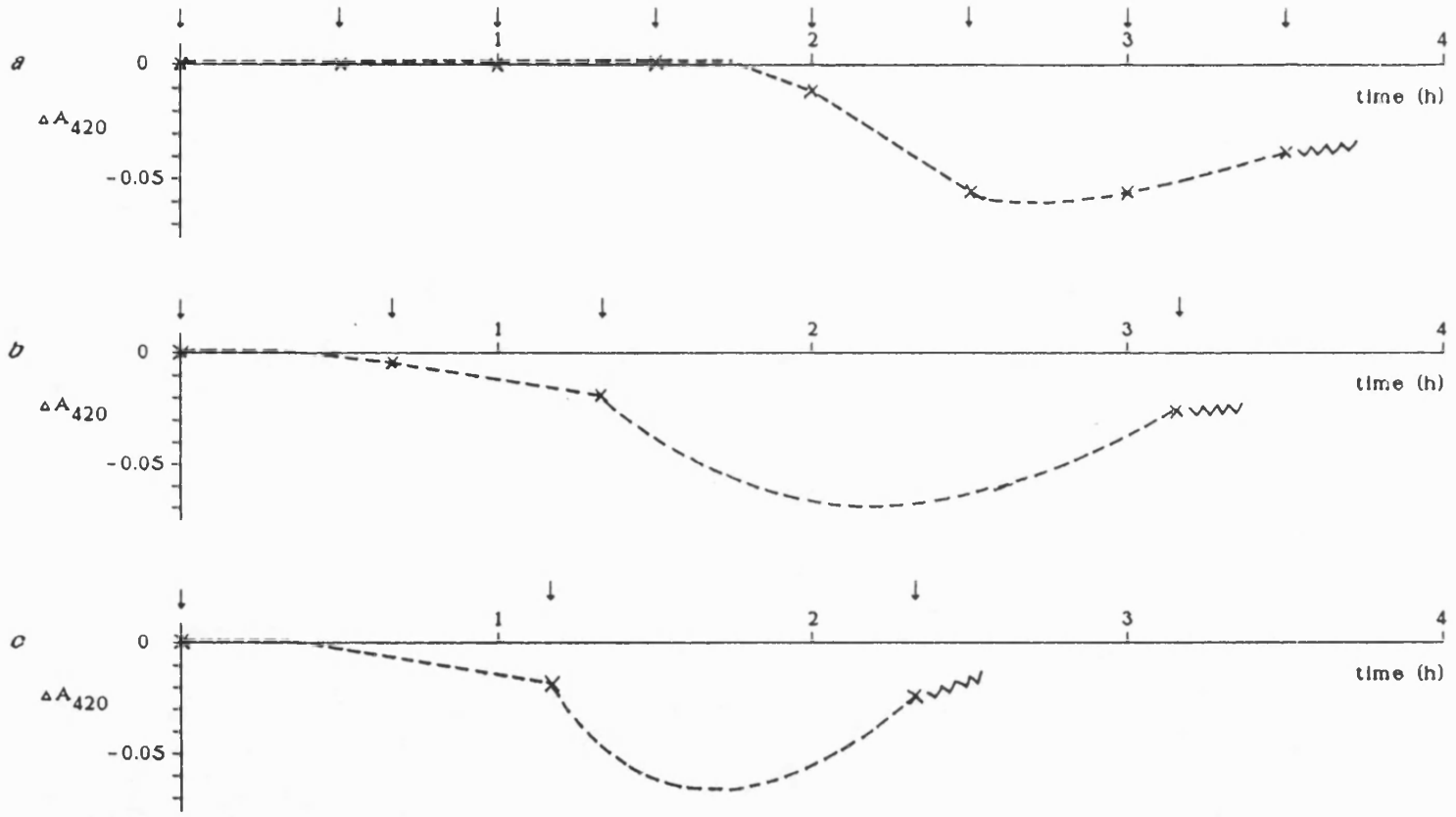

Figure 3.12 "Difference" traces for the protein-free controls in the presence and absence of zinc.

Final iron concentrations: *a* 0.44mM, zinc-with-iron, *b* 0.86mM, zinc-with-iron, *c* 0.95mM, zinc-before-iron.

Increments of ion solutions added at ↓, see table 3.3 for concentrations.

Table 3.5 A_{420} readings from the early stages of protein-free controls in the presence and absence of zinc.

increment number	0.44 mM Fe		0.86 mM Fe		0.95 mM Fe	
	+Zn with Fe	-Zn	+Zn with Fe	-Zn	+Zn before Fe	-Zn
3			0.289	0.350		
4	0.119	0.145			0.228	0.256
5			0.400	0.580		
6	0.236	0.305				

absolute absorbance readings taken during the course of the experiments. (These readings were taken for some of the earlier increments, before precipitation became a problem, at the end of the period allowed for the oxidation of each increment, see table 3.5.) Flocculation and precipitation of the products were extra reactions which did not take place in the presence of protein, therefore light scattering from the particles has to be considered. Also the reaction products were of different particle size, (see the results of the structural studies in section 3.3.2) and so would scatter light to different degrees. (The turbidity of a suspension is proportional to the number of scattering particles per unit volume and also to the square of the mass of the particles, Bull, 1964.) It was noted consistently during the experiments, that the reference cuvette (-Zn) would become cloudy before this was observed in the test cuvette.

Bearing in mind the above observations and reservations it is proposed that in these experiments zinc had its maximum effect on the rate of iron (II) oxidation at a concentration of between approximately 0.2 and 0.3 mM iron (0.02 and 0.03 mM zinc). Such a

conclusion may be possible if the disparity between the solutions in the cuvettes was not too great at this comparatively early stage of the reaction.

3 Reconstitution adding zinc before iron

The progress of iron oxidation in two apoferritin solutions (1 μM), one of which was pre-incubated with an increment of Zn^{2+} ions before each iron increment, was monitored at 420 nm. Figure 3.13 shows the uptake curves for two experiments; for the one with zinc the Zn^{2+} ions were incubated with the protein for 6-8 minutes before the next iron increment was added and the iron was allowed to oxidise for 50-60 minutes before the next increment of zinc was added, for the one without zinc, aliquots of distilled water were added as a control and the iron increments were added at 30 minute intervals. (The +Zn experiments required a longer time interval between increments due to the slower oxidation of iron in the presence of Zn^{2+} ions.) In a similar pattern to the uptake curves for the experiments with an apoferritin concentration of 0.5 μM where zinc was added with the iron (section 1 and figure 3.5, above), the curves were hyperbolic in shape and this shape tended to be more pronounced in the absence of zinc and in the early increments.

The Zn^{2+} was found to be an even more potent inhibitor of iron uptake by apoferritin if it was added before each iron increment, than when it was added along with the iron. The "difference" traces obtained in these experiments were of the pattern shown in figure 3.14 and features of the inhibition, measured from the traces are presented below.

The maximum effect of the zinc on the reaction under study was

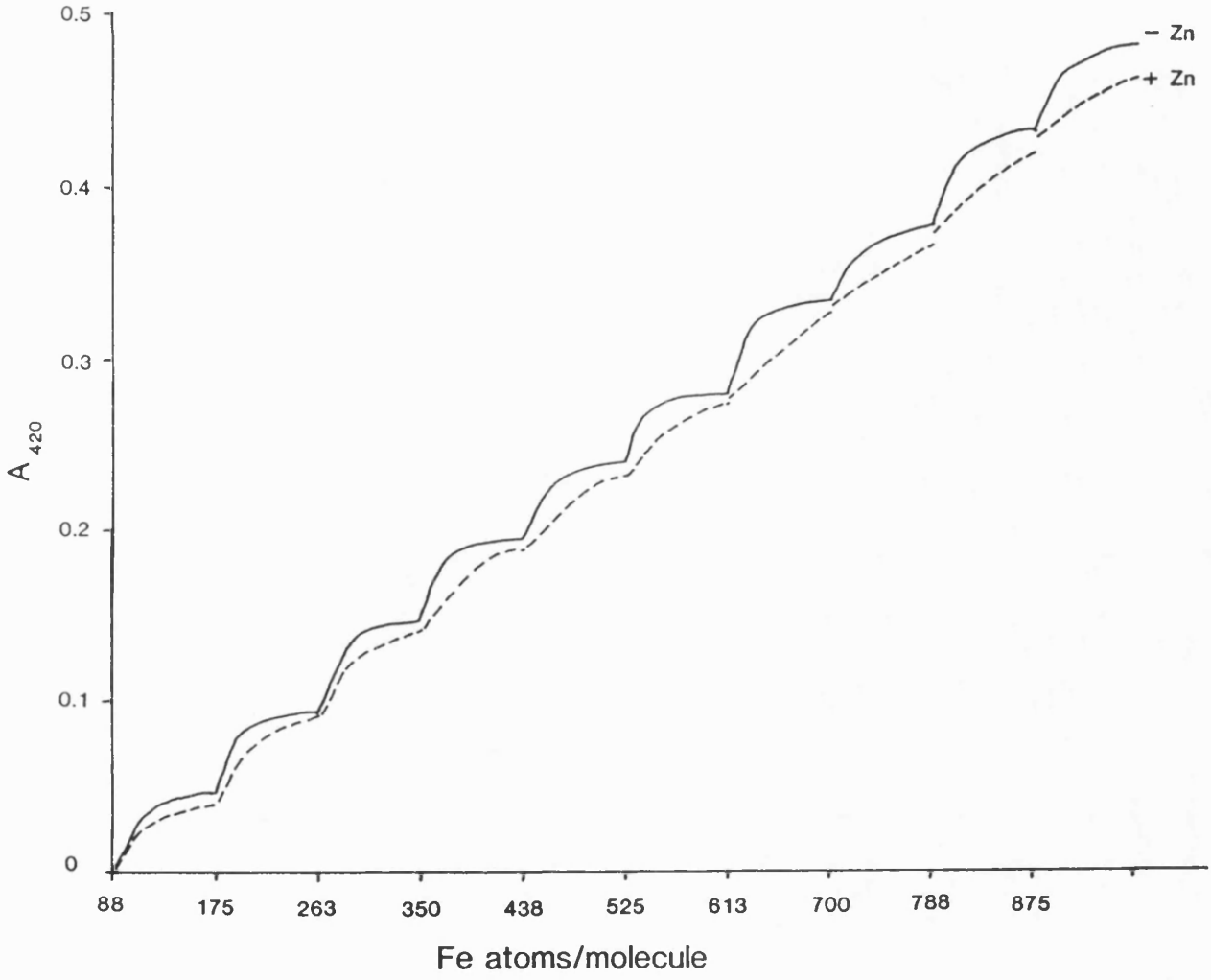

Figure 3.13 Zinc-before-Iron Graph showing the progress of reconstitution in the presence and absence of zinc for experiments at 1μM protein concentration, 0.95mM final iron concentration. For +Zn, zinc was added 6-8 minutes before each iron increment. The figure shows the shape of the reaction curves for 50 minutes (+Zn) and 30 minutes (-Zn) following the addition of each iron increment.

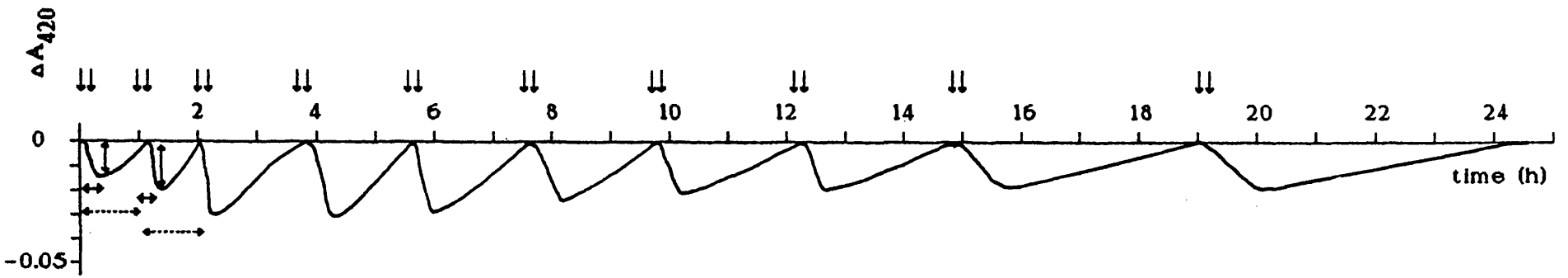

Key:- ⇊ increments of Fe + Zn added 6-8 minutes apart

↕ ΔA_{420} max

↔ time taken to reach ΔA_{420} max, t_{max}

⟷ time taken to regain original level, t_r

Figure 3.14 Zinc-before-Iron "Difference" trace for reconstitutions in the presence and absence of zinc. The graph shown was reproduced from a typical trace, (1μM protein concentration).

seen during the second and third increments when between approximately 175 and 263 iron atoms had been added per molecule, see figure 3.15. The plots followed a very similar pattern to those where zinc was added along with the iron (figure 3.9). Figure 3.15 illustrates the more potent nature of the inhibition by zinc when it was added before the iron in that the plots reach peaks at between -0.019 and -0.0315 absorbance units, whereas those for the experiments where zinc was added along with the iron (same protein concentration) peaked at between -0.0195 and -0.0235 absorbance units (figure 3.9).

The time taken for the difference trace to reach ΔA_{420} max. (t_{max}) after each iron increment is shown in figure 3.16. This figure shows that there was a tendency for t_{max} to decrease on the second increment, indicating a heightened effect of the zinc at this stage. However, after increment 5 there was a dramatic increase in t_{max}, which suggested, along with the decrease in ΔA_{420} max. that the zinc was less effective in the later stages of reconstitution.

The more potent inhibition of the reaction under study by zinc, when it was added before the iron is also illustrated in figure 3.17. In this figure the time taken for the trace to regain its original level (t_r) is plotted against the approximate number of iron atoms added per molecule. The results are shown for the experiments at 1 μM apoferritin in which zinc was added along with the iron and for these where it was added before the iron. As the figure shows, each increment of iron took longer to oxidise when the zinc was added before the iron.

The initial rate of iron oxidation again doubled on addition of the second iron increment in the absence of zinc. Where zinc had been added before the iron the initial rate did increase significantly, this was in contrast to the result for zinc added along with the

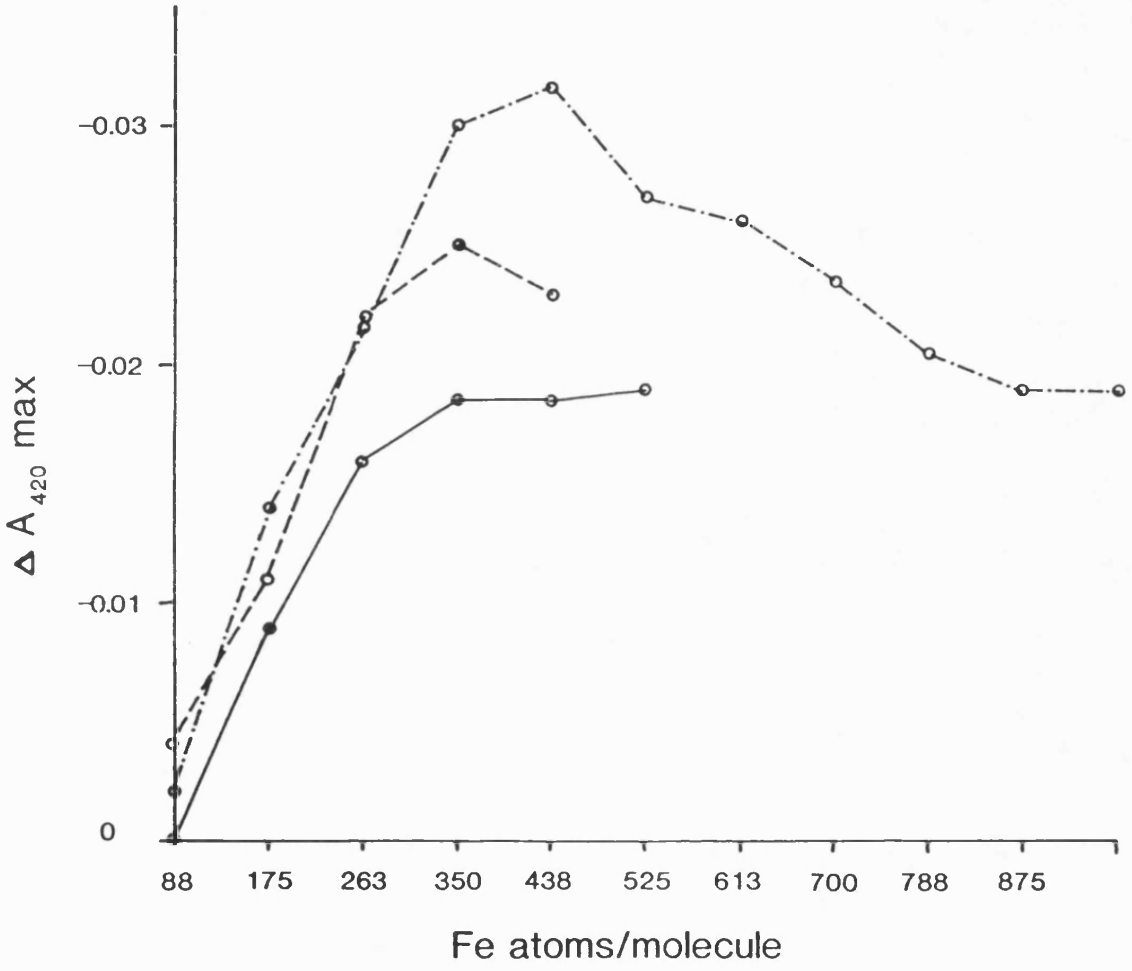

Figure 3.15 Zinc-before-Iron Graphs showing the maximum drop of the "difference" traces below their original level (ΔA_{420} max.) with each increment of iron. Data are shown from three experiments.

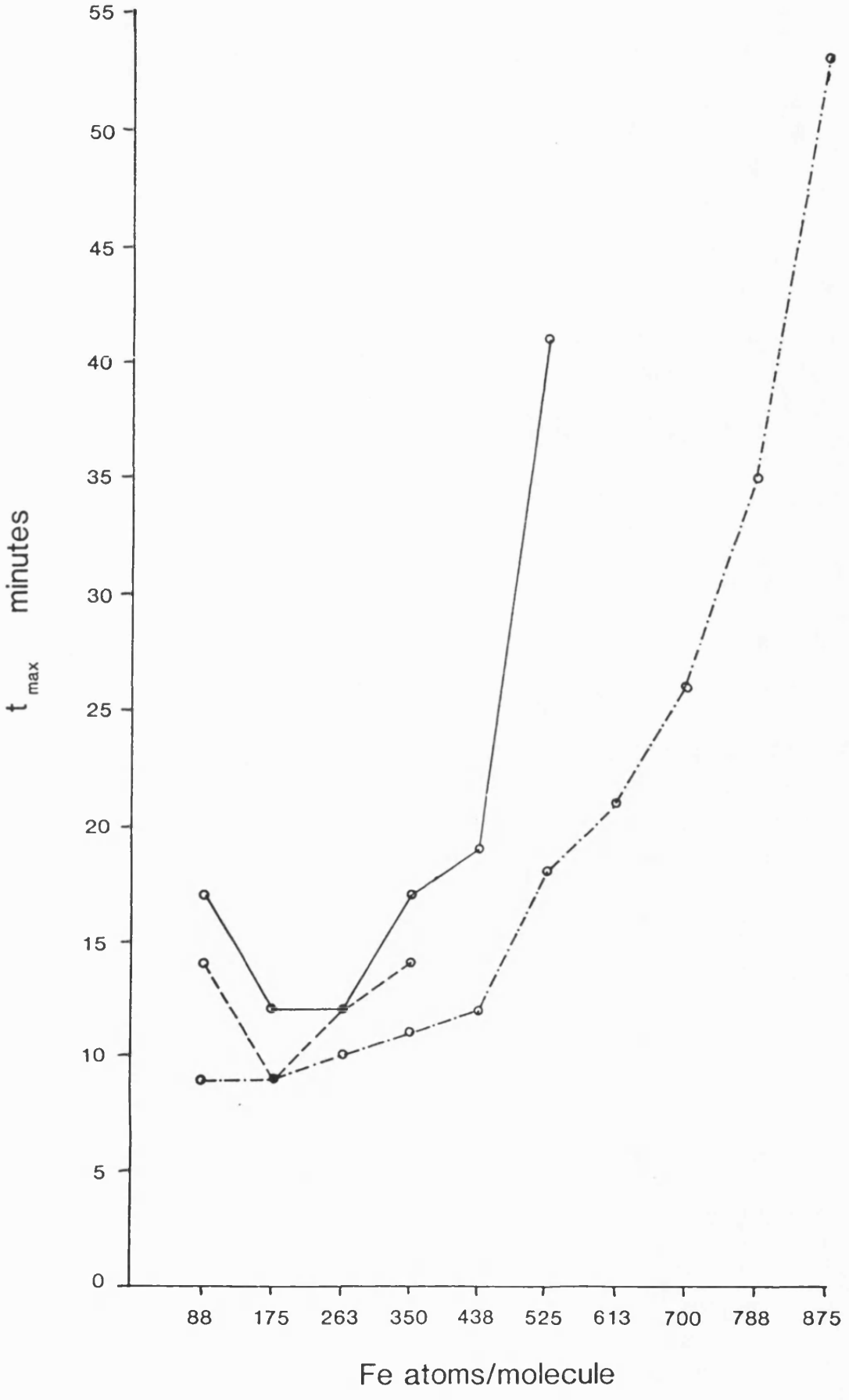

Figure 3.16 Zinc-before-Iron Graphs showing the time taken to reach ΔA_{420} max. (t_{max}) after the addition of each increment of ions. Data are shown from three experiments.

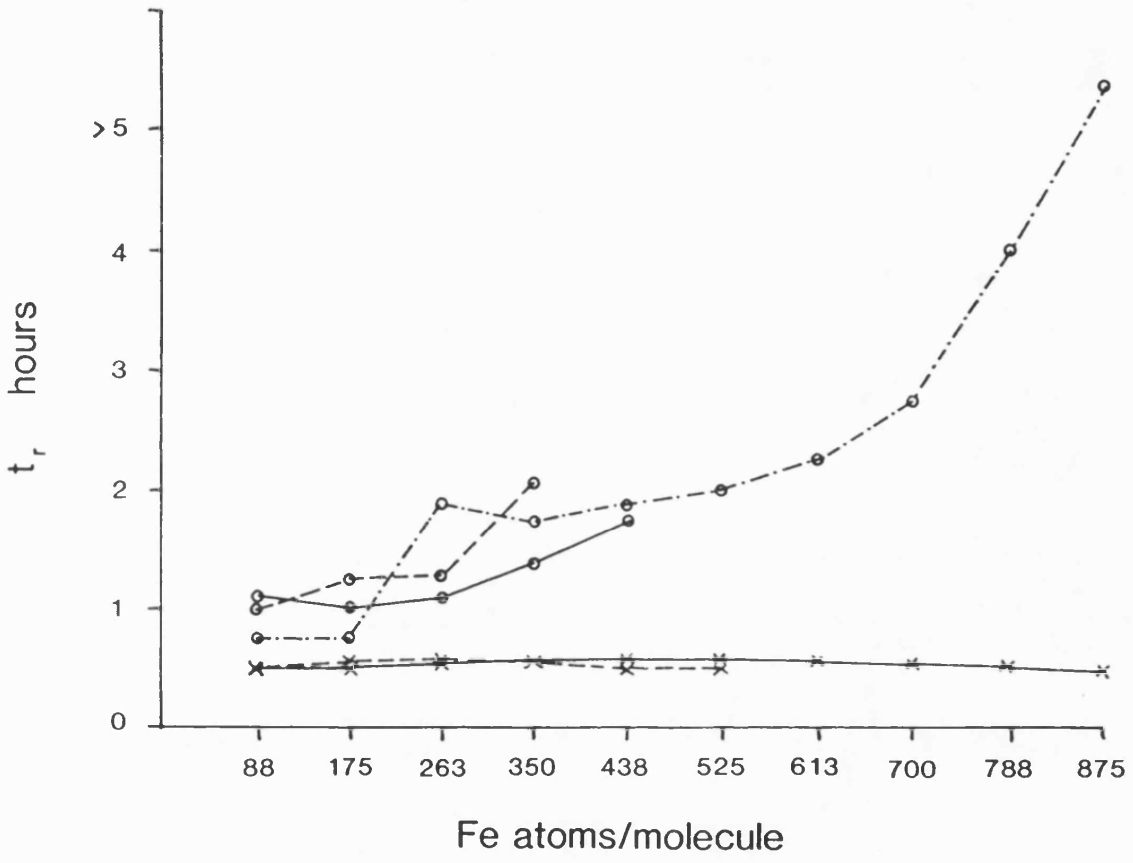

Figure 3.17 Graphs showing t_r after each iron increment for reconstitutions at 1μM protein concentration.
x--x zinc-with-iron, data from two experiments,
o--o zinc-before-iron, data from three experiments.

iron, where no increase in rate on addition of the second increment was seen. However, the rates in the presence of zinc were still well below those where zinc was not added. The initial rates are listed in table 3.4 and plotted in figure 3.7.

4 Protein-free control adding zinc before iron

Zinc had an effect on the rate of iron oxidation in the protein-free system during the first increment (0.12 mM iron concentration); the trace began to fall after about 22 minutes, see figure 3.12. The trace fell sharply after the addition of the second increment (0.24 mM), levelled off briefly and then began to rise, suggesting that the zinc had its maximum effect during the oxidation of this increment. After the third increment had been added (0.35 mM) the trace was unstable but moved up on the chart paper slightly, suggesting that the effect of the zinc was further diminished. Flocculation and precipitation in the cuvettes became a problem from then on.

Thus, as with the results from the experiments where iron and zinc were added together, the maximum effect of the zinc was again seen at concentrations of between approximately 0.24 and 0.30 mM iron (0.024 and 0.030 mM zinc). This conclusion is subject to the same reservations listed above for the other protein-free controls. A further consideration here was that the product formed in the presence of zinc was less crystalline than that formed in its absence, see section 3.3.2, and so should be regarded, to some extent, as a different product.

3.3.2 Structural Studies

1 Reconstitution adding iron and zinc simultaneously

Apoferritin was reconstituted to an average of 875 Fe atoms per molecule in the presence and absence of Zn^{2+} ions. The metal ions were added in a ratio of 10:1, Fe:Zn. After exhaustive dialysis of the ferritin against 0.15 M NaCl, this ratio was found by atomic absorption spectroscopy of five different samples to have decreased to between 33:1 and 74:1, which suggested that few zinc ions were strongly bound by the protein and that they were preferentially excluded from the core structure. Final iron loadings calculated from atomic absorption analysis varied between 705 and 827 iron atoms per molecule. Characterisation by TEM imaging showed no change in core morphology or size for samples reconstituted in the presence and absence of zinc. However, a slight difference between the samples was that the iron cores appeared to be slightly more well defined where they were reconstituted in the presence of zinc (plate 3.3). The mean core diameter for a typical +Zn sample was 4.71 nm, with a standard deviation of 0.58 nm. That for a typical -Zn sample was 4.87 nm (SD 0.68 nm). The particle size distribution was slightly narrower for the sample reconstituted in the presence of zinc, (see figure 3.18a&c).

Electron diffraction analysis showed that the cores were partially crystalline ferrihydrite and there was no difference in the crystallinity of the cores reconstituted in the presence of zinc compared with those reconstituted in its absence. (Table 3.6)

EdXa of the samples was carried out but the small amount of zinc present was not detectable by this method, (figure 3.19a).

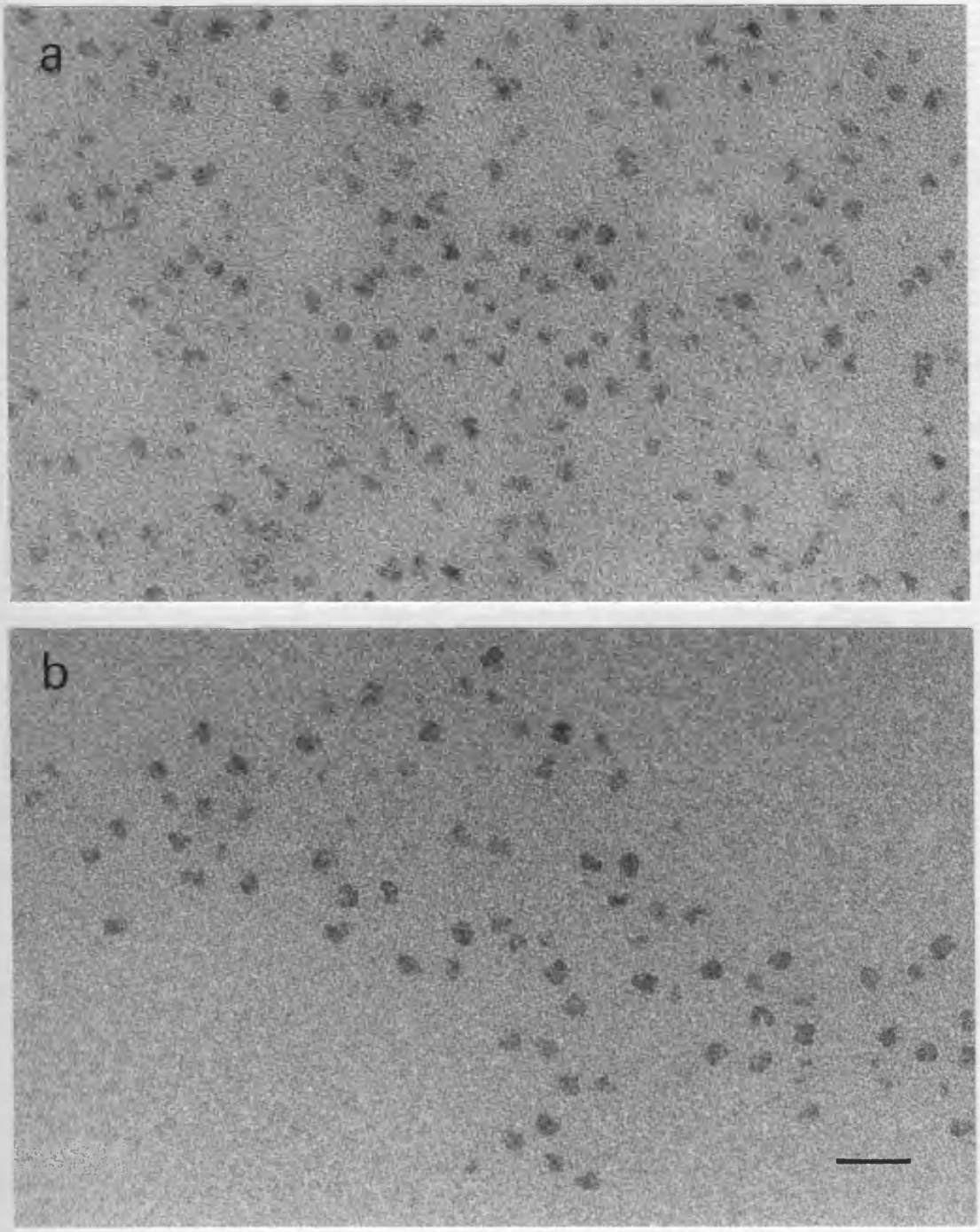

Plate 3.3 Electron micrographs of unstained ferritin reconstituted to ~875 Fe atoms/molecule. *a* -Zn, *b* +Zn, the zinc being added with the iron. Bar marker 20nm for *a & b*.

2 Protein-free control adding iron and zinc simultaneously

The oxidation products formed in these experiments, (at both concentrations) appeared in the electron micrographs as granular materials (plate 3.2), which, by electron diffraction, were a mixture of lepidocrocite and ferrihydrite. The presence or absence of zinc had no significant effect on the degree of crystallinity in the products (table 3.7). However, a noticeable effect when zinc was present was that the resultant particle size was much larger; the mean particle diameter was 10.75 nm, S.D. 2.22 compared with 4.96 nm, S.D. 1.04 and see figure 3.4 and plate 3.2. This increase in particle size suggested that the presence of Zn^{2+} ions inhibited nucleation; fewer nuclei formed which then grew to a larger final size.

Zinc ions were incorporated into the lepidocrocite/ferrihydrite mixture as shown by edXa (figure 3.19b) and atomic absorption spectroscopy, following exhaustive dialysis against 0.15M NaCl. Atomic absorption analysis of two samples, gave atomic ratios of 8:1 and 10:1, Fe:Zn. Therefore, the zinc is incorporated in a ratio closely similar to that in solution.

3 Reconstitution adding zinc before iron

Apoferritin was reconstituted to an average of 875 Fe atoms per molecule with Zn^{2+} ions added in a ratio of 10:1 (Fe:Zn) 6-8 minutes before each iron increment. Following exhaustive dialysis of the ferritin against 0.15M NaCl, the Fe:Zn ratio had decreased to 45 or 66 :1 (three samples assayed) which, as when the zinc was added along with the iron, suggested that the zinc ions were being preferentially excluded from the core structure and that few were strongly bound by the protein. The final iron loading for one sample was 812 iron

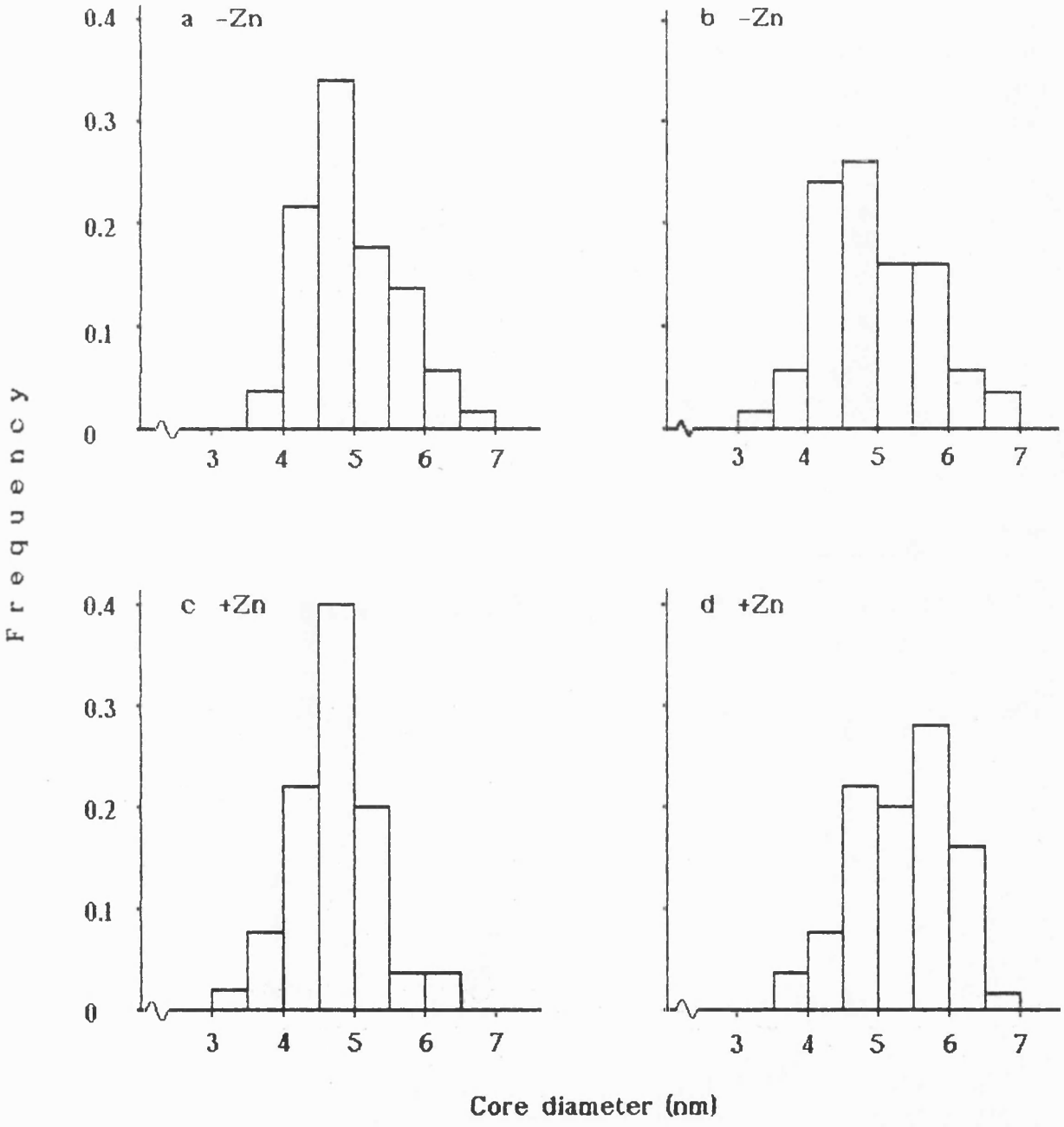

Figure 3.18 Particle size distributions for ferritin reconstituted to approximately 875 Fe atoms/molecule in the presence and absence of zinc. *a* & *c* : *a* control, *c* zinc added with iron, *b* & *d* : *b* control, *d* zinc added before iron.

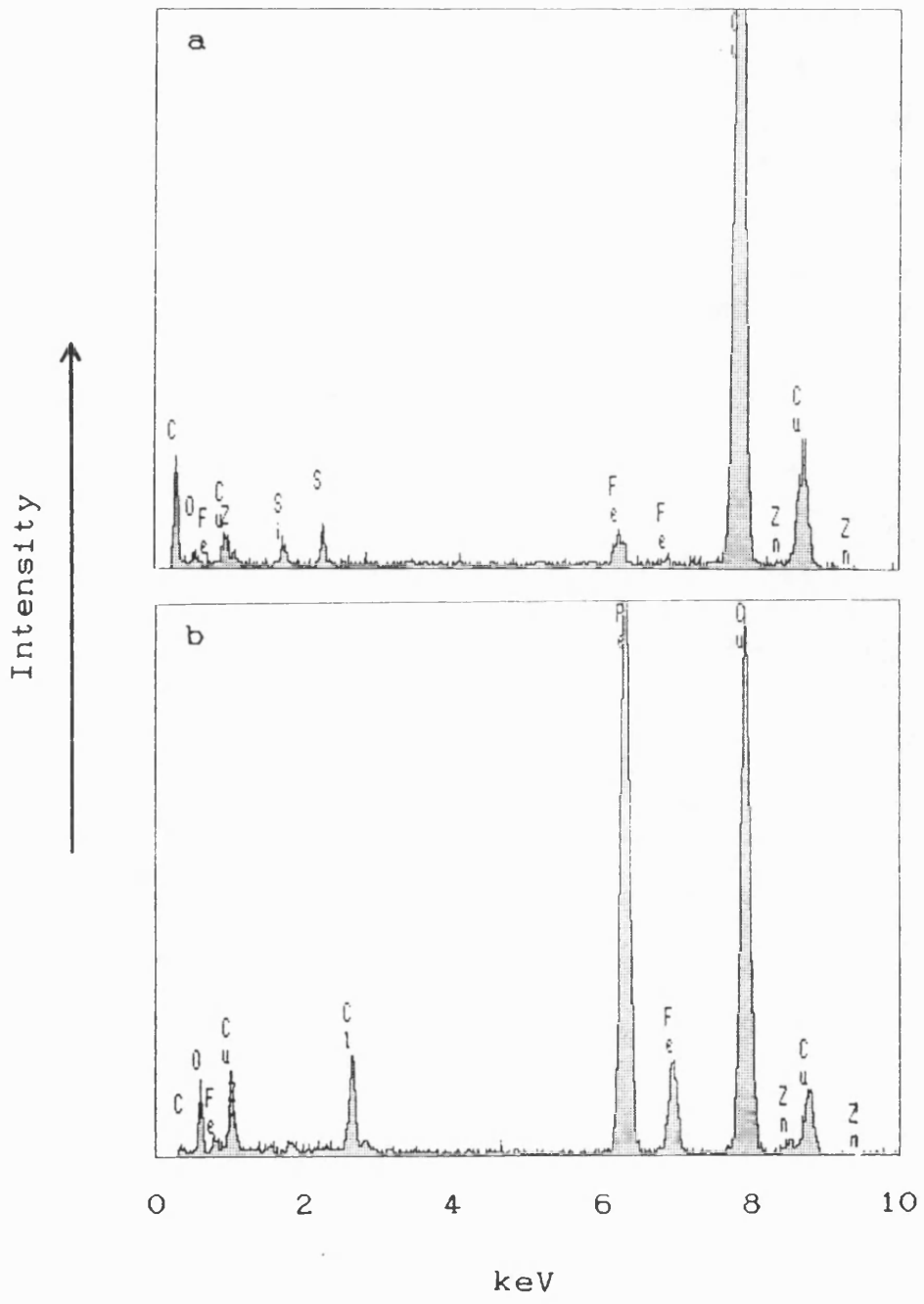

Figure 3.19 EdXa spectra. *a* ferritin reconstituted with iron and zinc (10:1, Fe:Zn), showing that the small amount of zinc present was not detectable by this method. *b* zinc-with-iron protein-free control. The zinc could just be detected in these samples by this method. The Cu peaks arise from the electron microscopy grids.

Table 3.6 Electron diffraction analysis of ferritins reconstituted in the absence and presence of zinc. Zinc being added simultaneously with iron.

-Zn		+Zn	
d(Å)	I	d(Å)	I
2.48	S	2.48	S
2.34 }	SBB	2.33 }	SBB
1.98 }		1.99 }	
1.54	W	1.50	W
1.50	S	1.45	S

Table 3.7 Electron diffraction analysis of oxidation products formed in the protein-free controls of the simultaneous Fe:Zn reconstitutions.
F = ferrihydrite, L = lepidocrocite.

-Zn		+Zn		assignment
d(Å)	I	d(Å)	I	
3.30	W	3.27	W	L
2.49	S	2.48	S	F/L
2.21	S	2.23	M	F
1.98	M	1.99	M	F/L
1.73	M	1.75	W	F/L
1.51	S	1.55	M	F/L
1.45	S	1.46	S	F
1.22	W			L
1.04	W			L
0.85	W	0.85	W	L

atoms/molecule. TEM showed no difference between these samples and those reconstituted in the absence of zinc as regards core morphology, but again the cores of the +Zn sample appeared to be more well defined than those of the -Zn sample, (plate 3.4a&b). The mean core diameter for the sample without zinc was 4.92 nm, with a standard deviation of 0.78 nm, whereas that for the sample with zinc was a little larger at 5.33 nm (SD 0.74 nm). The ranges of core diameters measured were 3.44 - 6.60 nm and 3.69 - 6.99 nm, respectively. The particle size histograms for both samples are shown in figure 3.18b&d; the frequencies between 5 and 6.5 nm for the +Zn sample are consistently higher than those for the sample without zinc.

Electron diffraction patterns from these samples revealed no difference in core structure between those reconstituted with and without zinc, they were quite well crystalline ferrihydrite. (Table 3.8) These cores were slightly more crystalline than those reconstituted in the experiments where iron and zinc were being added simultaneously; the diffraction patterns had five diffraction lines rather than four.

EdXa was carried out on these samples but, as above, the zinc was not detectable by this method.

4 Protein-free control adding zinc before iron

In this set of experiments the iron oxide formed in the absence of apoferritin was lepidocrocite, rather than a mixture of lepidocrocite and ferrihydrite. The material appeared to be thin plates or lamellae that had crumpled as they dried down onto the electron microscopy grids, (see plates 3.5 - 3.9). This morphology for synthetic lepidocrocite has been reported previously by Mackenzie

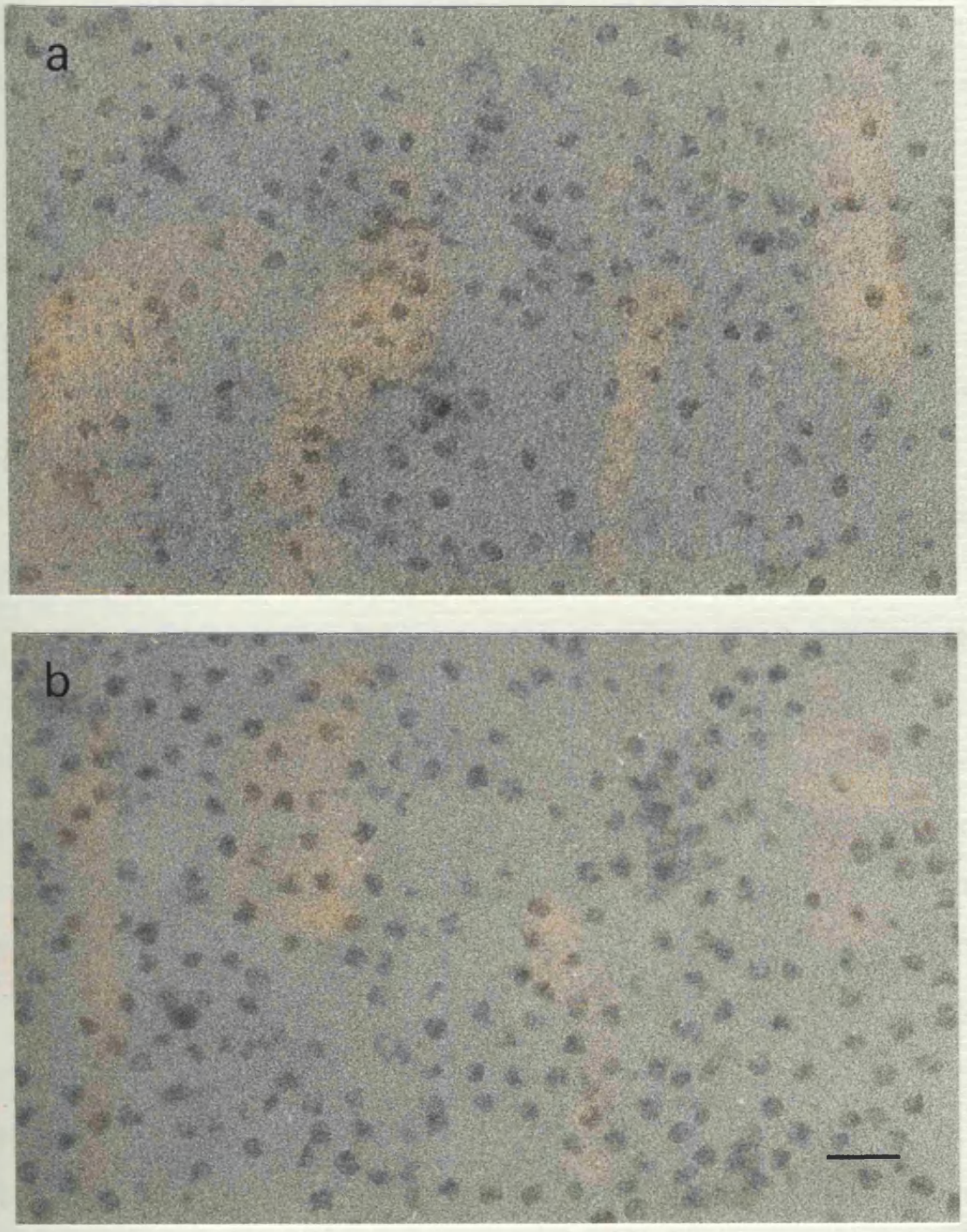

Plate 3.4 Electron micrographs of unstained ferritin reconstituted to ~875 Fe atoms/molecule. *a* -Zn, *b* +Zn, the zinc being added before the iron. Bar marker 20nm for both micrographs.

et al. (1971). The edges of the lamellae were irregular and those formed in the absence of zinc were clearly faceted. The electron micrographs also showed that the particles which had formed in zinc free solution were thicker than those formed in the presence of zinc. Electron diffraction analysis revealed that they were also more crystalline, since more diffraction rings could be seen on the patterns, (see table 3.9) and the rings were sharper. That the lamellae of lepidocrocite formed in the absence of zinc were thicker than those formed in its presence, suggested that the zinc was causing some inhibition of crystal growth in one direction (possibly along one crystallographic axis).

Due to the nature of the particles formed it was not possible to make an accurate assessment of overall particle size. However, measurements taken of 23 particles of two samples each, with and without zinc, (measuring the largest dimension across the particles on the thicker "spine-like" areas) showed again that the particle size was increased where zinc was present in solution, (figure 3.20).

Some zinc was incorporated in the lepidocrocite as shown by edXa (figure 3.21a&b) and atomic absorption analysis, the latter of which gave Fe:Zn ratios of 40:1 and 45:1 on two separate samples. In contrast therefore, to the protein-free system where iron and zinc were added together, the zinc was partially excluded from the crystal structure.

Plate 3.5 Electron micrograph of the crumpled lepidocrocite lamellae formed in the protein-free controls of the zinc-before-iron experiments. Those shown here were formed in the absence of zinc. Bar marker 200nm.

Plate 3.6 Higher magnification electron micrograph of the lepidocrocite lamellae formed in the absence of zinc. Bar marker 100nm.

Plate 3.7 Electron micrograph of what may be a single particle of lepidocrocite, formed in the absence of zinc. Bar marker 100nm.

Plate 3.8 Electron micrograph of the crumpled lepidocrocite lamellae formed in the presence of zinc, in the protein-free controls of the zinc-before-iron experiments. Bar marker 200nm.

Plate 3.9 Higher magnification electron micrograph of the lepidocrocite lamellae formed in the presence of zinc. Bar marker 100nm.

Table 3.8 Electron diffraction analysis of ferritin reconstituted in the absence and presence of zinc. Zinc being added before iron.

-Zn		+Zn	
d(Å)	I	d(Å)	I
2.53	S	2.53	S
2.30	M	2.27	M
1.98	M	2.01	M
1.54	W	1.53	W
1.49	S	1.48	S

Table 3.9 Electron diffraction analysis of oxidation products formed in the protein-free controls of the Fe:Zn reconstitutions, Zn being added before Fe.

γ-FeOOH standard			-Zn		+Zn	
d(Å)	I	hkl	d(Å)	I	d(Å)	I
3.29	90	120	3.29	S	3.27	SB
2.47	80	031	2.48	S	2.50	MB
2.36	20	111	2.36	M	2.33	
2.09	20	131, 060	2.09	VW		
1.937	70	051, 200	1.94	S	1.91	S
1.848	20	220	1.86	W		
1.732	40	151	1.73	M	1.67	W
1.535	20	002	1.54	S	1.53	S
1.389	10	122	1.38	M	1.39	W
1.261	10	091, 320	1.27	W		
1.213	10	280				
1.196	20	022, 191	1.20	M	1.20	M

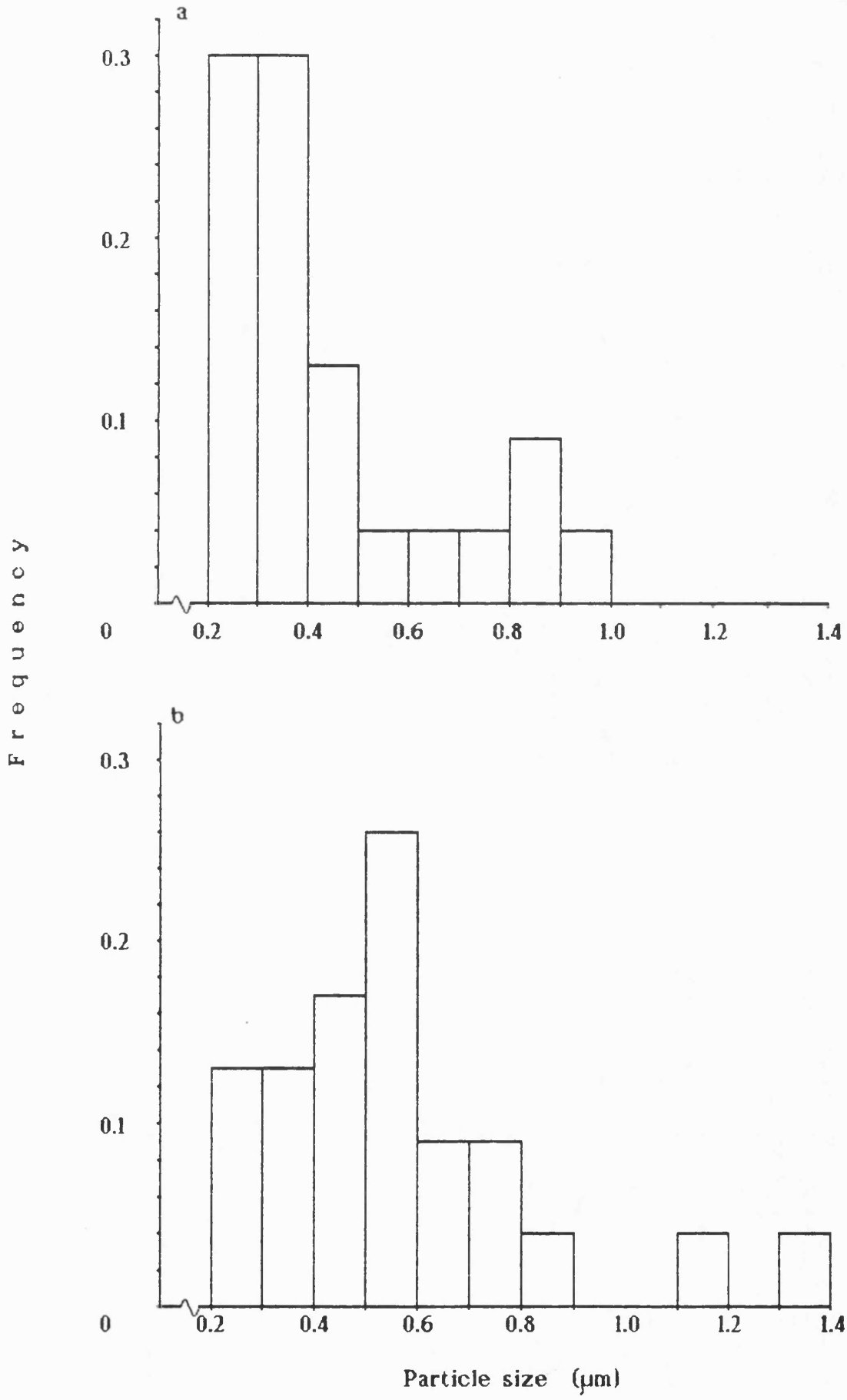

Figure 3.20 Particle size distributions for lepidocrocite lamellae formed in the Zn-before-Fe protein-free controls. a -Zn, b +Zn.

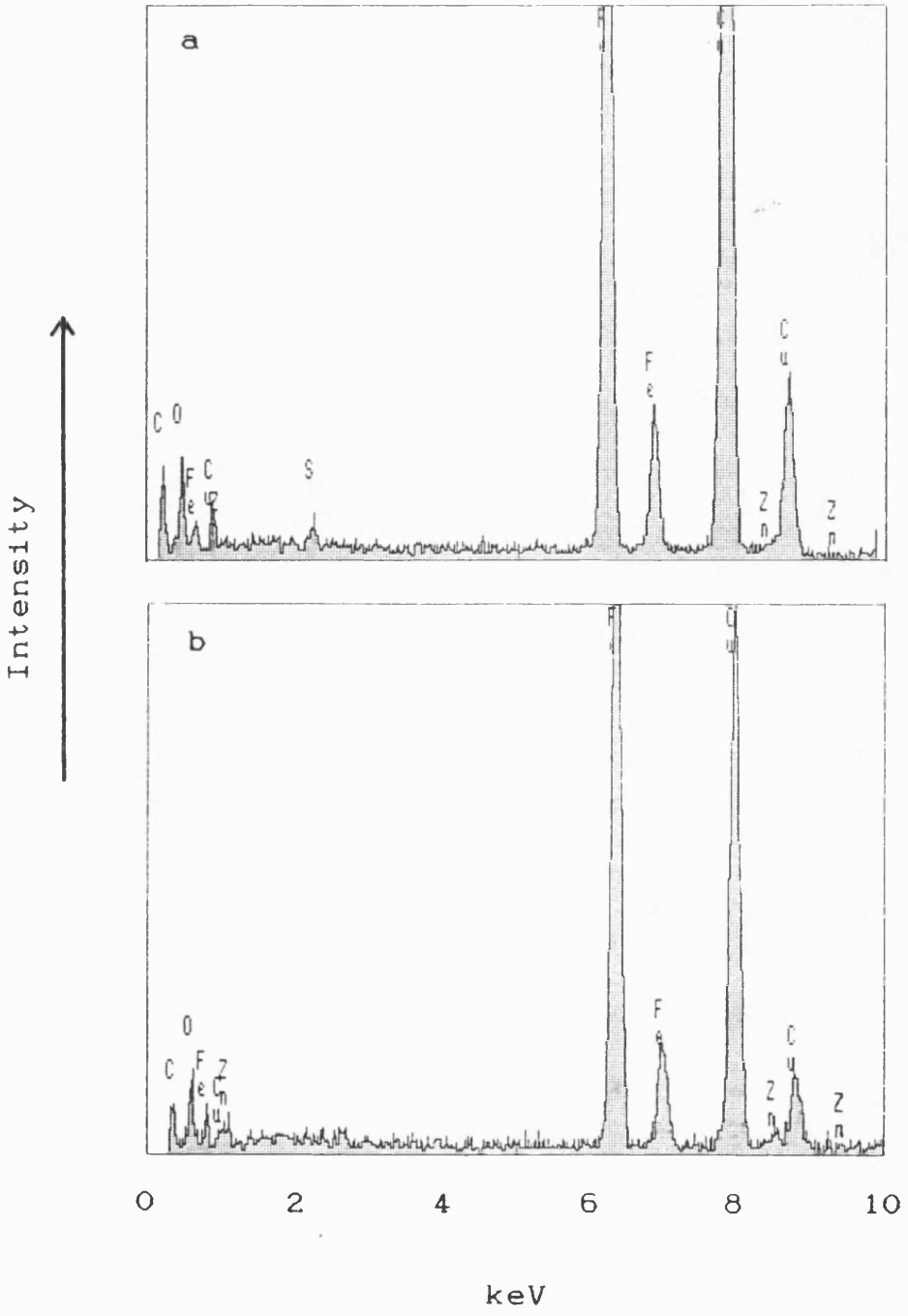

Figure 3.21 EdXa spectra of the lepidocrocite lamellae formed in the zinc-before-iron protein-free controls. *a* -Zn, *b* +Zn.

3.4 DISCUSSION

The results of the reconstitution experiments with horse spleen apoferritin presented in this chapter have shown that:

a) apoferritin catalyses iron oxidation,

b) the ferrihydrite core structure is established in a poorly crystalline form by ~200 Fe atoms/molecule and that the crystallinity improves as the cores grow,

c) zinc ions inhibit iron uptake by apoferritin and that the major effect of the Zn^{2+} ions is to inhibit nucleation of the ferrihydrite core.

Features of the structural and kinetic studies with apoferritin and the protein-free controls are discussed below and in the light of these, a size for the nucleation cluster inside the apoferritin cavity is proposed.

3.4.1 Iron reconstitution

a) Structural studies

At the lowest iron loading used (200/molecule) small cores were seen in the electron micrographs and not "iron staining" of the inside of the protein cavities, which would have been visible as rings. This suggested that at this stage of core growth a clustering of the Fe^{3+} and other ions, or nucleation of ferrihydrite, had occurred, at one site. Smaller clusters of the oxidation product may have formed at other sites within the cavity, which then migrated toward each other to form the particles seen. If this were the case it precludes the binding of such clusters to more than one site in the cavity. However, the formation of just one cluster or nucleus in each cavity may be more likely since, once such a cluster had formed it would compete successfully with any other potential sites for the

newly oxidised Fe^{3+} in the cavity, because it would be kinetically more favourable for the Fe^{3+} to add on to an existing cluster than to begin to form a new one. The possibility that the cores seen at this low loading were drying artefacts was unlikely since they exhibited some structure by electron diffraction, based on that of ferrihydrite.

At approximately 875 iron atoms/molecule the cores were irregular in shape which suggested that the mechanism of core growth was one of polymerisation at many edge sites, rather than one of a more classical crystal growth model. For the latter, where growth occurs in layers across specific faces, growth would be very regular and the resulting edges would be smooth. A polymerisation model for growth disagrees with the approach taken by Macara *et al.* (1972), where they assumed that the core grew from one point on the edge of the cavity, in layers across the cavity.

When 3500 iron atoms had been added per molecule the cores exhibited more regular shapes. This was probably a result of the size and shape constraints imposed on the larger cores by the protein cavity. Also, the mechanism of growth may have changed to one more like crystal growth, resulting in a more ordered structure with smoother edges. It was observed that a number of cores were square in shape; a roughly cubic morphology for the cores of full ferritin was suggested by the X-ray diffraction studies of Fischbach *et al.* (1969). In a TEM study of unstained native ferritin Massover (1985a) noted that some cores showed one or more straight edges, or a perimeter having some sharp angles. He proposed that such cores were being viewed parallel to a face or facet of the crystallite.

The ferrihydrite structure of the cores was established at ~200 iron atoms/molecule as shown by the 2 line electron diffraction patterns. These two lines, at 2.50 and 1.51Å, are correlated to the hexagonally close packed oxygens in the ferrihydrite (Towe & Bradley, 1967). The absence of the other diffraction lines suggested that the Fe^{3+} ions were all disordered. The ferrihydrite structure was apparently kinetically stable as a particle of around 3 nm across, and it is important to note again here that a core of 200 iron atoms only represents 40 unit cells of ferrihydrite. At the higher iron loadings the ferrihydrite structure was more clearly established; at ~875 iron atoms/molecule (175 unit cells) the diffraction patterns had 4 lines and at ~3500 iron atoms/molecule (700 unit cells) the diffraction patterns had 5 lines. An increase in particle size allowed more long range order in the cores, hence the greater crystallinity observed.

The oxidation product formed in the protein-free controls of these experiments (and those where zinc was added with the iron) exhibited a grain-like morphology. Synthetic lepidocrocite particles usually show acicular or crumpled lamellar morphologies, so this morphology of the mixed ferrihydrite/lepidocrocite product may represent a form of "proto-lepidocrocite".

b) Kinetic studies

The results of these experiments confirmed the catalysis of iron oxidation by apoferritin under the conditions used. Oxidation of the Fe^{2+} did occur in the absence of the protein, but by monitoring the appearance of the oxidation product in the presence and absence of

the protein at the same time, using the same stock solutions, the protein's catalytic effect was clearly demonstrated.

Hyperbolic uptake curves were observed after the addition of each increment of iron to the buffered protein solution. These results were in agreement with the findings of Macara *et al.* (1972 & 1973a), for their experiments at comparable iron concentrations, despite the differences in the other reconstitution conditions. (Macara *et al.* employed potassium iodate and sodium thiosulphate as an oxidant, an imidazole buffer at pH 7.45 and a higher protein concentration.) Macara *et al.* (1973a) concluded that such uptake curves were indicative of the protein's catalysis of the reaction and they proposed that binding of ferrous iron or $(Fe^{II}OH)^{+}$ to sites on the protein was an essential part of the protein's role. Once some hydrated Fe(III) was present in the cavity, binding sites on the forming core would also be available, augmenting the catalysis of the process.

The role of apoferritin in the catalysis of iron oxidation and the process of iron uptake is discussed more fully in chapter 4 in the light of work on homopolymers of human H and L ferritin subunits and human H-homopolymers which had changes in their primary structure at certain points in the sequence. The results of such studies have provided more detailed information as to which amino acids, at which positions in the protein's three dimensional structure, are directly involved in ion binding during apoferritin reconstitution. In addition to these very specific features, the quaternary structure of the protein may also enhance the rate of reaction by increasing the effective concentration of Fe^{3+} due to spatial localisation of these ions within the apoferritin cavity.

In the protein-free controls for these experiments the reaction

curves were linear rather than hyperbolic. This again indicates that the protein has an active role in the reaction.

In the control experiments with the "non-specific" protein bovine serum albumin, catalysis of the formation of the oxidation product, mediated by apoferritin, was not observed. That no precipitate was formed in these experiments is in agreement with the findings of Macara *et al.* (1972 & 1973c). Oxidation of the Fe^{2+} probably occurred quite readily in this system due to the conditions of pH and oxygen availability, but presumably the iron would have been bound by the BSA and the formation of oxo- and hydroxo-bridged iron clusters may have been inhibited for some hours.

3.4.2 Iron and zinc reconstitution

a) Structural studies

In order to discuss the results from the iron and zinc reconstitutions the effect of the zinc in the protein-free controls needs to be considered first, since it has a bearing on both the structural and kinetic studies. The very noticeable effect of zinc on particle size in the protein-free controls suggested that the major influence of the Zn^{2+} ions was to inhibit nucleation. The zinc ions, by binding to the forming clusters of Fe^{3+}, OH^- and H_2O caused fewer crystal nuclei to form and therefore, a larger final particle size. The Zn^{2+} ion is intermediate in size between Fe^{2+} and Fe^{3+}, the ionic radii (pm) in descending order being: Fe^{2+} 75, Zn^{2+} 70, Fe^{3+} 61. By binding to the surface of the forming crystals the zinc ions may prevent or diminish further growth from or around those sites, especially if the mechanism of growth is one involving the oxidation of Fe^{2+} to Fe^{3+} at sites on the surface of the particle.

In the granular ferrihydrite/lepidocrocite product formed in the experiments where the iron and zinc were added together, the Zn^{2+} ions may have been bound at surface sites and in discontinuities within the particles. It was noted that the lepidocrocite lamellae, (formed in the zinc-before-iron protein-free controls) were thinner and less well crystalline when formed in the presence of zinc. Here the Zn^{2+} ions may have caused inhibition of growth along the *a* axis, by binding between the layers of octahedra, as illustrated in figure 3.22. It may be assumed that there was inhibition of growth along this axis since the plane of the layers in the lepidocrocite crystal structure would correspond to the plane of the lamellae observed in the TEM. The poorer crystallinity of the +Zn lamellae may also be attributed to zinc binding at such sites, because this would disrupt the hydrogen bonding between the layers, resulting in the number of layers being reduced and possibly, in mis-alignment of layers above or below.

In the presence of apoferritin, where zinc was added either with or before each iron increment, the resulting cores appeared to be more well defined and this was attributed to the slower kinetics of the reaction in the presence of zinc.

When zinc was added before the iron the resultant mean core diameter increased from 4.92 to 5.33 nm. This may have resulted from a partial inhibition of nucleation by the zinc ions which caused fewer cores to nucleate in the early stages of the experiment. Those that did nucleate would have grown to a larger final size at the expense of other cores. The decrease in the overall rate of reaction would also have contributed to the formation of fewer and therefore larger cores.

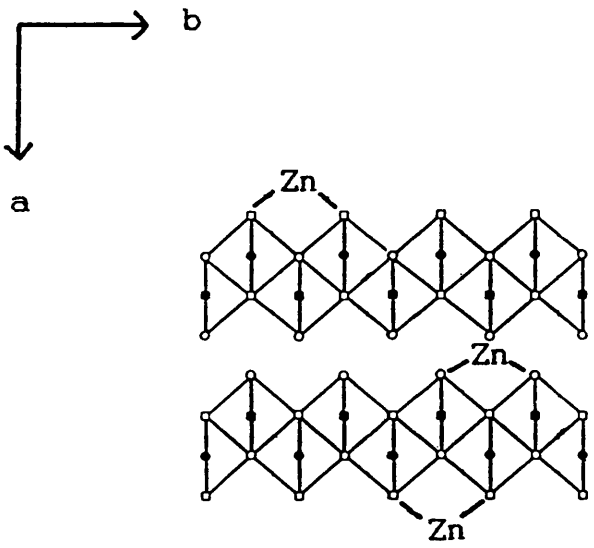

Figure 3.22 Diagram of the structure of lepidocrocite showing possible binding sites for Zn^{2+} between the layers of octahedrally coordinated iron. Projection along [001], (●) Fe at z = 0, (■) Fe at z = ½, (○) O at z = 0, (□) O at z = ½.

There was no difference in the degree of crystallinity of the ferrihydrite in the cores of samples reconstituted in the presence or absence of zinc, but those reconstituted in the slower experiment (where zinc was added before the iron) were more crystalline than those in the zinc with iron reconstitutions. This increase in crystallinity is another effect of the slower kinetics of the reaction.

Despite the presence of zinc ions and their effect in slowing down the kinetics of the reactions of iron oxidation and uptake by apoferritin, the product formed inside the protein was still ferrihydrite and not one of the more thermodynamically stable iron oxy-hydroxides such as goethite or lepidocrocite (α- and γ-FeOOH, respectively). This suggested that either the kinetics of the reaction were still too fast to permit the formation of the more thermodynamically stable iron oxy-hydroxides, or the protein prevented the formation of a more stable and ordered product, perhaps by the constraints of the reaction volume, or the geometry and nature of the ligands lining the cavity.

The zinc ions present during reconstitution, added either with or before each iron increment, were largely lost from the samples following exhaustive dialysis against 0.15 M saline. Only between 12 and 25% of the zinc remained bound. Presumably, only the zinc ions inside the cavity (and possibly, in the channels) would remain bound. Any ions very accessible to solvent would be removed by the dialysis regime. That the amount of bound zinc was less than that added suggested i) that the zinc ions were restricted from entering the cavity by the protein, or ii) they were segregated at the surface of the iron oxide core and then mostly lost. If the zinc ions were

restricted from entering the cavity, then, by implication, only a relatively few ions could have been involved in the inhibition of the reconstitution reaction.

In the protein-free controls where the zinc was added along with the iron, the zinc ions were not excluded from the ferrihydrite/ lepidocrocite product formed. This observation might suggest that the segregation of Zn^{2+} to the core surface in the ferritin reconstitutions was unlikely. However, in the protein-free control experiments where the zinc was added ahead of the iron, the zinc ions were largely excluded from the product: a lamella form of lepidocrocite. In these experiments the increments were added at longer time intervals, therefore the concentrations of the reactants increased more slowly. This would have led to slower reaction kinetics and accounts for the purer, more thermodynamically stable form of iron oxide being formed. The slower rate of formation may also account for the zinc being largely excluded from the crystal lattice; some of the bound Zn^{2+} could have been displaced by iron over the longer time scale. Or, perhaps the more ordered structure of the oxide itself led to the partial exclusion of the larger zinc ions. It is worth noting here that Zn^{2+} is softer than Fe^{2+} and Fe^{3+} in the Hard/Soft, Acid/Base classification and would therefore be expected to form less stable bonds than the iron species, with the hard oxygen ligands available in the iron oxide structures.

A greater degree of crystallinity in the oxidation products was achieved in the protein-free systems compared with those containing protein. This can be attributed to the slower rate of oxidation in the absence of apoferritin. Also, the spatial constraints of the

protein cavity may have prevented the stabilisation of the unit cell and usual morphologies of lepidocrocite.

b) Kinetic studies

In the experiments where zinc was added along with the iron, the maximum effect of the zinc was seen on the addition of the second and third increments, at both of the concentrations used. Where the zinc was added before the iron, the zinc's maximum effect was again seen during the oxidation of the second and third increments. The main effect of the zinc therefore, was dependent upon the stage of core loading which was between 175 and 263 iron atoms/molecule. This observation, together with results from the structural studies, suggested that nucleation was occurring at this stage in core development.

The presence of binding sites for Zn^{2+} ions on horse spleen apoferritin has been demonstrated by Macara *et al.* (1973b). These workers found that there were two classes of site and that those of the second class were probably located on the exterior of the assembled molecule. They also proposed that 1 or 2 zinc ions per subunit may be bound by the first class of site and 3 or 4 per subunit may be bound by the second class. This gives a maximum of 6 per subunit, or 144 per molecule. Macara *et al.* also noted that the Zn^{2+} was acting as a competitive inhibitor of the iron.

In the present study, the observation that zinc inhibited Fe^{2+} oxidation right from the very beginning of the experiments in the presence of apoferritin but not quite so early in the protein-free system indicated that the zinc was indeed interacting with the

protein in the reconstitution experiments. Also inhibition was seen for every increment. It is possible that the Zn^{2+} was binding in the intersubunit channels of the protein and also at the ferroxidase sites, so slowing the entry and oxidation of the Fe^{2+}. However these effects should have been independent of core loading. (The role of the ferroxidase site in these experiments may have been limited since horse spleen ferritin, 15% H-subunit, 85% L-subunit, only contains an average of 3.6 ferroxidase sites per molecule.) If the zinc was also binding to the forming core, inhibition would still be expected during each increment, but the extent of the inhibition may vary for each increment due to a dependence on the stage of core growth; this would seem to be the case here.

Where the zinc was added before the iron it had first access to binding sites both on the protein and on the growing core, this may explain why the inhibition was more potent and more prolonged.

Consider now the observations of the initial rates of reaction for the first few increments. In the absence of zinc the rate doubles for the second increment but then remains the same. This may be a result of several factors, two are noted here:

i) the oxidation product formed acts as an autocatalyst, this is true but one would expect a further increase in rate with subsequent increments as the core grew larger

ii) the protein is "activated" by the binding of Fe^{2+} and/or Fe^{3+} at specific and therefore saturable sites. All such sites are filled by the iron in the first increment, (therefore there must be less than approximately 88 per molecule or 3.6 per subunit), so no further activation can be achieved by subsequent increments.

The presence of zinc abolishes the increase in initial rate upon

the addition of the second increment for the experiments where zinc was added with the iron. Furthermore, it decreases the initial rate right from first increment for both sets of experiments (where zinc was added with and before the iron). These observations suggest the following:

i) the zinc must be binding to the protein and competing with the iron for, and thereby blocking, the "activation" sites. Could such activation sites be the few ferroxidase sites, the proposed nucleation site at the dimer interfaces, channel sites?

ii) the zinc is also binding to the growing core, diminishing its autocatalytic activity.

In the protein-free controls the presence of zinc did not have an effect on the rate of iron oxidation immediately, whether it was added with or before the iron, but the pattern of inhibition was broadly similar for all the experiments with the major effect of the zinc occurring at concentrations between 0.2 and 0.3 mM iron (0.02 and 0.03 mM zinc).

In the experiments carried out at a final iron concentration of 0.44 mM the effect of the zinc was first noticeable after 15 minutes following the addition of the fourth increment, which brought the iron concentration in the cuvette to 0.19 mM. In the experiments carried out at final iron concentrations of 0.86 and 0.95 mM the effect of the zinc was first seen after about 20 minutes following the addition of the first increment, (0.1 and 0.12 mM iron respectively). These time intervals may represent the induction times to nucleation, under the conditions used.

For reactions taking place in bulk solution the ions are free to move about throughout the whole volume of the solution. There is no

spatial constraint. Therefore, providing the total concentration is high enough for the formation of a critical nucleus, nucleation may occur at any stage. For the same reaction taking place in the presence of apoferritin the solution volume is "compartmentalised", as is the reaction because of the protein's ability to sequester iron. Therefore, nucleation may take place at a different absolute concentration to that required for nucleation in the protein-free system.

3.4.3 Further Conclusions

a) A kinetic summary

Taking into account the results of the kinetic and structural studies, the effects of zinc on the formation of ferrihydrite both in the presence and absence of apoferritin can be summarised by reference to the scheme in figure 3.23. Looking first at the reaction in the protein-free system: the rate constant k_2^* would seem to have been largely unaffected, k_3^* would probably have been greatly reduced by the zinc ions' inhibition of nucleation and k_4^* may have been reduced by the presence of bound zinc, as seen in the defect structure of the lepidocrocite formed. The autocatalysis rate constant k_a^* could have been reduced by the decreased rate of nucleation (and growth) and also, possibly, by the presence of zinc ions bound on the surface of the iron oxides, which may have diminished their autocatalytic activity.

Considering now the reaction in the presence of apoferritin: zinc may have reduced the rate constants k_1 and k_2 by binding to the protein channels or inner surface, respectively, k_3 may have been substantially diminished by the action of Zn^{2+} ions inhibiting

ferrihydrite nucleation. k_4 could have been reduced by both the binding of zinc to the surface of the growing core (although it would appear that most of any such zinc was displaced during core growth) and indirectly, via binding to the protein, thereby reducing k_1 and k_2. The autocatalysis rate constant k_a may also have been reduced due to the decrease in the rates of nucleation and core growth.

b) Proposed size of ferrihydrite nuclei in the reconstitution of apoferritin

The assessment of the number of ions required for the formation of a critical nucleus is difficult for a crystallisation reaction taking place in bulk solution, since the ions can occupy the whole volume or come together in any part of that volume. Estimations of the size of a critical nucleus therefore vary widely. Mullin (1972), in his book "Crystallisation" suggests that the number of molecules in a stable crystal nucleus can vary from about ten to several thousand and he proposes that ice nuclei may contain about 100 molecules. The size of the nuclei proposed below for ferrihydrite in ferritin is of the same order as Mullin proposes for ice, but may be higher than is generally considered for ferritin. For example, Macara *et al.* (1972) acknowledged that the number of iron atoms in a critical nucleus was not known, but they used only numbers between 1 and 10 in their computer model of core growth. Melikhov *et al.* (1987) state that the critical nuclei of iron hydroxide formation are the tetramers $[Fe(OH)_3]_4$. The largest discrete oxo-bridged poly-iron compound known, which has been synthesised as a model for the ferritin core, contains 11 iron atoms (Gorun & Lippard, 1986).

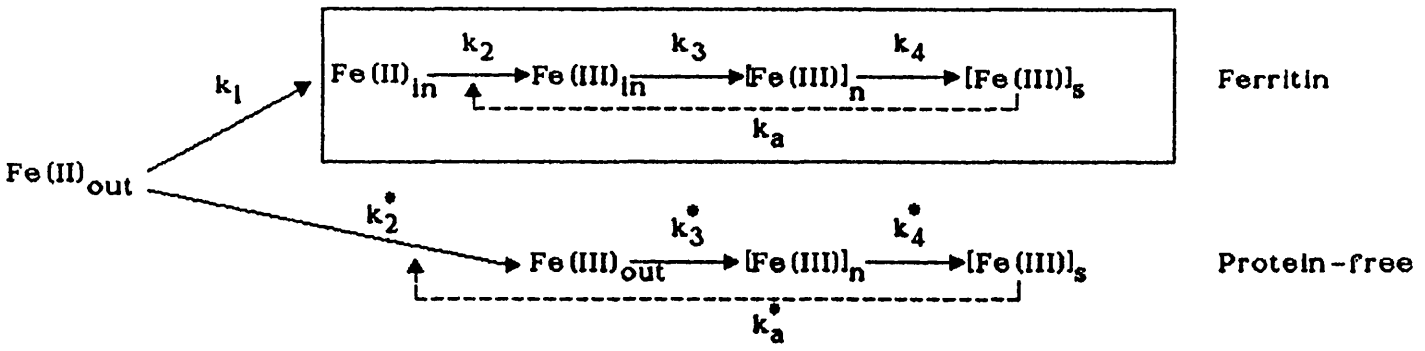

k_1 - diffusion into protein

k_2 - oxidation

k_3 - nucleation

k_4 - growth

k_a - autocatalysis

n - nucleus

s - solid

Figure 3.23 Schematic representation of the various kinetic steps of iron oxide formation in the presence and absence of ferritin.

For the "crystallisation" of ferrihydrite in the presence of apoferritin, with its ability to sequester iron, the number of iron atoms within each protein cavity can be estimated from the amount of iron added to the protein solution. With the addition of a nucleation inhibitor and a means of following the progress of the reaction, the stage at which nucleation occurs can be assessed, and from that the approximate size of the critical nucleus deduced. It is proposed that the nucleation of ferrihydrite cores in horse spleen apoferritin, during reconstitution, occurs at iron loadings of between approximately 170 and 260 iron atoms per molecule. This conclusion is based on three observations:

i) zinc had its maximum effect on iron uptake by apoferritin at iron loadings of between approximately 175 - 263 iron atoms per molecule, regardless of the absolute concentrations of any of the reactants,

ii) the major effect of the zinc in the protein free experiments seemed to be the inhibition of nucleation, so this was probably also its major effect in the reconstitutions,

iii) cores could be visualised in the TEM at iron loadings of ~200 iron atoms per molecule and these cores had a ferrihydrite based structure as revealed by electron diffraction.

Chapter 4

CORE STRUCTURE AND MORPHOLOGY IN RECOMBINANT AND VARIANT FERRITINS

4.0 INTRODUCTION

The work presented in this chapter was done in collaboration with Dr. P. Arosio, Dipartmento di Scienze e Tecnologie Biomediche, Universita di Milano, Italy and Professor P.M. Harrison and Dr. A. Treffry, Department of Molecular Biology and Biotechnology, University of Sheffield, U.K.

The aim of the study was to demonstrate the extent of influence that the protein shell of ferritin has over the structure, size and shape of the iron core that grows within it during *in vitro* reconstitution. Also, it was hoped that more could be learnt about the roles that the two types of subunit have in this process. In order to explore this problem homopolymers of human H- and L-subunits and rat L-subunit were generated by recombinant DNA techniques and also homopolymers of modified human H-subunits were produced using site-directed mutagenesis and recombinant DNA techniques. Furthermore, the naturally occurring human ferritin heteropolymers with differing H:L-subunit ratios isolated from brain (60% H, 40% L) and liver (10% H, 90% L) were compared with the recombinant H homopolymer.

The H- and L-subunits of ferritin are thought to have different roles *in vivo* since it has been shown that H-subunit rich heteropolymers take up and release iron faster than L-rich ones and that the L-rich ones accumulate more iron (see Chapter 1).

Boyd *et al.*, (1985) proposed that differences between the H- and L-rich heteropolymers in their ability to take up iron and to nucleate a core lay particularly with: a) the substitution in the 4-fold channel of histidine 173 in the H-subunit with leucine in the L-subunit; histidine having a particular affinity for iron and therefore facilitating its uptake and release, and b) the number of negatively charged residues exposed in the cavity, (carried on the B and D helices and on the C-terminus,) this number being reduced in the H-subunit so lowering the H-rich heteropolymer's "nucleation capacity" or "efficiency". Arosio concurs with this second point (pers. comm.), but Harrison *et al.*, (1989) suggest that if all potential metal ligands (not just carboxylate groups) on the inside surface are considered then the H-subunits have more such sites than L-subunits. Furthermore they suggest that the slightly more basic character of the inside surface in H-subunits may facilitate nucleation by aiding hydrolysis.

In the proposals made by Boyd *et al.* (1985), these workers are assuming that the 4-fold channels are the route by which the iron enters the cavity. Whether this is the case, or if the 3-fold channels or pathways through subunits are the route, remains to be shown. There are conflicting views; Ford *et al.*, (1984) and Harrison *et al.*, (1989) propose that either the 3- or 4-fold channels may be used, with a slight favouring of the 3-fold channels, although Harrison *et al.* cite Treffry *et al.*, (1989) as evidence that there is no specific mechanism involving the carboxylate residues in the

3-fold channels, in iron uptake. The ferroxidase centre (see Chapter 1 and Lawson *et al.*, 1989), has been located at a site within the subunit and it has been suggested that iron may be able to penetrate the protein shell via narrow channels through the subunit (Lawson *et al.*, 1989).

The present work can be divided into three sections, each of which should increase our understanding of the *in vitro* and *in vivo* functions of the H- and L-subunits.

1. study of homopolymers of H and L; the different properties of the two types of subunit should be accentuated if they are present as homopolymers.
2. study of H-subunit homopolymers that carry mutations at sites believed to be of importance since they are either conserved in many if not all the amino acid sequences known for H- and L-subunits, or they appear to be at key differences between the H and L sequences.
3. study of the effect of varying the proportion of H- and L-subunits in the assembled molecule according to the series 100% H, 60% H and 20% H.

The H-subunit variants studied here have been modified in the 3- and 4-fold channels, (one of the 4-fold variants, 102+150, has the His→Leu substitution highlighted by Boyd *et al.*, 1985), the "oxidation" site (Lawson *et al.*, 1989) and the proposed "nucleation" (Dr. Arosio, pers. comm.) site located in the same region of the B helix.

In addition, this work has demonstrated the effect of different reconstitution methods on the iron cores formed in a given protein.

The amino-acid sequences of the human H- and L-subunits are shown in Figure 4.1. Figure 4.2 shows the position and nature of each of the variations of H-subunit studied.

Description of the samples studied

The following samples were studied:

Native human liver ferritin (**HLFn**).

Reconstituted human liver ferritin (**HLF**), 10% H-subunit and 90% L-subunit, slower iron uptake kinetics and lower ferroxidase activity than rHF (see below), (Levi *et al.*, 1988).

Reconstituted human brain ferritin (**HBF**), 60% H-subunit and 40% L-subunit, faster *in vitro* rate of iron uptake than **HLF** (Prof. Harrison, pers. comm.).

Reconstituted recombinant L-subunit ferritin (**rLF**), (Levi *et al.*, 1989a).

Reconstituted recombinant H-subunit ferritin (**rHF**), (Levi *et al.*, 1988).

Reconstituted recombinant rat L-subunit ferritin (**r-rat LF**), the sequence of this protein has very extensive homology with human L-subunit, apart from an insertion (QPAQTGVA) between residues 161 & 162 (Harrison *et al.*, 1989) which forms a loop on the external surface of the assembled molecule (Harrison *et al.*, 1987).

Reconstituted H-subunit variants:

4-fold channel;

i) **R2**, Leu 169→Arg, substitution of the leucines (hydrophobic, neutral charge) in the middle of the 4-fold channels for bulky, positively charged arginines. This change together with the His

Figure 4.1. Amino-acid sequences of human H- and L-subunit ferritins

```
     1                                                  50
H  TTASTSQVRQ  NYHQDSEAAI  NRQINLELYA  SYVYLSMSXY  FDRDDVALKN
L       S..I..  ..ST.V...V  .SLV..Y.Q.  ..T...LGF.  ........EG

                                                       100
H  FAKYFLHQSH  EEREHAEKLM  KLQNQRGGRI  FLQDIKKPDC  DDWESGLNAM
L  VSHF.RELAE  .K..GY.R.L  .M.......A  LF......AE  .E.GKTPD..

                                                       150
H  ECALHLEKNV  NQSLLELHKL  ATDKNDPHLC  DFIETHYLNE  QVKAIKELGD
L  KA.MA...KL  ..A..D..A.  GSART.....  ..L...F.D.  E..L..KM..

                                       182
H  HVTNLRKMGA  PESGLAEYLF  DKHTLGDSDN  ES
L  .L...HRL.G  ..A..G....  ERL..KHD
```

Sequences from Harrison *et al.*, (1989).
For amino acid code see Appendix IV.

---

173 in the H-subunit must make this channel very different from that of the L-subunit homopolymer; positively charged from the inside, rather than hydrophobic all the way through.

ii) **102+150**, last 10 C-terminal residues → L-subunit sequence, including His 173→Leu, substitution of positive charge for a hydrophobic leucine, making this channel like that in the L-subunit homopolymer (hydrophobic all the way through). Also changing the charges and the charge density on the last 3 residues, as in L-subunit.

Also described in Levi *et al.*, (1989b).

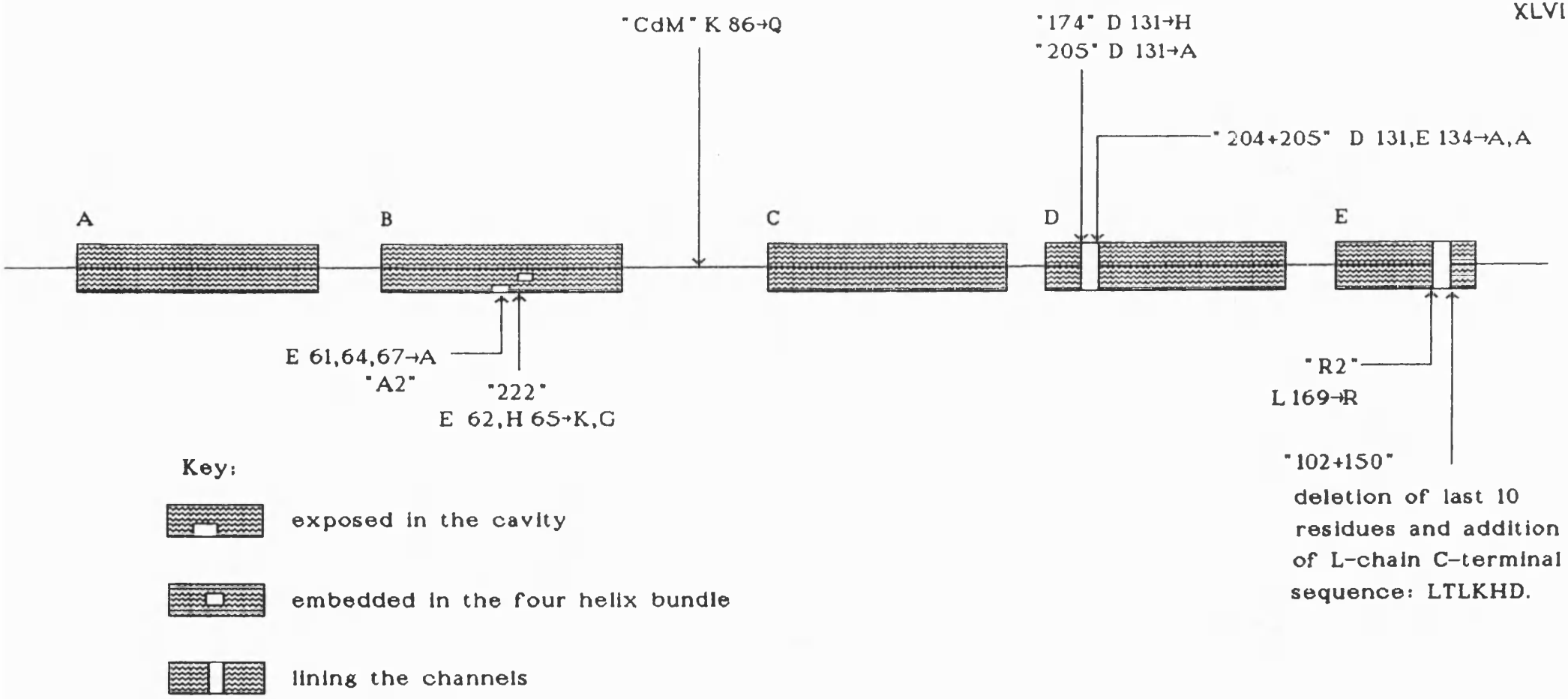

Figure 4.2

Schematic diagram of Human ferritin H-subunit showing the positions, names and types of mutations studied. The shaded boxes represent the five alpha helices, A to E. The "CdM" site is exposed on the outside of the assembled molecule. The other sites are located as given in the key.

A2, Glu 61,64 & 67 →Ala, putative "nucleation centre" (Dr. Arosio, pers. comm.), negatively charged acid groups replaced by smaller, non-polar, neutral charge alanines. These three glutamic acid residues are conserved in all ferritin sequences (H and L) known, (e.g. Harrison *et al.*, 1989). Dr. Arosio (pers. comm.) proposes that all three acid groups are exposed in the cavity, whereas Boyd *et al.*, (1985) indicate that only Glu 61 and Glu 64 are so exposed. Stereographs of the inner section of the dimer interface in horse L-subunit (Rice *et al.*, 1983) show Glu 61 to be more buried, Glu 64 to be at the edge of the "groove" and Glu 67 extending into the "groove". The neighbouring residues of the "ferroxidase" site (see below) were not altered.

CdM, this protein carries a crystallisation mutation Lys 86→Gln, (Treffry *et al.*, 1989 & Levi *et al.*, 1989b).

3-fold channel (superimposed on the **CdM** variant);

i) **174**, Asp 131→His, substitution of the inner carboxyl group, negative charge, for a positively charged histidine.

ii) **205**, Asp 131→Ala, substitution of the inner carboxyl group, negative charge, for a non-polar, neutral charge alanine of shorter side-chain length.

iii) **204+205**, Asp 131, Glu 134→Ala, Ala, substitution of both carboxyl groups, negative charges, for non-polar, neutral charge alanines of shorter side-chain length.

Also described in Treffry *et al.*, (1989) and Levi *et al.*, (1989b).

Later X-ray crystallography work on variant **205** (Prof. Harrison, pers. comm.) has shown that the proposed Asp 131→Ala substitution had

not in fact taken place, (the mutation that did occur was silent). So **205** carried only the **CdM** mutation and **204+205** only had the Glu 134→Ala substitution. From hereon therefore, **205** will be designated **205'** and **204+205** will be called **204**.

222, (superimposed on the **CdM** variant), Glu 62, His 65→Lys, Gly, "ferroxidase site", making the H-subunit like the L-subunit at these two residues. Ferroxidase activity has been attributed to the H-subunit alone (Levi *et al.*, 1988 & 1989a) and this site has been identified as the ferroxidase centre (Lawson *et al* ., 1989). Lawson *et al.* show that the residues concerned are buried within the subunit's four helix bundle, 7-10Å from the inside surface and this would be about 12Å from the centre of the groove or "pocket" formed between the two B helices (Prof. Harrison pers. comm.). Boyd *et al.*, (1985) also, do not indicate exposed positions for these two residues.

A222, this variant carries the **222** and **A2** mutations, superimposed on the **CdM** variant. Therefore, it has been modified in the ferroxidase site and the proposed nucleation site. All the glutamic acid residues in this region have been altered; numbers 61, 64 and 67 to smaller, non-polar, neutral charge alanines and number 62 to the larger lysine, which carries a positively charged amino group. Histidine 65 has been replaced by the small, neutral charge glycine.

4.1 EXPERIMENTAL

4.1.1 Reconstitution

The samples were reconstituted in Milan or Sheffield by various methods which are detailed below. The calculated loading was 2000 iron atoms per molecule in each case and freshly prepared ferrous ammonium sulphate solution was the source of the iron. The appropriate control protein was reconstituted on the same day, using the same solutions, as the proteins under direct study.

Method 1 Reconstitution of apoproteins in 0.1M HEPES pH 7.0 with Fe^{2+} in two increments, 20 minutes apart at room temperature. The samples were kept at room temp. for 1 hr. and then at 4°C for 18 hr.. They were then dialysed against 1mM Desferal to remove any non-specific oxidation products and then against 50mM HEPES pH 7.0. The final iron conc. was 2.0 mM and the protein conc. 0.4 mg/ml.

Method 2 Reconstitution of apoproteins in 0.1M MOPS pH 7.0 with two increments of Fe^{2+} solution at a 45 minute interval at room temperature and then 4°C overnight. The final iron conc. was 0.8mM and the protein conc. 0.2 mg/ml.

Method 3 Reconstitution of apoproteins in 0.1M MOPS pH 7.0 with two increments of Fe^{2+} solution at a one week interval. The increments were added at room temperature and the samples stored at 4°C. The final iron conc. was 0.8mM and the protein conc. 0.2 mg/ml.

Method 4 Reconstitution of apoproteins in 0.05M MES pH 6.45 by twenty increments of Fe^{2+} solution at a 15 minute interval and at room temperature. The final iron and protein concentrations were iron 0.8 mM and 0.2 mg/ml respectively.

Method 5 Reconstitution of apoproteins in 0.1M HEPES pH 7.0 with two increments of Fe^{2+}, 45 minutes apart at room temperature. The

solutions were kept at room temperature for 30 minutes and then overnight at 4°C. They were then microfuged for 5 minutes at 10,000 x g. The final iron conc. was 0.8mM and the protein conc. 0.2 mg/ml.

4.1.2 Characterisation of samples by transmission electron microscopy and electron diffraction

The size, shape, general appearance and relative crystallinity of the iron cores in these samples were assessed by TEM and electron diffraction, as described in chapter 2. Sample **A222** required a negative stain for successful imaging. Staining was achieved by incubating the electron microscopy grids containing the air-dried sample with 1.5wt% sodium silicotungstate solution for 1 minute at room temperature, followed by washing with distilled water.

The native human liver ferritin sample was in 0.02 M TRIS pH 7.4 + 0.02% azide. The reconstituted ferritin samples were in their respective buffers indicated above.

4.2 RESULTS

There was some variability in the data collected from samples of the same protein type reconstituted by different methods and even by the same method but on different days. Therefore, the results presented here are grouped according to individual sets of experiments, each with its own control. Comparisons are made between samples in the same experiment and conclusions drawn therefrom. In each case the same relative trends were observed. Some comparisons between samples of the same protein type reconstituted at the two different pH values (methods 1 and 4) are discussed in section 4.3.

4.2.1 Human liver ferritin

HLFn

This native sample is included, since it illustrates some of the changes in sample appearance on the electron microscopy grid and crystallinity induced by removal and then reconstitution, of the iron cores. This sample contained an average of 4050 iron atoms/molecule. Transmission electron micrographs showed that the iron cores were generally of very regular shapes. Many of them appeared round or square-shaped or were square with rounded corners. There were a few irregular shaped cores. The cores were discrete and aggregation on the electron microscopy grid was minimal. (Plate 4.1) The mean core diameter was 5.93 nm, with a standard deviation of 0.82 nm. The range of core size was 3.69 to 7.37 nm and a particle size distribution is shown in figure 4.3, see also table 4.1.

Electron diffraction analysis showed that the cores were well-ordered ferrihydrite, with all the possible six lines visible on the powder pattern, see plate 4.1c and table 4.2.

HLF

This sample was reconstituted by method 1.

Most of the iron cores in this sample were of irregular shape and compared with the **HLFn** sample they were of poor electron density. Some cores were oval-shaped, some were square-shaped and a few were round. The cores were discrete, but they were extensively aggregated on the electron microscopy grid. (Plate 4.1.) The data regarding iron core sizes for this sample are shown in table 4.1, and a particle size histogram is shown in figure 4.3.

The electron diffraction patterns from this sample revealed a defect ferrihydrite structure, with a line at 2.41Å and two broad

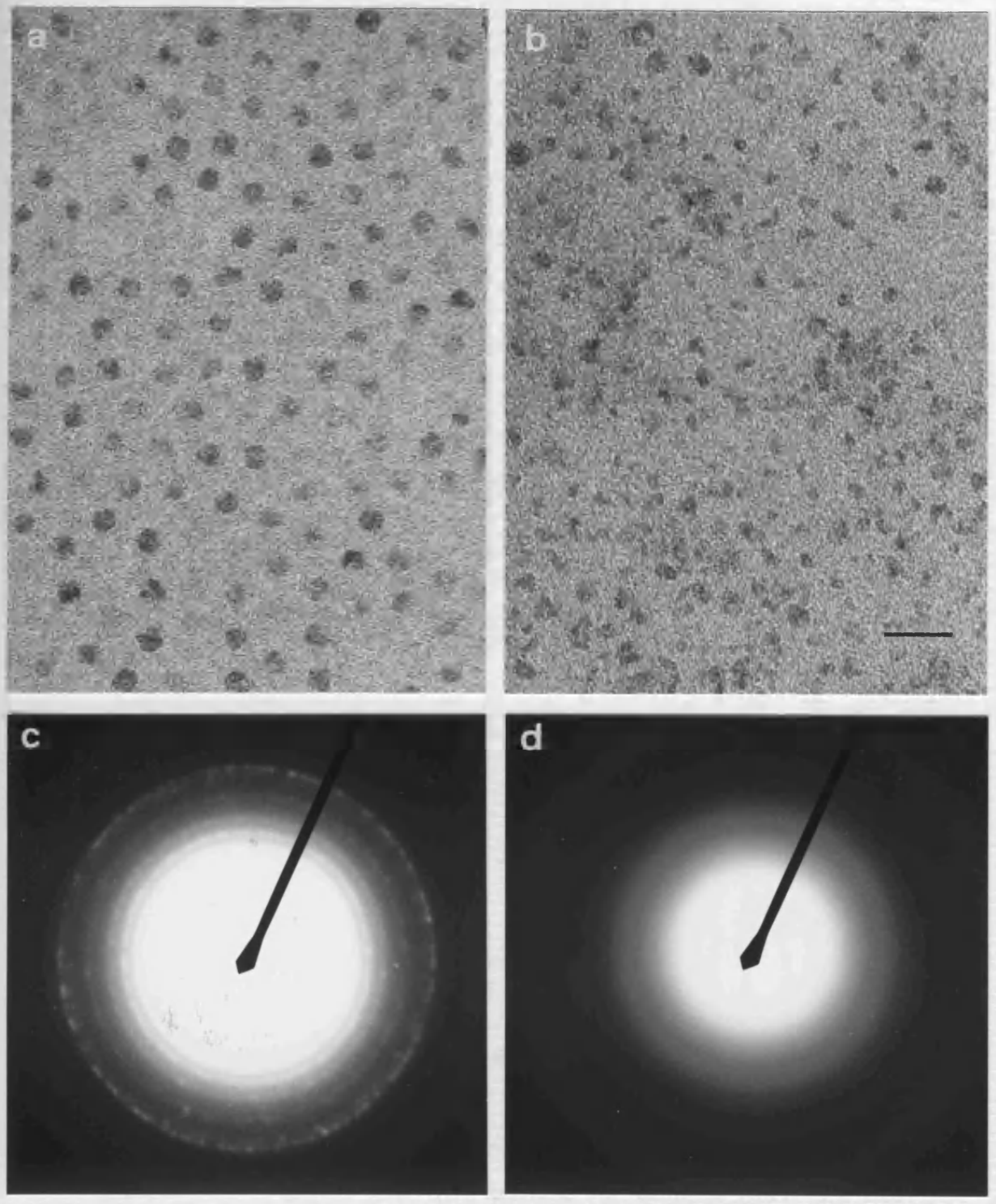

Plate 4.1 *a & c* Electron micrograph and diffraction pattern of unstained HLFn. *b & d* Electron micrograph and diffraction pattern of unstained reconstituted HLF (method 1). The diffraction pattern in *c* also illustrates the degree of crystallinity in the samples in the varying H:L ratio series reconstituted by method 4. That in *d* illustrates the degree of crystallinity in other samples reconstituted by methods 1, 2, 3 & 5. Bar marker 20nm for *a & b*, camera length 110cm for *c & d*.

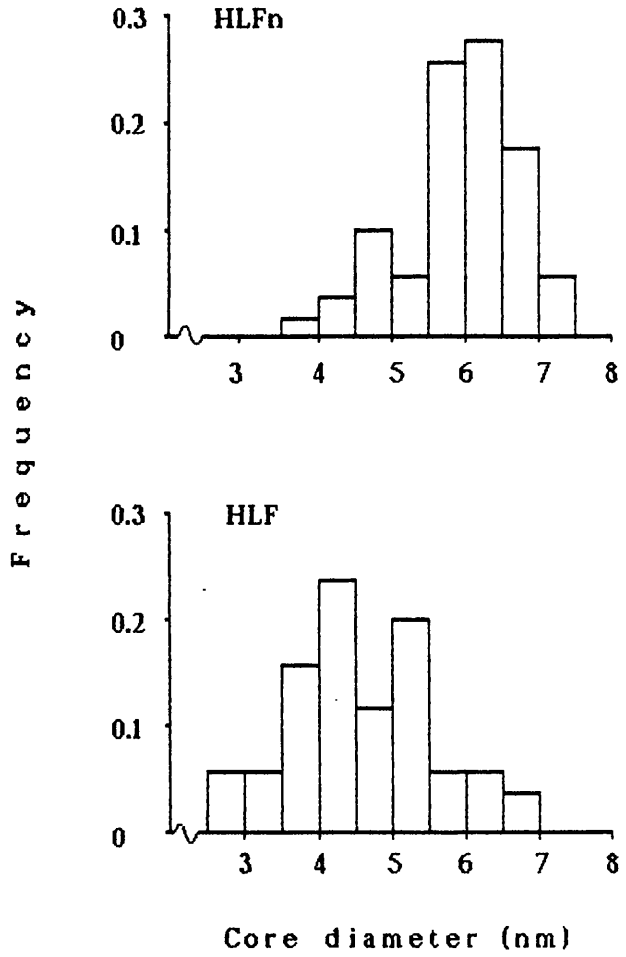

Figure 4.3 Particle size distributions for samples HLFn and HLF.
HLF reconstituted by method 1.

bands centred at 2.10 and 1.46Å, see plate 4.1d and table 4.2.

Comparing the structures of the native and reconstituted human liver ferritins both were ferrihydrite but the native sample was more crystalline than the reconstituted one. The reconstituted sample exhibited a greater degree of irregularity in the core morphology and a slightly increased range of core sizes. The smaller mean core diameter for the reconstituted sample was probably attributable to its much lower iron loading.

4.2.2 L- and H-subunit homopolymers

Two sets of experiments were performed with human recombinant L and H homopolymers using reconstitution methods 1 and 5. Recombinant rat-L homopolymer was reconstituted in a separate experiment by method 3.

Method 1, experiment 1

rLF

In this sample many large, well-formed cores were visible on the transmission electron micrographs, many of which were very rounded and some were square-shaped, see plate 4.2a. Most of the smaller cores were also of regular shape, although some were irregular. The cores were discrete but partially aggregated on the electron microscopy grid. Iron core size data are presented in table 4.1 and the particle size distribution from this sample is shown in figure 4.4a.

Electron diffraction analysis showed that the cores were partially crystalline ferrihydrite (table 4.2).

rHF

There were only a few large, well-formed, regular shaped cores visible in this sample. The cores of around the average size were a mixture of regular and irregular shapes, see plate 4.2b. Generally, the cores were less electron-dense and less well-defined than those of the **rLF** sample. The cores were discrete, but partially aggregated on the electron microscopy grid. Core size data are shown in table 4.1 and the particle size distribution from this sample is shown in figure 4.4c.

The electron diffraction patterns showed that, like the **rLF** sample, the cores in this sample were partially crystalline ferrihydrite (table 4.2).

Comparing the reconstituted **HLF** sample (method 1, above), which is 90% L-subunit, with the **rLF** sample also described above, there appeared to be a similar degree of crystallinity in each. However, with regard to core morphology and size the **rLF** sample contained more of the larger, well-formed cores.

Method 5, experiment 1

rLF

In general appearance on the electron microscopy grids this sample looked very similar to the **rLF** sample described above. However, as can be seen in table 4.1, its mean core diameter was reduced from 5.36 to 4.80 nm. The particle size histogram is shown in figure 4.4b.

There was no difference in the crystallinity of this sample compared with the **rLF** reconstituted by method 1.

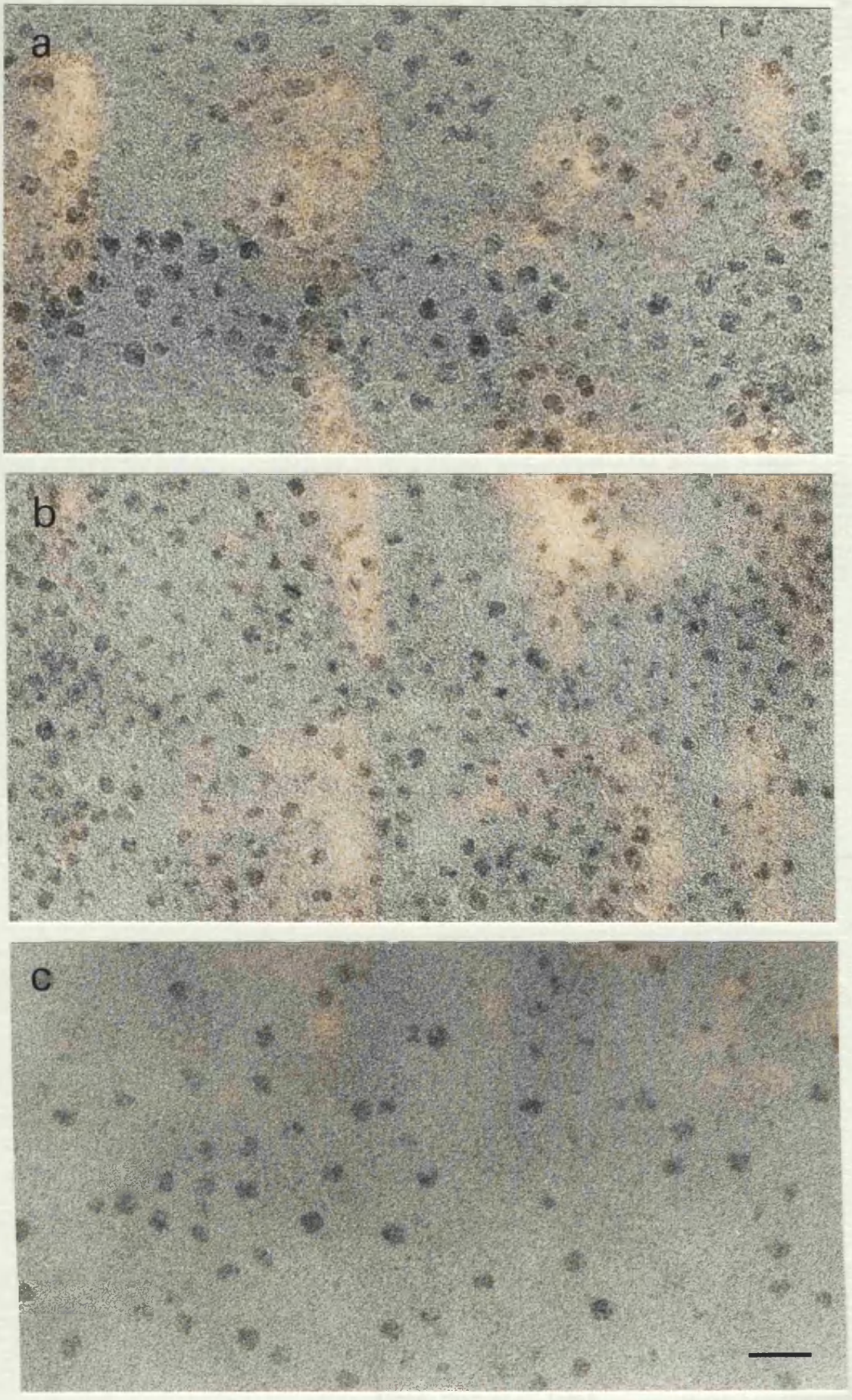

Plate 4.2 Electron micrographs of unstained reconstituted homopolymer ferritins. *a* rLF, *b* rHF, *c* r-rat LF. Bar marker 20nm for all micrographs.

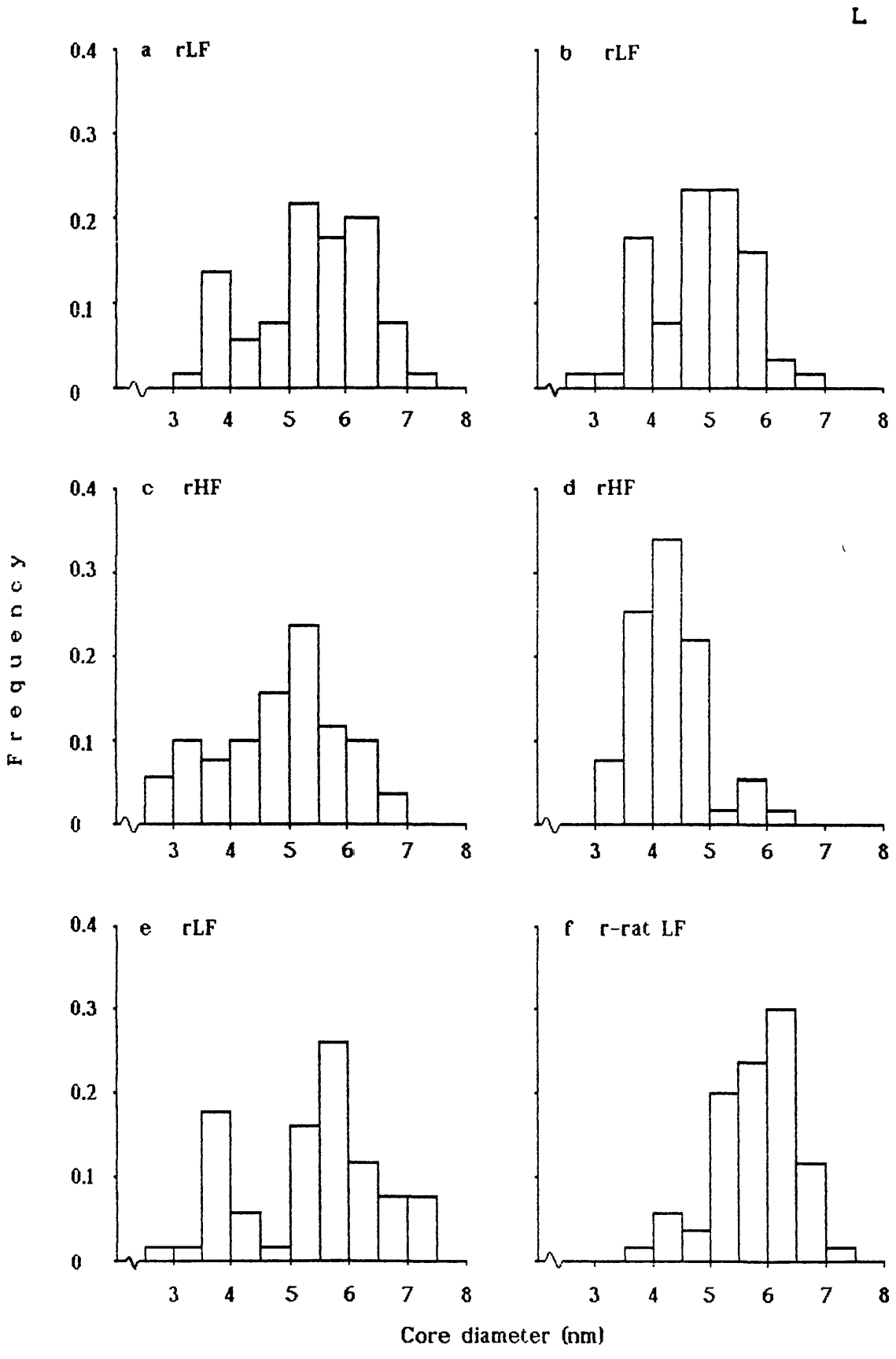

Figure 4.4 Particle size distributions for samples of rLF, rHF and r-rat LF. *a & c* method 1/1, *b & d* method 5/1, *e* method 1/3 and *f* method 3.

Together with a third sample of **rLF** (reconstituted by method 1 in a separate experiment, size data shown in table 4.1), it was noted that the distributions were all bimodal, to a greater or lesser degree (see figure 4.4e), which may suggest that there were two nucleation events during the iron uptake by this L homopolymer. Also, there was no difference in the crystallinity of the three samples.

rHF

The iron cores of this sample were less well-defined than those of the first sample, but they were discrete and aggregation varied across the electron microscopy grid. Core morphology was similar to the first sample, but the mean core diameter was reduced, as was the range of core diameters, see table 4.1 and figure 4.4d.

This sample was slightly less crystalline than that reconstituted by method 1, as judged by the quality of the diffraction patterns.

There was no difference in the crystallinity of the first sample and a third sample, reconstituted by method 1 as a control for the 4-fold channel variants, (see below).

Together, these two sets of results clearly showed marked differences between the two homopolymers in the size and morphology of their iron cores. However, there was no significant difference in the crystallinity of the ferrihydrite cores formed in the different homopolymers.

r-rat LF

Only one sample of this protein, reconstituted by method 3, was studied. The cores of this sample had various regular and irregular shapes, some of the largest ones were very regular in shape being round, square or square with rounded corners. (Plate 4.2c) Some of the smaller cores had very irregular shapes. The cores were discrete and they were not aggregated to any great extent. The mean core diameter was 5.78nm, with a standard deviation of 0.75nm. The range of core diameters measured was 3.82 - 7.06nm and a particle size distribution is shown in figure 4.4f. These size data are shown with those of the other homopolymers in table 4.1 and figure 4.4.

Contamination of this sample with the non-specific oxidation product lepidocrocite (γ-FeOOH) and NaCl made electron diffraction analysis difficult. Ferrihydrite lines could be seen among those attributed to lepidocrocite and NaCl hydrate, but the patterns were not suitable for comparison with those from the other recombinant samples.

4.2.3 Varying H:L ratios

All the samples in this series were reconstituted by method 4 in one experiment.

rHF

The iron cores in this sample were aggregated, but the sample had precipitated after it had been iron loaded. The cores were of a variety of shapes; rounded and angular, isometric and anisometric, see plate 4.3a. The mean core diameter was 4.48nm, with a standard deviation of 0.86nm. A particle size distribution is shown in

figure 4.5, the range of core diameters measured was 2.68 to 6.20nm.

Electron diffraction patterns from this sample were characteristic of quite well-ordered ferrihydrite, see table 4.3.

HBF

The iron cores of this sample were a mixture of shapes, many were rounded or square-shaped. A few were triangular and some were anisometric. Generally the cores were less angular than those in the sample of **rHF**, see plate 4.3b. The cores were fairly discrete, but they were quite extensively aggregated. Some of the large cores were particularly well defined. The mean core diameter was 4.84nm, with a standard deviation of 0.84nm. The diameters of the cores measured varied from 2.68 - 6.61nm, a particle size distribution is shown in figure 4.5.

Electron diffraction analysis revealed that the iron cores were well-ordered ferrihydrite, see table 4.3.

HLF

The cores in this sample were mostly of regular shapes, many were well-rounded or square-shaped. A few had irregular or elongated shapes. They were quite discrete and well-formed and aggregation was limited. Plate 4.3c. The mean core diameter was 5.40nm, with a standard deviation of 0.88nm. The smallest core measured had a diameter of 3.49nm and the largest a diameter of 7.02nm. A particle size distribution for this sample, which is slightly bimodal, is shown in figure 4.5.

Electron diffraction analysis showed the cores to be crystalline ferrihydrite, see table 4.3 below.

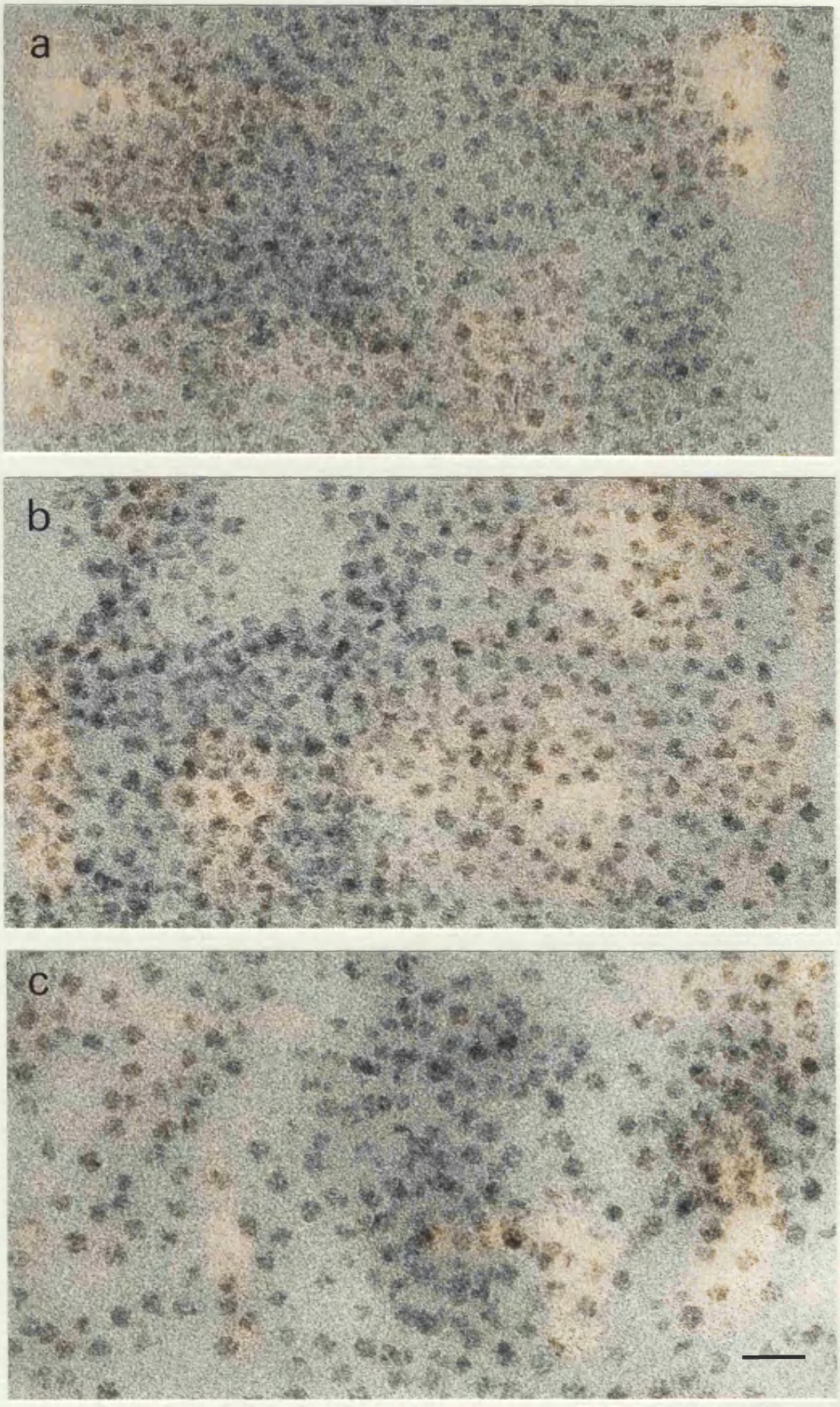

Plate 4.3 Electron micrographs of unstained reconstituted ferritins in the varying H:L ratio series. *a* rHF, *b* HBF, *c* HLF. Bar marker 20nm for all micrographs.

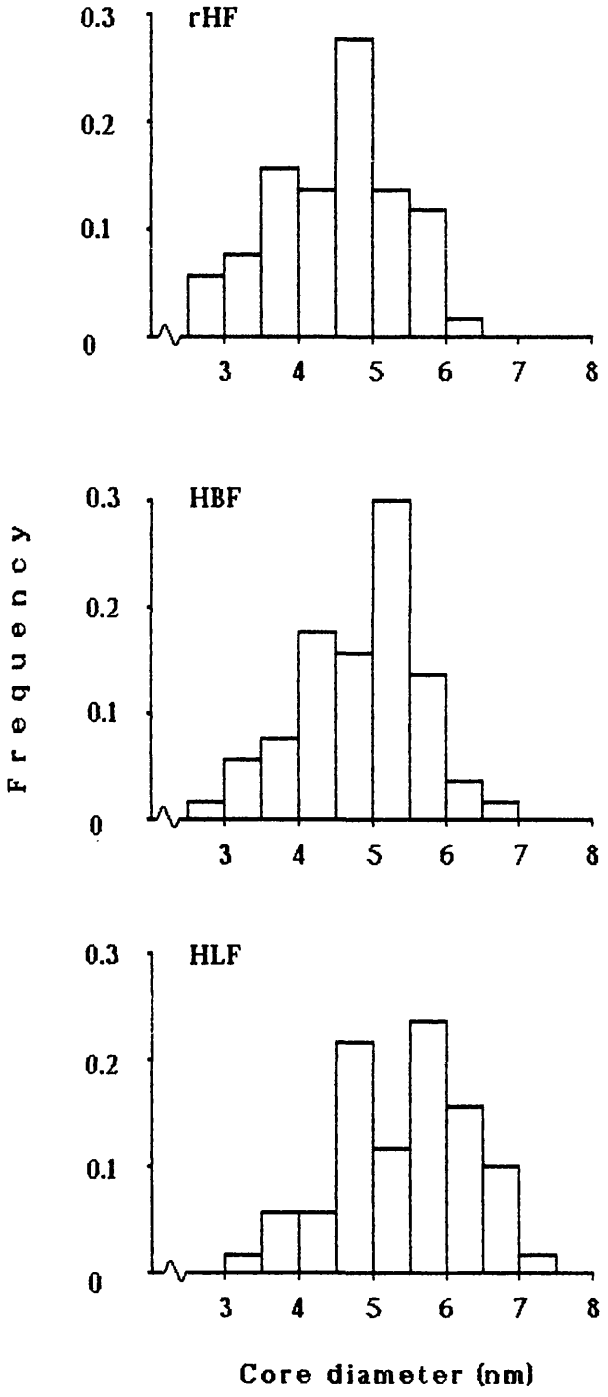

Figure 4.5 Particle size distributions for samples of varying H:L ratios, all reconstituted by method 4.

Table 4.1

Particle size data for reconstituted recombinant homopolymer ferritins and heteropolymer ferritins.

Method/ Expt.	Protein	Mean, nm	SD, nm	Range, nm
(native)	(HLFn)	(5.93)	(0.82)	(3.69 - 7.37)
1/1	HLF	4.57	0.97	2.63 - 6.67
	rLF	5.36	1.02	3.30 - 7.19
	rHF	4.79	1.06	2.80 - 6.72
5/1	rLF	4.80	0.84	2.63 - 6.57
	rHF	4.31	0.70	3.01 - 6.20
5/2	rHF†	4.30	0.65	2.77 - 5.74
1/3	rLF	5.35	1.17	2.91 - 7.39
1/2	rHF*	4.48	0.92	3.04 - 6.70
3	r-rat LF	5.78	0.75	3.82 - 7.06
4	rHF	4.48	0.86	2.68 - 6.20
	HBF	4.84	0.84	2.68 - 6.61
	HLF	5.40	0.88	3.49 - 7.02

† data also shown in table 4.4, with "nucleation site" mutant

* data also shown in table 4.4, with 4-fold channel mutants

Table 4.2

Electron diffraction data for human liver and homopolymer samples.

I= intensity of line judged by eye:- S = strong, M = medium, W = weak, B = broadened, BB = broad band.

HLFn		HLF		rLF		rHF	
d(Å)	I	d(Å)	I	d(Å)	I	d(Å)	I
2.46	S	2.41	S	2.46	S	2.54	S
2.23	S	2.28	SBB	2.28	SBB	2.29	MBB
2.00	M	1.92		1.98		2.04	
1.72	MW			very weak line here in these two			
1.51	W	1.48	SB	1.50	SB	1.52	SB
1.45	S	1.44					

Table 4.3.

Electron diffraction data for samples of varying H:L ratios.

rHF		HBF		HLF	
d(Å)	I	d(Å)	I	d(Å)	I
2.49	S	2.52	S	2.49	S
2.26	M	2.28	M	2.26	M
1.98	M	2.02	M	2.02	M/W
1.68	VW(approx.)	1.75	W	1.75	W
1.52	M	1.52	W	1.53	W
1.45	S	1.47	S	1.48	S

Intensities (I) judged as in Table 4.2.

4.2.4 H-subunit variants based on rHF

The 4-fold channel variants and the nucleation site variant were reconstituted in two sets of experiments using methods 1 and 5, each with an **rHF** control. A second sample of the nucleation site variant was reconstituted in another experiment but without the appropriate control.

Method 1, experiment 2

rHF

This sample was the control for the 4-fold channel variants. The cores had a variety of shapes; mostly angular with a few rounded ones, see plate 4.4a. They were discrete and aggregation varied across the electron microscopy grid. The core size data for this sample are presented in table 4.4. The mean core diameter and range were intermediate between those of the two other **rHF** samples described above in section 4.2.2. The particle size histogram is shown in figure 4.6a.

4-fold channel variants

i) **R2** The iron cores in this sample were generally of regular rounded or square shapes, several had irregular shapes. Plate 4.4b. The cores were fairly discrete but there was some extensive aggregation. The mean core diameter was 4.84 nm, with a standard deviation of 0.98 nm. The particle sizes varied from 2.70 to 6.68 nm and a distribution is shown in figure 4.6c.

ii) **102+150** There was a wide variety of shapes to the cores in this sample; they were regular or irregular, square or rounded. Plate 4.4c. Several cores were anisometric and several of the larger cores were rounded. The mean core diameter was 4.55 nm, with a

standard deviation of 0.83 nm. The particle size range was 2.87 to 6.24 nm and a distribution is shown in figure 4.6e.

On comparing the histograms for these three samples and the core size data in table 4.4, it was apparent that the iron cores of **R2** exhibited a slight increase in size, compared with the **rHF** control, whereas no change in size distribution could be seen for **102+150.**

The mean core diameter for **R2** was larger than that of **rHF**, although they had similar ranges. The frequencies of core diameters below 4.5 nm were significantly reduced in **R2** and the frequencies above 4.5 nm were slightly higher than those of **rHF.**

Comparisons between a number of electron diffraction patterns from each sample did not reveal any major structural changes in their iron cores. They were all poorly crystalline ferrihydrite giving a diffraction line at ~2.5Å and broadened lines centred at ~2.1 and ~1.5Å. See table 4.5 for the data from **R2.**

Method 5, experiment 2

rHF

This sample was the control for **A2.** Its iron cores were poorly defined but discrete and partially aggregated on the electron microscopy grid. They were generally of square and rectangular shapes, very few were rounded and several were anisometric. The core size data are shown in table 4.4 and a particle size histogram is shown in figure 4.6b. The data were very similar to those of the **rHF** sample reconstituted by method 5, in experiment 1, described above in section 4.2.2.

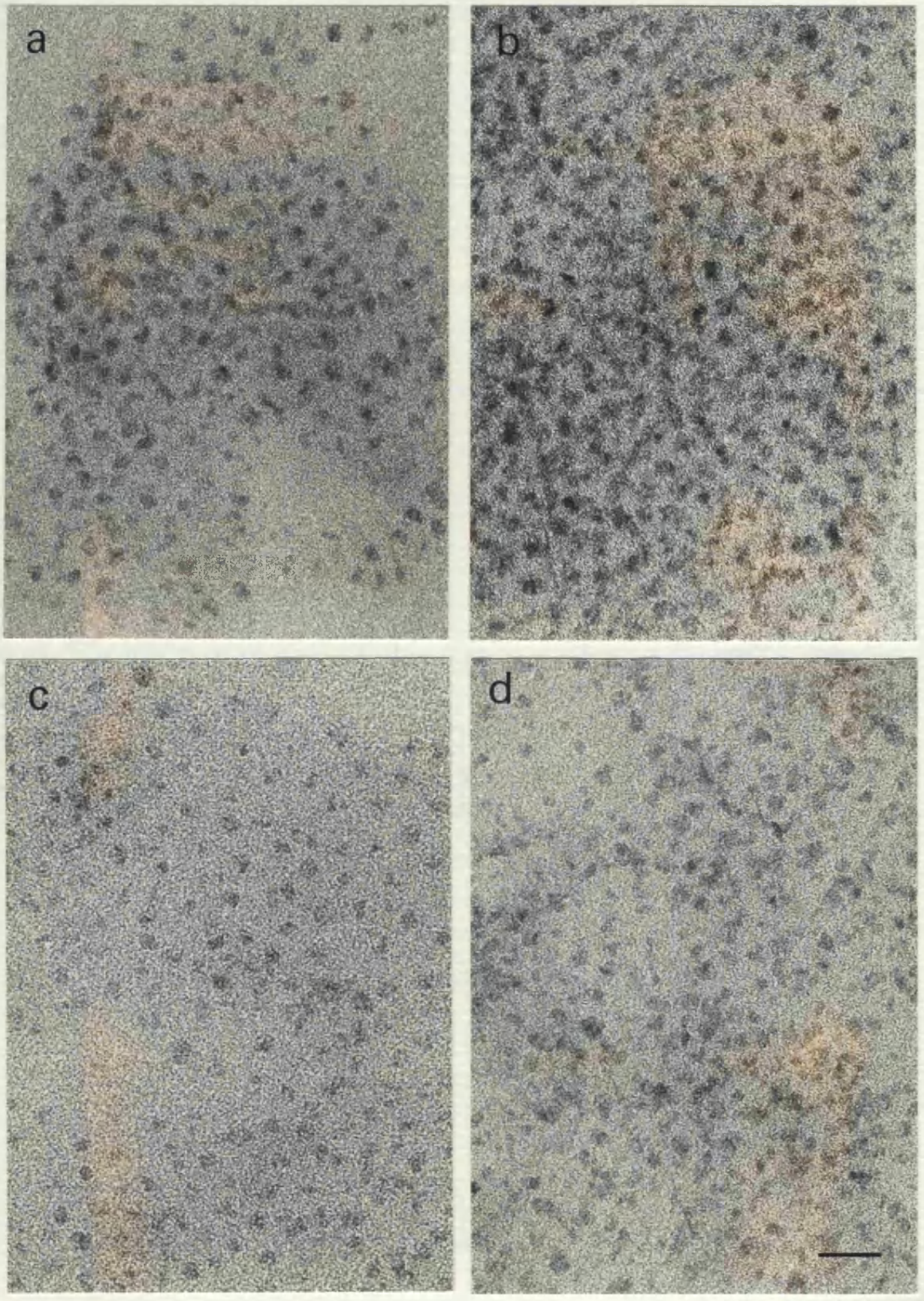

Plate 4.4 Electron micrographs of unstained reconstituted H-subunit variants based on rHF. *a* rHF, *b* R2, *c* 102+150, *d* A2. Bar marker 20nm for all micrographs.

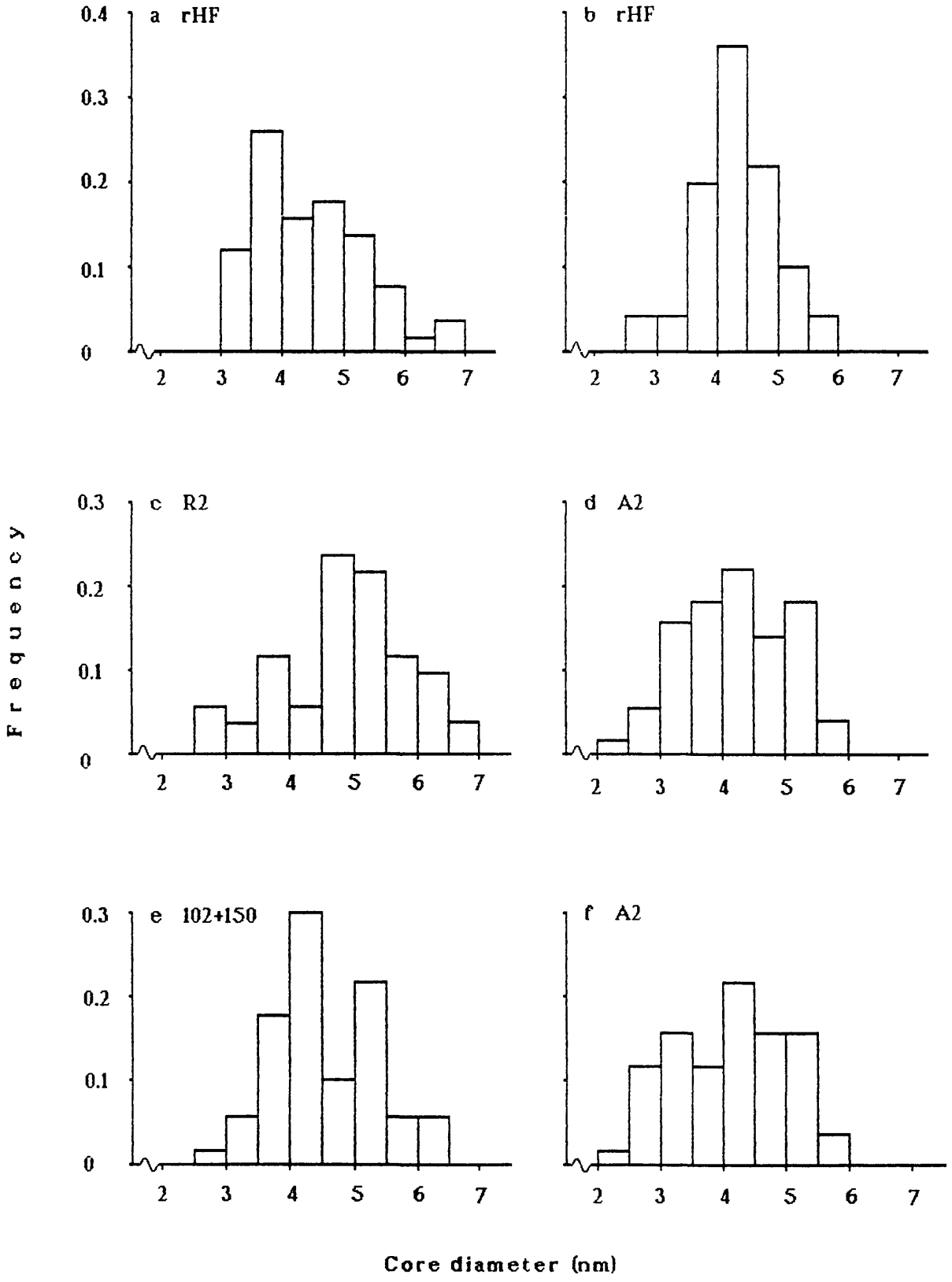

Figure 4.6 Particle size distributions for variants based on rHF.

a, c & e method 1/2, *b & d* method 5/2 and *f* method 1/3.

A2

The iron cores in this sample were also poorly defined. The extent of aggregation varied but the cores were reasonably discrete. Mostly, they had angular and irregular shapes, some were more rounded and several were anisometric (see plate 4.4d). The size data are shown in table 4.4 and a particle size histogram in figure 4.6d.

Method 1, experiment 3

A2

The cores in this sample were slightly more well defined than those of the first **A2** sample. The core morphology was similar; cores having a variety of shapes, but again the larger cores were generally of more regular rounded or square shapes than the smaller cores. Some cores appeared to be particularly discrete and the extent of aggregation of the cores varied across the electron microscope grid. The size data are shown with those of the other sample of **A2** in table 4.4 and a particle size histogram is shown in figure 4.6f.

The two particle size distributions for **A2** were quite similar and showed no cores with diameters above 6nm. Although there was no significant difference in the mean core diameters and size ranges of **A2** compared with the **rHF** control, the shapes of the distributions were rather different, with those of **A2** showing a broader distribution.

Electron diffraction analysis did not reveal any structural differences between the **A2** samples and their **rHF** control. They were all ferrihydrite of similar crystallinity to other samples reconstituted by the same or similar methods. The diffraction data for a sample of **A2** are presented in table 4.5.

4.2.5 H-subunit variants based on the CdM variant

1 CdM and the ferroxidase variant 222

Samples of each of these proteins reconstituted by methods 2, 3 and 5 were studied.

Method 2

CdM

The iron cores in this sample were small and poorly defined. They were of mostly angular shapes and extensively aggregated, see plate 4.5a. The mean core diameter was only 3.63 nm, this and the other core size data are shown in table 4.4. The particle size distribution (see figure 4.7a), showed that almost all of the core diameters lay between 2.5 and 5.0 nm.

The electron diffraction patterns from this sample were of ferrihydrite and showed a line at 2.56Å and two broad bands centred at 2.20 and 1.51Å (see table 4.5).

222

The electron micrographs of this sample were very different from those of **CdM**; there was a significant population of larger, more regular shaped cores, the cores were fairly well-defined and aggregation was not extensive. Many of the larger cores were round or square shaped. The "middle" sized and smaller cores were of less regular shapes. See plate 4.5b. The core size data are shown in table 4.4 and a particle size distribution is shown in figure 4.7d.

Electron diffraction analysis of this sample revealed ferrihydrite cores of similar crystallinity to those of the **CdM** sample, with diffraction lines at 2.46, 1.55 (weak) and 1.48Å and a broad band centred at 2.16Å (see table 4.5).

Method 3

CdM

The iron cores in this sample were again extensively aggregated and not well-defined, although they were slightly more well-defined than those in the sample reconstituted by method 2. They were of generally irregular shapes, like those of the first sample. There was no significant difference in the mean core diameter of this sample compared with that of the first, although the range of core sizes was reduced. Core size data are shown in table 4.4 and the particle size histogram is shown in figure 4.7b.

Electron diffraction analysis showed that this sample had the same structure as the first sample.

222

This sample was very similar in appearance and core size to that reconstituted by method 2. The size data and particle size distribution are shown in table 4.4 and figure 4.7e, respectively.

There was no difference in the structure of the cores in this sample compared with the first.

Method 5

CdM

In general appearance on the electron micrographs this sample looked very similar to the other **CdM** samples described above. Its mean core diameter was larger than those of the two previous samples, but the range of core sizes was intermediate between the two, see table 4.4. The particle size distribution is shown in figure 4.7c. All of the **CdM** particle size histograms showed quite narrow distributions with almost all of the core diameters measuring between 2.5 and 5.0 nm.

This third sample of **CdM** was less crystalline than the first two, with diffuse diffraction rings at approximately 2.5 and 1.5Å and a broad, diffuse band at approximately 2.2Å. This pattern was indicative of a defect ferrihydrite structure.

222

In this 222 sample there was also a noticeable population of the larger, regular shaped and well-defined cores, as had been apparent in the first two samples. The smaller cores were generally of angular shapes and aggregation varied across the electron microscopy grid. As the mean core diameter of the **CdM** sample reconstituted by this method had increased, so had that of this sample compared with the first two. The ranges of core size were all similar, see table 4.4. The particle size distribution, shown in figure 4.7f, was slightly bimodal. The histograms of all three 222 samples showed broad distributions, much broader than those of the **CdM** samples.

There was no difference in crystallinity between the three 222 samples.

There was a striking difference in the appearance of these two proteins, with and without the ferroxidase site, on the electron micrographs. The iron cores of **CdM** were small, poorly defined, of mostly irregular shape and often extensively aggregated, while those of 222 were more well-defined, discrete and contained a significant population of larger, mostly regular shaped cores. The particle size distributions reflected these observations (figure 4.7) as did the core size measurements (table 4.4).

The iron cores were all poorly ordered ferrihydrite. The degree of crystallinity was similar in all the samples studied apart from

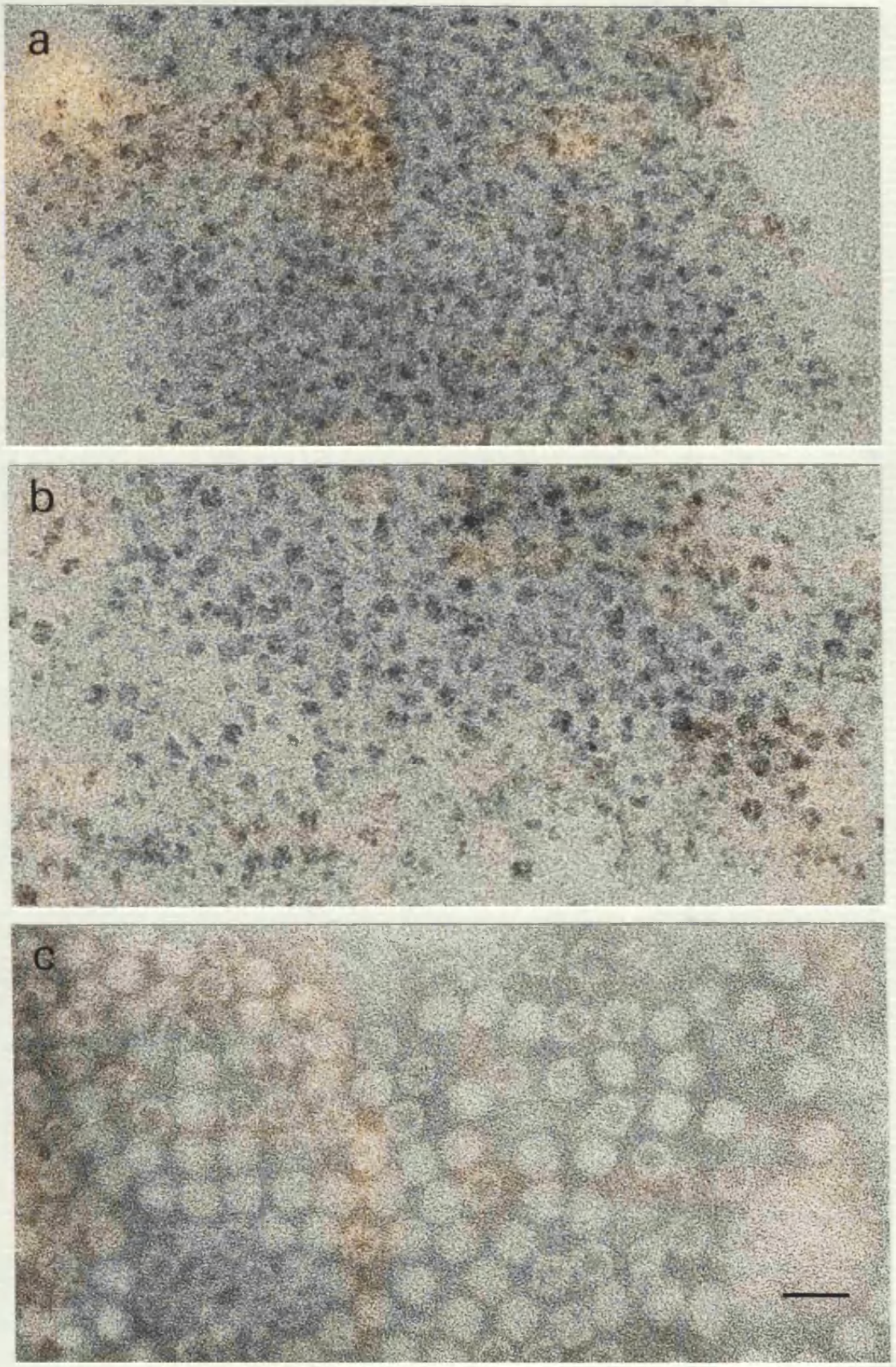

Plate 4.5 Electron micrographs of reconstituted H-subunit variants based on CdM. *a* CdM, *b* 222, *c* A222 (*a* & *b* unstained, *c* negatively stained with sodium silicotungstate, courtesy of Miss F. Meldrum. The occasional dark centres observed in *c* are staining artefacts; no cores were seen in the corresponding unstained protein.) Bar marker 20nm for *a*, *b* & *c*.

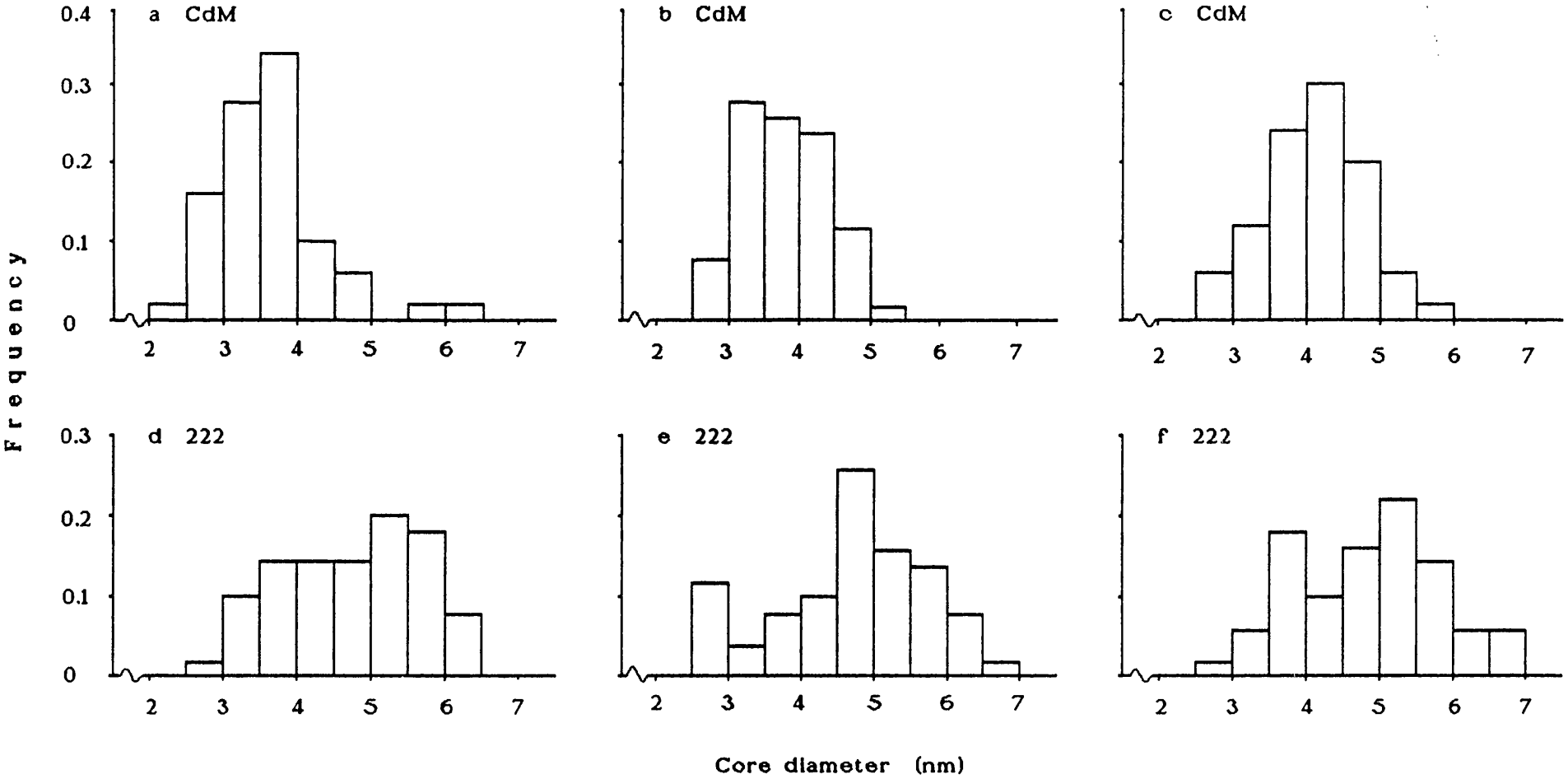

Figure 4.7 Particle size distributions for samples of CdM and 222.
a & d method 2, *b & e* method 3 and *c & f* method 5.

the final one of **CdM** (method 5), which appeared to be less crystalline.

2 The ferroxidase and nucleation site variant **A222**

One sample of this protein, reconstituted by method 5 (experiment 2, along with **rHF** and **A2** described in section 4.2.4) was studied.

No iron cores were visible in the electron micrographs of this sample, although intact apoferritin could be seen when the grids had been negatively stained with sodium silicotungstate (plate 4.5c). This indicated that this variant was incapable of taking up and retaining iron to any appreciable extent. It was noted by Dr. Arosio, who's group reconstituted this sample, that there was a much higher proportion of non-specific oxidation product formed here, than with any of the other samples studied.

3 **205'** and the 3-fold channel variants **174** and **204**

The control sample for this set of experiments was **205'**, which carried just the **CdM** mutation. One sample of each protein was studied, each reconstituted by method 1 in the same experiment.

205'

The cores of this sample were generally of regular squarish shapes. There were some which were more rounded and a few were anisometric, see plate 4.6a. The mean core diameter was 4.65 nm, with a standard deviation of 0.87 nm. The particle sizes ranged from 2.84 - 6.27 nm and a distribution is shown in figure 4.8.

3-fold channel

i) **174** The iron cores in this sample were of mostly angular shapes, very few cores were rounded. The shapes were both isometric and anisometric. Plate 4.6b. The mean core diameter was 4.35 nm, with a standard deviation of 0.86 nm. The particle sizes ranged from 2.40 - 5.98 nm and a distribution is shown in figure 4.8.

ii) **204** These cores were also mostly angular in shape, see plate 4.6c. The mean core diameter was 4.18 nm, with a standard deviation of 0.86 nm. The particle sizes ranged from 2.25 - 6.06 nm and a distribution is shown in figure 4.8.

When the particle size histograms for these samples were compared no significant change in the size distributions could be seen for sample **174**, but a slight reduction in core sizes could be seen for sample **204**.

The distributions for **205'** and **204** were of very similar shapes, but that of **204** appeared to have been shifted down in size by 0.5nm. This meant that in **204** the frequencies of core diameters above 5nm were significantly reduced and for diameters between 3.5 and 4nm, the frequency of 0.2 was 0.12 higher than that in **205'**.

See also the core size data in table 4.4.

Comparisons between a number of electron diffraction patterns from each of these samples did not reveal any major structural changes in their iron cores. They were all poorly crystalline ferrihydrite giving a diffraction line at ~2.5Å and broadened lines centred at ~2.1 and ~1.5Å. (See table 4.5 for the data from sample **205'**.)

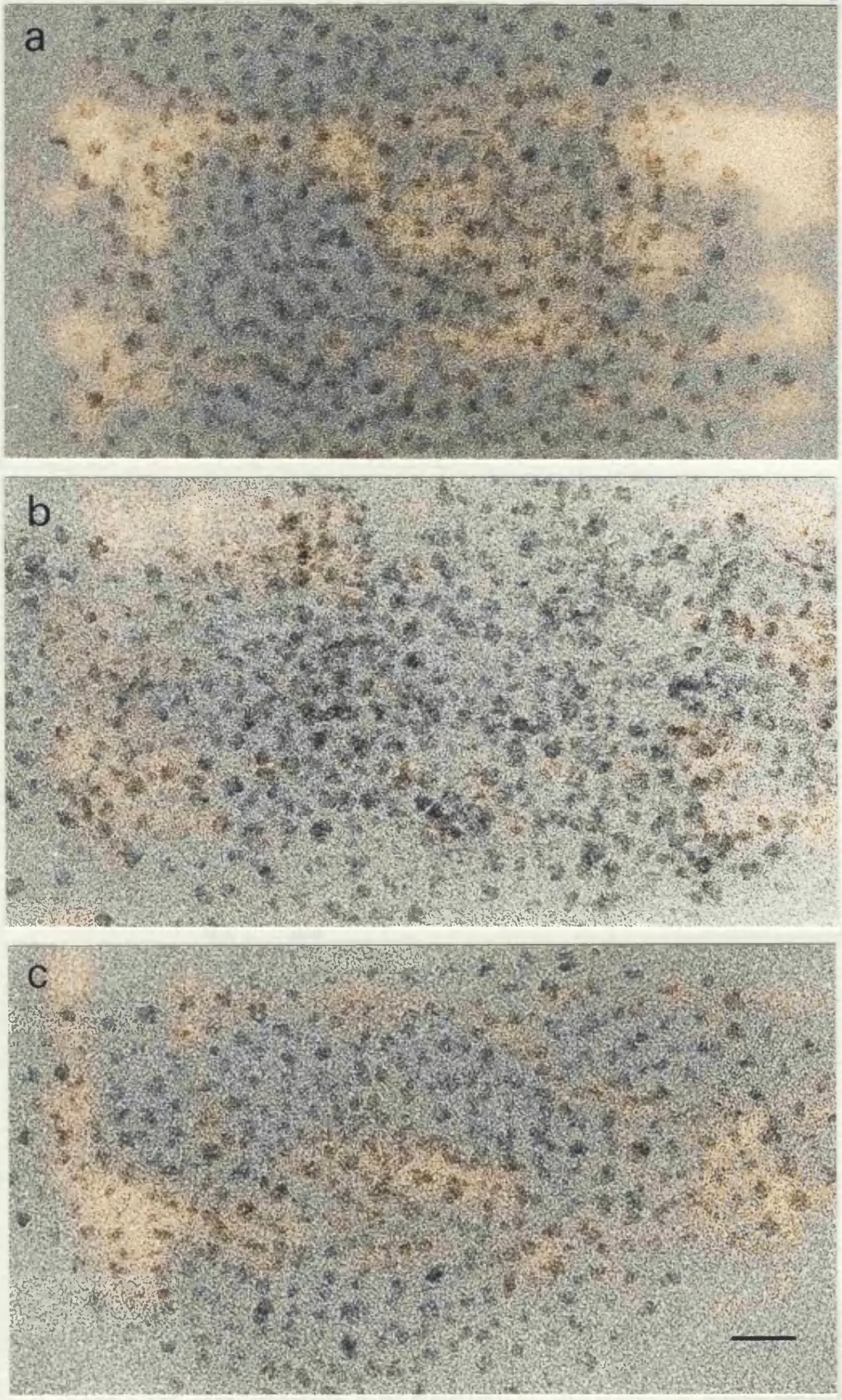

Plate 4.6 Electron micrographs of unstained reconstituted ferritins 205' (*a*) and the 3-fold channel variants 174 (*b*) & 204 (*c*). Bar marker 20nm for all micrographs.

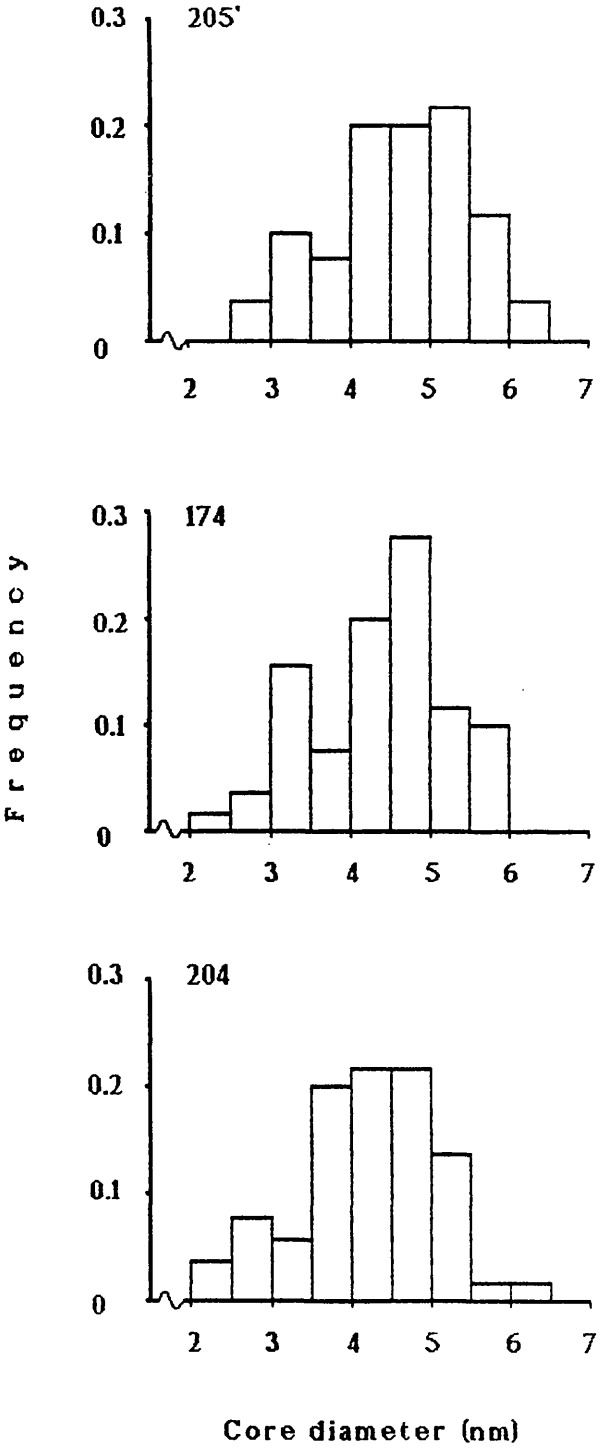

Figure 4.8 Particle size distributions for the 3-fold channel variants and their control sample, all reconstituted by method 1.

Table 4.4

Particle size data for reconstituted recombinant H-subunit ferritins.

Method/ Expt.	Protein	Mean, nm	SD, nm	Range, nm
1/2	rHF	4.48	0.92	3.04 - 6.70
	R2	4.84	0.98	2.70 - 6.68
	102+150	4.55	0.83	2.87 - 6.24
5/2	rHF	4.30	0.65	2.77 - 5.74
	A2	4.19	0.87	2.08 - 5.91
1/3	A2	4.13	0.92	2.15 - 5.79
2	CdM	3.63	0.74	2.40 - 6.10
	222	4.76	0.99	2.71 - 6.46
3	CdM	3.75	0.58	2.64 - 5.04
	222	4.74	1.04	2.58 - 6.66
5	CdM	4.13	0.65	2.79 - 5.63
	222	4.85	1.03	2.62 - 6.85
1	205'	4.65	0.87	2.84 - 6.27
	174	4.35	0.86	2.40 - 5.98
	204	4.18	0.86	2.25 - 6.06

Table 4.5

Electron diffraction data for some of the H-subunit variant samples.

R2		A2		CdM		222		205'	
d(Å)	I	d(Å)	I	d(Å)	I	d(Å)	I	d(Å)	I
2.47	S	2.51	S	2.56	S	2.46	S	2.54	S
2.33	MB	2.28	M	2.41	M	2.35	S	2.32	M
1.96		2.03	M	1.99		1.97		1.96	
1.53	MB	1.51	W	1.53	M	1.55	VW	1.53	W
1.46		1.47	S	1.49		1.48	MS	1.46	S

Intensities (I) as judged in Table 4.2

4.3 DISCUSSION

The work presented in this chapter will be discussed under four headings initially and then a broader discussion will follow. Some of the principal results on core size and morphology are represented schematically in figure 4.9.

4.3.1 Homopolymers

The results of this study of homopolymers comprising either H- or L-subunits showed that iron cores were formed in each, but in the L homopolymer, both human and rat, there was a significant population of larger cores with a more regular and rounded morphology, (see figure 4.9). rLF and r-rat LF lack ferroxidase activity (Levi *et al.*, 1989a & Harrison *et al.*, 1989 respectively) and rLF takes up iron more slowly than rHF (Levi *et al.*, 1989a). It may be proposed that

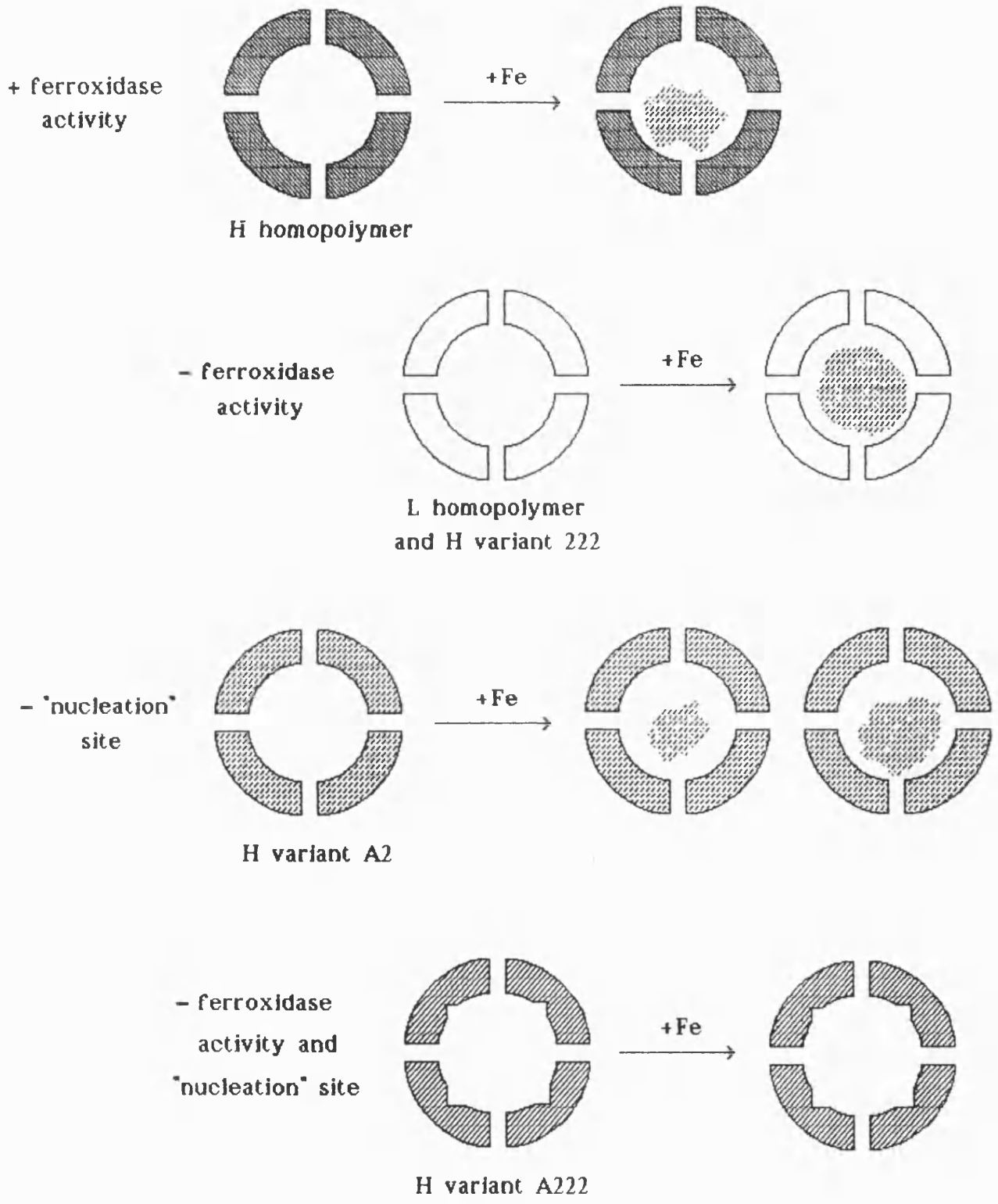

Figure 4.9 Schematic representation of some of the principal results on core morphology and size, following reconstitution of H and L homopolymers and H-subunit variants.

during reconstitution, because there is no ferroxidase activity, the effective concentration of Fe^{3+} in solution is low, so only a few cores nucleate early in the reconstitution process. These few cores attain a relatively large size, since autocatalysis favours their growth. As the Fe^{3+} concentration increases through autooxidation more cores nucleate (a second nucleation event was indicated by the bimodal particle size distributions), but they do not grow as large. The large cores have a more regular, rounded shape because as the protein cavity becomes full the shape of the iron core is increasingly influenced by the shape of the cavity.

Differences in the processes of core formation in H and L homopolymers may also be discussed with reference to the kinetic scheme used in the discussion of chapter 3 (figure 3.23). In L homopolymers, because of the lack of ferroxidase activity, the rate of oxidation (k_2) would be diminished compared with H homopolymers and the rate of nucleation (k_3) would become the rate determining step.

rLF may be exhibiting a greater nucleation capacity or efficiency in that cores grow inside the protein despite the lack of ferroxidase activity. Such a greater capacity was proposed by Boyd *et al.* (1985) on the grounds of a higher number of potential iron binding residues exposed in the cavities of L-rich ferritins compared with H-rich ferritins. More recent sequence and X-ray crystallography data (Harrison *et al.*, 1989) have shown that in addition to the three glutamic acid residues of the proposed nucleation site, which are common to both H- and L-subunits, the L-subunits have two additional conserved glutamic acid residues (Glu 57 & 60, H-subunit numbering) which are close to the cavity surface, (these residues are histidines in H-subunits). These additional carboxylate groups may enhance the

ability of L homopolymers to sequestrate iron and nucleate cores in the absence of ferroxidase activity.

The extent to which H-subunits modify the properties of a heteropolymer is illustrated by comparing the core sizes and morphologies in samples **rLF** and **HLF** both reconstituted by method 1. The small proportion of H-subunit (10%) has abolished the increase in core size and the effect of producing more cores with a rounded morphology. These observations confirm the proposal that ferritin's catalytic activity is attributable to the H-subunit (Levi *et al.*, 1988) and they suggest that 10% H-subunit is sufficient to "activate" the molecule.

The differing core morphologies of **HLF**, **rHF** and **rLF** may explain the different kinetics of iron release from these samples (Dr. Arosio pers. comm., see figure 4.10a), although the nature of the 4-fold channels may have some effect also. The smaller, more irregular shaped cores of **HLF** and **rHF** would be more readily solubilised by the reductant than the larger, more rounded cores of **rLF**. The smaller cores would have a larger and more accessible surface area, while the larger cores were probably in closer contact with the protein and would have had a smaller surface area to volume ratio.

4.3.2 Varying H:L ratios

This study showed that a reduction in the proportion of H-subunits present in the heteropolymer led to an increase in core size and crystallinity and that the cores became more rounded in shape and less aggregated on the electron microscopy grid. Kinetic studies have compared **HLF** with **rHF** and **rLF** (Levi *et al.*, 1989a and Levi *et al.*, 1988); **HLF** having initial iron uptake rates between those of **rHF** and

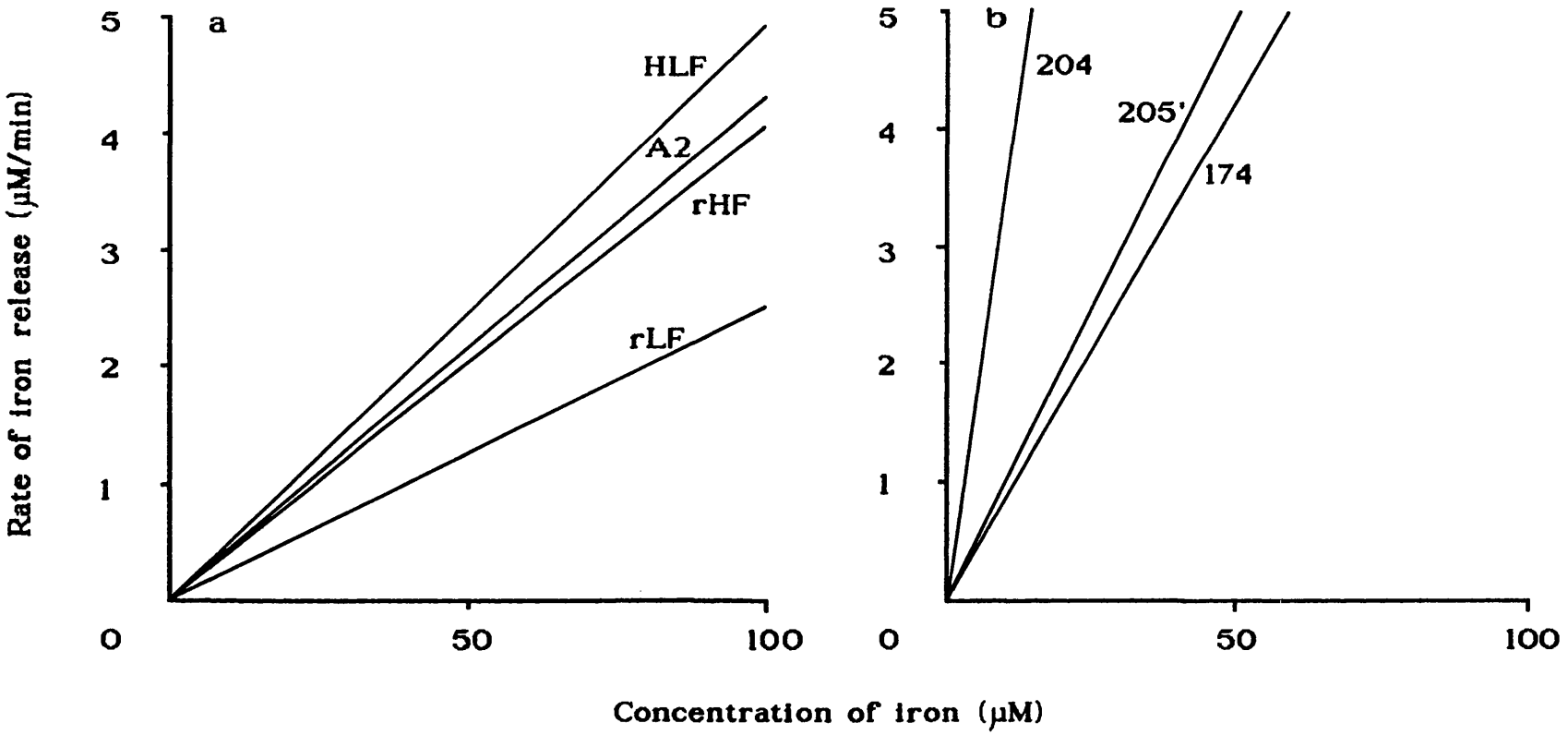

Figure 4.10 Initial rates of iron release from some of the reconstituted ferritins. Studied by incubating various concentrations of the ferritins with thioglycollic acid (50 mM) and bipyridine (2 mM) in 0.2 M sodium acetate buffer pH 5.6 at 30°C and monitoring the formation of the red bipyridine Fe (II) complex at 520 nm for 1-3 minutes. Data courtesy of Dr. Arosio.

rLF, but closer to those of rLF, and HBF is known to have faster uptake kinetics than HLF (Prof. Harrison, pers. comm.). So, as in the study of homopolymers, it is apparent that the H-subunit contributes to the faster kinetics of H-rich heteropolymers and this leads to smaller, more irregular shaped cores.

With this sample of HLF, as with that reconstituted by method 1, a slightly bimodal distribution was seen in the histograms, again suggesting that two nucleation events occurred during the process of reconstitution of these proteins. This bimodal pattern was not seen with rHF or HBF and a similar argument as to why this occurs as that given above for rLF may be invoked.

An increase in core crystallinity was apparent for samples HBF and HLF compared with rHF, this may be explained by the slower iron uptake in HBF and HLF allowing a more crystallographically ordered core to form. Such an increase in crystallinity was not seen when rHF and rLF reconstituted by method 1 were compared. The conditions of reconstitution are probably responsible for this effect; the kinetics of the overall reaction being driven more by the physiochemical conditions in solution than the properties of the proteins (see 4.3.4 below). Core size and morphology may more readily reflect a change in the rate of iron loading than an increase or decrease in crystallinity. Thus, the former is seen in reconstitutions at both pH 6.45 and 7.0, whereas the latter is only seen in the reconstitution at pH 6.45.

4.3.3 H-subunit variants

a) 4-fold channel

In **R2** there was a slight increase in core size. This may be explained by the slightly reduced iron uptake kinetics reported for this protein in Levi *et al.*, (1989b). As for rLF homopolymers, though not to such an extent, the slower iron uptake resulted in a larger average core size. However, the cause of the slower uptake was not the same for these two proteins; for rLF homopolymers it was the lack of the ferroxidase site, whereas for **R2** it may have been the increase in positive charge and bulk of the group in the centre of the 4-fold channel. The four symmetry related arginines present at the narrowest part of the channel may have partially or completely blocked the channel. These channel changes may have reduced the diffusion of reactants into the cavity, or products out of the cavity. Thus, k, in figure 3.23 may have been reduced and become more important in determining the overall rate of reaction.

There was no significant difference in the core size of **102+150**, so the alteration of the 4-fold channel to the L-subunit sequence does not appear to have had any great effect. This is also borne out by the very similar iron uptake kinetics reported in Levi *et al.*, (1989b) for this H-subunit variant compared with **rHF**. These results indicate, contrary to the proposals of Boyd *et al.* (1985), that the differences in the 4-fold channels between H and L homopolymers are not significant in core formation. See also c) ferroxidase site below.

b) "nucleation" site

In **A2** there was no change in the average core size, but the distribution of core sizes was broader than that for the **rHF** control, (see figure 4.9). These observations suggest that the alteration of the proposed nucleation site has had some effect. It is interesting to note here that the initial iron uptake kinetics for **A2** were approximately 20% of those of **rHF** (Dr. Arosio pers. comm.), but the release kinetics were about the same as **rHF** (figure 4.10a).

The residues altered in **A2** are close to the ferroxidase site and this may account for the diminished iron uptake kinetics of this variant. The substitution of Glu 61 may have been the most important change since this one is closest to the ferroxidase residues Glu 62 and His 65, (see figure 1.10 in chapter 1). A reduction in the activity of the **A2** site(s), may have caused feed-back inhibition of the ferroxidase centre. The broadened size distributions of **A2** may indicate that nucleation was occurring at different times in the population of cavities, due to the diminished rate of iron uptake/ deposition. Whereas, in **rHF**, there would have been essentially one nucleation event. That the release kinetics of **A2** were similar to those of **rHF** can be attributed to the similar core size. The conservation of the 3- and 4-fold channel sequences may also be important, but as yet a pattern in the data is not clear, (for example see e) 3-fold channel, below).

It was noted that a high proportion of non-specific oxidation product formed during the reconstitution of this protein, compared with its control (**rHF**, Dr. Arosio, pers. comm.). The variant is therefore competing less effectively than **rHF** with the iron oxidation and precipitation taking place in bulk solution. This may be as a result of partial inhibition of the ferroxidase activity discussed

above or a decrease in the protein's nucleation capacity or efficiency. With reference to the kinetics scheme in figure 3.23 either k_2 or k_3 may be diminished compared with k_2 and k_3 for rHF and a decrease in k_3 would lead to a reduced rate of autocatalysis (k_a).

c) ferroxidase site

The results from the samples of **222**, like those from the **rLF** homopolymers, clearly show the effect of the lack of ferroxidase activity on the size and morphology of the iron cores formed in these proteins, (figure 4.9). Also, like **rLF**, the iron uptake kinetics for **222** were reduced compared with its control (**CdM**, Prof. Harrison pers. comm.). So again, with reference to figure 3.23, k_2 would have been reduced and k_3 would have become the rate determining step.

It appears from these results and those from variant **A2**, that the ferroxidase centre is more important to ferritin's function than the proposed nucleation site; the changes in core morphology and size in **222** compared with **CdM** were more marked than those for **A2** compared with **rHF**.

Similarities between the reconstituted cores of **rLF** and **222** suggest again that the properties of the 4-fold channels formed in H and L homopolymers are not significant in core formation, since the channels of **222** remain like those of an H homopolymer.

d) ferroxidase and nucleation site

A222 was the only protein studied in which reconstituted iron cores failed to form, (see figure 4.9). The quaternary structure of the protein had been conserved, but its functional activity had been lost. The alteration of amino acid residues at both the ferroxidase and nucleation sites had abolished the protein's ability to store

iron, whereas alteration of just one or the other only modified its performance. Two other variants of H-subunit ferritin have been described (Levi *et al.*, 1989b) which could not form cores, but both of these were drastically altered at the C-terminus; one having the E-helix deleted and in the other the E-helix was displaced outside the assembled molecule.

The attempted reconstitution of **A222** resulted in non-specific oxidation and precipitation in bulk solution (Dr Arosio pers. comm.). The substitution of glutamic acids 61, 64 and 67 for alanines, together with substitutions at the ferroxidase centre, appears to have diminished the protein's ability to sequester Fe(II) and/or stabilise incipient Fe(III) nuclei to such an extent that it could no longer compete successfully with the reaction taking place in bulk solution. Once nucleation was achieved outside the protein, further precipitation of the non-specific oxidation product would be favoured by autocatalysis.

e) 3-fold channel

In sample **204** there was a reduction in core size and an increase in the rate of initial iron release compared with **205*** (figure 4.10b). The reduction of charge and increase in hydrophobicity of the 3-fold channel may have affected core growth by reducing the flux of iron or other necessary species (eg. O_2, H_2O) into the cavity, or by reducing the efflux of the by-products of ferrihydrite formation (eg. H^+) from the cavity, (reduced k_1 in figure 3.23). The Glu 134 residues which had been substituted are located toward the outside of the 6Å channel, whereas the Asp 131 residues (substituted in **174**, below) are further down the channel. Modification of the "receptor" end of the channel appears to have had a greater effect on core

reconstitution. The smaller core size and the channel change may have facilitated iron release since the smaller cores would have presented a larger surface area to the reducing agent and the reduced charge in the channel may have facilitated the influx/efflux of reductant/iron-chelate complex to and from the cavity.

In **174** both core size and initial iron release (figure 4.10b) did not appear to be affected by the Asp→His change in the 3-fold channel; the sign of the charge has changed but there has not been a reduction in the number of charged residues.

In all the H-subunit variants studied, in which iron cores were formed, there was no marked difference in the structure of the cores formed under the conditions of reconstitution used, despite their differing uptake kinetics. This may be attributed to the physiochemical conditions in solution, as discussed in section 4.3.2 and below.

4.3.4 Reconstitution conditions

The results from the above studies have illustrated the differences induced in core size, shape and structure in a given protein by the conditions of reconstitution.

When samples of **rHF** reconstituted by methods 1 and 4 were compared there was no change in core shape or size and the size distributions remained broad, but there was a marked increase in the crystallinity of the cores. The sample reconstituted at pH 6.45 with 20 increments gave a 5-line electron diffraction pattern, whereas that reconstituted at pH 7.0 with 2 increments gave only a comparatively diffuse, 3-line pattern (see Tables 4.2 & 4.3).

When samples of HLF reconstituted by methods 1 and 4 were compared method 4 resulted in better crystallinity (again see tables 4.2 & 4.3), larger cores (4.57 vs. 5.40nm, also see histograms in figures 4.3 & 4.5) and more discrete cores, with more regular shapes and less aggregation (see plates 4.1b & 4.3c).

Increased core crystallinity would be induced by slower iron uptake/core formation. The slowing of these processes can be achieved by the reconstitution conditions employed (lower pH and many small increments) or having a higher percentage of L-subunits. However, increased crystallinity is only seen for this second case in reconstitutions at pH 6.45 where the kinetic differences between H and L are more apparent.

4.3.5 Broader discussion

1 Relation of the quaternary structure of ferritin to its function

The results presented in this chapter demonstrate that ferritin can tolerate a number of amino acid substitutions without loss of function, although its efficiency may be reduced. These findings suggest that the quaternary structure of the protein, which dictates the size and architecture of its internal cavity, is the most important factor in core formation, rather than the precise sequence of residues. The cavity provides a restricted reaction volume in which iron oxidation and hydrolysis can occur and ferrihydrite can nucleate and grow. The residues lining the cavity surface would appear to enhance ferrihydrite deposition as demonstrated by the specific reconstitution of L homopolymers and the ferroxidase

depleted H-subunit variant 222, but precise structural correspondence at the core-protein interface is apparently not required.

2 The *in vivo* functions of H and L subunits

This study of homopolymers and heteropolymers has given some insight into the roles of the two subunits *in vivo*. That H-rich ferritins take-up and release iron more rapidly than L-rich ferritins may be accounted for by the presence on the H-subunits of the ferroxidase centre and the formation within the ferritin of small, irregular shaped cores. With ferroxidase activity, storage would seem to be achieved rapidly and small, irregular shaped cores would present a large and accessible surface area to facilitate iron mobilisation. However, the role of the ferroxidase site *in vivo* is not altogether clear, since it has yet to be established if ferritin takes up Fe(II) or Fe(III) *in vivo*.

The large core sizes demonstrated in L-homopolymers suggest that a significant proportion of the protein shells remain empty. This is consistent with the finding that native apoferritin is composed entirely of L-subunits, (Arosio *et al.*, 1978). L-rich ferritins, with a small proportion of H-subunits, store more iron *in vivo* than H-rich ferritins. This may be a result of an enhanced nucleation capacity in the L-type cavity and would be to physiological advantage because larger cores mean that more iron is stored per ferritin molecule. This is economical on protein and the iron is less readily mobilised and so less toxic in conditions of iron overload. Also, *in vivo*, the ferrihydrite in L-rich heteropolymers may be more crystalline than that in H-rich ones, due to slower loading. This would also make the iron less readily mobilised and so less toxic in iron overload.

L-rich ferritins are found in liver and spleen. These are the major organs of iron storage and those first affected by iron overload, (see chapter 5). H-rich ferritins are found in tissues such as brain, heart, pancreas and kidney where a lower level of storage and a higher rate of iron metabolism than, for example in liver, is required. "Tumour-specific" isoferritins are also reported to have higher proportions of H-subunits than are found in most normal tissues (Arosio *et al.*, 1978). Presumably this is due to a high rate of iron metabolism in the rapidly growing tumour. In idiopathic haemochromatosis, an iron loading syndrome, the isoferritin profile of some organs changes as loading proceeds. Ferritins from heart, pancreas and kidney which are normally H-rich, become L-rich and also closely resemble the liver ferritin in iron content and amino acid composition (Powell *et al.*, 1974).

The nature of bone marrow ferritin is interesting, considering the large amounts of iron handled by this tissue. Bone marrow contains two types ferritin which have been distinguished by their electrophoretic mobilities. The ferritin with a faster anodal mobility, and therefore rich in H-subunit, has been classified as "anabolic" since it receives iron for haem synthesis. The other ferritin, which had the same electrophoretic mobility as the ferritins from liver and spleen (therefore L-rich), has been classified as "catabolic". This ferritin acquires its iron from haemoglobin degradation. The "anabolic" ferritin had a lower iron content than the "catabolic" ferritin, the former is presumed to be erythroblast ferritin and the latter present in the marrow RE cells, (Gabuzda & Pearson, 1968, Mazur & Carleton, 1963).

Chapter 5

FERRITIN AND HAEMOSIDERIN IN IRON OVERLOAD

5.0 INTRODUCTION

The work presented in this chapter is a structural and morphological study of a number of ferritins and haemosiderins isolated from human, horse and reindeer liver and spleen under different iron-loading conditions. The work was done in collaboration with Drs. R.J. Ward and T.J. Peters, Clinical Research Centre, Harrow and Dr. D.P.E. Dickson and Miss N.M.K. Reid, Liverpool University.

The primary objective of the study was to find out, using TEM and electron diffraction, if there were any observable differences between these haemosiderins that could account for their differing Mössbauer behaviour. The Mössbauer spectroscopy of various haemosiderins has been documented by Fischbach *et al.*, (1971), Bell *et al.*, (1984), Williams *et al.*, (1986), Dickson *et al.*, (1987) and St. Pierre *et al.*, (1987). A wider objective was to understand further the nature of haemosiderin and its relationship with ferritin.

The study demonstrates that in human iron overload the nature of the haemosiderin formed is disease specific and different to that formed in the non-iron-loading situation. Also the disease forms of human haemosiderin are different to the haemosiderins formed in horse and reindeer.

Haemosiderin is less well characterised than ferritin, but there are similarities between the two which suggest that they are related, with haemosiderin possibly deriving from ferritin. Haemosiderin iron cores are smaller than those in ferritin and there is a reduced amount of protein associated with them, (Williams *et al.*, 1986). Transmission electron microscopy shows that the iron cores tend to aggregate and the protein shells are less well defined. Generally iron uptake and release by haemosiderin is slower than these processes in ferritin. Haemosiderin is insoluble in water. In iron overload diseased states in mammals and birds it is the levels of haemosiderin, rather than ferritin that rise. These properties suggest that haemosiderin is used for longer term iron storage than ferritin, (Harrison *et al.*, 1974).

5.0.1 Iron homeostasis

Iron homeostasis in mammals is achieved largely by regulation of uptake of this element from the diet. However, mammals other than man, do have a limited capacity to excrete iron, mainly via the gastrointestinal tract, if excessive amounts should enter the body (Finch, *et al.*, 1978). Man seems to be unique among the mammals in having no physiological route for the excretion of excess iron (Jacobs, 1980). It is worth noting also that man has the most limited ability to absorb iron from the diet (Finch, *et al.*, 1978). This very restricted iron exchange probably accounts for man's predisposition to pathological conditions of anaemia and overload (Finch, *et al.*, 1978).

Iron storage in the body is an important aspect of normal iron metabolism, since iron containing molecules are subject to metabolic

turn-over and there are normal physiological variations in the iron demand of various tissues. The initial site of iron storage is in ferritin. Figure 5.1 shows the most important tissues involved in iron storage. If the iron is not mobilised from ferritin because the body has too much iron then haemosiderin is formed. In the early stages of iron overload this storage complex accumulates in the cells of the liver or spleen, depending on the cause of the overload, but as the loading continues haemosiderin builds up in many other tissues, including the heart, (Jacobs 1980).

5.0.2 Iron overload

Iron overload in mammals arises under a number of circumstances. Horses, in their old age, accumulate haemosiderin in the spleen. This is thought to be due to enhanced red blood cell destruction, (Dr. T.J. Peters pers. comm.). Spitzbergen reindeer suffer a seasonal iron overload as their feeding pattern is dictated by climatic factors. In summer, when grazing is available, food reserves are laid down in the reindeer's body. In winter, when food is scarce, these reserves are used up and the tissue iron is turned over and stored in the liver and spleen. The following summer, as the reindeer feeds again and regains weight, the stored iron is mobilised, (Dickson, *et al.*, 1987).

Human subjects in iron balance have very little or no haemosiderin. Recently, Ward *et al.*, (1989), isolated a small amount of haemosiderin from the spleen of a 76 year-old female who had no symptoms of iron overload. There are two human pathological conditions under which iron overload occurs: primary and secondary haemochromatosis.

Idiopathic haemochromatosis, a form of primary haemochromatosis, is an inherited disorder of iron metabolism where too much iron is taken up from the diet. The initial site of deposition is the liver and other tissues are affected if the condition is left untreated. Where the iron accumulates severe tissue damage results. Once this condition has been diagnosed regular removal of blood (by venesection or phlebotomy) from the body will reduce accumulated iron stores and prevent subsequent loading. If the condition is correctly diagnosed early on, complete reversal of any tissue damage can be expected.

In secondary haemochromatosis the iron overload is secondary to another disorder and is indeed caused by the treatment of the primary disorder. Most commonly the primary disorder is thalassemia, particularly β-thalassemia. The thalassemias are disorders of haemoglobin synthesis, leading to severe anaemia, which is treated by regular transfusions of whole blood. Increased amounts of iron enter the body, 200-250mg per unit of blood (Peter, 1985), having by-passed the regulatory uptake mechanism. Overload results because the excess iron cannot be excreted. The extra iron is in the form of haemoglobin in red blood cells and thus is handled by the reticuloendothelial system (RES) in the spleen. Therefore, this is the organ initially affected by the overload. If the excess iron is not removed by chelation therapy, other tissues such as liver and heart become affected. In this iron-loading syndrome, in contrast to primary haemochromatosis, the iron causes little tissue damage until the parenchymal loading is substantial (in the very last stages), when fibrosis occurs and the liver and myocardium may be affected, (Jacobs, 1980).

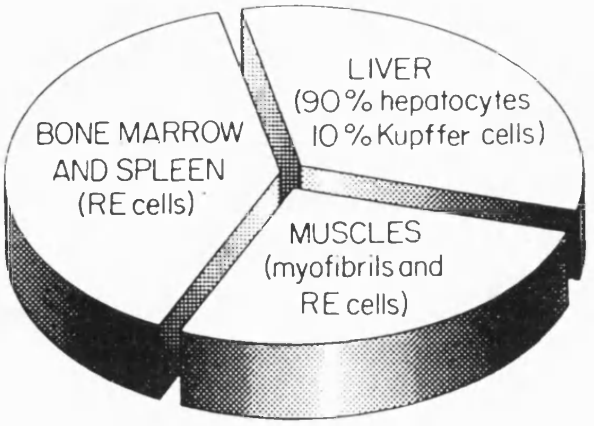

Figure 5.1 Location and relative sizes of the major sites of iron storage in normal human subjects. After Bothwell *et al.* (1979).

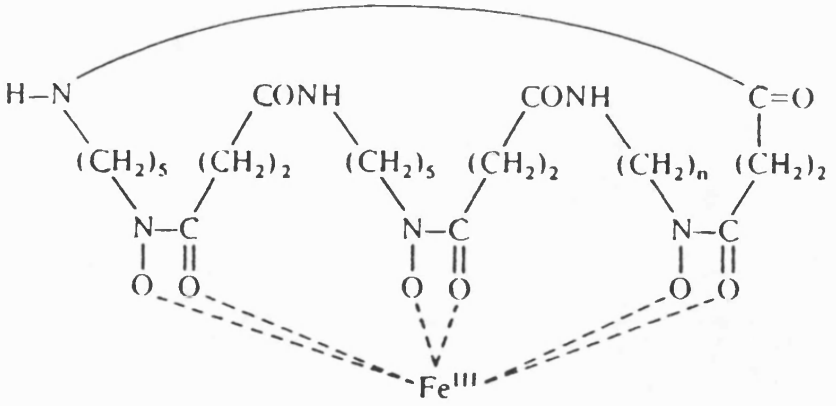

Figure 5.2 Diagram of the structure of the desferrioxamine complex with Fe(III).

Chelation Therapy

In secondary haemochromatosis iron chelating drugs have to be administered to mobilise the excess stored iron in non-toxic form which can be eliminated from the body by excretion. At present the only such drug available for clinical use is desferrioxamine.

Desferrioxamine, molecular weight 539, is a bacterial siderophore with three hydroxamic acid groups. A very stable complex, $k = 10^{30.6}$ (Peter, 1985), is formed with Fe^{3+}, satisfying the preferred six coordination of iron in this oxidation state. Reynolds (1989) reports that 100 mg desferrioxamine binds 8.5 mg iron and that in solution at pH 6 its binds ferric and ferrous iron maximally, whereas at lower pH values it combines well with Fe(III) but not with Fe(II). When bound, the metal ion is completely enclosed within the complex. The complex has a hydrophilic character and is therefore water soluble. The chelate also has some lipophilic character and can therefore mobilise parenchymal iron from hepatocytes via the bile, as well as RE iron via the urine, (Hershko *et al.*, 1985).

Ciba-Geigy produce desferrioxamine by large scale fermentation of a *Streptomyces* strain and market it under the brand name Desferal as the methanesulphonate salt. The structure of the desferrioxamine complex with Fe^{3+} is shown in figure 5.2.

The chelate's high affinity for ferric ions means that it can compete with transport proteins for "chelatable iron", transferrin has a complex-formation constant of ~ 10^{30}. Desferrioxamine's high selectivity for iron is very important so that other essential metal ions such as Zn^{2+} and Ca^{2+} are not removed from the body.

Two severe disadvantages for the clinical use of this drug are that it is not active after oral ingestion and that it is cleared very rapidly from the plasma after injection. The subcutaneous

infusion of a low dosage of desferrioxamine over a period of hours, daily, is the most effective use of the drug, but this makes treatment more expensive and less than ideal for use with children and adolescents over the long periods of therapy that are necessary, (Peter, 1985).

5.0.3 Relation between ferritin and haemosiderin

It is widely assumed that haemosiderin is derived directly from ferritin by partial lysosomal degradation of the protein shell, (Ford *et al.*, 1984 and Hoy & Jacobs, 1982). With its protein shell rendered incomplete the ferritin becomes insoluble and clumps together. It has been suggested that high iron loading and high intracellular concentrations of ferritin may predispose it to enzymatic attack leading to aggregation of the ferritin molecules and lysosomal processing to form haemosiderin (Jacobs, 1980). There is evidence that the protein in haemosiderin is the same as that in ferritin; immunological cross-reactivity between the two has been demonstrated and sodium dodecyl sulphate - polyacrylamide gel electrophoresis (SDS-PAGE) of the protein subunits from haemosiderin resolves protein fragments which are cleavage products of the ferritin subunits (O'Connell *et al.*, 1988 and Andrews *et al.*, 1987a&b).

5.0.4 The biochemical nature of haemosiderin

a) The protein

Andrews *et al.*, (1987a&b) have studied the *in vivo* processing of excess iron by rat liver when the overload is achieved by intraperitoneal injection of iron dextran. This group has demonstrated that the iron is processed by liver siderosomes, these are iron-laden secondary lysosomes, enriched in cathepsin D activity, which appear under the TEM as roughly spherical membrane-bound bodies packed with electron-dense particles resembling ferritin cores. The siderosomes contain soluble ferritin and an insoluble iron-protein complex deemed to be haemosiderin. Other cell constituents are present only as minor impurities. Siderosomes are not found in control rats, but in the iron-loaded rats these bodies are found in all types of liver cell, and are particularly concentrated in the Kupffer cells, (Andrews, 1986). The ferritin isolated from the siderosomes has a faster electrophoretic mobility than the cytosolic ferritin and it has been shown to comprise 69% of a small "F-subunit", 24% L-subunit and 7% H-subunit. This "F-subunit" has been isolated and characterised as a peptide derived from the L-subunit of ferritin: it has a nominal molecular weight of 17.3 kDa and arises from cleavage at Glu163, Val164 on the extended loop between helices D and E located on the exterior of the assembled 24-subunit ferritin molecule, see figure 5.3. Again this type of subunit is not found in control rats. There is no evidence of cleavage of the H-subunit. A similar F-subunit has been isolated from the spleens of the iron-loaded rats and this is probably also of siderosomal origin.

Immuno- and gold-staining of the haemosiderin peptides showed a complex pattern. Anti-rat ferritin antiserum confirmed the presence of ferritin within the insoluble haemosiderin by identifying

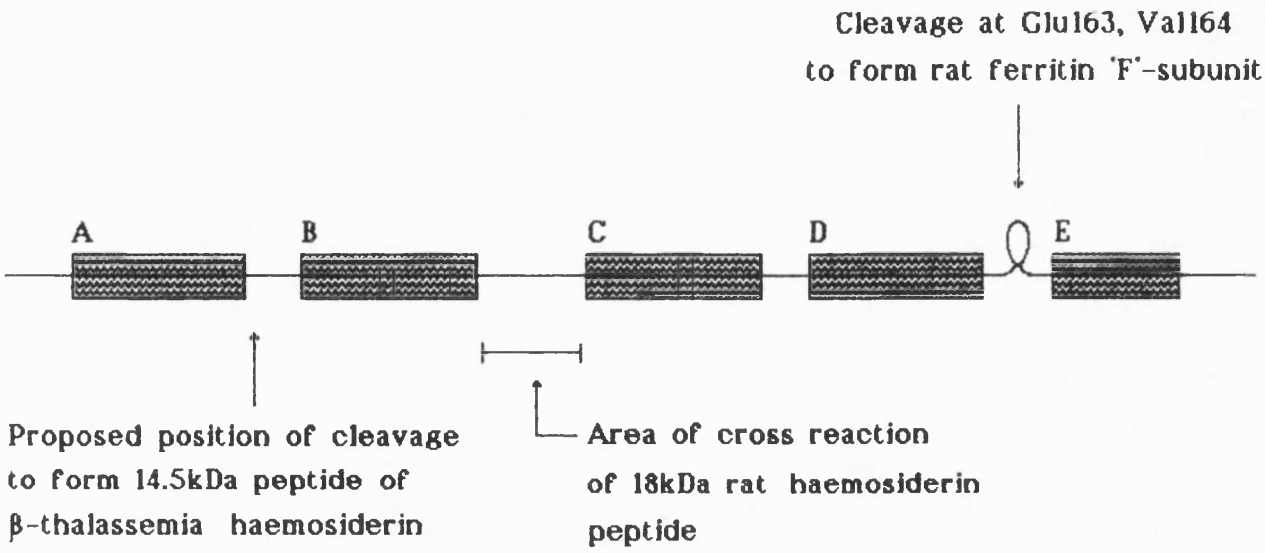

Figure 5.3 Schematic diagram of the ferritin L-subunit showing its relationship to siderosomal ferritin and haemosiderin in rat and the major peptide present in β-thalassemia haemosiderin. The shaded boxes represent the five alpha helices, A to E. Human and rat L-subunits share extensive homology, apart from the rat sequence having an eight residue insertion between residues 161 and 162, which is represented by the extended loop between helices D and E.

L-subunit, the 17.3 kDa F-subunit and a band at about 7 kDa. Gold-staining revealed the 7 kDa peptide, small amounts of F- and L-subunits, several bands of relatively high molecular weight and a major band at about 18 kDa which was not present in the soluble ferritins. This major peptide cross-reacts with sera raised against a peptide representing amino-acids 83-91 of the human L-subunit (loop between helices B & C, see figure 5.3) where rat and human L-subunit differ only by two amino-acids. So this would suggest that it is a ferritin L-subunit peptide. It is unclear at present how the various peptides isolated from the soluble ferritins and the insoluble haemosiderin fit into a pattern of degradative steps.

Massover (1985b) identified an 18 kDa subunit from siderotic mouse liver which was present as a minor component together with a 22 kDa subunit, similar to that in the major ferritin. He proposed that this smaller species may be produced *de novo* as a response to siderosis but it is possible that it arises in a similar way to the F-subunit in siderotic rat liver.

The peptide composition of haemosiderin isolated from the spleens of patients suffering from β-thalassemia (and hence secondary iron-overload) has been shown (Weir *et al.*, 1984) to be different to that of rat. SDS-PAGE demonstrated a range of peptide bands, the main feature of which was a peptide with an apparent molecular weight of 14,500, additional bands were seen at 12,900, 14,100, 15,500, 16,600, 17,800 and 42,000. The peptides of molecular weight lower than a ferritin subunit were suggested to be ferritin cleavage products. The 42,000 band corresponded to a covalently linked ferritin subunit dimer. More recent work by O'Connell *et al.*, (1988), has confirmed, using immuno-blotting techniques, that the smaller peptides are derived from ferritin and these workers have also proposed that the

14,500 peptide is a C-terminal fragment of the ferritin L-subunit cleaved at around residue 40, see figure 5.3.

Ward *et al.*, (1989) have separated, again by SDS-PAGE, the peptides in liver haemosiderin isolated from patients suffering from idiopathic haemochromatosis (primary iron overload). The major peptide band in this material, in contrast to other haemosiderins, has a molecular weight of around 20,000, similar to unmodified ferritin subunit. It is not clear at present if this indicates therefore that the ferritin protein is not subject to any form of cleavage in this condition. Immunological cross-reactivity of the haemosiderin with the corresponding ferritin anti-sera has yet to be demonstrated.

The process by which cleavage of the ferritin subunits occurs is not clear. Since intact ferritin has been shown to be resistant to proteolytic degradation *in vitro* (Coffey & de Duve, 1968) it seems likely that an alternative initiation of damage and degradation is necessary. Free radical oxidation of susceptible amino-acid residues, such as those with aromatic or thiol side chains, in ferritin could cause the initial damage. Human and horse spleen ferritins promote the formation of hydroxyl radicals in reaction mixtures containing ascorbic acid and H_2O_2 at both pH 4.5 and pH 7.4 (O'Connell *et al.*, 1986a). This promotion is attributed to the mobilisation of the ferritin iron. These authors suggest that ferritin iron may promote damage to ferritin protein thereby predisposing the ferritin to conversion to haemosiderin. SDS-PAGE of ferritin incubated with ascorbate at pH 4.5 or pH 7.4 has demonstrated that the protein is damaged (O'Connell *et al.*, 1986b). A high proportion of tyrosine residues in the region of residue 40 in human L-subunit could be

susceptible to free radical oxidation, so generating the 14,500 peptide seen in human β-thalassemic spleen haemosiderin, (O'Connell *et al.*, 1988). Comparison of the amino-acid compositions of ferritin and β-thalassemic spleen haemosiderin (Weir *et al.*, 1984) shows a number of differences; the loss of tyrosine, phenylalanine and methionine residues is consistent with oxidation occurring during the conversion of ferritin to haemosiderin. Again, it is not clear if the ferritin protein in idiopathic haemochromatosis is subject to free-radical oxidation, since it is apparently not cleaved when the haemosiderin is formed.

O'Connell *et al.* (1986a) also suggest that the formation of haemosiderin might represent a biological protective mechanism since the iron in the haemosiderin they studied is less active in promoting the formation of free radicals than that in ferritin. This does not seem to be the case with the haemosiderin formed in primary haemochromatosis. (See section on core solubility studies in the discussion.)

b) The iron core

The iron cores of haemosiderin are smaller than those of most ferritins and this is attributed to some iron loss or partial dehydration of the ferrihydrite. In the fast ferritin isolated from rat liver by Andrews *et al.* (1987a), the number of iron atoms per molecule was considerably smaller than that of the cytosolic ferritin (2170 ± 420 and 3050 ± 70, respectively) and this smaller core size was proposed to be similar to that found in the haemosiderin. This may be further evidence that this siderosomal ferritin is a precursor of haemosiderin and that iron loss occurs during conversion to haemosiderin.

It has been assumed that the nature of the mineral core is essentially unchanged; X-ray diffraction studies, for example by Fischbach *et al.* (1971) and Ford *et al.* (1984) and the Mössbauer study in the Fischbach *et al.* paper led to this conclusion for horse and human β-thalassemic haemosiderin. These authors concluded that the structures of the iron cores were indistinguishable and that the haemosiderin cores were smaller than the ferritin cores by XRD and TEM (Fischbach *et al.*, 1971). However, work presented in this chapter demonstrates for the first time that there are distinct structural differences between ferritin cores and those of the various haemosiderins isolated from different human disease states. It is also shown, that in animal and 'normal' human haemosiderin, the core structure does remain unchanged.

c) Other constituents

1. Sugars

Galactose (200μM/g), mannose (100μM/g) and fucose (20μM/g) were found in β-thalassemic human spleen haemosiderin (Weir *et al.*, 1984). However, the authors proposed that these may be contaminants since sialic acid and hexosamines, the common constituents of mammalian carbohydrate side chains, were not found. Also, previous reports suggested low and variable carbohydrate compositions.

2. Lipids

A total lipid content of approximately 6.7% (w/w) in haemosiderin has been found, (Weir *et al.*, 1984). This is a substantial quantity, but it is not clear if this material is a contaminant or not. The amounts of phospholipid and cholesterol present do not indicate direct derivation from either lysosomal or erythrocyte membranes. However, lipid may be an intrinsic part of haemosiderin

since ferritin accumulates on lamellar structures before the formation of haemosiderin in lysosomes, (Weir *et al.*, 1984 and references therein). O'Connell *et al.*, (1986b) suggest that peroxidising lipids may play a part in the conversion of ferritin to haemosiderin and so they may well be closely associated with the product.

3. Phosphate

The phosphate to iron ratio found by Weir *et al.* (1984) was 1:6 and this was deemed to be mostly core absorbed. Andrews *et al.*, (1988) reported ratios of 1:8.1 (±1.3) and 1:3.1 (±0.44) for their rat liver haemosiderin, the lower ratio (1:8.1) being found in insoluble clumps of material rather, than that brought into suspension by sonication in 10mM tetramethyl-ammonium hydroxide plus 1% w/v Nonidet-P40.

4. Magnesium

This element appeared to be core associated, possibly bound to the phosphate and was present at a level of 13.8 ±7.8 mmol/mol iron, (Weir *et al.*, 1984).

d) Iron:protein ratios

A high iron:protein ratio is characteristic of haemosiderin and Weir *et al.*, (1984) report a weight ratio of 1.4 - 2.0 for haemosiderin compared with 0.1 - 0.4 for ferritin, (ref. therein). Williams *et al.*, (1986) report a weight ratio of 1.86 for siderosomal haemosiderin in rat liver overloaded by intraperitoneal injection of iron dextran. Ward *et al.*, (1989) found ratios of 0.56 and 0.41 for the haemosiderins from β-thalassemic spleen and liver, respectively and in idiopathic haemochromatosis liver the ratio was 0.34. In iron-loaded horse spleen and liver haemosiderins the ratios were 0.21 and

0.51 respectively (Dr. R.J. Ward pers. comm.). The ferritins corresponding to these last five samples had ratios between 0.07 and 0.20.

5.0.5 Solubility studies

Various authors have reported *in vitro* studies of iron availability. O'Connell *et al.*, (1985) showed greater mobilisation of iron by ascorbate and 1,10-phenanthroline from ferritin (horse and human spleen) than from human β-thalassemic haemosiderin. At 37°C and pH 7.4 (50mM Tris/HCl) 0.5 mM ascorbate (equi-molar to Fe) mobilised approximately eight times more iron from the ferritins than from the haemosiderin. At 37°C and pH 4.5 (50mM sodium acetate/acetic acid), even in the absence of ascorbate, about five times more iron was mobilised. The iron availability was being measured in this paper by the iron's ability to mediate lipid peroxidation of phosphatidyl-choline liposomes. With 1,10-phenanthroline at pH 7.4 (concentration, buffer and temperature used not given), about twice as much iron was mobilised from ferritin than from haemosiderin.

Andrews *et al.*, (1988) compared iron release from rat and human β-thalassemic haemosiderin and ferritin to 1,2-dimethyl-3-hydroxypyridin-4-one (6.75mM, 15-fold excess to Fe) at 37°C and pH 7.0 (0.1M Hepes). After 24 hours both ferritins had released similar amounts of iron, approximately 38%. The rat haemosiderin had released slightly more iron, approximately 48%, but the human haemosiderin had released significantly less, approximately 20%. Here, the mobilised iron was being reduced and assayed colourimetrically as its complex with 2,2'-bipyridyl.

5.0.6 Mössbauer spectroscopy

The variable temperature Mössbauer spectra of ferritins from mammalian species, animal haemosiderin and β-thalassemic human haemosiderin exhibit superparamagnetic behaviour which is characteristic of a magnetically ordered material present as small particles, (see appendix II).

Mössbauer studies of ferritin and haemosiderin isolated from iron-loaded mammals and birds (horse: Fischbach *et al.*, (1971), reindeer: Dickson *et al.*, (1987), rat: Williams *et al.*, (1986) & St. Pierre *et al.*, (1987), hornbill: St. Pierre *et al.*, (1987)) have established a pattern in which the haemosiderin has a lower mean blocking temperature (T_B) than the corresponding ferritin. Since T_B is related to particle volume, as shown by the equation:

$$T_B\, k = K\, V$$

where k = Boltzmann constant

K = magnetic anisotropy constant

V = particle volume,

the decrease in the value of T_B has been attributed to the smaller particle size in the haemosiderin, as demonstrated by XRD and TEM. A difference in the value of K was not anticipated because the nature of the iron oxide material was the same in both iron-protein complexes.

However, work reported by Bell *et al.*, (1984) on the haemosiderin formed in β-thalassemia revealed that this material had anomalous Mössbauer behaviour in that the haemosiderin's T_B (~70K) was higher than that of the corresponding ferritin (~40K), despite the haemosiderin having a smaller particle size demonstrated by TEM. Bell *et al.*, concluded that the higher value of T_B must be related to

a higher value of K, although it was hard to see why this should be different since the structure of the iron oxide in both materials was believed to be the same. They concluded that the difference may be due to the incompleteness of the protein shells in the haemosiderin.

This proposal was proved incorrect by later work of the same group, (St. Pierre *et al.*, 1988) who could not produce an elevation of T_B by various treatments of ferritin including the total removal of the protein shell. So the reason for a larger value of K must still lie with the nature of the iron oxide core itself.

The structural differences in the iron cores of haemosiderins isolated from different iron overload conditions which are characterised and presented in this chapter explain both the anomalous Mössbauer behaviour and the differences in iron availability of these iron-protein complexes.

5.1 EXPERIMENTAL

The human samples of ferritin and haemosiderin and the horse and reindeer haemosiderins used in this study, were isolated by conventional methods (ferritin: Chan *et al.*, 1985 and haemosiderin: Weir *et al.*, 1984) and supplied by Dr. R.J. Ward, Clinical Research Centre, Harrow. Three types of human haemosiderin were studied; the first was isolated from the spleen of a female (76 years) in iron balance, post mortem. The second type was β-thalassemia haemosiderin, isolated from liver or spleen following post mortem or splenectomy. All the β-thalassemia subjects had undergone multiple transfusion and iron chelation therapy. The third type was idiopathic haemochromatosis haemosiderin, isolated from liver, post mortem.

These subjects had received venesection therapy. The horse haemosiderin was isolated from spleen (27 years). The horse spleen ferritin was Cd-free from Boehringer Corporation Ltd. See table 5.1.

Sample preparation, transmission electron microscopy, electron diffraction and data analysis were all performed as described in chapter 2. The ferritin samples were in 0.15 M NaCl solution (Fisons, A R grade) and the haemosiderin samples in 20 mM tetramethyl ammonium hydroxide, (pentahydrate, Aldrich Chemical Co., after Weir *et al.*, 1984, who demonstrated that this solution disaggregated the haemosiderin without causing disruption to the cores).

Microdensitometer traces of certain electron diffraction pattern negatives were obtained using a Joyce Microdensitometer. This was done in order to assess, perhaps more accurately than could be done by eye, any changes in the intensities of diffraction lines on the patterns.

5.2 RESULTS

5.2.1 Normal human sample

One sample of haemosiderin isolated from a normal human spleen was studied.

Sample NHs

The iron cores in this sample were generally of well rounded shape, although some irregular shapes could be seen. The cores were aggregated but discrete, see plate 5.1a. The mean core diameter was 5.81 nm, with a standard deviation of 0.59 nm. A particle size histogram is shown in figure 5.4a.

Table 5.1 Reference Table of Samples Studied

Sample source	Disease state	Ferritin or Haemosiderin	Code
Female A, spleen	---	Haemosiderin	NHs
Male G, spleen	β-thalassemia	Ferritin	TF1s
Male G, spleen	β-thalassemia	Haemosiderin	TH1s
Male J, spleen	β-thalassemia	Haemosiderin	TH2s
Male X, liver	β-thalassemia	Ferritin	TF31
Male X, liver	β-thalassemia	Haemosiderin	TH31
Y, liver	I. Haemochromatosis	Ferritin	IHF11
Y, liver	I. Haemochromatosis	Haemosiderin	IHH11
Z, liver	I. Haemochromatosis	Haemosiderin	IHH21
Horse spleen	---	Ferritin	EFs
Horse spleen	---	Haemosiderin	EHs
Reindeer spleen	---	Haemosiderin	RHs
Reindeer liver	---	Haemosiderin	RHl

The six-line electron diffraction pattern showed that the material was crystalline ferrihydrite, (but several of the d-spacings were lower than those of the standard; the 2.50, 1.72, 1.51 and 1.48 Å lines had moved in to 2.47, 1.69, 1.49 and 1.44 Å respectively, see table 5.2.)

5.2.2 β-thalassemia samples

a) Ferritins Two individual samples of ferritin from patients with β-thalassemia were studied.

i) Sample TF1s

The iron cores in this sample were discrete, well separated and generally of a regular, rounded shape, plate 5.1b. The mean core diameter was 6.83 nm, with a standard deviation of 0.36 nm. The histogram of core diameters (figure 5.5a) showed that the size distribution was skewed to the right indicating that the ferritin was full, which was to be expected in this condition.

The d-spacings calculated from the electron diffraction patterns of this sample (table 5.3) showed that the structure of the iron cores was that of crystalline ferrihydrite.

ii) Sample TF31

This liver ferritin sample looked much like the IHF11 sample (see below) with discrete cores which were generally angular in shape, being four- or five-sided, plate 5.1c. The mean core diameter was 6.39 nm with a standard deviation of 0.48 nm. A histogram of particle size is shown in figure 5.5b, the distribution was approximately normal about the mean.

The electron diffraction patterns from this sample showed the cores to be quite well-ordered ferrihydrite, see table 5.4.

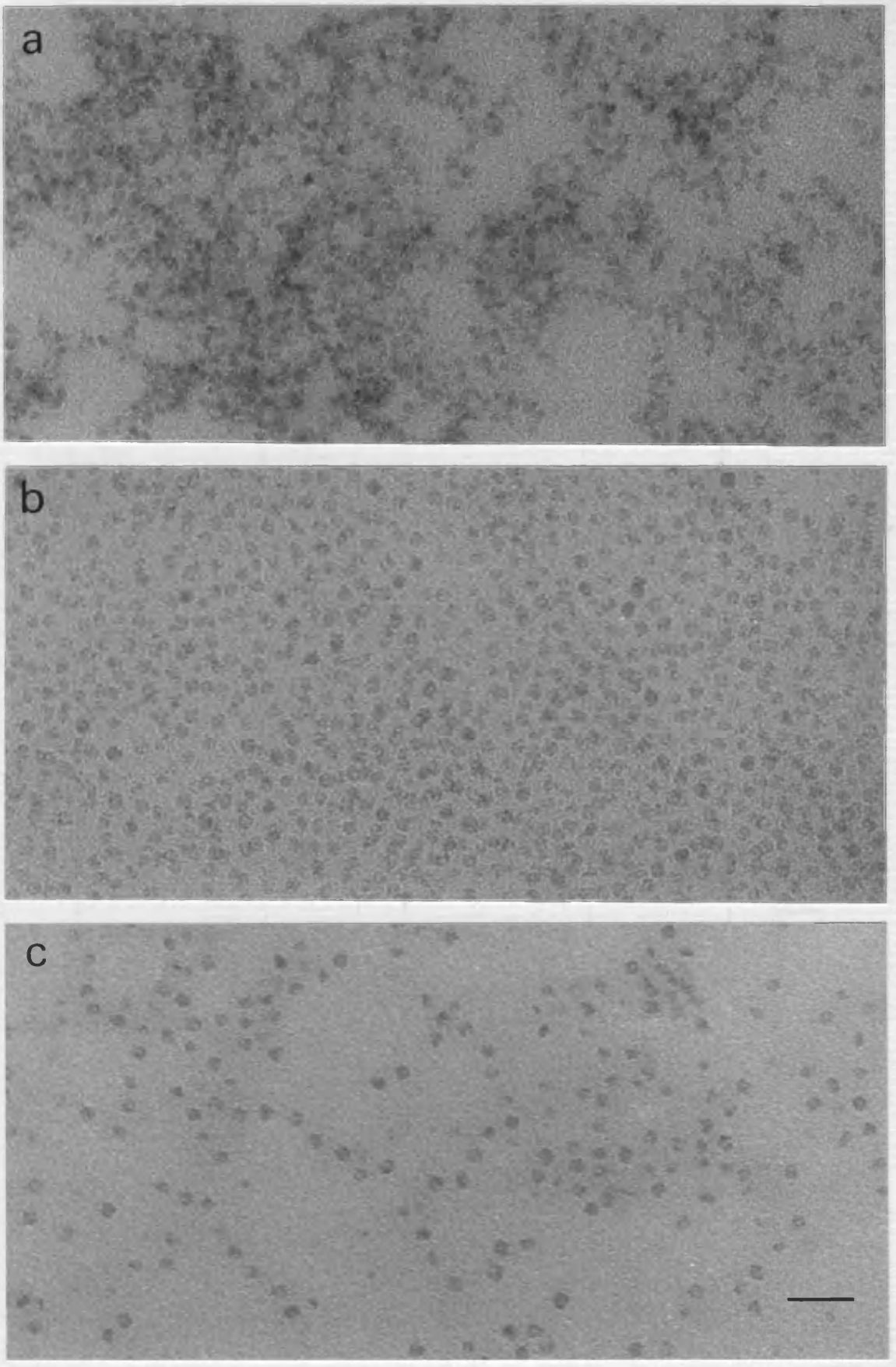

Plate 5.1 Electron micrographs of unstained haemosiderin and ferritin. *a* Normal human spleen haemosiderin (NHs), *b* β-thalassemia spleen ferritin (TF1s), *c* β-thalassemia liver ferritin (TF3l), bar marker 30nm for *a*, *b* & *c*.

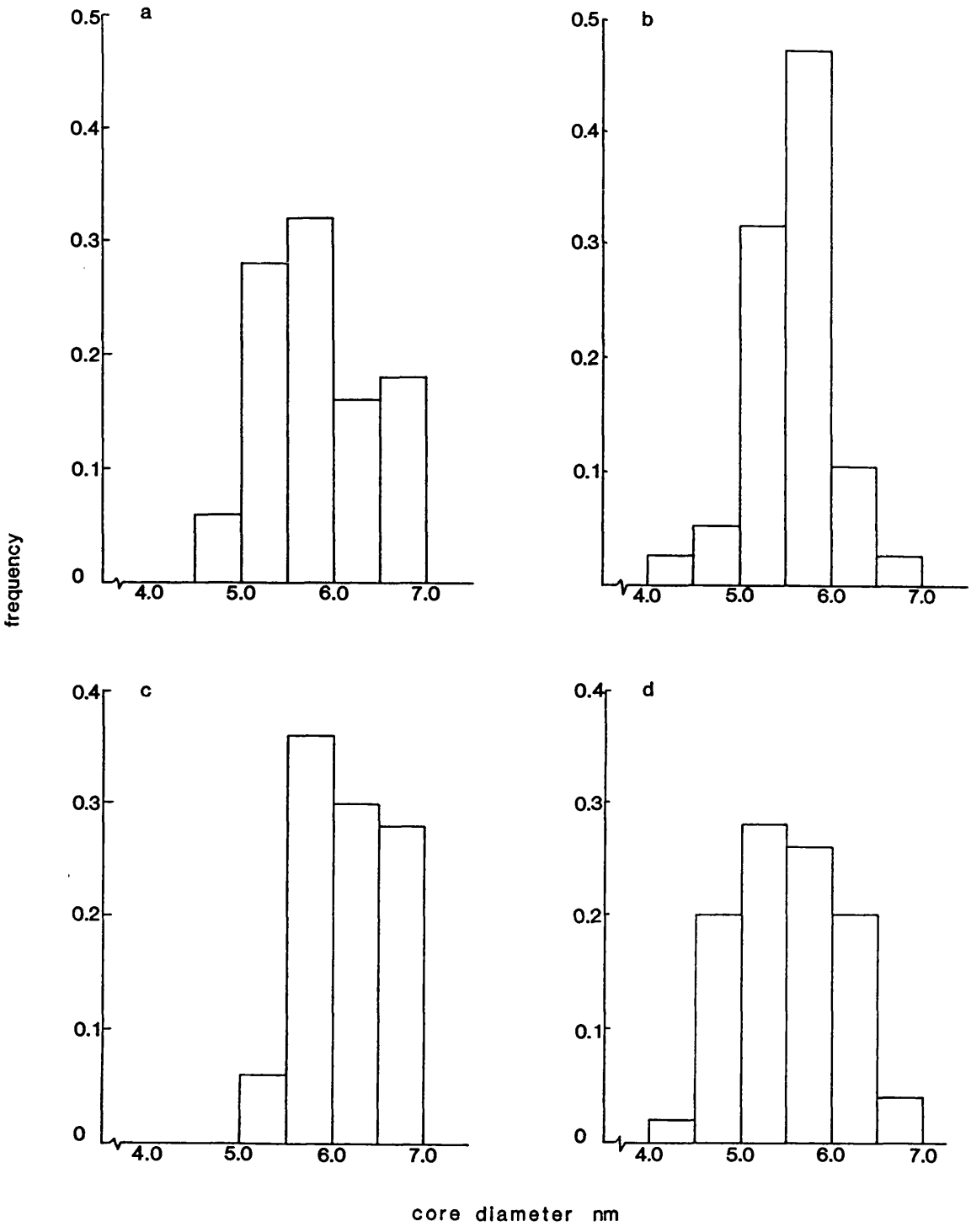

Figure 5.4 Particle size distributions for haemosiderins isolated from normal human spleen and β-thalassemia spleen and liver. *a* NHs, *b* TH1s, *c* TH2s, *d* TH31.

Table 5.2 Electron diffraction data for Sample NHs

d(Å)	I	assigned material
2.47	S	F
2.21	M	F
1.96	M	F
1.69	W	F
1.49	W	F
1.44	S	F

Table 5.3 Electron diffraction data for Sample TF1s

d(Å)	I	assigned material
2.47	S	F
2.22	S	F
1.96	M	F
1.71	W	F
1.48	W	F
1.44	S	F

I = intensity of line judged by eye: S = strong, M = medium,
W = weak.
F = ferrihydrite.

b) Haemosiderins Three individual samples of haemosiderin from patients with β-thalassemia were studied.

i) Sample THis

These cores were more discrete than those of normal human spleen haemosiderin, but again they showed some aggregation. They were more irregular in shape than those of the corresponding ferritin (TFis); there were more anisometric and angular cores, plate 5.2a. The mean core diameter was 5.57 nm with a standard deviation of 0.48 nm; this diameter is smaller than that of the ferritin isolated from the same tissue sample. A histogram of core diameters is shown in figure 5.4b. It is an approximately normal distribution around the mean.

The electron diffraction patterns from this sample were different to those of the corresponding ferritin and sample NHs; there are more than six lines present, some of the d-spacings have changed, as have the intensities of some lines. The 4.25 Å line was not present in all patterns. The 2.5 Å line was missing, possibly being split into the 2.68(2.66) and 2.45(2.40) Å lines. The increase in the intensity of the line at around 1.70 Å was very noticeable and this feature was probably the most consistent in indicating altered structure in the β-thalassemia haemosiderin samples. There were extra, weak lines at 1.54, 1.33 and 1.13 Å. See table 5.5 and plate 5.2d. The electron diffraction data indicated that this haemosiderin was more crystalline than the corresponding ferritin and that it was a goethite (α-FeOOH)-like phase. Several of the diffraction lines could be indexed as goethite or ferrihydrite, but the lines at ~4.2, 2.68 and 2.45Å and the increase in the intensity of the 1.7Å provide firm evidence for the presence of goethite albeit in a defect form.

A microdensitometer trace across a diffraction pattern negative was obtained and this confirmed the increase in the intensity of the

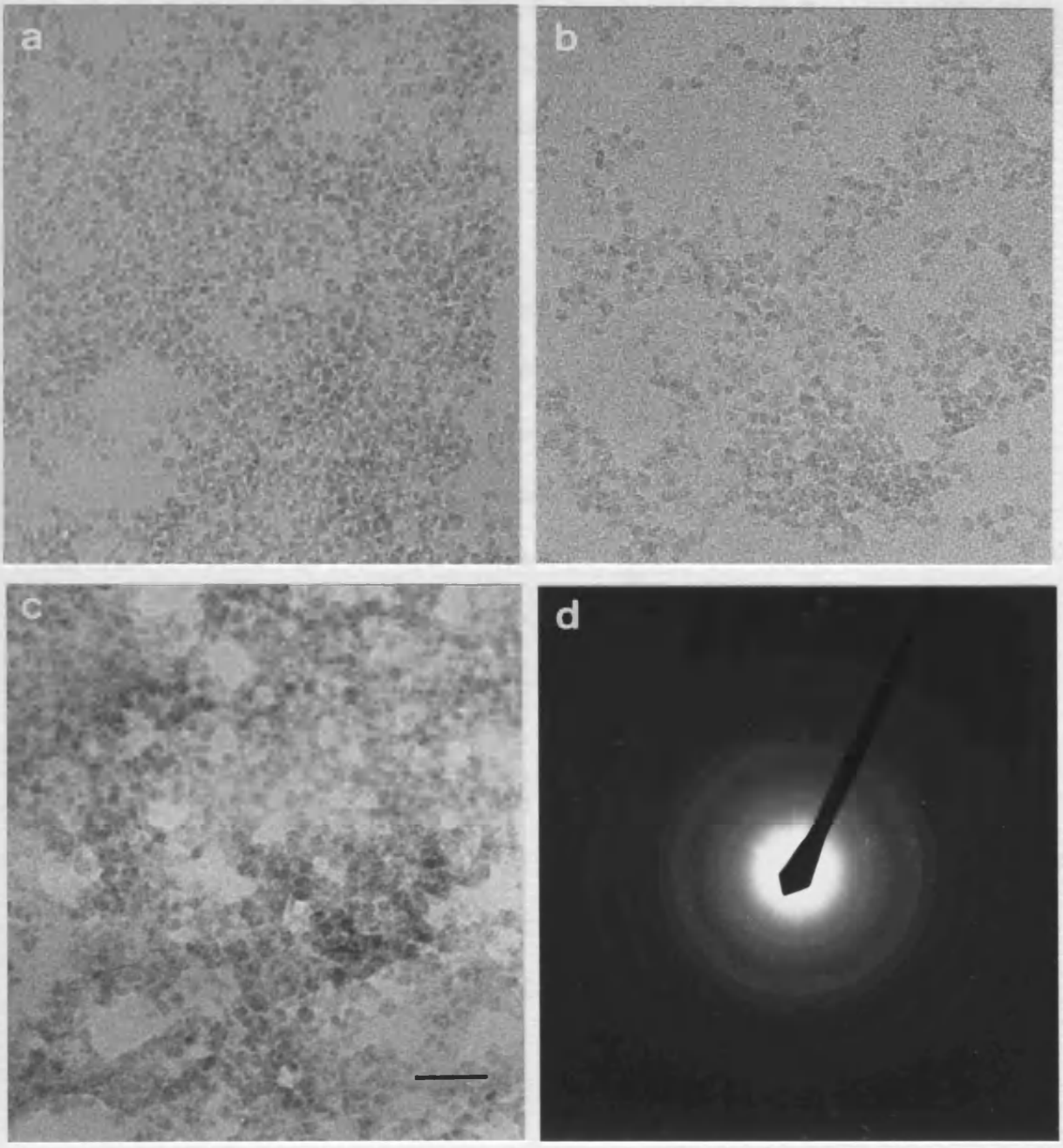

Plate 5.2 Electron micrographs and diffraction pattern of unstained β-thalassemia haemosiderins. *a* spleen (TH1s), *b* spleen (TH2s), *c* liver (TH3l), bar marker 30nm for all images. *d* electron diffraction pattern from sample TH1s, camera length 164cm.

line at around 1.70 Å, when compared to traces from diffraction pattern negatives of horse ferritin and haemosiderin, i.e. normal ferrihydrite structure, (see figure 5.6).

ii) Sample TH2s

The cores in this spleen haemosiderin were again discrete but aggregated, plate 5.2b. They appeared to be very similar to the TH1s sample in the range of shapes. However, a larger average particle size was noted: the mean core diameter was 6.14 nm with a standard deviation of 0.43 nm. This average and the maximum diameter (6.90 nm) were still below those of the TF1s sample (6.83 and 7.35 nm respectively). The particle size distribution was narrow, see figure 5.4c.

Electron diffraction patterns of this sample were not entirely consistent, but on careful inspection α-FeOOH structure could be seen in all of them; again note the increased intensity of the reflection at 1.70 Å. The most obviously different pattern was obtained from a very dense clump of material. See table 5.6.

iii) Sample TH31

This liver sample had aggregated cores which were not as discrete as those in the spleen samples. The cores were irregular in shape but generally more rounded than those in the human spleen haemosiderin samples (TH1s and TH2s), plate 5.2c. The mean core diameter was 5.49 nm, with a standard deviation of 0.55 nm. Again the mean core diameter was smaller than that of the corresponding ferritin (TF31). A particle size histogram is shown in figure 5.4d, the distribution was slightly broader than that of sample TH1s.

Electron diffraction patterns from this liver sample showed that

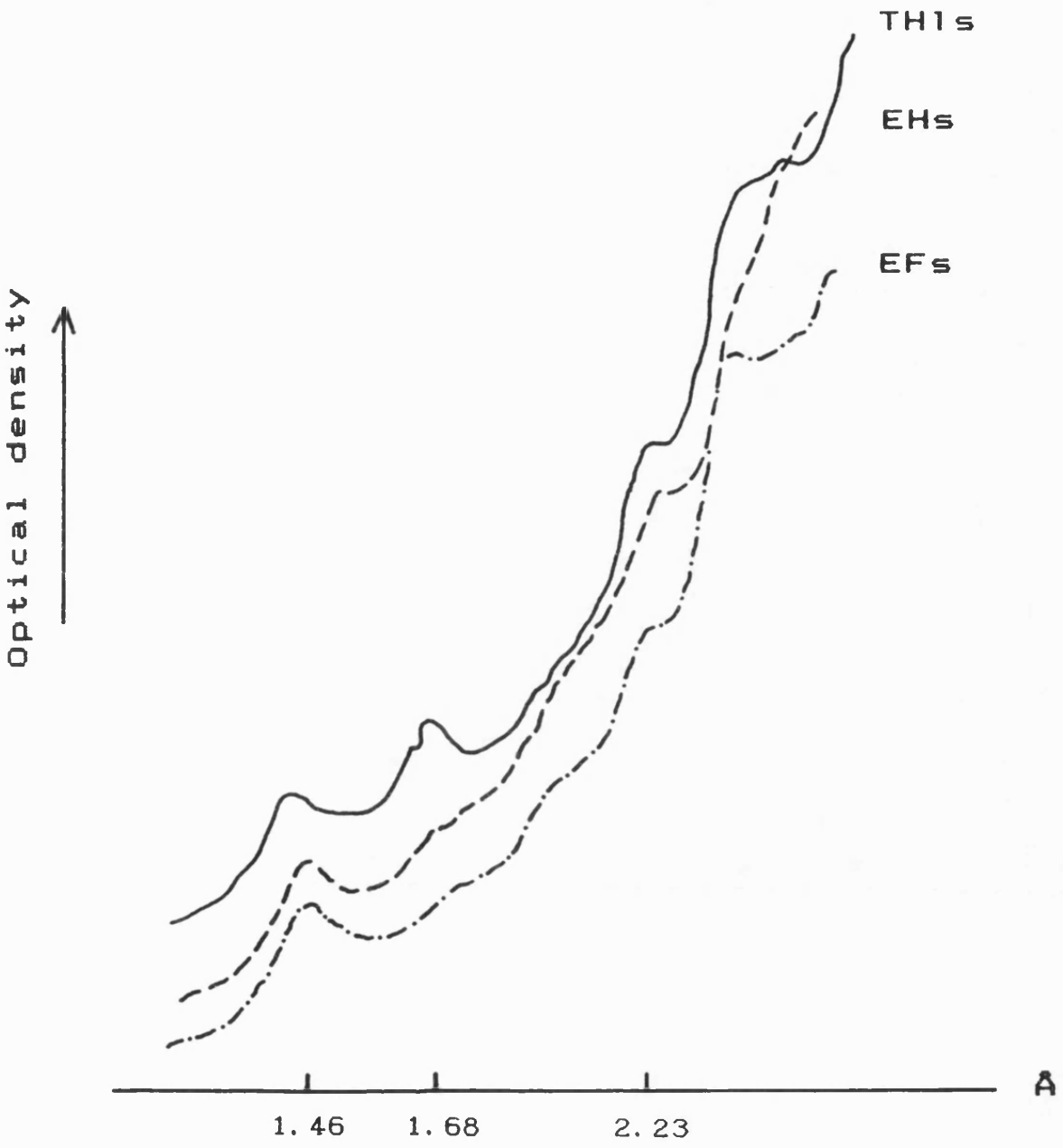

Figure 5.6 Densitometer traces across electron diffraction pattern negatives of β-thalassemia spleen haemosiderin (THIs), horse spleen haemosiderin (EHs) and horse spleen ferritin (EFs).

Table 5.4 Electron diffraction data for Sample TF31

d(Å)	I	d(Å)	I	assigned material
2.44	M	2.43	S	F
2.21	S	2.19	S	F
1.97	M	1.91	M	F
1.69	W	1.68	W	F
1.47	W	1.47	W	F
1.44	S	1.42	S	F

Table 5.5 Electron diffraction data for Sample TH1s

d(Å)	I	d(Å)	I	assigned material
4.25	M			G
2.68	M	2.66	M	G
2.45	S	2.40	S	G
2.20	S	2.17	S	G/F
1.99	W	1.93	W	F
1.71	S	1.68	S	G/F
1.54	W			G
1.47	M/W	1.45	W	F
1.43	S	1.41	S	F
1.33	VW			G
1.13	VW			

G = goethite.

this haemosiderin had the same α-FeOOH based structure as the spleen haemosiderins isolated from other patients with the same disorder. The mineral phase was different from ferrihydrite with an extra line at 4.13 Å, the 2.50 Å line split into 2.65 and 2.45 Å lines and an increase in the intensity of the 1.72 Å line, see table 5.7.

5.2.3 Idiopathic haemochromatosis samples

a) Ferritin One sample of ferritin from the liver of a patient with idiopathic haemochromatosis was studied.

Sample IHF11

This ferritin had discrete, well separated iron cores of generally irregular shape, see plate 5.3a. It appeared to be morphologically very similar to the liver ferritin of secondary iron-overload (sample TF31, plate 5.1c). The mean core diameter was 6.02 nm (S.D. 0.45 nm) and the particle size histogram is shown in figure 5.5c.

The electron diffraction patterns from this sample were markedly different from those of the other human ferritins studied. Only three lines at 2.45, 1.68 and 1.47 Å and a broad band centred at 2.13 Å were visible. These indicated that the cores were poorly ordered ferrihydrite, (see table 5.8).

Table 5.6 Electron diffraction data for Sample TH2s

d(Å)	I	d(Å)	I	d(Å)	I	assigned material
2.64	M?	2.62	M			G
				2.50	S	F
2.46	S	2.48	S			G
2.21	S	2.21	S	2.21	S	F
1.96	M	1.96	M	1.97	W	F
1.70	M	1.68	S	1.70	M	G/F
1.46	S	1.49	M	1.49	W	F
		1.44	S	1.44	S	F
		1.33	W			G
		1.07	W			
		0.85	VW			

Table 5.7 Electron diffraction data for Sample TH31

d(Å)	I	assigned material
4.13	M	G
2.65	M	G
2.45	S	G
2.22	S	F
1.97	VW	F
1.72	S	G/F
1.49	W	F
1.46	S	F

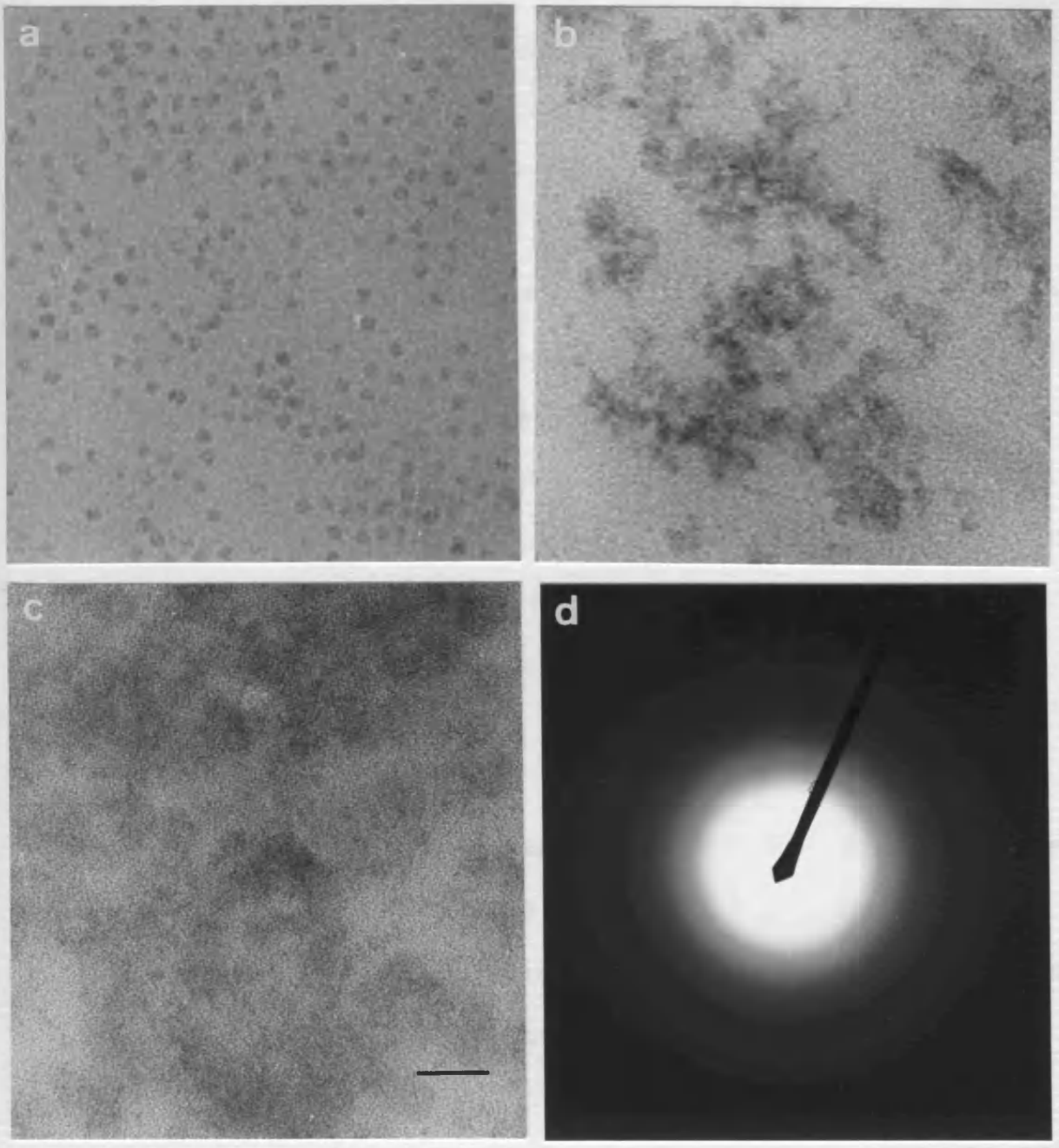

Plate 5.3 Electron micrographs and diffraction pattern of unstained idiopathic haemochromatosis samples. *a* liver ferritin (IHF11), *b* liver haemosiderin (IHH11), *c* liver haemosiderin (IHH21), bar marker 30nm for all images. *d* electron diffraction pattern from haemosiderin sample IHH11, camera length 122cm.

b) Haemosiderins Two samples of haemosiderin from patients with idiopathic haemochromatosis were studied.

i) Sample IHH11

This material was extensively aggregated and the individual cores not readily distinguishable. The indistinct particles were of irregular shape and of low electron density. (Plate 5.3b.) Only a few isolated particles were visible on the micrographs and these had diameters ranging between 5.36 and 6.31 nm.

The electron diffraction patterns showed one line at 2.49 Å and two broad bands centred at 2.12 and 1.53 Å suggesting the presence of a largely amorphous iron (III) oxide with partial ordering based on the ferrihydrite structure. (Table 5.9 and plate 5.3d.)

ii) Sample IHH21

This material looked very similar to sample HH11, except it was even less electron dense, (plate 5.3c).

The electron diffraction patterns from this sample had no lines on them which indicated that the material was amorphous by this technique.

5.2.4 Animal samples

Samples of ferritin and haemosiderin from iron-loaded horse spleen and haemosiderin from iron-loaded reindeer spleen and liver were studied.

a) Ferritin

Sample EFs

This material is the "standard" ferritin and the TEM image showed characteristic discrete, well separated and well rounded iron cores, (plate 5.4a). The mean core diameter was 7.22 nm,

Table 5.8 Electron diffraction data for Sample IHF11

d(Å)	I	assigned material
2.45	S	F
2.33 }		
1.93 }	S	F
1.68	VW	F
1.47	S	F

Table 5.9 Electron diffraction data for Sample IHH11

d(Å)	I	assigned material
2.49	S	F
2.33 }		
1.91 }	S	F
1.56 }		
1.50 }	S	F

Table 5.10 Electron diffraction data for Sample EFs

d(Å)	I	assigned material
2.49	S	F
2.23	S	F
1.99	M	F
1.72	W	F
1.52	W	F
1.46	S	F

(S.D. 0.44 nm). A particle size histogram is shown in figure 5.5d and this shows a fairly narrow distribution.

The electron diffraction pattern had six lines characteristic of well crystalline ferrihydrite. (Table 5.10.)

b) Haemosiderins

i) Sample EHs

The iron cores in this material were discrete but aggregated, many had irregular shapes, see plate 5.4b. The mean core diameter was 6.12 nm, with a standard deviation of 0.51 nm. The average size was therefore smaller than the horse spleen ferritin, sample EFs. A particle size histogram is shown in figure 5.7a and this shows a slightly broader distribution than that for sample EFs.

The d-spacings calculated from the electron diffraction patterns of this sample were virtually identical to those of the horse spleen ferritin. So this material was also well crystalline ferrihydrite. (Table 5.11.)

ii) Sample RHs

In this sample the cores were again discrete but aggregated. They were generally of a rounded appearance, but a few were irregular in shape, (plate 5.4c). The mean core diameter was 5.88 nm, but there was a wider variation in size than had been seen in other samples, from different species. This is reflected in the standard deviation of 0.81 nm and illustrated in the particle size histogram shown in figure 5.7b.

Electron diffraction analysis showed that the material was crystalline ferrihydrite, see table 5.11.

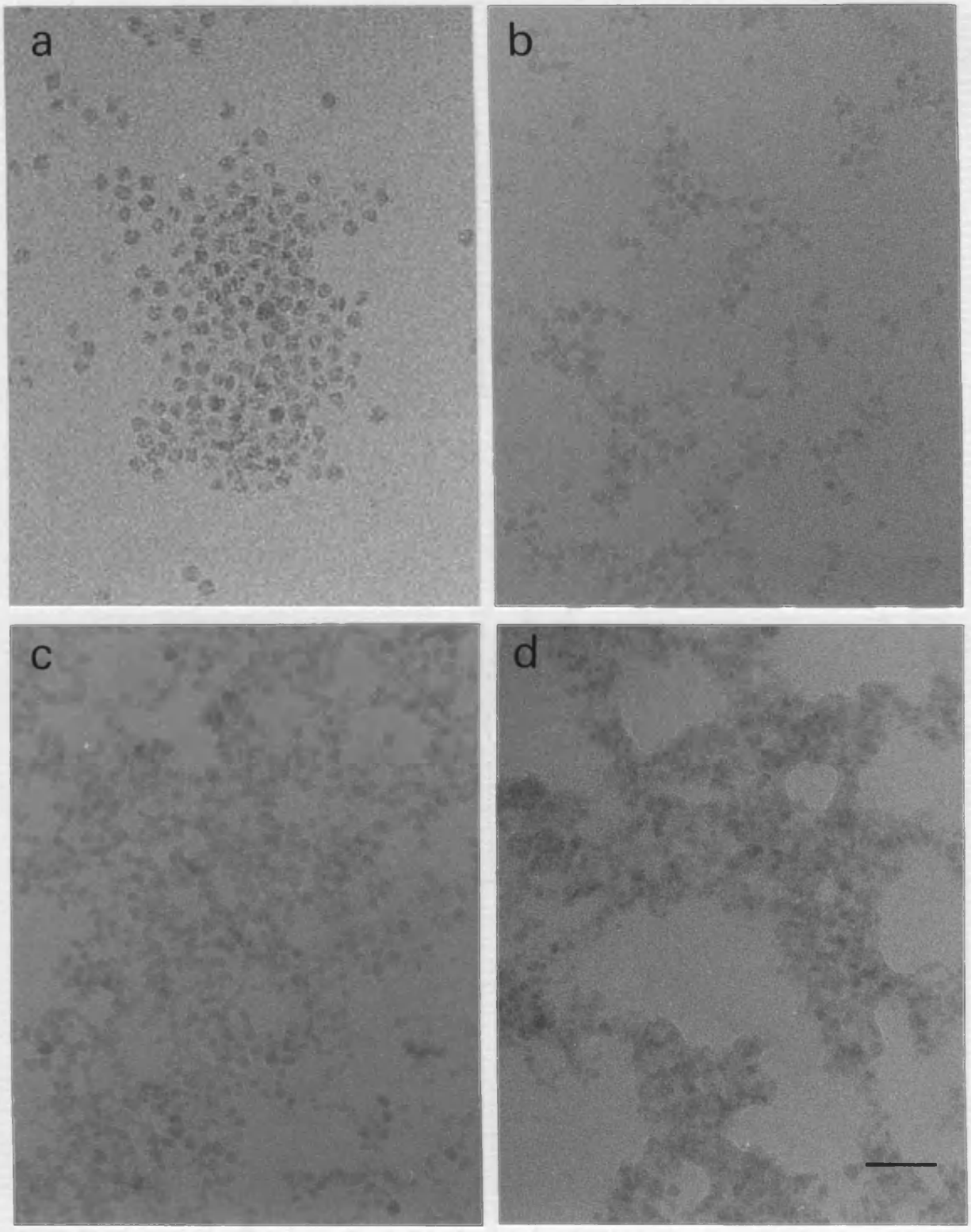

Plate 5.4 Electron micrographs of unstained animal samples. *a* horse spleen ferritin (EFs), *b* horse spleen haemosiderin (EHs), *c* reindeer spleen haemosiderin (RHs), *d* reindeer liver haemosiderin (RHl), bar marker 30nm for all micrographs.

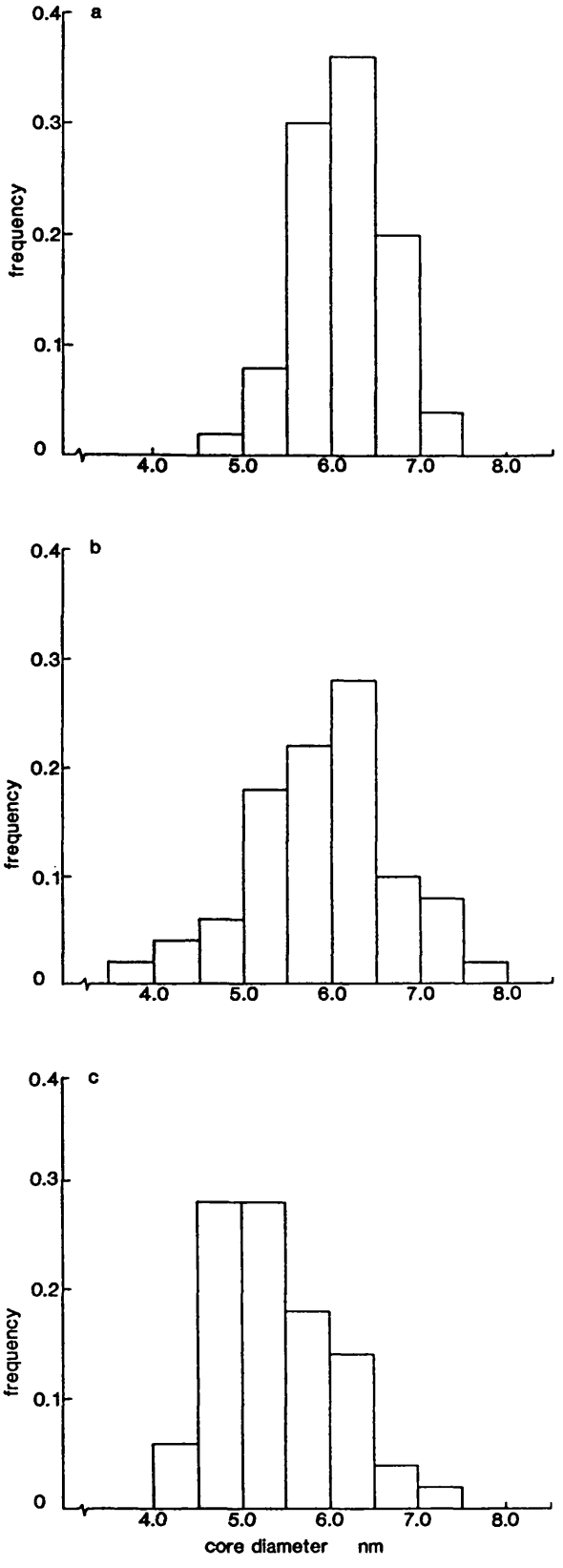

Figure 5.7 Particle size distributions for the animal haemosiderins.
a EHs, *b* RHs, *c* RHl.

iii) Sample RH1

In comparison to many of the other haemosiderins studied the iron cores in this sample were not very discrete, plate 5.4d. They were more discrete than those of human idiopathic haemochromatosis haemosiderin (IHH11 and IHH21) but not as discrete as those of human β-thalassemia (TH1s, TH2s and TH31), normal human (NHs) and horse (EHs) haemosiderin. Also, they were less discrete and more extensively aggregated than the reindeer spleen sample, RHs. Where individual cores could be seen they were of fairly regular shape. The mean core diameter was 5.39 nm, with a standard deviation of 0.71 nm. Again there was a wider size distribution than seen in other species. A particle size histogram is shown in figure 5.7c and this also shows that the cores in this sample were generally smaller than those in the spleen sample RHs.

Electron diffraction patterns from this sample showed that the cores were ferrihydrite, (table 5.11). Comparing a number of patterns from the reindeer liver and spleen samples, it appeared that the liver haemosiderin was slightly less crystalline than the spleen haemosiderin.

A summary of the structural data presented above is shown in table 5.12.

Table 5.11 Electron diffraction data for the Animal haemosiderins

EHs		RHs		RHl		
d(Å)	I	d(Å)	I	d(Å)	I	assigned material
2.50	S	2.50	S	2.46	S	F
2.24	S	2.23	S	2.21	S	F
1.99	M	1.95	M	1.92	M	F
1.71	W	1.69	W	1.69	W	F
1.51	W	1.50	VW	1.49	VW	F
1.46	S	1.45	S	1.46	M	F

Table 5.12 Summary of structural data

The relative crystallinity was judged by the quality of the electron diffraction patterns.

Sample code	Relative crystallinity	Nature of iron oxide
TF1s	Good	F
TF31	Good	F
IHF11	Poor	F
EFs	Good	F
NHs	Good	F
TH1s	Very good	G/F
TH2s	Very good	G/F
TH31	Very good	G/F
IHH11	Very poor	F
IHH21	Amorphous	---
EHs	Good	F
RHs	Good	F
RH1	Fair	F

5.3 DISCUSSION

5.3.1 Summary of the TEM and electron diffraction studies

i) Comparison of core morphology:

The iron cores in the spleen ferritins studied were generally of a rounded shape and those of the liver ferritins of more angular shapes. The spleen haemosiderins had iron cores with a mixture of rounded and irregular shapes. The liver haemosiderins of both idiopathic haemochromatosis and β-thalassemia were less discrete than the spleen haemosiderins, but where the particles were distinguishable they were generally of more rounded shapes.

ii) Comparison of core size:

The ferritin iron core sizes were all similar. The ranges of sizes denoted by the S.D. of the mean overlapped between all the human samples and between samples TF1s, TF31 and EFs, only sample IHF11 failed to overlap with EFs. Generally the ferritins had narrower size distributions than the haemosiderins.

All the ranges of core sizes measured for the haemosiderins overlapped. The haemosiderins had lower mean core diameters and smaller maximum core sizes than the ferritins isolated from the same tissue sample or tissue type. This pattern of smaller size was reflected in the other samples studied.

iii) Comparison of core structure:

All the ferritins studied were ferrihydrite. They were all well crystalline except for sample IHF11 which only gave four out of the six possible diffraction lines. Two of these, at 2.45 and 1.47 Å, are correlated to the hexagonally close packed oxygens in the ferri-hydrite structure (Towe & Bradley, 1967), the other diffraction lines

indicate that some of the Fe^{3+} are in ordered sites.

The normal human haemosiderin (NHs) and the animal haemosiderins were also all ferrihydrite. Generally, they too were well crystalline, only sample RH1 was slightly less crystalline as judged by the quality of the electron diffraction patterns.

All the β-thalassemic haemosiderins were very well crystalline and had a goethite-like structure. Many of the electron diffraction lines could be assigned to either ferrihydrite or goethite but the diffraction lines at ~4.2 and 2.7 Å and the increase of the intensity of the line at ~1.7 Å showed unequivocally the presence of a goethite-like phase. It was not a stoichiometric, well-ordered goethite since many of the weaker goethite lines were missing.

The idiopathic haemochromatosis haemosiderins were essentially amorphous. In sample IHH11 there were only three diffraction lines, two of which were broadened and indistinct. Those at 2.49 and ~1.53 Å are again correlated to the hexagonally close packed oxygens. The other lines indicate that some of the iron is ordered, but less so than that in the ferritin sample, IHF11. Sample IHH21 gave no diffraction lines at all.

5.3.2 Mössbauer study

A Mössbauer spectroscopy study of all the samples investigated was carried out by Dr. D.P.E. Dickson and Miss N.M.K. Reid and it is relevant that a summary of those results is given here. The methods used and a fuller description of the results are reported in Dickson *et al.*, 1988.

The variable temperature Mössbauer spectra of all the ferritin samples (TF1s, TF31, HF11 and EFs), the normal human (NHs) and

β-thalassemia (TH1s, TH2s and TH31) haemosiderins and the animal haemosiderins (EHs, RHs and RH1) showed characteristic superparamagnetism between the temperatures of 77 and 1.4K. However, as demonstrated previously for horse ferritin and animal and β-thalassemia spleen haemosiderins (Fischbach *et al.*, 1971, Bell *et al.*, 1984, Williams *et al.*, 1986, Dickson *et al.*, 1987 and St. Pierre *et al.*, 1987) the values of T_B vary from sample to sample; the ferritins all had T_B's of around 40K, the normal human and animal haemosiderins had T_B's between 20 and 30K and the β-thalassemia haemosiderins (liver and spleen) had T_B's of 63 and ~70K respectively.

The Mössbauer spectra of the normal human spleen haemosiderin (NHs) at 77, 20, 4.2 and 1.4 K are shown in figure 5.8. The spectra were very similar to those of the horse and reindeer haemosiderins (spectra from the horse haemosiderin shown in appendix II). Sample NHs had a value for T_B of around 25 K. The variable temperature Mössbauer spectra of the β-thalassemia liver sample (TH31) are shown in figure 5.9. These spectra were very similar to those of the spleen haemosiderins (TH1s and TH2s) and spectra previously reported for β-thalassemia spleen haemosiderin by Bell *et al.* (1984). Sample TH31 had a T_B of 63 K.

The Mössbauer spectra of the idiopathic haemochromatosis haemosiderins (IHH11 and IHH21) were quantitatively and qualitatively different from all the others. Those of sample IHH11 appeared to represent two iron-containing components, see figure 5.10. One of these which corresponded to about 20% of the total iron present, appeared to be similar to the animal and normal human haemosiderins, with a T_B of around 15-20 K. The other, major component, did not show resolved magnetic splitting until well below 4.2 K and the spectral

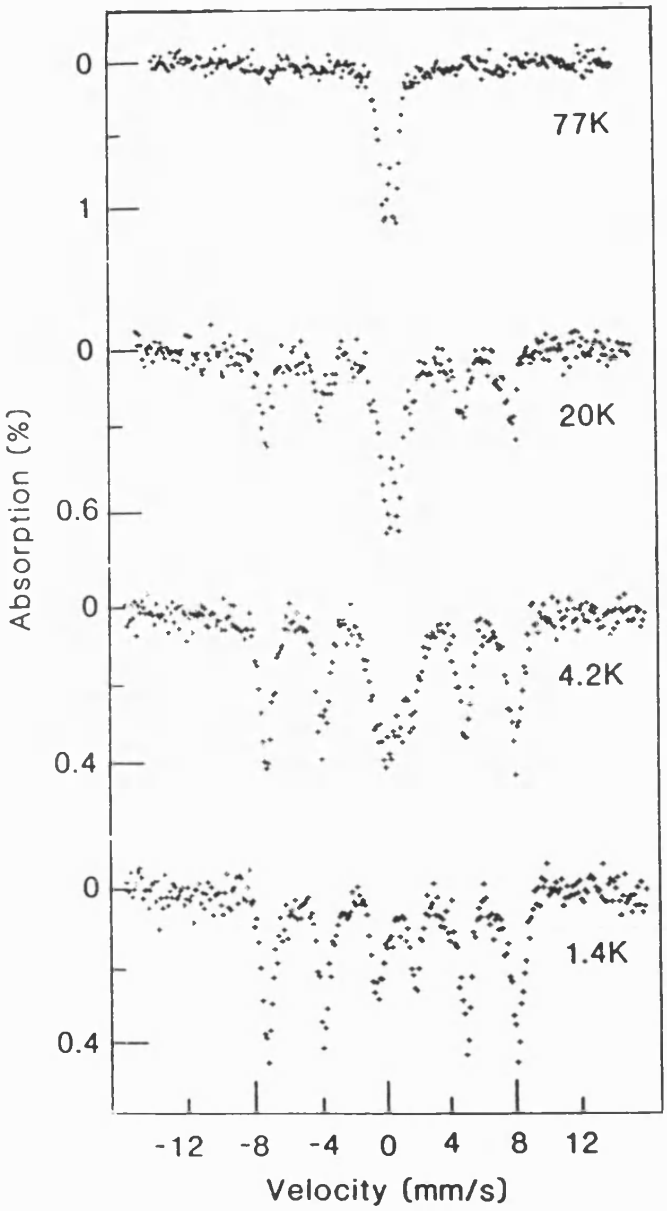

Figure 5.8 Variable temperature Mössbauer spectra of the normal human spleen haemosiderin sample.

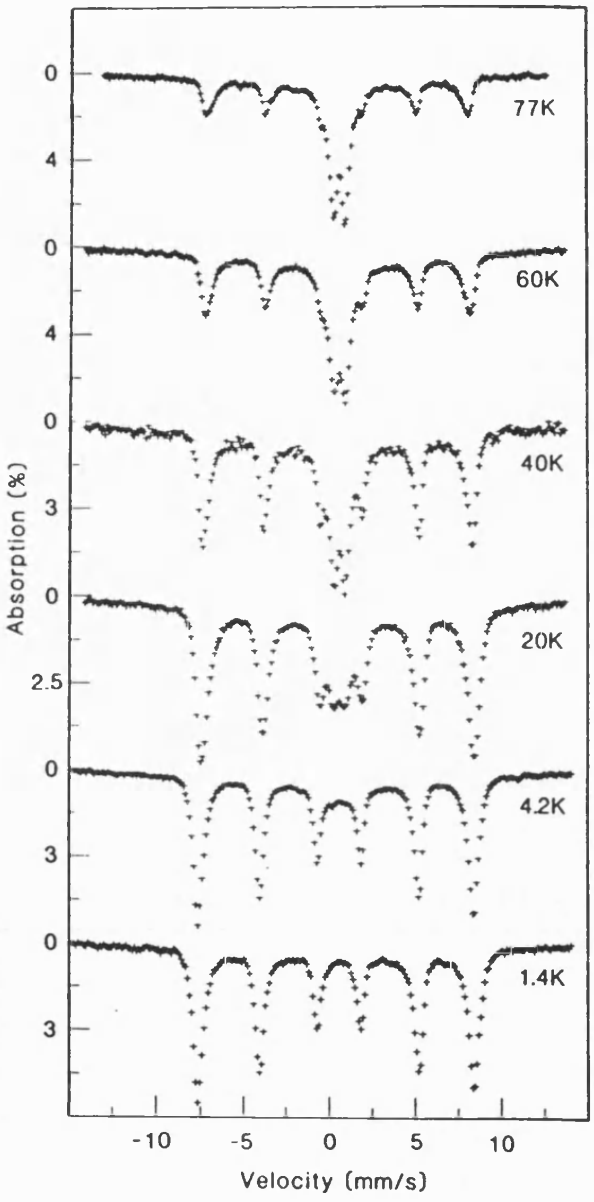

Figure 5.9 Variable temperature Mössbauer spectra of the β-thalassemia liver haemosiderin sample.

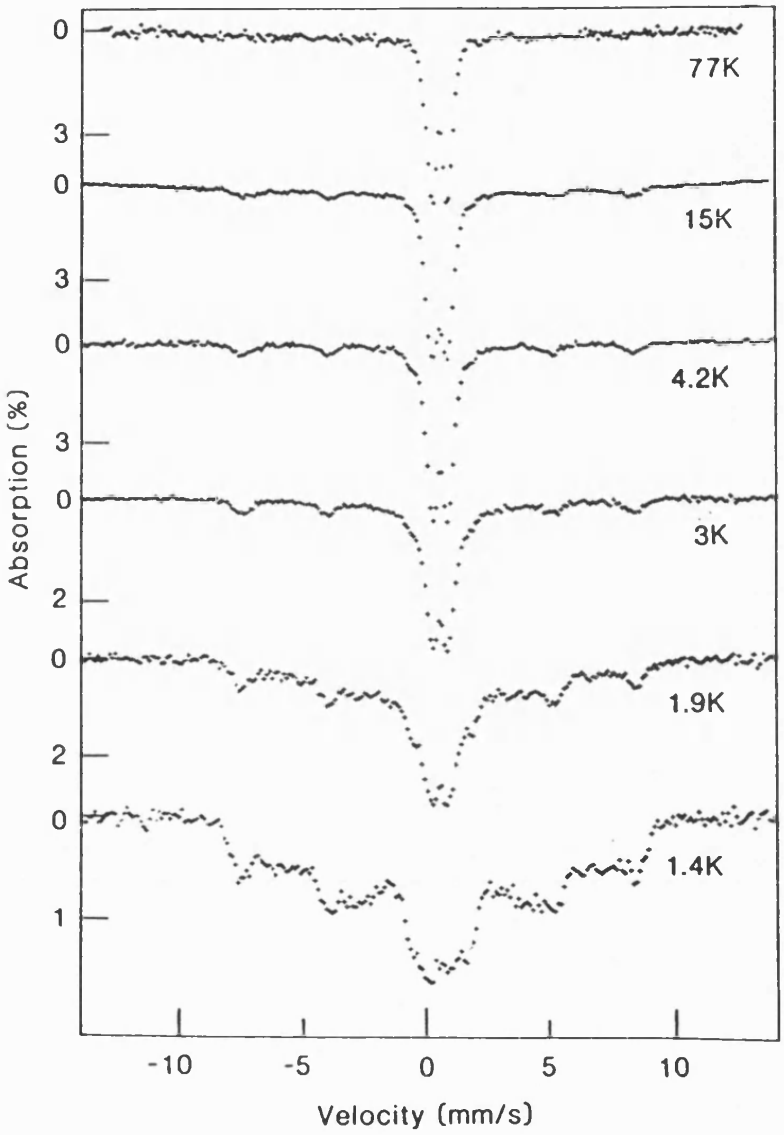

Figure 5.10 Variable temperature Mössbauer spectra of the idiopathic haemochromatosis liver haemosiderin sample IHH11.
(Figures 5.8, 5.9 & 5.10 from Dickson *et al.*, 1988).

behaviour was qualitatively different to superparamagnetism. This component is similar in its Mössbauer behaviour to the bacterial ferritins of *E. coli* (Bauminger, *et al.*, 1980) and *P. aeruginosa* (St. Pierre *et al.*, 1986) and also to the iron-containing materials found in iron-overloaded heart cell cultures (Bauminger *et al.*, 1987). The spectra of sample IHH21 showed only the behaviour of the major component in IHH11.

These Mössbauer results correlate well with the electron diffraction analyses of the samples. The normal human and animal haemosiderins were all ferrihydrite and since their particle sizes were smaller than the ferritins', their values of T_B were also lower.

The β-thalassemia haemosiderins were all goethite-like and more highly ordered than ferrihydrite. Consequently, their values of T_B were higher than those of the corresponding ferritins since more highly ordered solids have higher magnetic anisotropy constants, (the value of K is related to magnetic differences between crystal axes and therefore is expected to be greater in a more well-ordered system, Dickson *et al.*, 1988).

The two idiopathic haemochromatosis samples need to be considered separately. Sample IHH11 had two components: that with a ferrihydrite-based structure contributed the sextet to the Mössbauer spectrum at the higher temperatures, (4.2 - ~40 K) and gave the three lines of the electron diffraction pattern. The amorphous component contributed nothing to the electron diffraction pattern but did contribute the broadened sextet which appeared at very low temperatures in the Mössbauer spectrum. Sample IHH21 was totally amorphous by electron diffraction and so there was no sextet component in the Mössbauer spectrum at the higher temperatures. This

material gave rise to the broadened sextet at the very low temperatures.

5.3.3 Solubility study

The rate of dissolution to oxalate discriminates between various iron oxides and oxyhydroxides, (Schwertmann, 1964). Carlson and Schwertmann (1987), published X-ray diffractograms of a ferrihydrite with some goethite before and after oxalate treatment, which clearly show that the ferrihydrite is preferentially dissolved; the X-ray diffractogram of the remaining material shows only enhanced goethite lines.

This oxalate solubility technique, 0.2M oxalate/ammonium oxalate pH 3.0, 25°C, was used by Dr. R.J. Ward in conjunction with the work presented in this chapter (the results from the human samples are published in Ward *et al.*, 1989). After a two hour incubation approximately 55-65% of the iron in the ferritins of idiopathic haemochromatosis and β-thalassemia had been released, whereas for the haemosiderins of these two conditions the amounts released were 80 and 40% respectively, see figure 5.11. Samples of horse spleen ferritin and haemosiderin had also released about 40% of their iron, after 2 hours. After 24 hours, further iron was released from all samples; 75-85% for the human ferritins, approximately 100% for the idiopathic haemochromatosis haemosiderin, 70% for the β-thalassemia haemosiderins and 75-80% for the horse ferritin and haemosiderin. A similar pattern of release was found for the human samples using the clinically relevant chelator desferrioxamine (1 mM), although the total amount of iron released was not as great.

The pattern that emerges from these *in vitro* studies and others

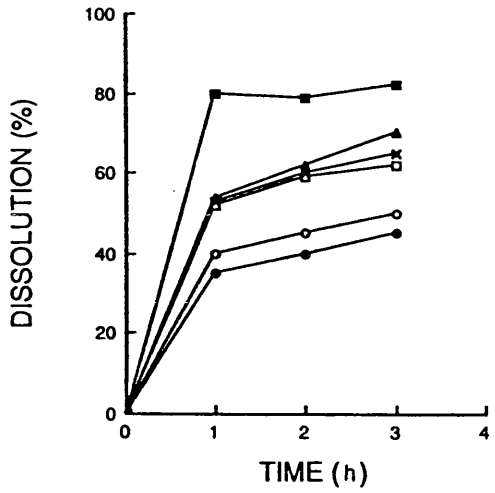

Figure 5.11 Rate of dissolution of iron from some of the human ferritin and haemosiderin samples. The iron protein was incubated with 0.2M oxalic acid/ammonium oxalate buffer (pH 3.0), at 25°C in the dark. Values (% dissolution) are the mean of two determinations. (□) IHF11, (■) IHH11, (x) TF1s, (●) TH1s, (▲) TF31, (○) TH31. (From Ward *et al.*, 1989.)

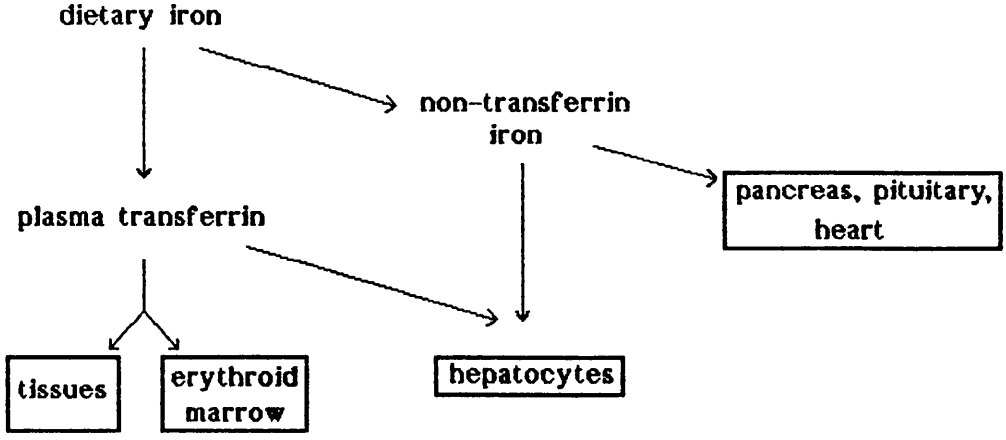

Figure 5.12 Schematic representation of the pathways of internal iron transfer relevant to idiopathic haemochromatosis, see text for details.

noted in the introduction (section 5.0.5), is that, in most cases, the iron in the ferritins and in the animal haemosiderins can be mobilised at similar rates and that these rates are faster than those for β-thalassemia haemosiderin. (It is not clear why, at two hours the amount of iron released to oxalate from the horse spleen ferritin and haemosiderin was only as much as that from the β-thalassemia haemosiderins. However, at 24 hours more iron had been released from the horse spleen samples than from the β-thalassemia haemosiderins.) The iron in the idiopathic haemochromatosis haemosiderin is more easily mobilised than that in the ferritins.

These solubility results for the human samples correlate well with the results of the structural studies of the iron cores. All the ferritin samples had ferrihydrite structures and exhibited similar rates of dissolution. The β-thalassemia haemosiderins had goethite-like structures which were more crystalline and more thermodynamically stable than the ferrihydrite of the ferritin cores. The two haemosiderin samples exhibited similar rates of dissolution which were slower than those of the ferritins. The idiopathic haemochromatosis haemosiderins had poorly ordered ferrihydrite-based structures which had greater solubility than the crystalline ferrihydrite cores of the ferritins. Therefore, the haemosiderin samples exhibited faster rates of dissolution.

In addition to the chemical and structural nature of the iron cores, the protein component of the haemosiderins may influence the rate of dissolution of the iron complexes. It has been proposed (Ward *et al.*, 1989) that the seemingly intact protein shell of the idiopathic haemochromatosis haemosiderin (in that no proteolytic degradation of ferritin subunits has been found to have occurred) may maintain the iron at a higher degree of solubility and facilitate its

release, in comparison to β-thalassemia haemosiderin where degradation of the protein shell has occurred. However, if the iron oxide component of the idiopathic haemochromatosis haemosiderin is not surrounded by the protein shell, as its appearance under the TEM might suggest (discussed below), then the iron would be very accessible to the oxalate, enhancing its solubility.

5.3.4 P:Fe ratios

The P:Fe ratios in ferritin cores have been fairly widely studied among various species and there is a correlation between phosphate content and crystallinity (as discussed in chapter 1, section 1.7.2). The phosphate contents of haemosiderins have not been well documented yet, but preliminary measurements on some of the samples studied in this work have been made (Dr. R.J. Ward, pers. comm.). The results are given in table 5.13, along with the published ratios for haemosiderins cited in section 5.0.4c and some published ratios for ferritins.

It can be seen from the table that the P:Fe ratios for haemosiderins vary widely, as previously found for ferritins. A correlation between the ratios and the crystallinity of the samples is evident, along similar lines to that discussed in chapter 1 for ferritins. The Mössbauer spectral behaviour of the samples also fits into this pattern. The horse spleen and rat liver haemosiderins have "medium" P:Fe ratios which do not affect their crystallinity or Mössbauer behaviour. Thus, these haemosiderins are similar to the corresponding ferritins. The P:Fe ratios for the β-thalassemia spleen haemosiderins all fall into the "medium" to "low" range, so crystallinity is very good and the samples exhibit superparamagnetism.

Table 5.13 P:Fe ratios for some haemosiderin and ferritin samples.

Sample	P:Fe	Crystallinity
Haemosiderins		
horse spleen (EHs)	1:3.2	good
β-thalassemia spleen (TH1s)	1:10.5	very good
β-thalassemia spleen (TH2s)	1:9.8	very good
β-thalassemia spleen[a]	1:6	---
idiopathic haemochromatosis (IHH11)	1:1.2	very poor
rat liver[b]	1:8.1, 3.1	good
Ferritins		
horse spleen	1:6.5[c], 8[d]	good[c, d]
β-thalassemia spleen[d]	1:20	good
P. aeruginosa [e]	1:0.58	amorphous

P:Fe ratios for all haemosiderins, except [a] and [b], from Dr. R.J. Ward, pers. comm., crystallinity from table 5.12 of this chapter, [a] Weir *et al.*, 1984, [b] Andrews *et al.*, 1988. Ferritin data: [c] Dr. R.J. Ward and this chapter, [d] Treffry *et al.*, 1987, [e] Mann *et al.*, 1986a).

For the idiopathic haemochromatosis haemosiderin the high P:Fe ratio of 1:1.2 falls within the range proposed by St. Pierre *et al.*, 1989 (P:Fe ratios higher than 1:2) at which the phosphate in the iron oxide structure disrupts the magnetic exchange interactions in the

iron cores. The haemosiderin is very poorly crystalline and the major component revealed in the Mössbauer spectra does not exhibit superparamagnetism, the sample is akin, in these respects, to the bacterioferritin of *P. aeruginosa* (Mann *et al.*, 1986a & St. Pierre *et al*, 1986a).

5.3.5 Possible mechanisms/pathways of formation of the different forms of haemosiderin

1 Normal human and animal haemosiderin

The similarities between the iron cores of mammalian ferritins and the normal human and animal haemosiderins, i.e. in the type of iron oxide (ferrihydrite) and the degree of crystallinity, may suggest that these two forms of iron storage are closely related. The haemosiderin may derive directly from ferritin by lysosomal processing. The studies of rat siderosomal ferritin and haemosiderin by Andrews *et al.* (1987a&b) suggest that this is so. However, the protein component(s) of the haemosiderins isolated from normal human spleen, horse spleen and reindeer liver and spleen have yet to be studied.

2 Idiopathic haemochromatosis haemosiderin

The largely amorphous nature of the iron oxide in haemosiderin isolated from primary haemochromatosis liver suggests that the iron/protein complex is deposited very rapidly. The appearance of this material under the TEM indicates that deposition of the oxide may occur outside as well as inside the protein shells. Possibly, the rate of iron uptake into the hepatocytes is so rapid that the available ferritin molecules cannot sequester the iron quickly enough

to prevent some deposition outside the ferritin protein shells.

An explanation for the different forms of haemosiderin deposited under the two human pathological conditions studied here may lie in the nature and mechanism of the tissue iron loading. In idiopathic haemochromatosis the iron is of dietary origin. In the normal situation the small amount of iron required by the body is absorbed from the diet and passes to the plasma transferrin, which delivers it to the iron requiring tissues, (the erythroid marrow being the greatest user of iron, but receiving much of its iron from the RES). This is illustrated on the left-hand side of figure 5.12. Excessive absorption of iron from the diet leads to saturation of the plasma transferrin and, since little of this iron is required by the erythroid marrow, the excess iron loaded transferrin is taken up by the hepatocytes via the endocytic pathway, (centre, figure 5.12). When the transferrin is saturated, the liver removes most of the non-transferrin, low molecular weight iron complexes by an alternative mechanism, (centre, figure 5.12). Much of the plasma iron in idiopathic haemochromatosis patients is in the form of iron-citrate complexes (Grootveld *et al.*, 1989). The alternative route of iron uptake appears to be restricted to certain cell types: hepatocytes, exocrine pancreatic cells, pituitary chromophobe cells and possibly cardiac muscle fibres (right-hand side, figure 5.12). Thus, these organs are susceptible to damage (Lombard, 1990). The uptake of large amounts of iron by hepatocytes in such low molecular weight forms may result in the iron by-passing or over-loading the normal assimilatory routes so that an amorphous ill-defined material results.

The presence of a protein component in this haemosiderin which is similar to the ferritin subunit (Ward *et al.*, 1989) suggests that ferritin may be a precursor to the haemosiderin. However, the TEM

appearance of this material may show that in this condition, the "ferritin-stage" is by-passed by at least some of the iron entering the hepatocytes.

It is important to note again here that the ferritin isolated from idiopathic haemochromatosis liver is also of poor crystallinity, which suggests a rapid rate of iron uptake by the ferritin in this disease state.

3 β-thalassemia haemosiderin

In β-thalassemia the main source of excess iron is haemoglobin in effete erythrocytes. The main sites of haemoglobin degradation are the RE cells of the spleen, bone marrow and liver (Kupffer cells). If lysis of erythrocytes occurs in the bloodstream the haemoglobin dissociates into dimers and should oxidation of the iron occur the haem moiety dissociates from its polypeptide chain. The haemoglobin dimers are bound by haptoglobin and haem is bound by haemopexin. Both complexes are taken up by the hepatocytes. The rate at which haemolysis occurs is elevated in β-thalassemia, due to ineffective erythropoiesis. Should the haptoglobin capacity be exceeded, haemoglobin dimers are filtered through the glomeruli of the kidney and taken up by the renal tubular cells where they are catabolysed and the iron stored as haemosiderin within these cells. This iron is lost when these cells exfoliate, (Bothwell *et al.*, 1979). Iron loading of parenchymal cells, predominantly of the liver and heart, only occurs when the RES is saturated (Lombard, 1990). Following the degradation of haemoglobin in Kupffer cells, iron is released as ferritin which is taken up by the hepatocytes via specific receptors (Ward *et al.*, 1989). The pathways of iron exchange involved in the iron loading syndrome of β-thalassemia are represented schematically

in figure 5.13. Some iron of dietary origin, due to enhanced absorption, gives rise directly to parenchymal loading in the liver.

The deposition of a relatively well-ordered, more thermodynamically stable iron oxide in β-thalassemia haemosiderin points to the rate of formation of the product being slow. Assuming that the haemosiderin is derived from ferritin, (and there is good evidence that this is so (Weir *et al.*, 1984, O'Connell *et al.*, 1988)) the goethite-like material must be derived from ferrihydrite and not deposited *de novo*. It is important to note that the *in situ* transformation of ferrihydrite to goethite is not possible since ferrihydrite has an hexagonal structure and that of goethite is orthorhombic, i.e. they are not closely related, (see chapter 1, section 1.3). So a dissolution re-precipitation process must occur. Such a process may or may not involve the reduction of some of the Fe(III) present to Fe(II) during the dissolution step.

The conditions and processes by which the goethite-like material could form are outlined below, (see also chapter 1, figure 1.5):

a) slow oxidation of aqueous Fe(II)

The Fe(II) may be supplied by reductive dissolution of the Fe(III) in the ferritin. Cornell and Schneider (1989) have shown that L-cysteine can facilitate the transformation of ferrihydrite to goethite at physiological pH and temperature. Interaction of the thiol group with the ferrihydrite surface occurs and the mechanism may also involve enhanced dissolution of the ferrihydrite. Additional Fe(II) may arrive at the site of haemosiderin deposition in the form of haemoglobin. The rate of oxidation of this Fe(II) would be slowed down:

i) by a low concentration of the Fe(II) or

ii) by a low concentration of O_2,

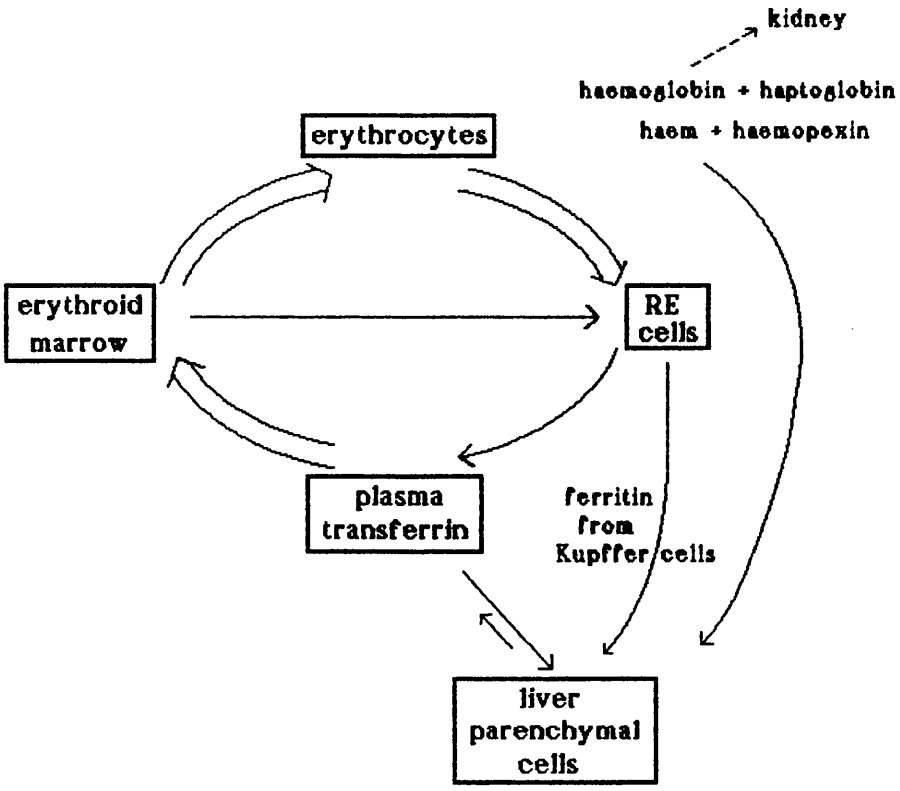

Figure 5.13 Pathways of internal iron exchange relevant to β-thalassemia, see text for details.

iii) by the low pH present in the lysosomes or,

iv) if the Fe(II) was present as a complex, eg. in haemoglobin, with thiol groups.

b) slow dissolution and re-precipitation of Fe(III)

Some Fe(III) may be removed from the ferritin core without reduction by complexing agents and these complexes slowly degraded to form the goethite-like oxide. Such complexing agents might include citrate and ascorbate, desferrioxamine will also be available, although it may not mobilise Fe(III) directly from ferritin. Additional Fe(III) may arrive in cells such as the hepatocytes, as transferrin iron. Carbonate ions will be released along with this iron and this would also favour the formation of goethite (see Taylor & Schwertmann, 1978 or chapter 1, section 1.3).

While the transformation of the ferrihydrite ferritin cores into a goethite-like phase is occurring, it is feasible that some degradation of the ferritin protein shells would occur, possibly by free radical oxidation as proposed by O'Connell *et al.*, 1988.

5.3.6 Clinical implications

In the two human iron overload syndromes considered here the structure of the haemosiderin cores is altered from that of the ferritin and the final form is different in each. Since neither of these forms occur in animal iron overload conditions (natural or induced), this could be the reason why an accurate animal model of

human overload has not been produced with the accompanying cellular and tissue damage or the very high levels of loading.

The haemosiderin iron of idiopathic haemochromatosis is very labile, whereas that of β-thalassemia is much less readily mobilised. The structural differences that give rise to these features explain the lower toxicity of the haemosiderin formed in β-thalassemia, compared to that of idiopathic haemochromatosis. The lower intrinsic solubility of the β-thalassemia haemosiderin also means however, that the iron is less readily mobilised by desferrioxamine, as has been demonstrated *in vitro* (Ward *et al.*, 1989). The discovery that the iron oxide component of β-thalassemia haemosiderin is a goethite-like phase rather than ferrihydrite, as had been assumed, has implications for the design of new iron chelating agents for clinical use. The iron in this haemosiderin will be less readily mobilised than expected from predictions based on a ferrihydrite model.

The more complete characterisation of the haemosiderins formed in iron loading syndromes may contribute to our understanding of the biological processing of the iron in each disease state.

Chapter 6

RECONSTITUTION WITH MANGANESE

6.0 INTRODUCTION

The *in vitro* removal and formation of the iron core of ferritin relies on one of the transition metal characteristics of iron, that of the ability to exist in more than one oxidation state, and that at neutral pH the interconversion of Fe^{2+} and Fe^{3+} is energetically easy. Manganese, a transition metal of atomic number just one below iron, also exists in a number of oxidation states. However, the larger standard redox potential for the conversion of Mn^{2+} to Mn^{3+} requires a higher pH to drive the oxidation, than is necessary for iron. The standard reduction potentials are:

$$Fe^{3+} + e^- \leftrightarrow Fe^{2+} \quad E^\circ = 0.770V$$

$$Mn^{3+} + e^- \leftrightarrow Mn^{2+} \quad E^\circ = 1.510V$$

and oxidation to Mn(III) is thermodynamically favourable under alkaline conditions since:

$$Mn(OH)_3 + e^- \leftrightarrow Mn(OH)_2 + OH^- \quad E^\circ = -0.40V$$

$$O_2 + 2H_2O + 4e^- \leftrightarrow 4OH^- \quad E^\circ = 0.401V$$

The aims of the present study were to attempt to load apoferritin with manganese in a similar way to reconstitution with iron and if possible, to follow the kinetics of the reaction. Such experiments would demonstrate whether or not apoferritin was just specific for iron with regard to metal ions that could be assimilated

into its internal cavity and precipitated in a "solid" form. Kinetic studies would show if the protein influenced the rate of oxidation of Mn^{2+}, as it does that of Fe^{2+}. The successful formation of manganese cores may suggest the possibility of using the apoferritin protein shell as a reaction volume for the formation of particles of other inorganic materials of nanometre dimensions. Also, if the protein influenced the kinetics of Mn(II) oxidation by promoting the rate of reaction, this would demonstrate some "flexibility" in the oxidase activity of the protein, with implications for the function of the amino-acid side chains involved, at the atomic/molecular level. If, however, the apoferritin inhibited the rate of oxidation, this may imply a role, perhaps particularly for the external surface of the shell, in binding Mn^{2+} and inhibiting the clustering or polymerisation of manganese ions into a solid form.

6.0.1 Aqueous oxidation of Mn(II)

In aqueous solution, at acid and neutral pH, Mn(II) exists as the aqua ion $[Mn(H_2O)_6]^{2+}$ which is stable to aerial oxidation. Under basic conditions, it exists as $Mn(OH)_2$ which is readily oxidised, as illustrated above, even by air. It follows that the rate of oxidation is strongly enhanced by increasing pH.

The pathways followed during the oxidation of Mn(II) in aqueous systems are not fully understood. A variety of oxide and oxyhydroxide products can be formed initially, depending on the experimental conditions. These include hausmannite (Mn_3O_4), groutite (α-MnOOH), feitknechtite (β-MnOOH) and manganite (γ-MnOOH), (Murray *et al.*, 1985), which are all insoluble and are thus precipitated. However, in this complex system, further reaction occurs and may proceed through

a number of intermediates before the final product is reached (Burns & Burns, 1979 and Giovanoli, 1980). A study of the oxidation and precipitation of Mn(II) in artificial lake water (pH 7-8) by Stumm and Giovanoli (1976) revealed the initial product to be a mixture of hausmannite and feitknechtite, which changed in time to manganite. Murray *et al.* (1985), in a study at pH 9.0, observed that the initial precipitate comprised mainly hausmannite, with some feitknechtite and a trace of manganite also present. The proportion of feitknechtite increased at first, but then decreased and after five months no feitknechtite remained. The dissolution of hausmannite was shown to be a slower process. The amount of manganite increased with aging and after nine months it was the only phase present.

Kinetic and thermodynamic considerations

The oxidation of aqueous Mn(II) is subject to kinetic limitations. In the neutral pH range Mn(II) is stable because the oxidation rate is very slow. Like the oxidation of Fe^{2+}, the reaction is autocatalytic and obeys an equivalent rate law:

$$\text{rate} = k\,[Mn^{2+}]\,[O_2]\,[OH^-]^2\,[MnO_x]$$

where MnO_x is the general formula for the oxidation product. At alkaline pH, Mn^{2+} ions are adsorbed onto the surface of manganese oxides where they are rapidly oxidised (Stumm & Morgan, 1970). Any oxidised manganese precipitate is able to catalyse the reaction.

In the natural environment the highest oxidation state attained by manganese is Mn(IV) (Stumm & Morgan, 1970). The oxidation reaction of Mn(II) to MnO_2 can be summarised as

$$Mn^{2+} + \tfrac{1}{2}\,O_2(aq) + H_2O \leftrightarrow MnO_2 + 2H^+ \qquad (1)$$

The mechanism for this reaction is thought to be a two step process involving Mn(III) first oxidising to a metastable intermediate, which

should then alter to a more stable, more highly oxidised form. At room temperature, the initial oxidation product is hausmannite:

$$3Mn^{2+} + 3H_2O + \tfrac{1}{2} O_2(aq) \leftrightarrow Mn_3O_4 + 6H^+ \quad (2)$$

(Hastings & Emerson, 1986).

Murray *et al.* (1985) have shown that the hausmannite undergoes spontaneous protonation to MnOOH:

$$Mn_3O_4 + 2H^+ \leftrightarrow 2MnOOH + Mn^{2+} \quad (3)$$

the form of the oxy-hydroxide being β or γ initially with the β-MnOOH transforming to γ-MnOOH with time.

Theoretically, the hausmannite should disproportionate to form MnO_2:

$$Mn_3O_4 + 4H^+ \leftrightarrow MnO_2 + 2Mn^{2+} + 2H_2O \quad (4)$$

However, this reaction has not been experimentally demonstrated and it is generally thought that manganese oxides with an oxidation state greater than (III) do not readily form in laboratory systems, except under extreme experimental conditions (Hastings & Emerson, 1986 and Stumm & Morgan, 1970).

A non-equilibrium thermodynamic model which describes the *relative* stability of the various phases that form from the aqueous oxidation of Mn^{2+} has been developed (Hem & Lind, 1983 and Hastings & Emerson, 1986) and a scheme for the model is shown in figure 6.1. The figure is not a true stability diagram since, over most of the Mn(II) concentration and pH range illustrated, MnO_2 would be the most stable phase. (Concentration is equated with activity here, as it was in Hastings & Emerson, 1986.) The equilibrium lines for each reaction are drawn from thermodynamic data and for known solution conditions it is possible to predict which phase is thermodynamically stable. For a solution with Mn and pH values to the right of line 2 the formation of hausmannite (Mn_3O_4) has a negative free energy so the forward reaction is thermodynamically favourable. For a solution to

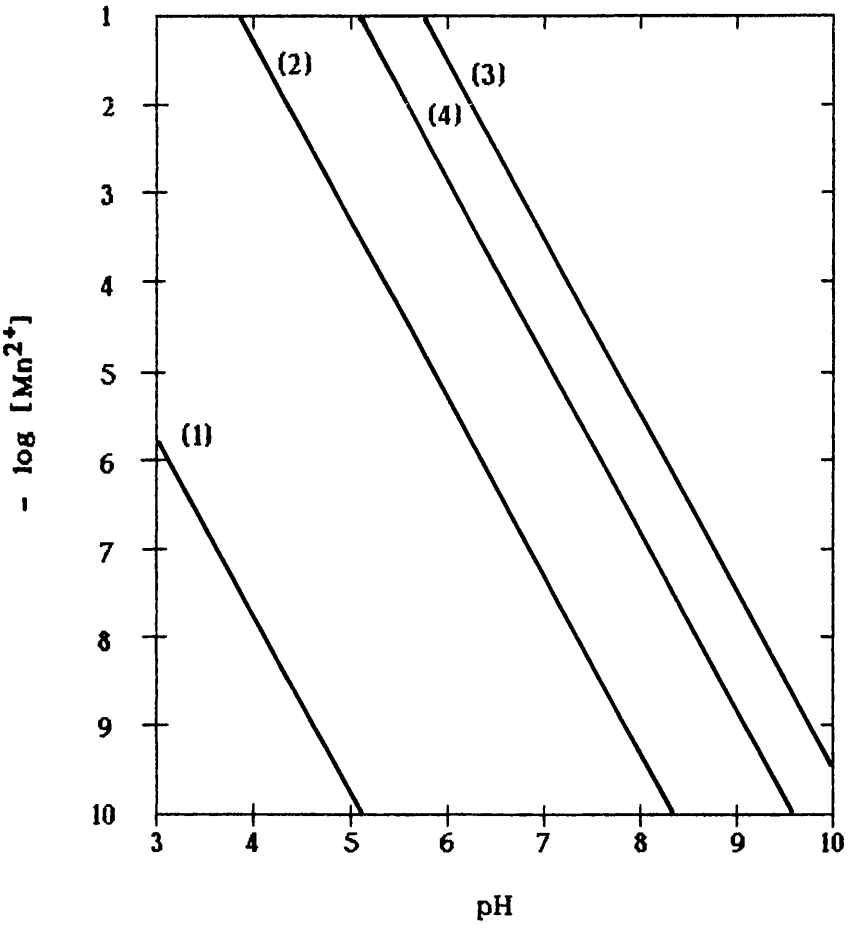

Figure 6.1 Mn^{2+} activity - pH equilibrium relationships

(1) $Mn^{2+} + {}^{1}/_{2}O_2 + H_2O \leftrightharpoons MnO_2 + 2H^+$

(2) $3Mn^{2+} + 3H_2O + {}^{1}/_{2}O_2 \leftrightharpoons Mn_3O_4 + 6H^+$

(3) $2\ \gamma MnOOH + Mn^{2+} \leftrightharpoons Mn_3O_4 + 2H^+$

(4) $MnO_2 + 2Mn^{2+} + 2H_2O \leftrightharpoons Mn_3O_4 + 4H^+$

(After Hastings & Emerson, 1986.)

the right of line 3 hausmannite is stable with respect to manganite (γ-MnOOH) and for a solution to the right of line 4 hausmannite is stable with respect to MnO_2.

The model is incomplete as it does not show the relative stabilities of α- and β-MnOOH. However, it is clear from the work of Murray *et al.* (1985) that β-MnOOH is less stable than γ-MnOOH. Also, it is important to note that the model gives no indication of the kinetics of the system.

6.0.2 The Morphologies of Manganese oxides

Mackenzie *et al.* (1971) reported that feitknechtite (β-MnOOH) forms hexagonal platelets, which may be of regular or irregular shapes. Hem and Lind (1983) have added that this material is poorly crystalline. Manganite (γ-MnOOH) forms lath like crystals, elongated along the c-axis, the crystals generally having blunt rather than pointed ends, (Mackenzie *et al.*, 1971). Murray *et al.* (1985) describe manganite as needle-like. Hausmannite (Mn_3O_4) has a square-like morphology, some crystals having rounded corners, (Mackenzie *et al.*, 1971). It can appear to be granular (Dana, 1932) or take the form of bipyramids, (Murray *et al.*, 1985). Groutite (α-MnOOH) has a rod-like morphology (Giovanoli & Leuenberger, 1969).

6.0.3 Mn^{2+} binding to apoferritin

In 1973 Macara *et al.* reported that apoferritin could bind Mn^{2+} at pH 5.55 at two classes of site, one class having a higher binding constant than the other. Apoferritin was found to bind Mn^{2+} at the sites with the higher binding constant, at a ratio close to one ion

per subunit dimer and this ratio suggested that binding may take place at the 2-fold axes of symmetry on the assembled molecule. The other class of binding site was thought to be on the external surface of the molecule.

In later work Wardeska *et al.* (1986) studied the binding of Mn^{2+} by apoferritin at pH 7.0 and pH 6.2. At pH 7.0 they reported a binding of 0.67 ions per subunit, this decreased to 0.26 ions per subunit at pH 6.2. These binding ratios suggested that the protein was binding one and two ions per three subunits, which in turn suggested binding of one and possibly two Mn^{2+} within each 3-fold channel. They also reported that additional weaker binding sites were observed at the two values of pH studied.

The binding sites that exist for manganese on apoferritin will undoubtedly have a role in the binding and possible uptake of Mn^{2+} investigated in the present study. This study should reveal if, once the relatively few available binding sites are saturated, the manganese remains in the bulk solution or if it enters the protein cavity. Its oxidation in either environment should lead to the precipitation of an insoluble oxide.

6.1 EXPERIMENTAL

6.1.1 Reconstitution methods

Apoferritin was reconstituted with manganese by one 0.5ml addition of an aqueous Mn^{2+} solution ($MnCl_2.4H_2O$ BDH Analar) to a buffered apoferritin solution. The final protein and manganese concentrations were; 0.8 μM protein in borate standard buffer pH 9.2 and 2.67 mM manganese, or 2.4 μM protein in 0.05M HEPES (Aldrich Chemical Co. Ltd.) pH 8.0 or 0.1M MOPS pH 7.5 and 9.76 mM manganese.

The concentrations were calculated to give approximately 3300 and 4000 Mn atoms per molecule in the pH 9.2 and the pH 8.0/7.5 preps. respectively. The solutions were left open to the air at room temperature. For the reconstitutions at pH 8.0 the absorbance of the solutions at 385nm was read at intervals in a Cecil CE 595 UV/visible spectrophotometer with distilled water in the reference cell. The increase in absorbance at this wavelength gives a measure of the appearance of the oxidation product, (ascertained by scanning the absorbance of solutions of both the starting materials and the product over a range of wavelengths).

Protein-free controls at all the pH values used were also performed.

6.1.2 Kinetics methods

For the initial experiments with manganese the continual change in absorbance of the solution at A_{385} with each Mn^{2+} addition was recorded for the first 5 hours on the flat-bed chart recorder, on its most sensitive setting, linked to the Cecil CE 595. For the later experiments, the A_{385} was recorded at intervals during days 1 - 14.

6.1.3 Transmission electron microscopy

Sample preparation for TEM, electron diffraction and data analysis were all performed as described in chapter 2.

6.1.4 Sample preparation for X-ray photoelectron spectroscopy

A sample of manganese loaded ferritin was prepared by incubation with Mn^{2+} at pH 8.0 for 6 days. Successful loading of the protein and the absence of any significant amount of non-specific oxidation product was confirmed by TEM. The sample was centrifuged at high

speed in a Microfuge for two minutes and the supernatant withdrawn. This was then dialysed exhaustively against 0.001M NaCl to remove the buffer and reduce the amount of other ions present. The sample was then divided between four Eppendorf tubes, frozen in solid CO_2 and freeze-dried over 6 hours.

A sample of native horse spleen ferritin was dialysed against 0.001M NaCl and freeze-dried in a similar way in order that XPS could be carried out on this also.

The protein samples and the manganese oxide standards, were mounted with double-sided sticky tape onto stainless steel stubs. All the samples were placed in a circular mount, introduced via a number of vacuum chambers into the spectrometer, and were then analysed in turn. For the standards, narrow regions of the photoelectron spectrum were scanned: the manganese 2p, the manganese Auger and the oxygen 1s regions. For the manganese protein sample these regions were scanned in the same way and also a wide scan across the whole available range of energies (0 - 1500 eV) was performed. For the ferritin sample the iron 2p, iron Auger, oxygen 1s and wide scans were carried out.

For all the analyses step size, scan speed and number of scans was selected, by the operator, in order to maximise the signal-to-noise ratio.

Abbreviations used:

HEPES 4-(2-hydroxyethyl)-1-piperazineethanesulphonic acid

MOPS 3-(*N*-Morpholino) propane-sulphonic acid

6.2 RESULTS

6.2.1 Structural studies

Experiments at pH 9.2

1. with apoferritin

Transmission electron microscopy of samples taken after 3 hours showed that discrete cores of electron dense material of the right size and appearance to be inside the ferritin cavity could be imaged. Also oxidation products which had formed outside the protein (non-specific oxidation products) could be seen. (Plate 6.1a.) The presence of manganese in the samples at this stage was confirmed by EdXa, see figure 6.2a. Electron diffraction analysis of areas of the grid where only cores were visible did not reveal any structure, but it was difficult to find a sufficient density of cores to be sure of obtaining a pattern. The non-specific oxidation products were hausmannite (Mn_3O_4) of poorly crystalline and defect structure, see table 6.1.

TEM images of samples taken after 3 days showed massive aggregation of the manganese cores, plate 6.1b, probably caused by the high pH damaging the protein shells. The resulting oxide aggregates had a defect hausmannite structure, table 6.1.

2. protein-free control

The oxidation products formed in the absence of apoferritin exhibited various morphologies. The product which had formed by 3 hours appeared as granular aggregates (see plate 6.2a) and the two broad rings on the diffraction patterns at between 1.47 - 1.62Å and 2.41 - 2.78Å suggested that it was hausmannite. By three days some of the product had a very thin sheet-like appearance and some remained granular, plate 6.2b & c. These morphologies and the electron

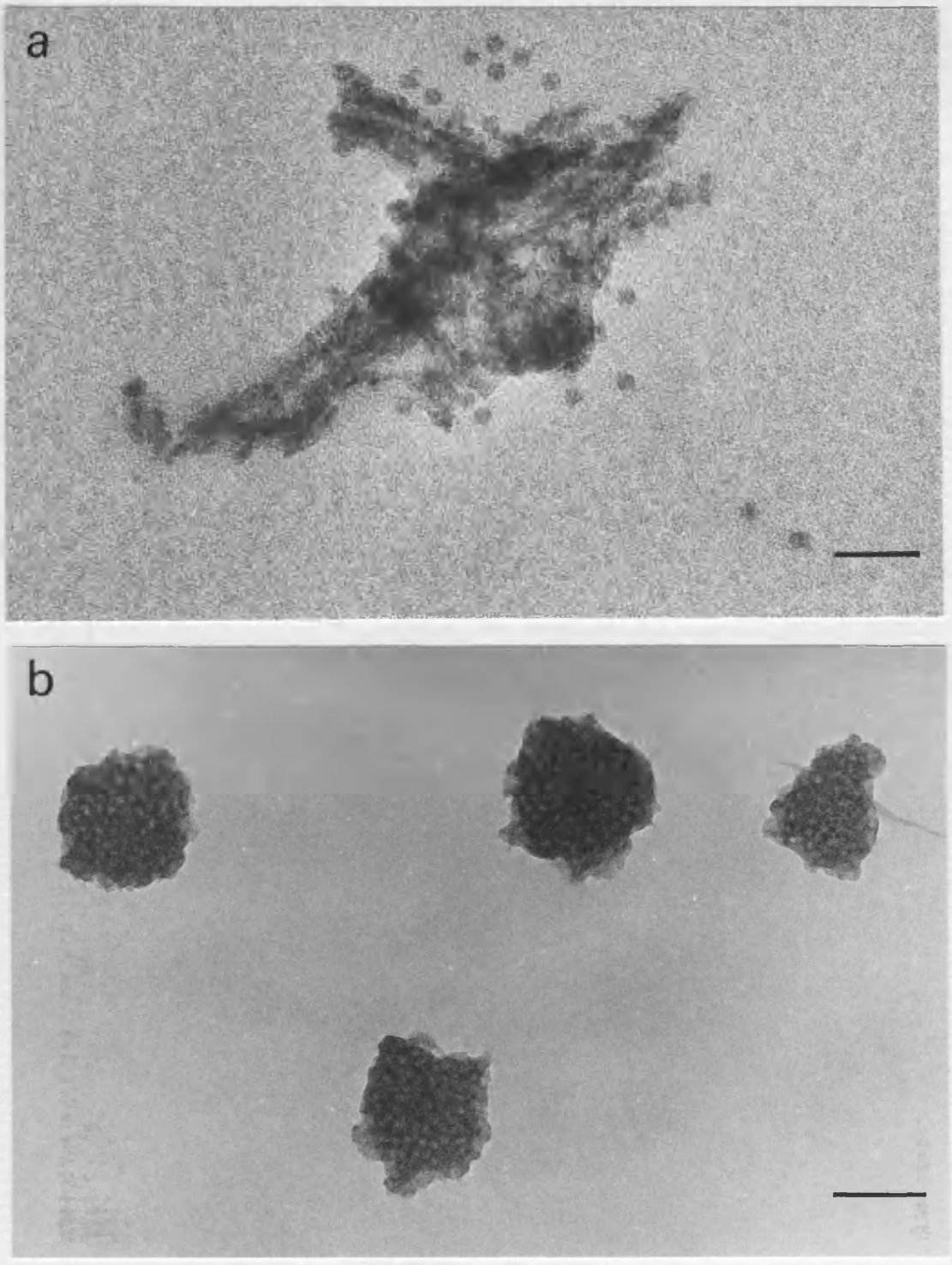

Plate 6.1 Electron micrographs of products formed in the presence of apoferritin at pH 9.2. *a* at 3 hours, manganese ferritin cores and non-specific oxidation product, bar marker 30nm. *b* at 3 days, aggregated manganese cores, bar marker 100nm.

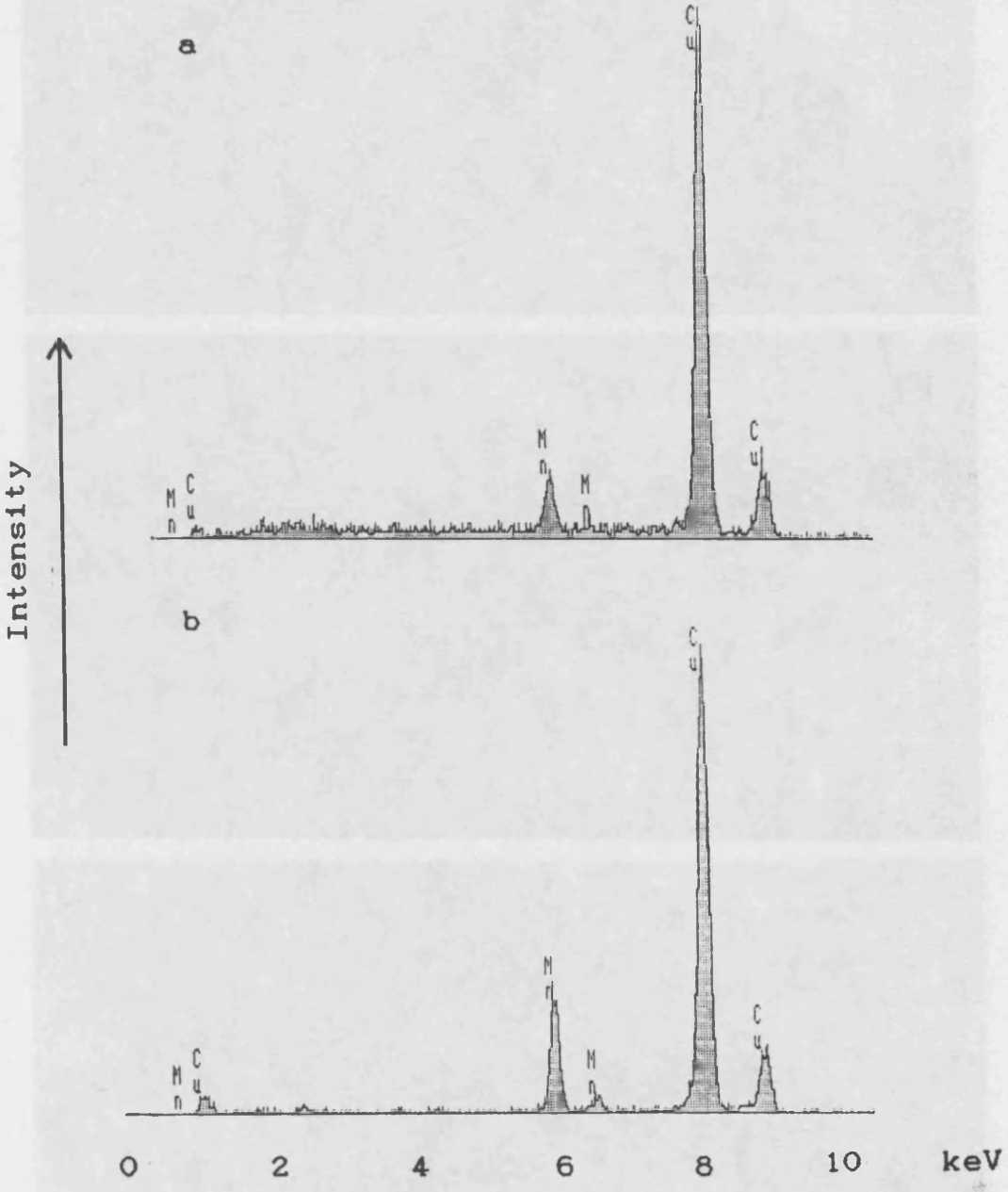

Figure 6.2 EdXa spectra of samples from experiments at pH 9.2. *a* in the presence of apoferritin, from an area of cores and non-specific oxidation product. *b* in the absence of apoferritin, from the material shown in plate 6.2c.

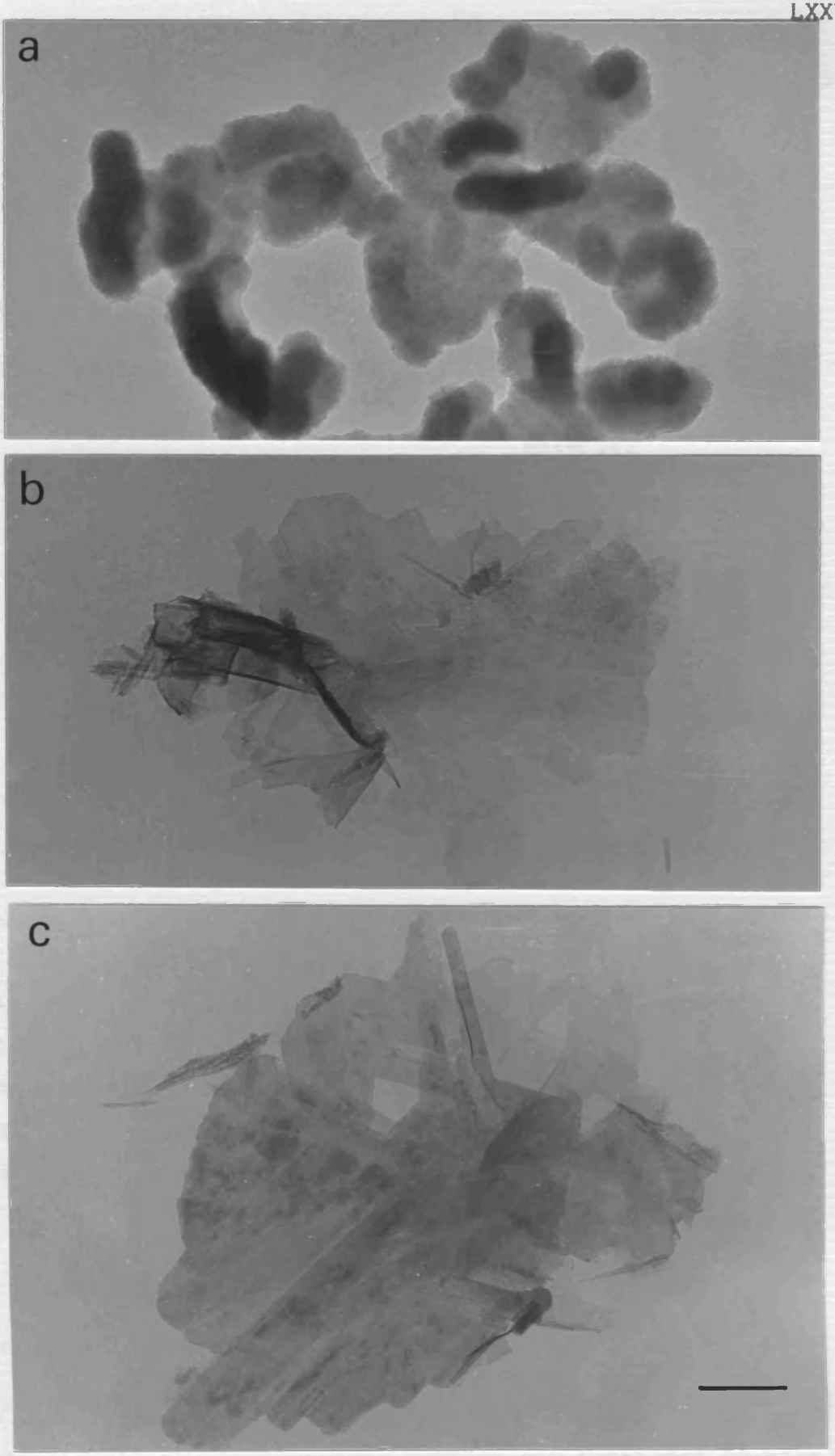

Plate 6.2 Electron micrographs of products formed in the protein-free controls at pH 9.2. *a* at 3 hours, *b* & *c* at 3 days, bar marker 200nm for *a*, *b* & *c*.

Table 6.1. Electron diffraction data for the non-specific oxidation product formed in the presence of apoferritin at pH 9.2, after 3 hours and after 3 days.

3 hours		3 days		
d(Å)	I	d(Å)	I	assigned material
2.75	S	2.73	M	H
2.38	M	2.42	SB	H
2.12	M	2.11	W	H
1.96	M	1.98	W	H
1.73	M			H
		1.58	W	H
1.49	W	1.48	M	H
1.36	W			H
	M	1.26	M/W	H

For all electron diffraction analysis the intensities of the diffraction lines were judged by eye: S = strong, M = medium, W = weak, B = broadened.
The assigned manganese oxides are designated as follows:
H = hausmannite, F = feitknechtite, G = groutite, M = manganite.

diffraction data (table 6.2) suggested that the material was a mixture of hausmannite and feitknechtite (β-MnOOH). The presence of manganese in all the protein-free samples was confirmed by EdXa and a spectrum taken from the material shown in plate 6.2c is shown in figure 6.2b.

Experiments at pH 8.0

1. with apoferritin

After incubation with Mn^{2+} for 2 days discrete, well-defined cores of a very regular round or square shape were visible on the electron microscope grid (plate 6.3a). The mean core diameter was 6.64 nm, with a standard deviation of 0.42 nm, and a particle size histogram is shown in figure 6.3a. The smaller cores, had more irregular, anisotropic shapes. There was little non-specific oxidation product. The cores appeared to be amorphous by selected area electron diffraction. The density of cores on the grids was not as high as that achieved routinely with iron reconstituted samples, but was thought to be high enough to obtain a diffraction pattern if some structure existed in the cores. EdXa confirmed the presence of manganese in the cores, see figure 6.4a.

After 4 days incubation, the cores were again discrete, well defined and of rounded or squarish shape (plate 6.3b). The mean core diameter was a little larger than that at 2 days: 6.71 nm, with a standard deviation of 0.41 nm (see particle size histogram shown in figure 6.3b). A few smaller, less regular cores were visible on the grid but not as many as were seen in the 2 day sample. The electron diffraction patterns again showed just diffuse carbon rings. There was little non-specific oxidation product.

After 7 days incubation the cores were still discrete, well defined and of regular round or square shape, see plate 6.4a. There was a little non-specific oxidation product. The cores appeared to be amorphous by electron diffraction. They were large, with a mean core diameter of 7.14 nm (SD 0.46 nm). There were very few smaller cores visible in this sample. A particle size histogram is shown in figure 6.3c.

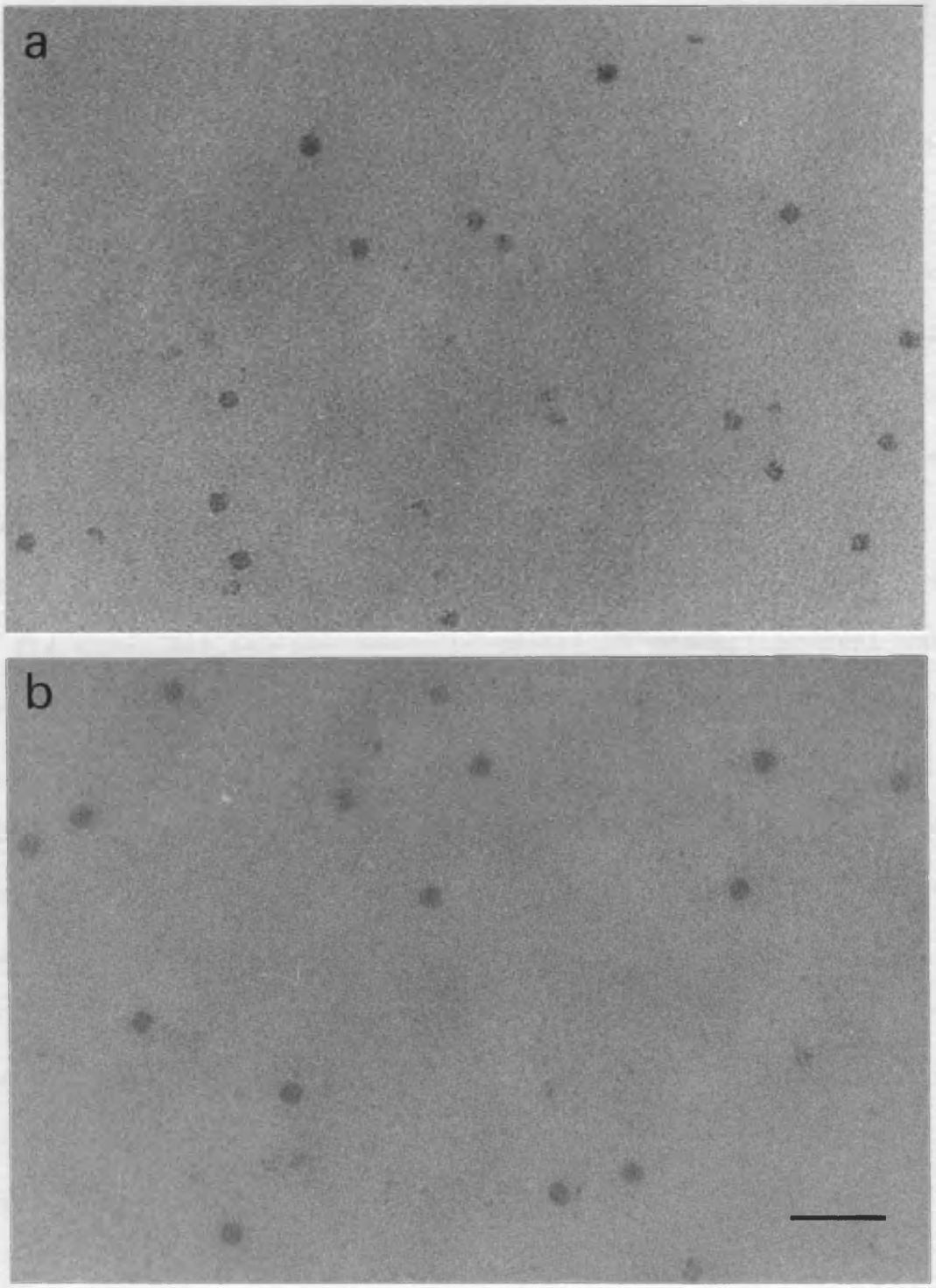

Plate 6.3 Electron micrographs of manganese ferritin cores formed in the experiments at pH 8.0. *a* at 2 days, *b* at 4 days, bar marker 30nm for both *a* & *b*.

Following a 14 day incubation with manganese the samples contained discrete and well defined cores (plate 6.4b) and an increased amount of non-specific oxidation product (plate 6.4c). The cores were again of generally regular shapes, they had a mean core diameter of 6.88 nm, with a standard deviation of 0.33 nm and there were no very small cores visible in these samples. The particle size distribution, shown in figure 6.3d, illustrates the slightly narrower distribution of cores sizes in these samples as compared with those after 7 days, although the modal core diameter remains unchanged. Electron diffraction analysis again showed no structure in the cores but it did show that the non-specific oxidation product present was hausmannite, (see table 6.3).

Since selected area electron diffraction had proved unsuccessful in providing structural information about the manganese loaded cores, high resolution TEM was carried out on samples reconstituted at pH 8.0 after 2, 4 and 7 day incubations. However, this approach was also unsuccessful. No structural order could be imaged in any of the cores; they appeared disordered with little contrast against the background film of amorphous carbon, as illustrated in plate 6.4d.

2. protein-free control

At 2 days the material in the controls was predominantly of granular and cuboid morphology, with some rod or needle shaped particles. (Plate 6.5a). The electron diffraction patterns taken from areas of mixed morphologies revealed diffraction lines attributable to hausmannite, see table 6.4. The rod and needle shaped particles were probably groutite.

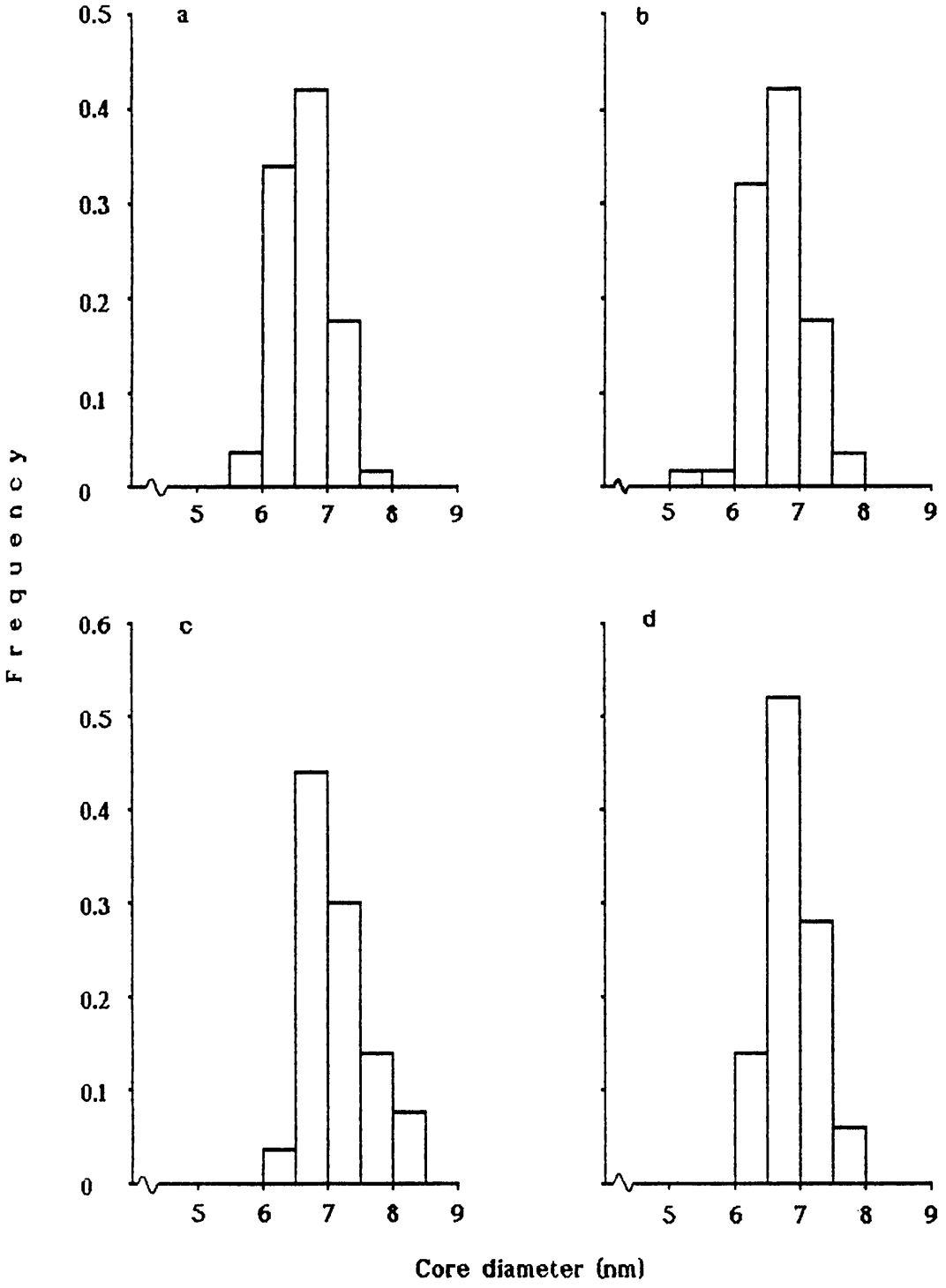

Figure 6.3 Particle size distributions for ferritin reconstituted with manganese at pH 8.0. *a* 2 days, *b* 4 days, *c* 7 days, *d* 14 days.

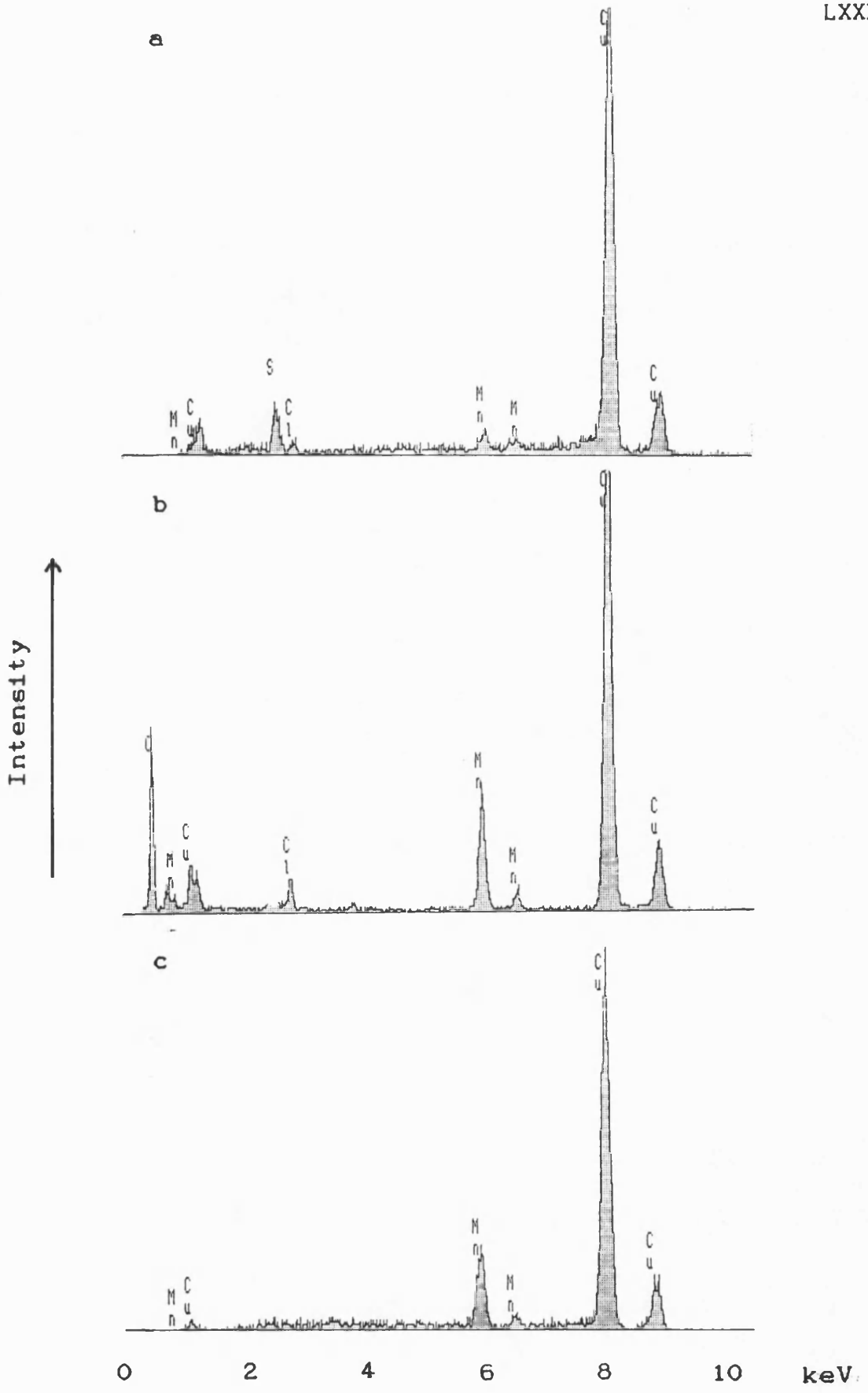

Figure 6.4 EdXa spectra of samples from experiments at pH 8.0 and pH 7.5. *a* manganese loaded ferritin after two days incubation at pH 8.0, *b* protein-free control after seven days at pH 8.0, *c* protein-free control after seven days at pH 7.5.

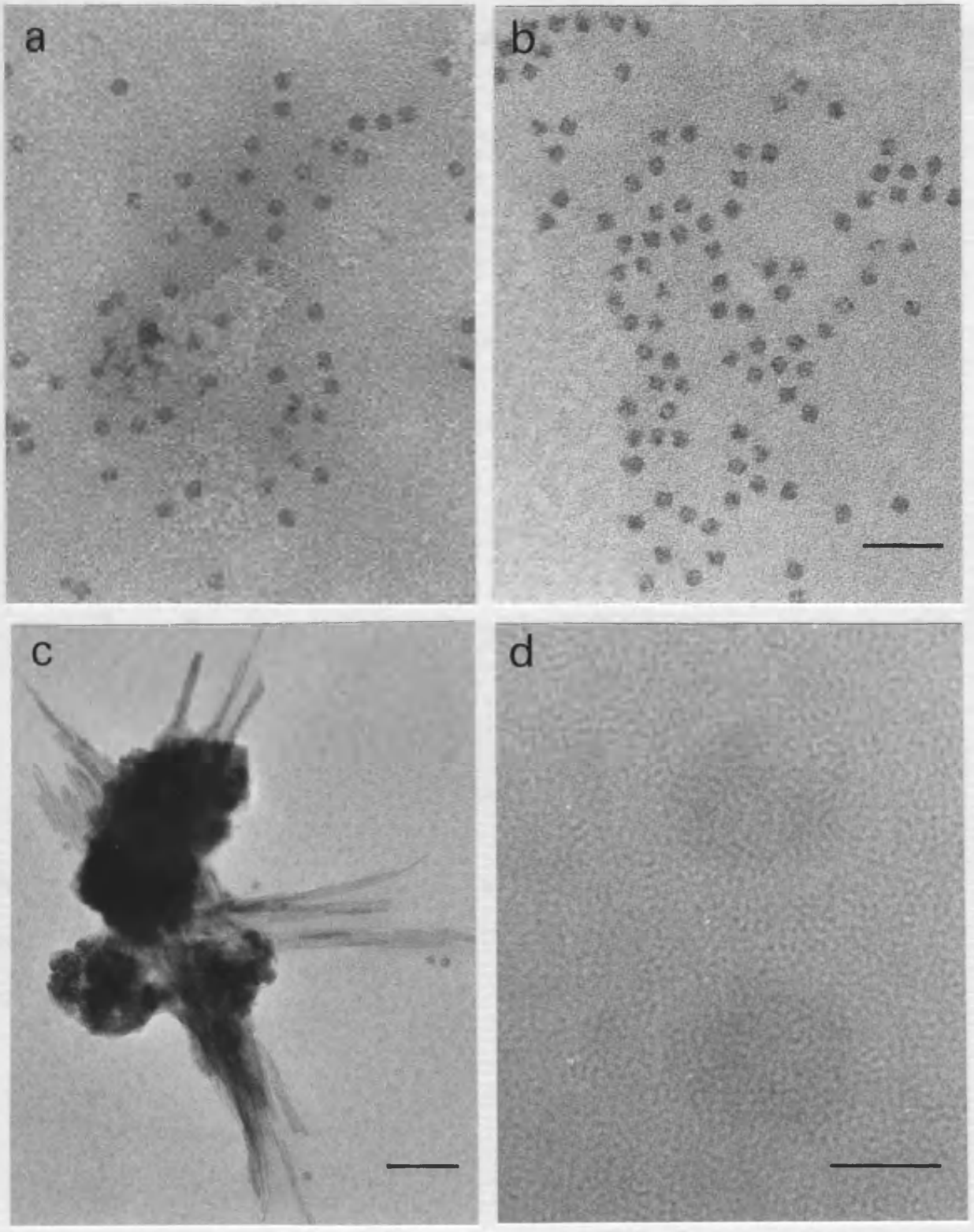

Plate 6.4 Electron micrographs of products formed in the experiments at pH 8.0. *a & b* manganese ferritin cores at 7 and 14 days respectively, bar marker 30nm for both micrographs. *c* manganese ferritin cores and some non-specific oxidation product formed at 14 days, bar marker 50nm. *d* high resolution image of two manganese ferritin cores, bar marker 5nm.

Table 6.2. Electron diffraction data for the non-specific oxidation product formed after 3 days at pH 9.2. Data from two patterns taken from the two areas shown in plate 6.2b & c.

d(Å)	I	d(Å)	I	assigned material
2.53	S	2.49	S	H
2.12	M			H
1.49	S	1.49	S	F
1.43	S	1.43	S	H
1.27	W	1.30	W	H
1.23	M	1.25	M	H
0.97	W	0.97	W	H
0.83	M	0.83	W	
0.74	W	0.74	W	
0.72	W			

Table 6.3. Electron diffraction data from the non-specific oxidation product formed after 14 days at pH 8.0 in the presence of apoferritin.

d(Å)	I	assigned material
4.93	S	H
3.12	W	H
2.78	M	H
2.49	S	H
2.38	W	H
2.06	M	H
1.82	W	H
1.58	MB	H
1.46	M/W	H

After 4 days well-defined rods of fairly uniform width but varying length were imaged, they appeared to have grown from some poorly-defined material, see plate 6.5b. The rod-shaped morphology and electron diffraction data (table 6.5) suggested that this material was groutite (α-MnOOH). The poorly defined material was probably hausmannite.

The oxidation products visible after 7 days all had a plate-like morphology which is indicative of feitknechtite. Indeed, some plates of ~350 × 250 nm dimensions gave hexagonal single crystal electron diffraction patterns which corresponded to feitknechtite, see plate 6.6a & b. The diffraction pattern was the same from both the lighter and darker areas shown in plate 6.6a. Some larger plates, ~2 × 1.5μm (plate 6.7a), gave powder electron diffraction patterns having many sharp lines, which showed preferred orientation of the crystallites in the plates and some of the lines occurred in pairs indicative of a spinel structure, (plate 6.7b). The d-spacings of these lines (table 6.6) and the good crystallinity suggested that this material may have been hausmannite but the strongest lines at 4.79 and 1.61Å do not match the hausmannite standard lines well; the 4.79Å line was below the standard line at 4.924Å and the intensity of the 1.61Å line was too high for it to match the standard line at 1.641Å. Also the plate-like morphology was inconsistent with the material being hausmannite. From the morphology, feitknechtite was the only likely form of oxide and the two strong d-spacings could be attributable to this poorly crystalline oxide. Therefore, the material may have been a mixture of the two.

The presence of manganese in these plate-like materials was also confirmed by EdXa, see figure 6.4b.

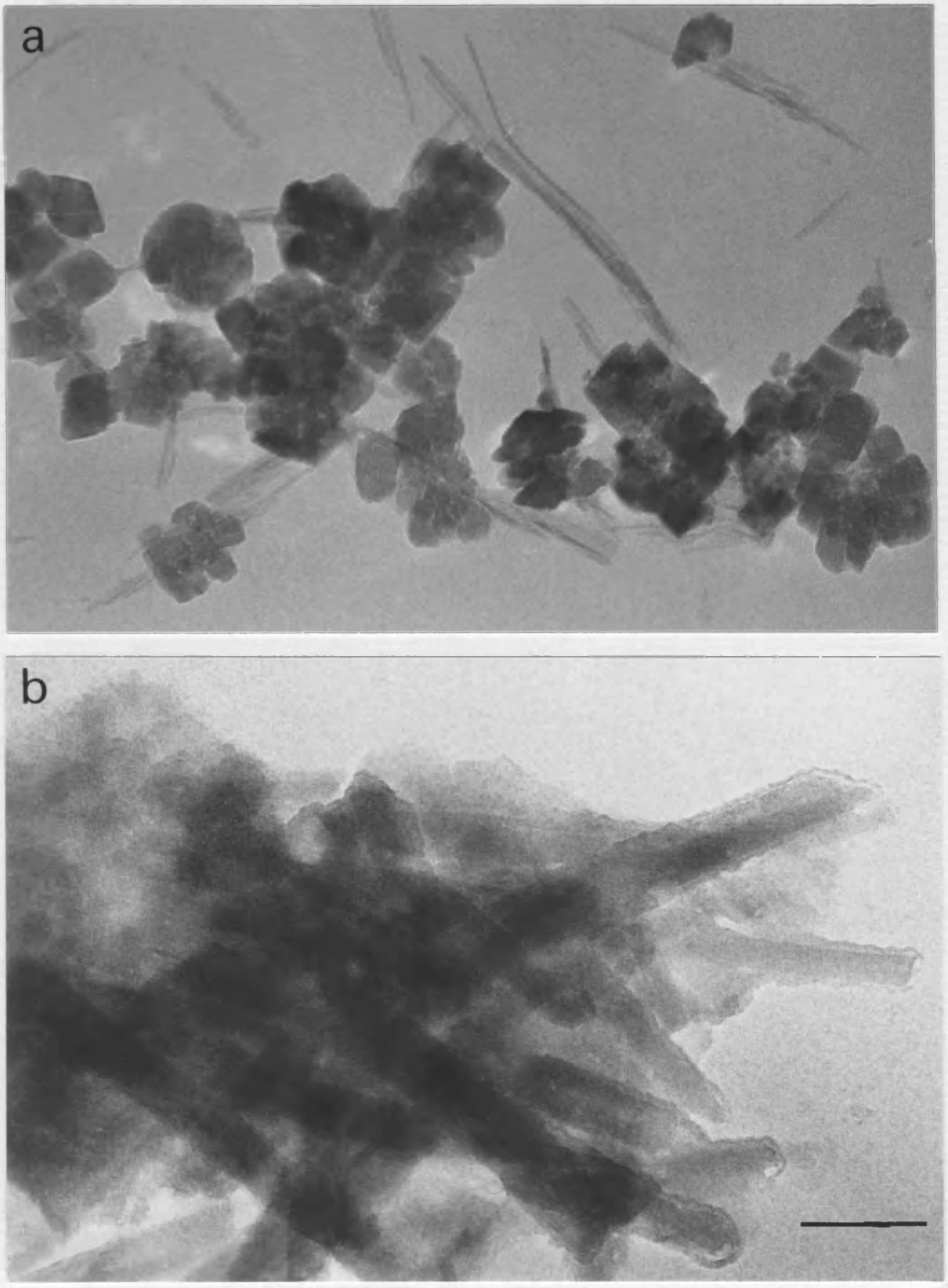

Plate 6.5 Electron micrographs of products formed in the protein-free controls at pH 8.0. *a* at 2 days, *b* at 4 days, bar marker 100nm for both micrographs.

Table 6.4. Electron diffraction data for the non-specific oxidation product formed after 2 days at pH 8.0.

d(Å)	I	assigned material
2.89	M	H
2.74	M	H
2.48	S	H
2.33	W	H
2.04	W	H
1.79	W	H
1.57	W	H
1.53	M/W	H
1.44	M	H
1.27	W	H

Table 6.5. Electron diffraction data for the rod-shaped non-specific oxidation product formed after 4 days at pH 8.0.

d(Å)	I	assigned material
2.19	W	G
1.80	M	G/H
1.59	M	G
1.54	W	G/H
1.36	S	G

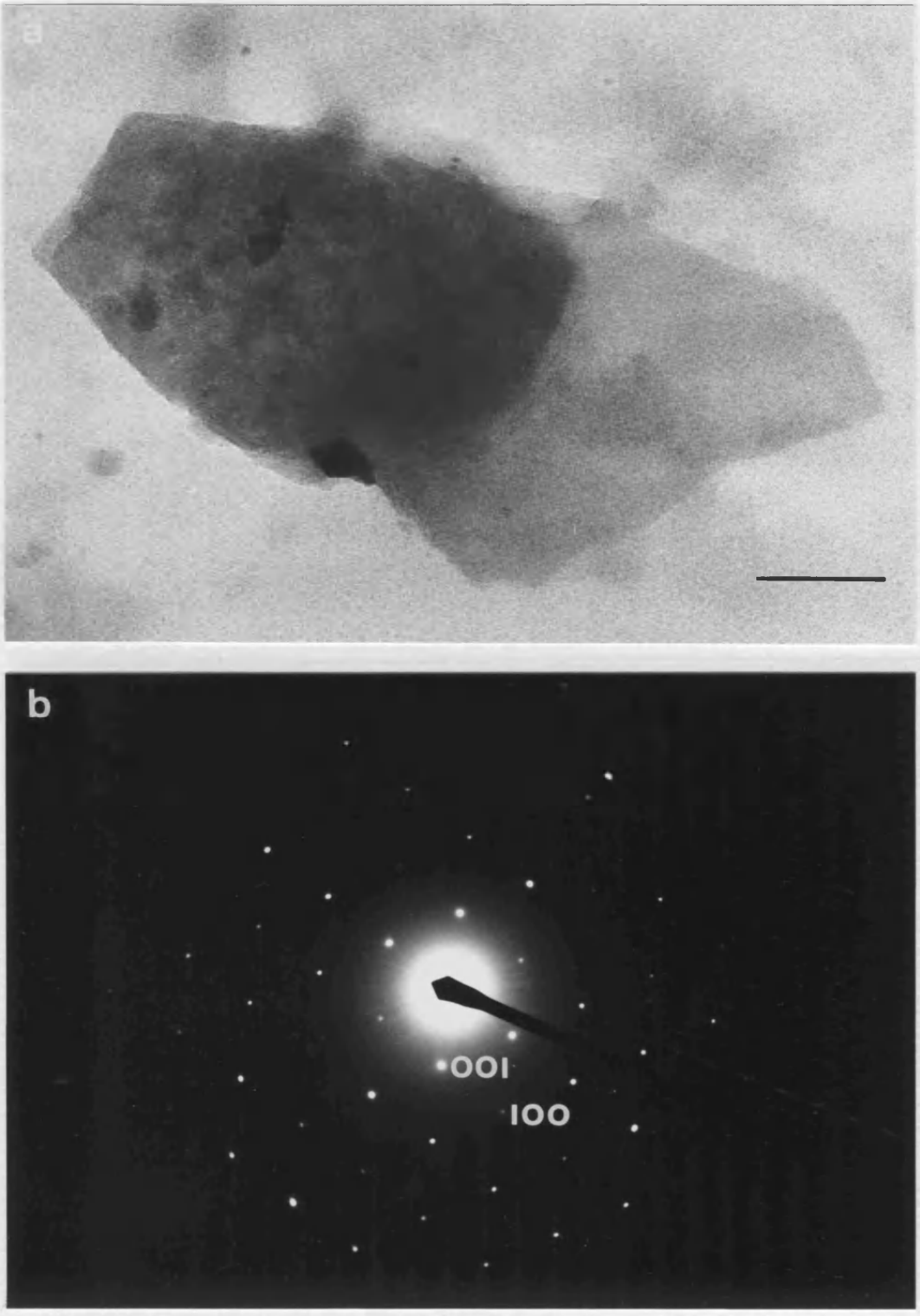

Plate 6.6 Electron micrograph and single crystal diffraction pattern from the products formed in the protein-free controls at pH 8.0 after 7 days. Bar marker 100nm in *a*, camera length 135cm in *b*.

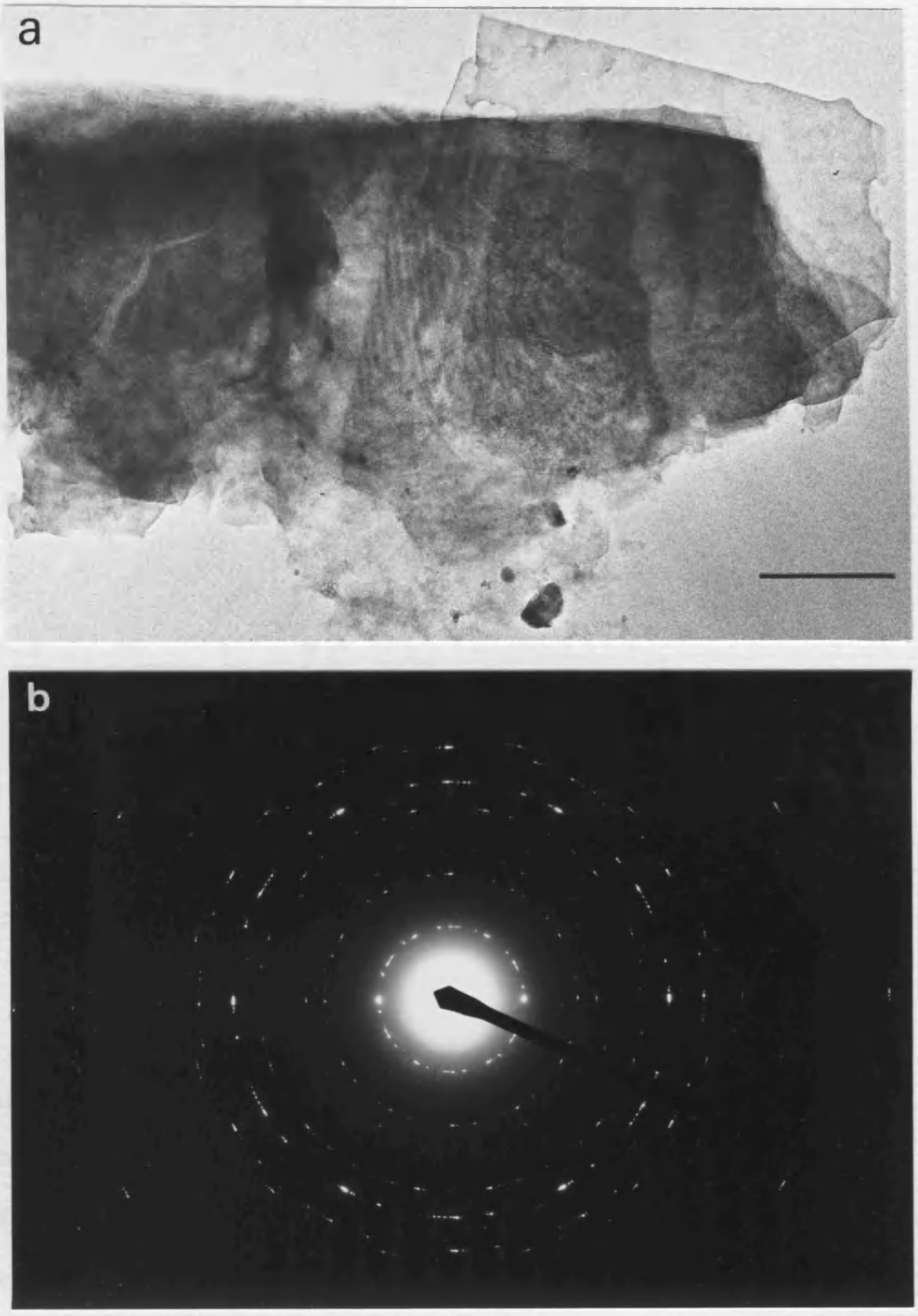

Plate 6.7 Electron micrograph and powder diffraction pattern from the products formed in the protein-free controls at pH 8.0 after 7 days. Bar marker 500nm in *a*, camera length 135cm in *b*.

Table 6.6. Electron diffraction data from non-specific oxidation product of plate-like morphology formed after 7 days at pH 8.0.

d(Å)	I	assigned material
4.79	S	H/F
2.79	M	H
2.41	M/W	H
1.82	M	H
1.61	S	H/F
1.40	M	H
1.34	M/W	H
1.10	W	H
1.06	W	H
0.93	M/W	H
0.87	W	

d-spacings bracketed together formed pairs of rings on the diffraction pattern.

Experiments at pH 7.5

1. with apoferritin

After 2 days incubation discrete cores of regular shape, round or square, could be seen on the grids, however, they were fewer in number than those formed in the experiments at pH 8.0 at this stage. There was very little non-specific oxidation product present. (Plate 6.8a.)

After 7 days incubation the sample contained discrete, well-formed cores, see plate 6.8b, and a little more non-specific oxidation product.

The very low density of cores in these pH 7.5 experiments precluded any attempts at characterisation by electron diffraction and there were too few cores present for EdXa to be successful. The low total numbers of cores also prevented the measurement of populations of cores for particle size distributions. However, some core size measurements were made: for the 2 day sample, 12 cores with diameters ranging from 5.76 to 7.49 nm were measured and for the sample after 7 days, 14 cores were measured which had diameters between 4.93 and 7.07 nm.

2. protein-free control

After 2 days the non-specific oxidation product appeared as granular material, see plate 6.8c, which was amorphous by electron diffraction.

After 7 days the material present was irregular rod-like particles approximately 50 - 200 nm long, see plate 6.8d. This morphology suggested that the material was groutite, the electron diffraction pattern indicates a mixture of groutite, hausmannite and, possibly manganite (γ-MnOOH), see table 6.7. EdXa analysis confirmed the presence of manganese in this material, see figure 6.4c.

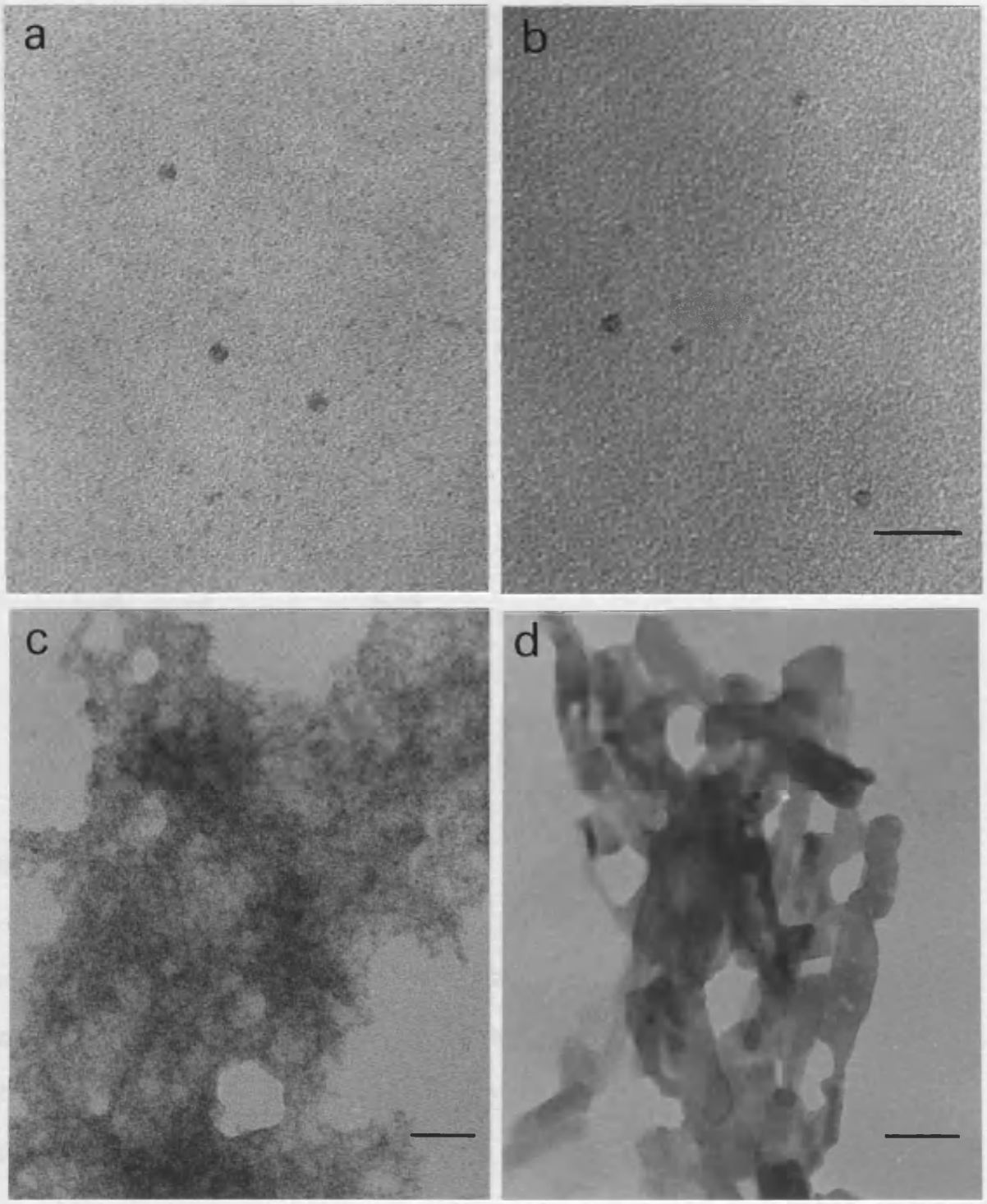

Plate 6.8 Electron micrographs of products formed in the experiments at pH 7.5. *a & b* manganese ferritin cores at 2 and 7 days respectively, bar marker 30nm for both micrographs.
c & d oxidation products formed in the protein-free controls at 2 and 7 days respectively, bar markers 50nm.

Table 6.7. Electron diffraction data from the non-specific oxidation product of rod-like morphology formed after 7 days at pH 7.5.

d(Å)	I	assigned material
3.45	S	G/M
3.28	W	
2.89	M	H
2.73	M	H/M
2.36	S	G
1.85	W	
1.77	W	G/M
1.42	M	H/M
1.36	W	G/M

6.2.2 Kinetic Studies at pH 8.0

The kinetics of the oxidation of Mn^{2+} in the presence and absence of apoferritin was monitored at 385 nm over the course of several days. When the reaction was monitored continuously over the first five hours no oxidation could be detected in either the solution containing apoferritin or the protein-free control. The results of readings taken at later time intervals for three separate experiments are shown in figure 6.5. The figure shows that oxidation did occur in both solutions and that the apoferritin had a catalytic effect on the reaction under the conditions used. For one of the experiments (plot c) the increase in A_{385} of both solutions was monitored over the following 10 days. The solution containing protein attained an absorbance of 4.6 (calculated from the A_{385} of a dilution) and that of the protein-free control reached 0.2. During

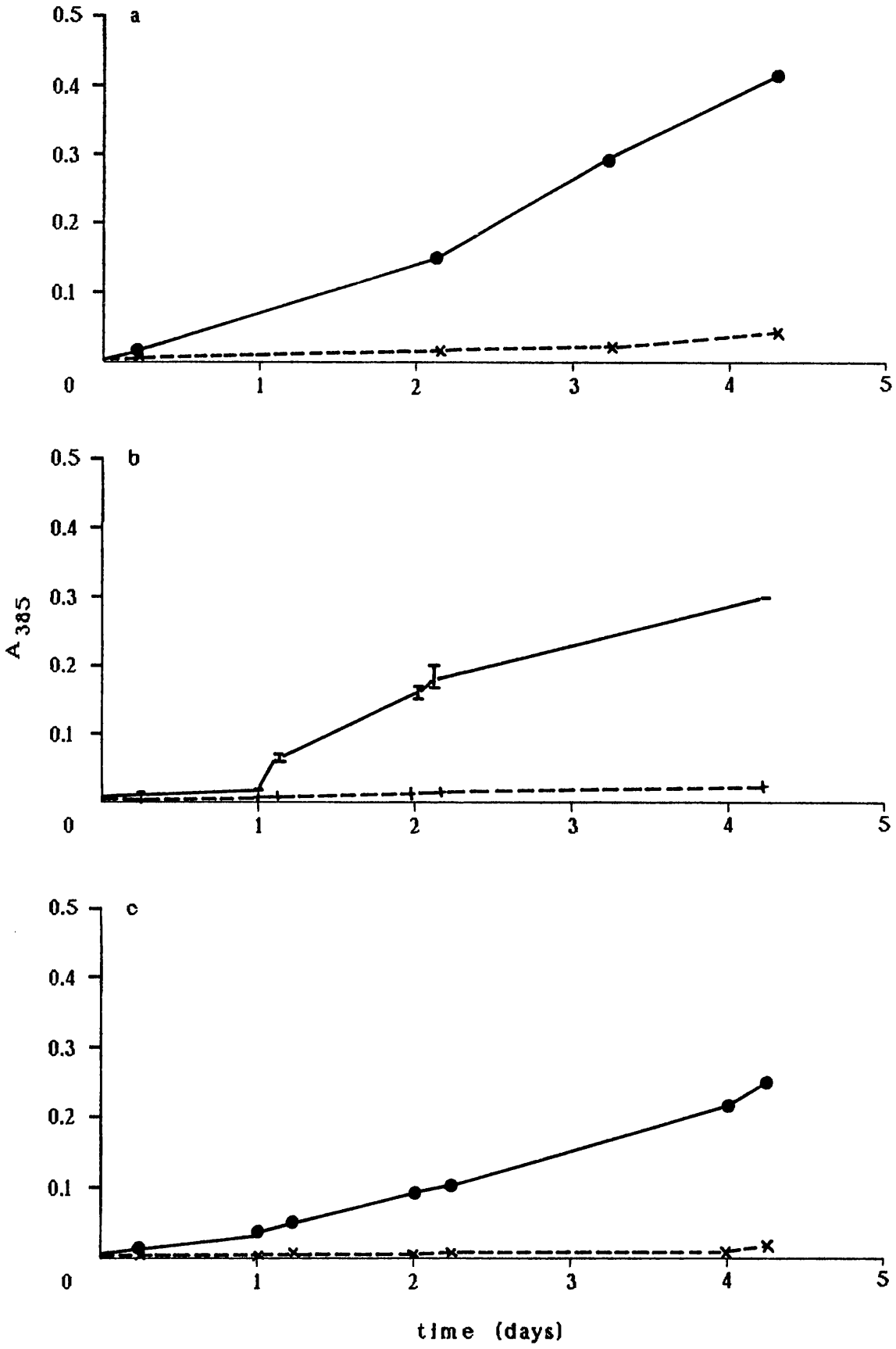

Figure 6.5 Progress curves for manganese oxidation in 3 separate experiments at pH 8.0 in the presence (—) and absence (---) of apoferritin.

days 5 - 14 both solutions became cloudy and contained particles which tended to settle out of solution, so the further increase in absorbance may have increasingly reflected flocculation of the products, rather than just oxidation of Mn^{2+}.

6.2.3 X-ray Photoelectron Spectroscopy

Electron diffraction analysis of the manganese loaded ferritin yielded no information about the cores, so in order to further investigate the nature of the manganese oxide cores XPS was carried out on a sample of the manganese loaded protein. It was hoped that this technique would reveal the oxidation state of the manganese.

Characterisation of standards

Three manganese oxide standards were characterised by XRD to confirm their structure and thus, the oxidation state of the Mn they contained. The Mn(II,III) oxide, Mn_3O_4 was confirmed as hausmannite, the Mn_2O_3 was a synthetic Mn(III) oxide, and the MnO_2 was the Mn(IV) oxide pyrolusite (βMnO_2). The observed d-spacings and those from the X-ray diffraction file for each of the three oxides are shown in tables 6.8, 6.9 and 6.10.

XPS

Due to charging of the samples the observed binding energies were higher than the theoretical values. When the values of the O 1s energies observed were compared with the theoretical value they showed that readings obtained were 2 - 3 eV higher than the theoretical values.

Table 6.8. XRD data for hausmannite.

Expt. data		File data, no. 24-734		
d(Å)	I	d(Å)	I	hkl
4.89	W	4.924	30	101
3.038	W	3.089	40	112
2.746	S	2.768	85	103
2.429	S	2.487	100	211
		2.463	20	202
1.789	W	1.7988	25	105
1.568	M	1.5762	25	321
1.536	S	1.5443	50	224
1.436	M	1.4405	20	400

Table 6.9. XRD data for the Mn(III) oxide.

Expt. data		File data, no. 31-826		
d(Å)	I	d(Å)	I	hkl
3.827	W	3.84	25	211
2.694	S	2.72	100	222
2.338	W	2.35	12	400
1.991	W	2.01	14	332
1.835	W	1.845	14	431
1.656	S	1.664	30	440
1.448	W	1.4524	10	541
1.414	M/S	1.4191	14	622
1.385	W	1.3875	6	631

Table 6.10. XRD data for pyrolusite.

Expt. data		File data, no. 24-735		
d(Å)	I	d(Å)	I	hkl
3.112	S	3.110	100	110
2.405	M/S	2.407	55	101
2.108	M	2.110	16	111
1.967	W	1.9681	5	210
1.623	SB	1.6234	55	211
1.557	MB	1.5554	14	220
1.434	M/W	1.4370	8	002

1. The Mn 2p region.

The peaks in binding energy observed in this region for the three manganese oxide standards coincided, see figure 6.6, so the difference in oxidation state of the manganese in these oxides could not be resolved by this method. The scan of this region for the manganese ferritin sample showed broadened peaks corresponding to the $2p^3$ and $2p^1$ energies, see figure 6.6d.

2. The Mn Auger region.

In this energy region, again no difference was observed between the spectra from the three manganese oxide standards, see figure 6.7. The scan of the Mn Auger region of the manganese protein sample was weak, due to a poor count rate, and no clear peak was observed, see figure 6.7d.

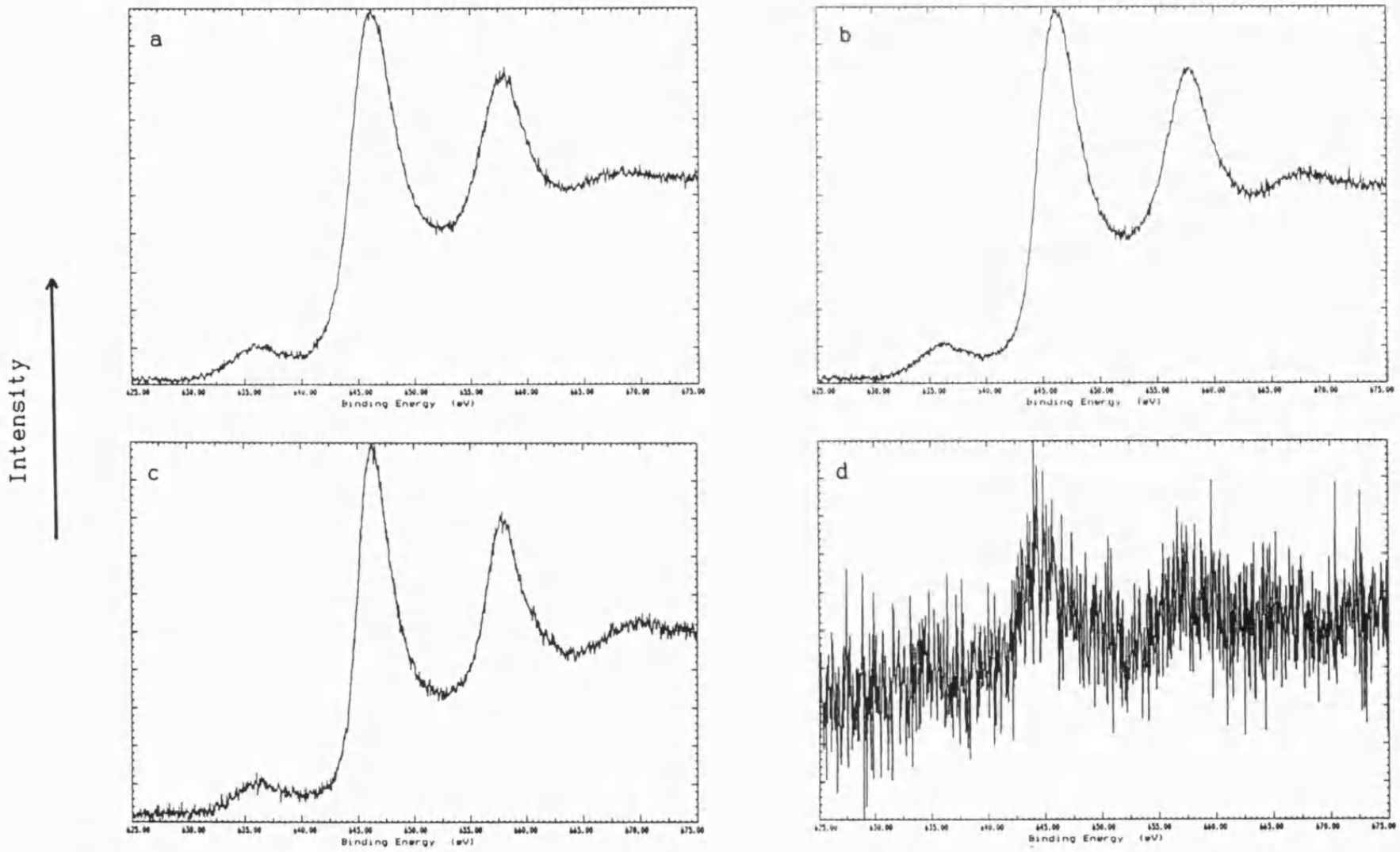

Figure 6.6 X-ray photoelectron spectra of the Mn 2p region. *a* Mn_3O_4, *b* Mn_2O_3, *c* MnO_2, *d* manganese loaded ferritin. Step size 0.05 eV, 5 scans of 60 secs per scan.

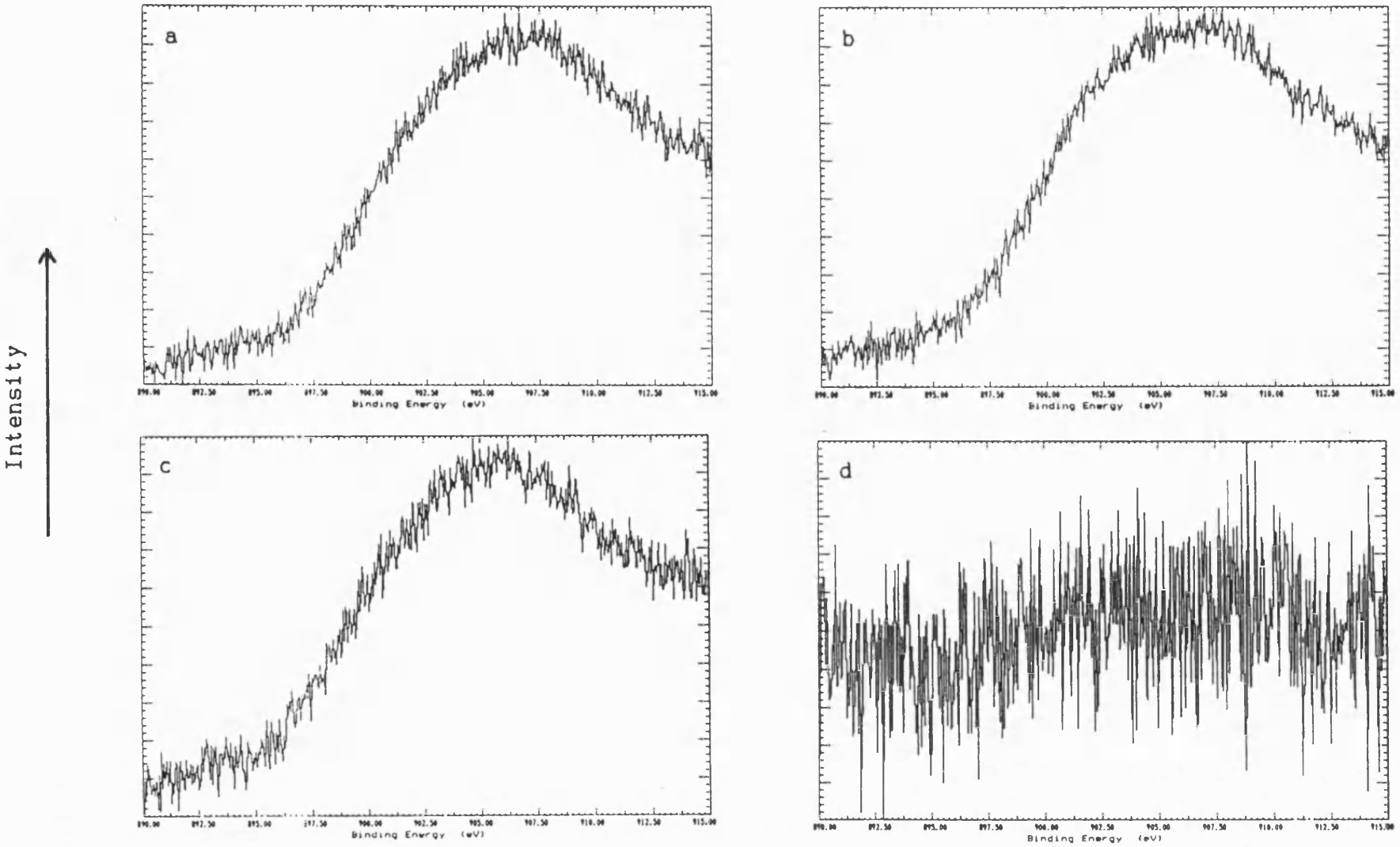

Figure 6.7 X-ray photoelectron spectra of the Mn Auger region. *a* Mn_3O_4, *b* Mn_2O_3, *c* MnO_2, *d* manganese loaded ferritin. Step size 0.05 eV, 5 scans of 30 secs per scan.

3. The O 1s region.

In this region clear peaks corresponding to the 1s energy level were obtained for all samples, see figure 6.8. The energy at which this peak was observed for each manganese oxide standard was slightly different. For hausmannite (Mn II,III) the peak occurred at 534.25 eV, for the Mn (III) oxide it occurred at 533.875 eV and for pyrolusite (Mn IV) it occurred at 533.25 eV. The peak shape for the Mn (IV) sample was different in that it had a shoulder on the higher energy side from around 535.00 to 538.75 eV, see figure 6.8c. The peak for the manganese protein sample occurred at 5.33.75 eV (figure 6.8d), and as such was most similar in energy to the Mn (III) standard. Its peak shape was similar to both the Mn (II,III) and Mn (III) standards.

4. The wide scan.

The scan of binding energies from 0 - 1500 eV, figure 6.9, confirmed again the presence of manganese in the manganese protein sample. It also showed the presence of other elements originating from the protein (eg. S, N and C), the dialysate (NaCl) and the sticky tape (Si).

5. The native horse spleen ferritin sample.

The results of the XPS scans performed on this sample are shown in figure 6.10. The Fe 2p region (spectrum a) showed peaks of binding energy corresponding to $2p^3$ and $2p^1$. The Fe Auger scan (b) showed a broad peak around 788.75 eV. This spectrum was slightly stronger than that of the Mn Auger region for the manganese protein sample due to a higher count rate. The O 1s scan (c) showed a peak of binding energy at 534.25 eV, which was most similar in energy to that of the Mn

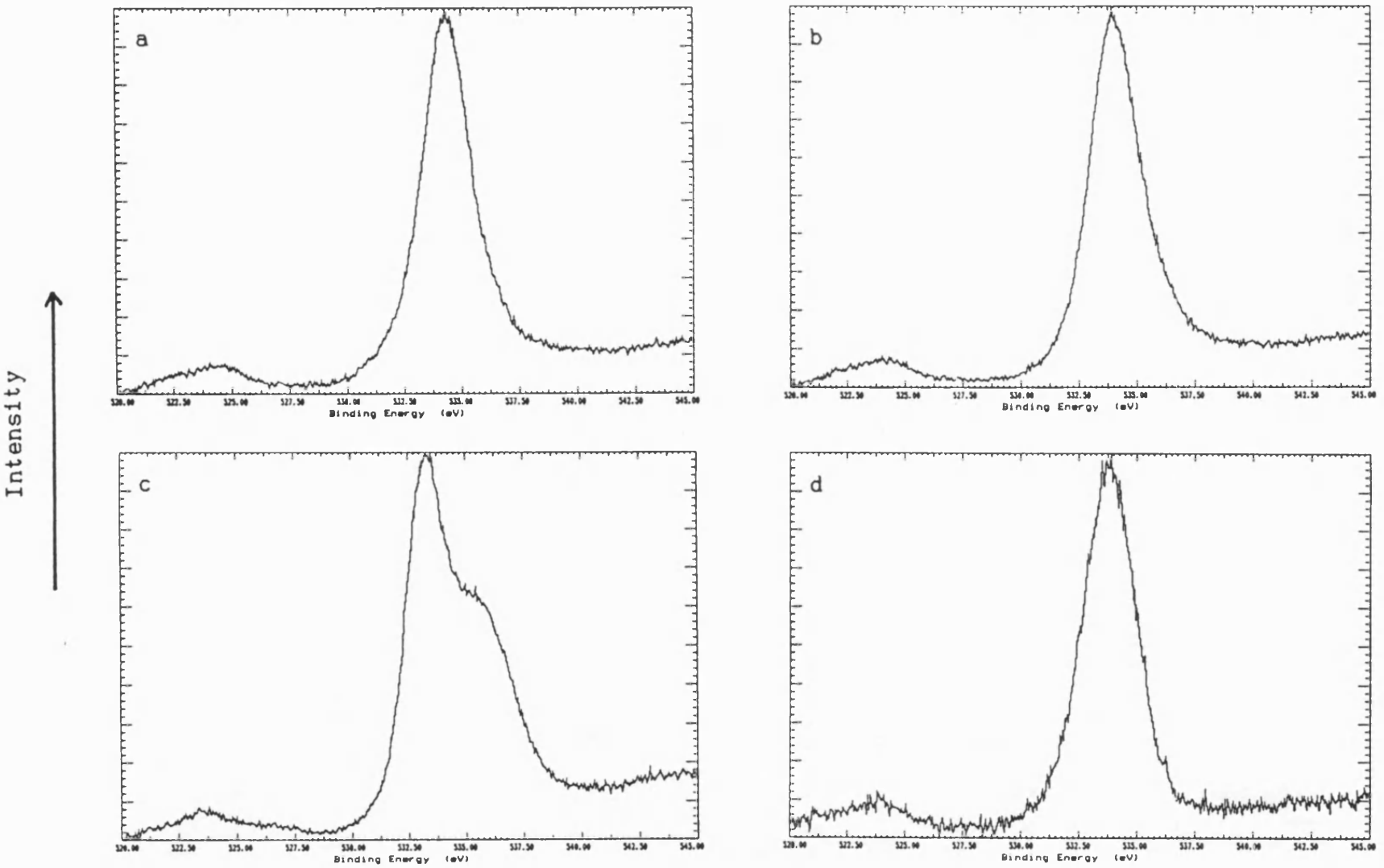

Figure 6.8 X-ray photoelectron spectra of the O 1s region. *a* Mn_3O_4, *b* Mn_2O_3, *c* MnO_2, *d* manganese loaded ferritin. Step size 0.05 eV, 5 scans of 30 secs per scan.

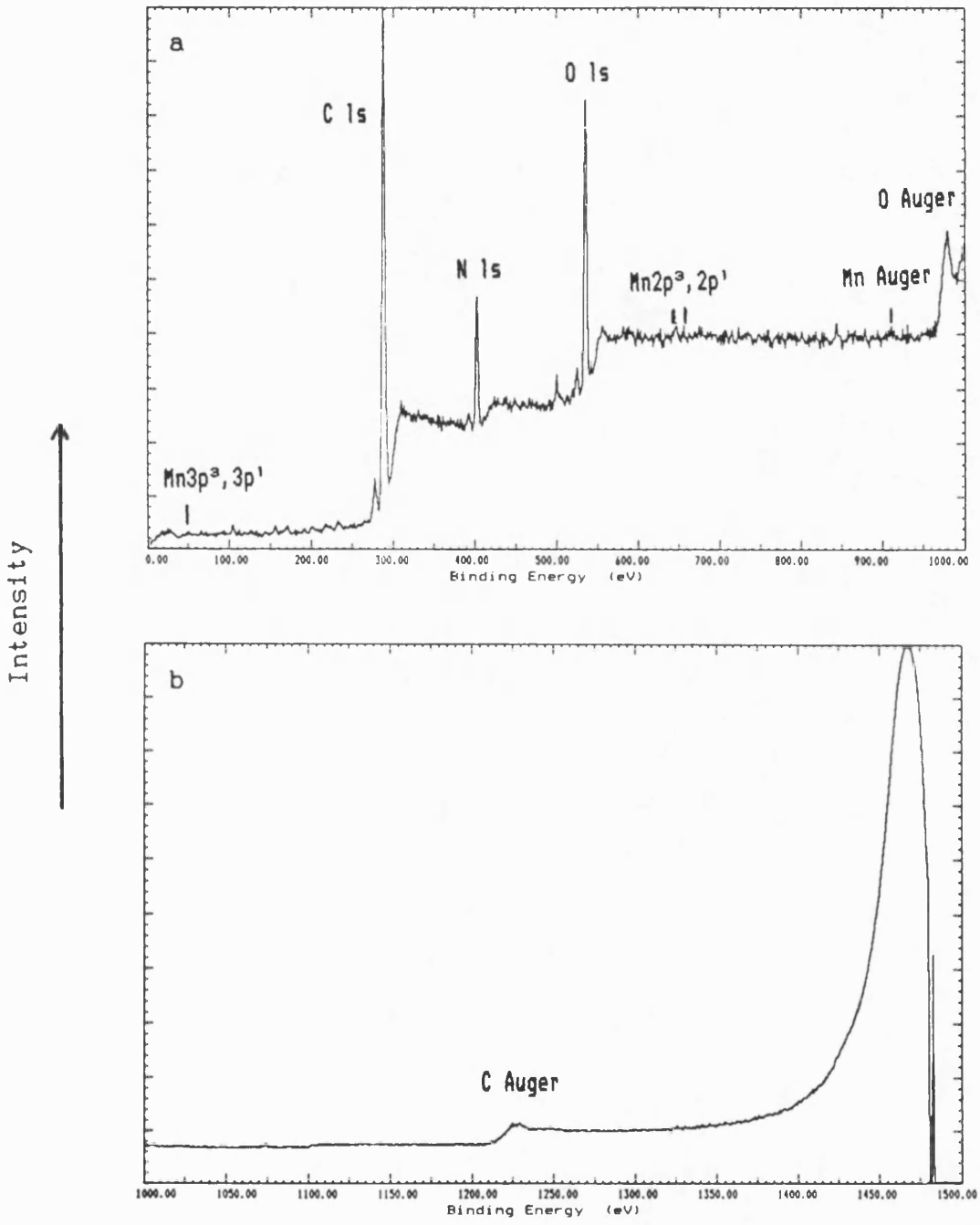

Figure 6.9 X-ray photoelectron spectrum, wide scan of the manganese loaded ferritin. Step size 0.25 eV, *a* 5 scans of 40 secs per scan, *b* 5 scans of 20 secs per scan.

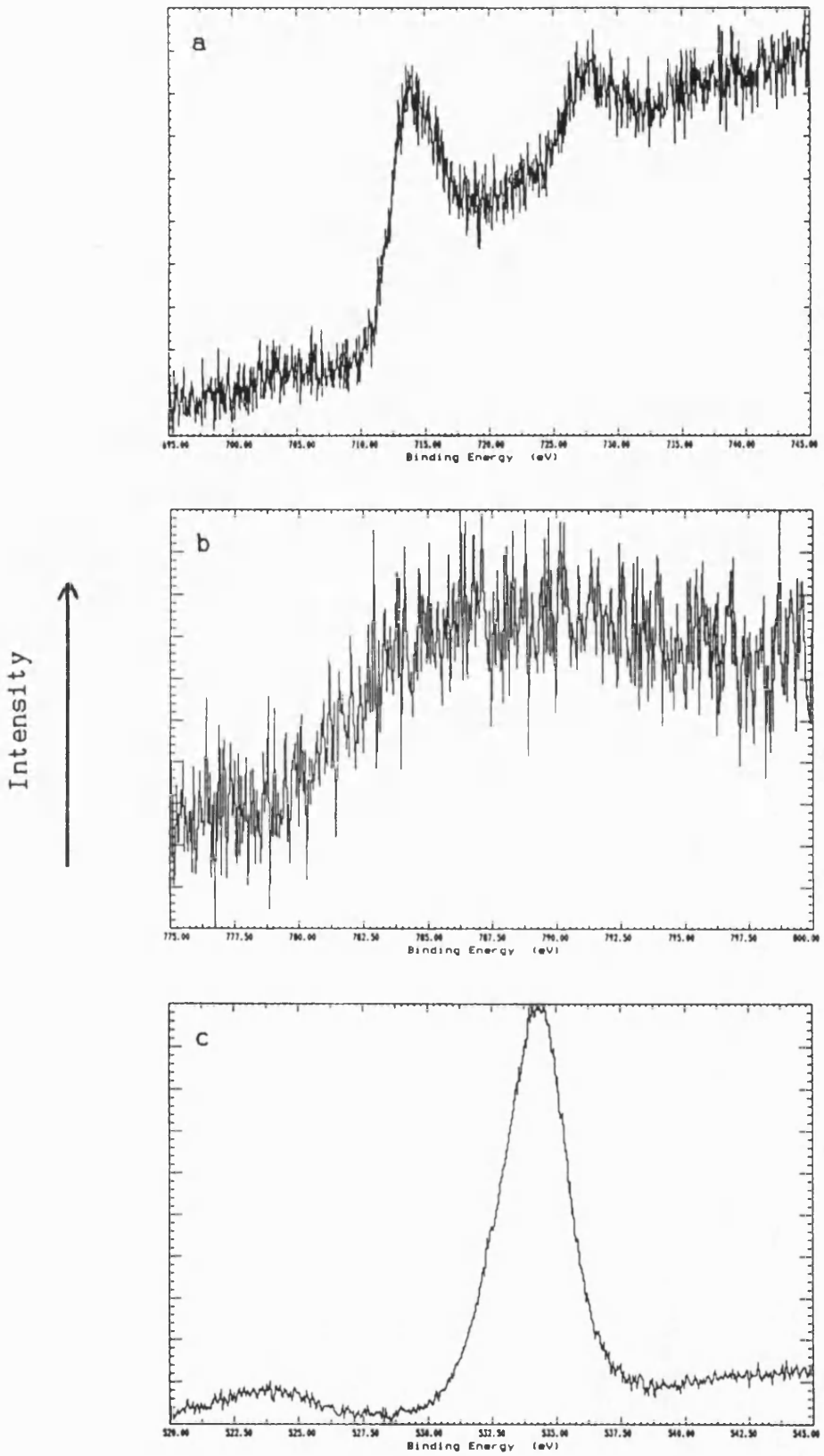

Figure 6.10 X-ray photoelectron spectra of native ferritin.
a the Fe 2p region, *b* the Fe Auger region, *c* the O 1s region.
Step size 0.05 eV, *a* 5 scans of 60 secs per scan, *b* & *c* 5 scans of 30 secs per scan.

(II,III) oxide standard. It was very similar in shape to that of the manganese protein sample. The wide scan (figure 6.11 a & b) again revealed the presence of elements in the protein, dialysate and sticky tape.

Table 6.11. Photoelectron and Auger lines (eV) of the elements observed by XPS, (theoretical values).
The * denotes the strongest line.

S	3s	17	O	1s	* 531
Cl	3s	17	Na	Auger	536
O	2s	23	Na	Auger	565
Na	$2p^1$	31	Mn	$2p^3$	* 641
Mn	$3p^3$	48	Mn	$2p^1$	652
Mn	$3p^1$	49	Fe	$2p^3$	* 710
Fe	$3p^3$	55	Fe	$2p^1$	723
Fe	$3p^1$	56	Mn	2s	770
Na	2s	64	Fe	Auger	* 786
Mn	3s	83	Fe	Auger	841
Fe	3s	93	Fe	2s	847
Si	$2p^3$	* 102	Mn	Auger	853
Si	$2p^1$	103	Fe	Auger	892
Si	2s	153	Mn	Auger	* 903
S	$2p^3$	* 165	Mn	Auger	948
S	$2p^1$	166	O	Auger	* 976
Cl	$2p^3$	* 199	O	Auger	997
Cl	$2p^1$	201	O	Auger	1012
S	2s	229	Na	1s	* 1072
Cl	2s	270	N	Auger	* 1108
C	1s	* 287	C	Auger	* 1226
N	1s	* 402	Cl	Auger	* 1304
Na	Auger	* 497	S	Auger	* 1336

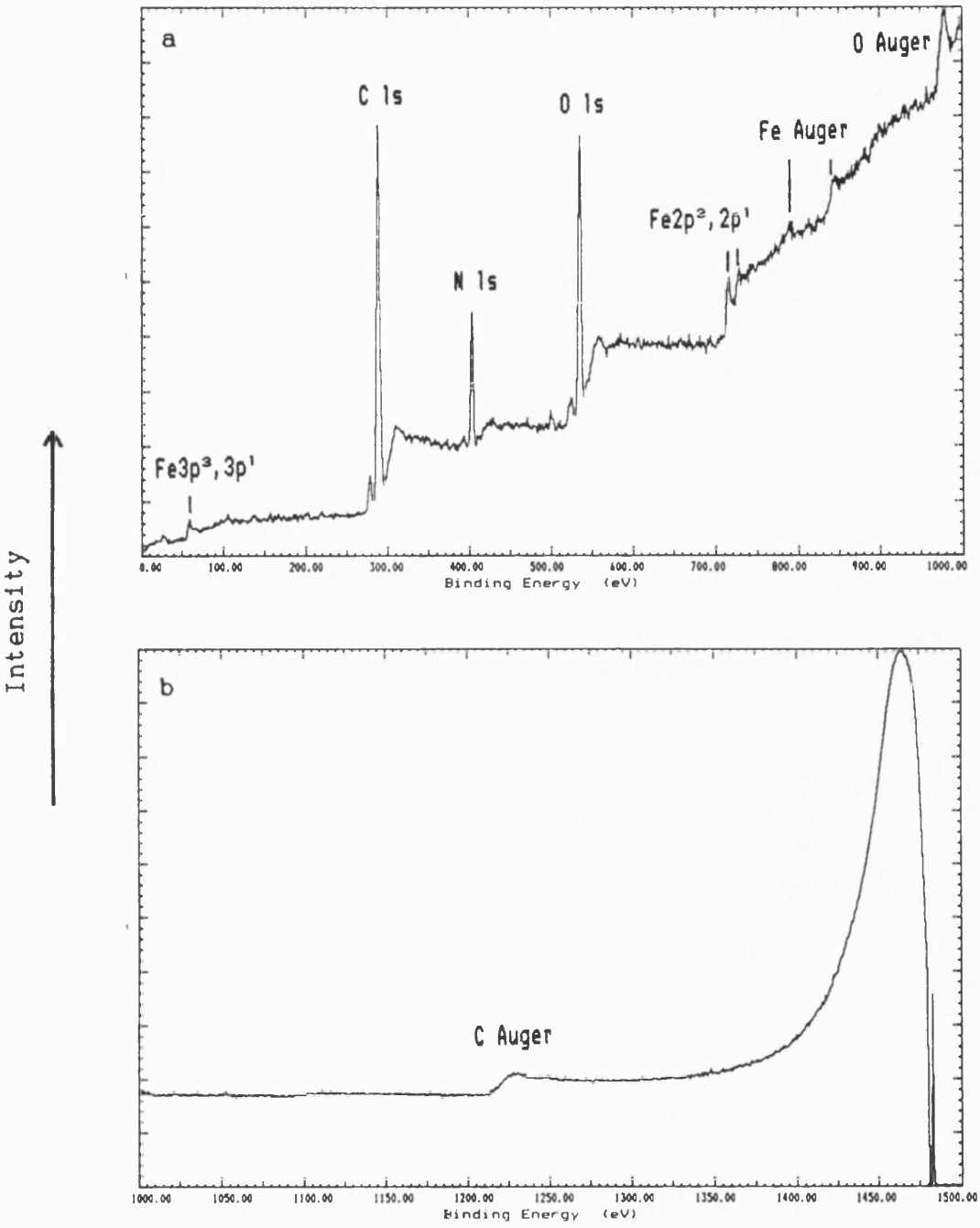

Figure 6.11 X-ray photoelectron spectrum, wide scan of native ferritin. Step size 0.25 eV, *a* 5 scans of 40 secs per scan, *b* 5 scans of 20 secs per scan.

6.3 DISCUSSION

The work presented in this chapter has illustrated that apoferritin is not just specific for iron with regard to the metal ions that can be assimilated into its internal cavity and precipitated in a "solid" form. Manganese oxide cores can also be formed, when Mn^{2+} is supplied in mM quantities, in the presence of oxygen at pH values between pH 7.5 and pH 9.2. Also, apoferritin is capable of catalysing the oxidation of Mn^{2+} and favouring the development of the hydrated kinetic product in a seemingly similar way to that for iron assimilation.

6.3.1. Manganese uptake by apoferritin

Core formation, morphology and structure

Some general observations of the manganese cores formed in apoferritin in the experiments described were i) that the cores were of very regular shapes, ii) the cores were present at a lower density than that routinely observed in iron reconstitutions at similar protein concentrations, iii) the reaction of apoferritin with manganese may not have been so specific as that with iron.

Taking first the morphology of the cores; most were of very regular shapes, being rounded or square with rounded corners. Also, many of the cores appeared to be of a size that would fill the protein cavity, (however, measurements of cores could only be made in two dimensions). This regularity of cores shape may have been a result of slow loading, mediated by the slow kinetics of manganese oxidation, and the influence of the cavity shape on the large cores. The large size of the cores may also be explained by the slow kinetics of the reaction, since the continued growth of cores which nucleate early in the course of the reaction is favoured over the

formation of more nuclei. Consequently, the cores which nucleate early grow large. This reaction may be similar, with regard to kinetics (nucleation driven) and resultant core morphology, to the reconstitution of recombinant human L-subunit ferritin with Fe(II) (chapter 4).

It was established in chapter 4 that apoferritin provides a nucleation site (or sites) which is operative during reconstitution with iron. The formation of manganese oxide cores suggests that the protein does have a nucleation activity with Mn^{2+} ions. If the protein's "nucleation efficiency" was diminished, (compared to that with iron,) this would also lead to the formation of large, regular shaped cores. This follows the same argument as above; that cores that nucleate early grow, at the expense of others, to fill the cavity.

Such arguments imply that some, if not many, ferritin molecules remain essentially as apoferritin. This may explain the second general observation, that the cores were present in a lower density than observed for iron reconstituted ferritin, at similar protein concentrations.

It was difficult to judge if the reaction of apoferritin with manganese was less specific than that with iron, since the conditions employed were different, (higher pH, higher loading, longer time scale). However, non-specific oxidation products were seen in many of the preparations, so it may be presumed that once the known binding sites for manganese (see introduction 6.0.3) are saturated, some manganese goes into the protein cavity and some remains in bulk solution. It has been shown that insoluble oxides were produced external to the protein but the nature of the product inside the cavity remains unclear. Is it a true solid, or more like a large

cluster or polymer of manganese ions, oxygen, hydroxide and water which is trapped in the cavity? The lack of evidence for any crystallinity in the cores, by electron diffraction and high resolution TEM, does not favour or rule out either possibility. XPS provided evidence for the presence of Mn(III) which implies that oxidation had taken place. The similarity between the chemistry of iron and manganese would suggest the formation of a "solid" product, produced by the kinetics of the system and stabilised by the protein cavity. A similarity to the polymerised uranyl oxyhydroxide product formed from apoferritin and UO_2^{2+} in Meldrum *et al.* (1991), seems less likely.

Wardeska *et al.* (1986) have proposed that iron and manganese bind at the same sites in the 3-fold channel of apoferritin. They suggest that with iron, these sites may be involved in the initiation of core formation, since upon oxidation of Fe(II) to Fe(III), at pH 7.0, there is regeneration of Mn(II) binding sites, which implies translocation of the iron. It is possible, therefore, that a similar route is followed during reconstitution with manganese, as the Mn(II) is oxidised to Mn(III).

The successful reconstitution of apoferritin with manganese has demonstrated that the protein cage of ferritin may be useful as a reaction volume for the formation of particles of other inorganic materials, with nanometre dimensions. (See also Meldrum *et al.*, 1991.)

Kinetics

Apoferritin has been shown to catalyse the oxidation of Mn^{2+} at pH 8.0, an effect similar to that seen with Fe^{2+} at pH values of around 6.5. However, the reaction of manganese with apoferritin was not as rapid and may not have been so specific as that with iron. The reconstitution with manganese required days, whereas that with iron requires only minutes or hours. Some non-specific oxidation product appeared in the manganese experiments on a similar time scale to the observation of cores, when, on the faster time scale of iron reconstitution, the observation of oxide exterior to the protein would be uncommon. Also, the flocculation of the manganese loaded sample after two weeks may have indicated the formation of an increasing amount of non-specific oxidation product, or this may have been due to damage to the protein shells caused by the relatively high pH, (although the latter was not indicated by the TEMs taken of the sample after two weeks). Furthermore, binding of manganese to the outside of the protein over this long period may have caused aggregation.

Whether the mechanism by which the ferritin influences the oxidation of Mn^{2+} is the same as that which operates for the oxidation and uptake of iron is a matter for speculation. It is probable that they would be the same, given the similarities between the two metals. If the manganese is oxidised at the "ferroxidase" sites, (Glu 62, His 65, present on the H-subunits, see chapter 4) this implies some flexibility in the sites as to the size of ion that can be coordinated there, since the ionic radii of the ions under consideration are: Fe^{2+} 75 pm, Fe^{3+} 61 pm, Mn^{2+} 80 pm, Mn^{3+} 66 pm. This also implies that there is not "recognition" at the atomic level. If the manganese is handled by the ferroxidase site less

efficiently than iron would be, on the grounds of ionic radius and the higher redox potential of Mn^{2+}, this may explain the slight reduction in specificity of the reaction.

6.3.2 The non-specific manganese oxide products

The products formed in the protein-free control experiments are summarised in table 6.12. The initial products observed at all three pH values appeared to be hausmannite of varying morphology and degree of crystallinity. This was also the only form of non-specific oxide observed in the presence of apoferritin. The hausmannite in the protein-free controls then tended to transform into groutite and feitknechtite. It could be proposed that groutite is formed more readily from hausmannite than feitknechtite, since groutite but not feitknechtite was formed by day 7 at pH 7.5 and groutite had formed by day 4 at pH 8.0, but feitknechtite was not observed until day 7. At pH 9.2 some feitknechtite had formed by day 3 and groutite was not observed at all. It is possible that the higher pH caused either the groutite "intermediate" to be bypassed, or that it formed and was transformed during the time between the observations made at 3 hours and 3 days. In all cases the transformation of hausmannite to either groutite or feitknechtite must involve a dissolution and reprecipitation process since hausmannite has a tetragonal structure, whereas groutite has an orthorhombic structure and feitknechtite has an hexagonal structure.

The oxides observed were those predicted, in the literature, to form from the oxidation of aqueous Mn^{2+}. That hausmannite was the initial product in all the experiments is in agreement with the findings of Stumm and Giovanoli (1976) and Murray, *et al.* (1985).

Table 6.12 Summary of the oxides formed in the protein-free control experiments.

pH	time	morphology	assigned material
9.2	3 hours	granular aggregates	H
	3 days	plates, granular	F, H
8.0	2 days	granular, cuboid	H
		(small needles)	(G)
	4 days	rods, (granular)	G, (H)
	7 days	plates	F, F/H
7.5	2 days	granular	H?
	7 days	irregular rods	G/H(M)

In both studies, carried out at pH values between 7 and 9, feitknechtite was also formed, although over a period of months both the hausmannite and feitknechtite were transformed to manganite.

The formation of hausmannite as the initial oxidation product, under all the conditions used, is in agreement with the thermodynamic model illustrated in figure 6.1. The conditions of Mn^{2+} concentration and pH all lie to the right of line 3, where hausmannite is predicted to form and be stable with respect to both manganite and MnO_2, ($\log[Mn^{2+}]$ -2.5 and -2.0, pH 9.2, 8.0 and 7.5). With the formation of hausmannite and continuing oxidation, the levels of Mn^{2+} in solution would decrease and so any prediction of the course of the reaction from this stage is difficult. Transformation to manganite or MnO_2 may

be possible, even probable, given sufficient time, and may involve groutite and/or feitknechtite as intermediates.

6.3.3 X-ray Photoelectron Spectroscopy

Since no difference was observed in the binding energies of the Mn 2p and Mn Auger electrons in the three manganese oxide standards, the spectra of these binding energy regions from the manganese ferritin sample cannot indicate the oxidation state of the manganese in the protein cavity. The spectra from the O 1s regions did show slight differences though and the peak of binding energy from the manganese ferritin suggested that it was very close to that of the Mn(III) oxide, the peak shape was similar to that of the Mn(II,III) and Mn(III) oxides and unlike the Mn(IV) oxide. This evidence, together with the consideration that the oxidation of Mn^{2+} to Mn^{4+} is unlikely, kinetically, under the conditions used, most probably rule out the presence of Mn(IV) in the protein. The oxidation state of the manganese was therefore, probably 3+, although a mixture of 2+ and 3+ cannot be ruled out.

Murray *et al.* (1985) found that Mn(II) could be distinguished from Mn(III) and Mn(IV) by observing the $2p_{3/2}$ binding energies of MnO, γ-MnOOH and βMnO_2. However, Mn(III) could not be distinguished from Mn(IV) using 2p binding energies.

Oxygen atoms in the protein as well as the manganese oxide cores may have contributed to the O 1s energy spectrum from the manganese ferritin. However, it would seem that this contribution was insignificant since the spectrum from the protein sample was so

similar to those from the Mn(II,III) and Mn(III) oxides and the step size, scan speed and number of scans was the same in each case.

For the native ferritin sample, the peak of binding energy in the O 1s region was closest in energy to the Mn(II,III) oxide standard and it was very similar in shape to the that of the manganese ferritin sample. These observations may provide indirect evidence that the oxidation state of the manganese in the manganese ferritin was no higher than 3+. Since, in native ferritin the iron is all Fe^{3+} and the peak of binding energy of the O 1s electrons was the same as that of the Mn(II,III) oxide and the peak shape was similar to those of the Mn(II,III) and Mn(III) oxides and not the Mn(IV) oxide.

Chapter 7

TRANSMISSION ELECTRON MICROSCOPY OF SOME RECENTLY ISOLATED FERRITINS

7.0 INTRODUCTION

All the samples which are described in this chapter were supplied by Prof. P.M. Harrison, University of Sheffield. They include a native human brain ferritin, a plant ferritin isolated from garden pea seeds, in its native and a reconstituted form, and a reconstituted *E. coli* bacterioferritin. These ferritins, from diverse sources, have not been widely studied and have not previously been characterised by TEM and electron diffraction. The aim of the study, therefore, was to survey the general appearance, morphology, size and structure of the iron cores of each of the samples. Such work will increase our knowledge, and hopefully therefore, our understanding, of this almost ubiquitous protein.

7.1 EXPERIMENTAL

Sample preparation, transmission electron microscopy, electron diffraction and data analysis were all performed as described in chapter 2.

7.2 RESULTS

7.2.1 Native human brain ferritin

This ferritin sample was isolated from the brain tissue of an Alzheimers patient taken at post-mortem. It contained 1507 ± 226 iron atoms per molecule and had a iron to phosphate ratio of 11.1 ± 3.7. It is interesting to note that no significant differences have been found in iron and phosphate content between ferritins isolated from the brain tissue of Alzheimers and non-Alzheimers patients (Dr. A. Treffry, pers. comm.).

The cores in this sample were generally of fairly regular shapes, several were approximately rectangular and others were rounded or square-shaped, see plate 7.1a. The mean core diameter was 5.60 nm, with a standard deviation of 0.93 nm. The range of diameters measured was 2.94 - 7.01 nm and the particle size distribution is shown in figure 7.1a. Compared with other native samples studied during the course of my research the iron cores of this sample were not very discrete or well-defined, they were relatively small and they were slightly aggregated. Also, the core size distribution was somewhat broader than would normally be expected for a native sample. These differences in the appearance of the sample on the electron microscopy grid are probably due to the higher proportion of H-subunit in this native sample (60% H-subunit, 40% L-subunit) compared to any other native proteins studied (mostly liver and spleen which have a high proportion of L-subunit, ~90%). The more rapid iron uptake kinetics exhibited by H-subunit rich ferritins would be expected to result in smaller, more irregular and less well-defined cores, with a greater variation in size. (See chapter 4.)

The electron diffraction patterns from this sample were characteristic of well-ordered ferrihydrite, see table 7.1.

When this native sample was compared with the human brain ferritin reconstituted to 2000 iron atoms/molecule, described in chapter 4, the particle size distributions (figures 7.1 & 4.5, respectively) and the mean core diameters (5.60 & 4.84 nm, respectively) indicated that the majority of the cores in the native sample were larger in size than those of the reconstituted sample. The iron cores of both samples had a well-ordered ferrihydrite structure: both had characteristic six-line patterns.

7.2.2 Reconstituted *E. coli* bacterioferritin

The *E. coli* bacterioferritin (BFR) protein was isolated from an over-expressing strain grown in a rich broth (L-broth), without added iron. Purified BFR (0.2 mg/ml) containing approximately 60 iron atoms per molecule, was further iron loaded in 20 mM HEPES buffer pH 7.0 with four aliquots of 0.1 M ferrous ammonium sulphate over 1¼ hours, with constant stirring. The sample was then precipitated with 45% $(NH_4)_2SO_4$, spun down, redissolved and dialysed against 10 mM Tris-HCl (pH 7). The reconstituted BFR was then, twice, sedimented by high speed centrifugation and redissolved in 10 mM Tris-HCl (pH 7). The calculated iron loading was 1820 iron atoms/molecule, but the final Fe:protein ratio was not determined.

The iron cores in this sample were very discrete and aggregation was very limited, (plate 7.1b). Many of the cores had regular rounded shapes, some were four- or five-sided and a few had less regular shapes. A particle size distribution is shown in figure 7.1c, this was fairly narrow with most of the core diameters lying between 5 and 7 nm. The mean core diameter was 5.83 nm, with a standard deviation of 0.96 nm. The range of core diameters measured was 2.89 - 7.44 nm.

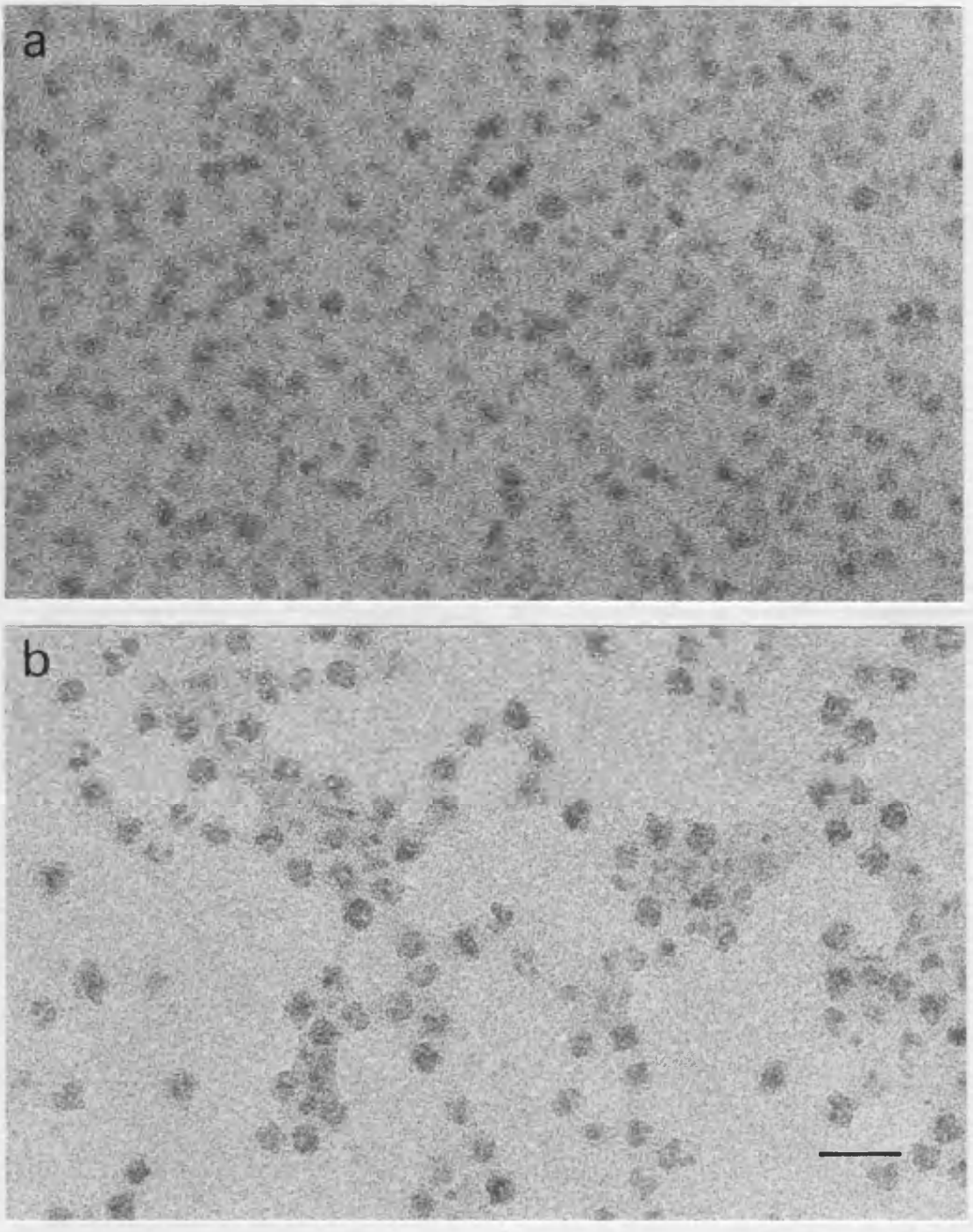

Plate 7.1 Electron micrographs of unstained ferritins. *a* native human brain ferritin. *b* reconstituted *E. coli* ferritin. Bar marker 20nm for both micrographs.

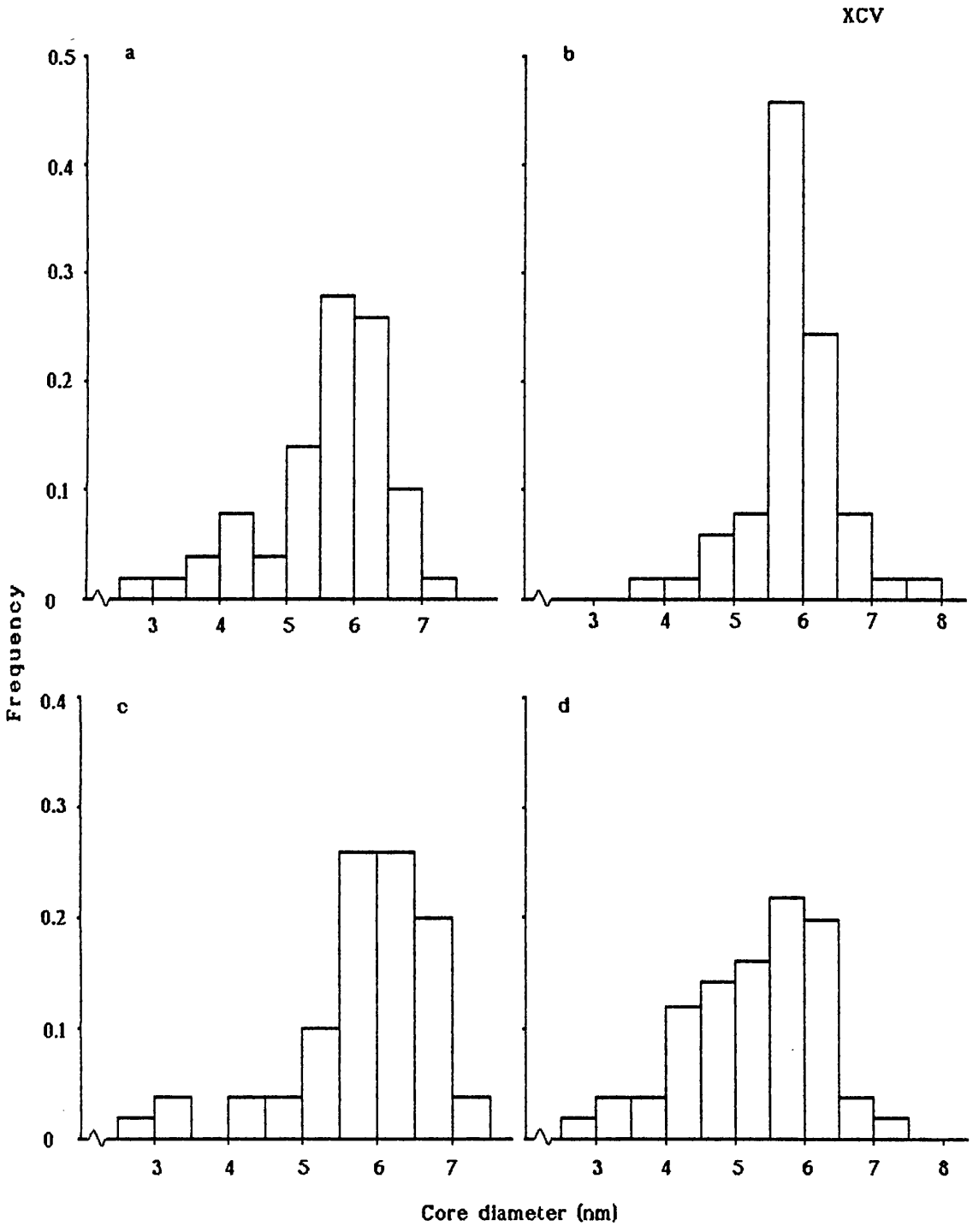

Figure 7.1 Particle size distributions for samples: *a* native human brain ferritin, *b* native pea seed ferritin, *c* *E. coli* BFR, *d* reconstituted pea seed ferritin.

Again, many of the cores were quite large. Is this a reflection of the bacterial protein (other bacterioferritins have large cores despite a low iron loading, Mann *et al.*, 1987b and see below) or a consequence of loading a protein that has not been subjected to the rigours of reduction to remove its iron core? The sample's appearance on the electron microscopy grid reminds one of a native sample.

Electron diffraction analysis revealed that this sample was well crystalline ferrihydrite, see table 7.1.

7.2.3 Plant ferritin

a) Native This plant ferritin sample isolated from seeds of the garden pea contained an average of approximately 1860 iron atoms per molecule, unfortunately its phosphate content was not known. The iron cores in this sample were discrete but not well-defined in the electron micrographs due to their lack of crystallinity; the cores were amorphous by electron diffraction (see plate 7.2). They were not aggregated. The lack of definition of the cores on the micrographs made the measurement of the core diameters even more inaccurate than with other samples and also precluded any real assessment of cores shapes, although the impression was that they were of generally regular shapes. From the measurements taken a mean core diameter of 5.87 nm, with a standard deviation of 0.66 nm, was calculated. The cores sizes measured ranged from 3.94 - 7.60 nm. The particle size distribution was quite narrow, (see figure 7.1b).

b) Reconstituted The plant apoferritin was reconstituted in 0.1 M MOPS pH 7.0 with 2000 iron atoms/molecule (no phosphate) in two increments at a 45 minute interval, at room temperature and then kept

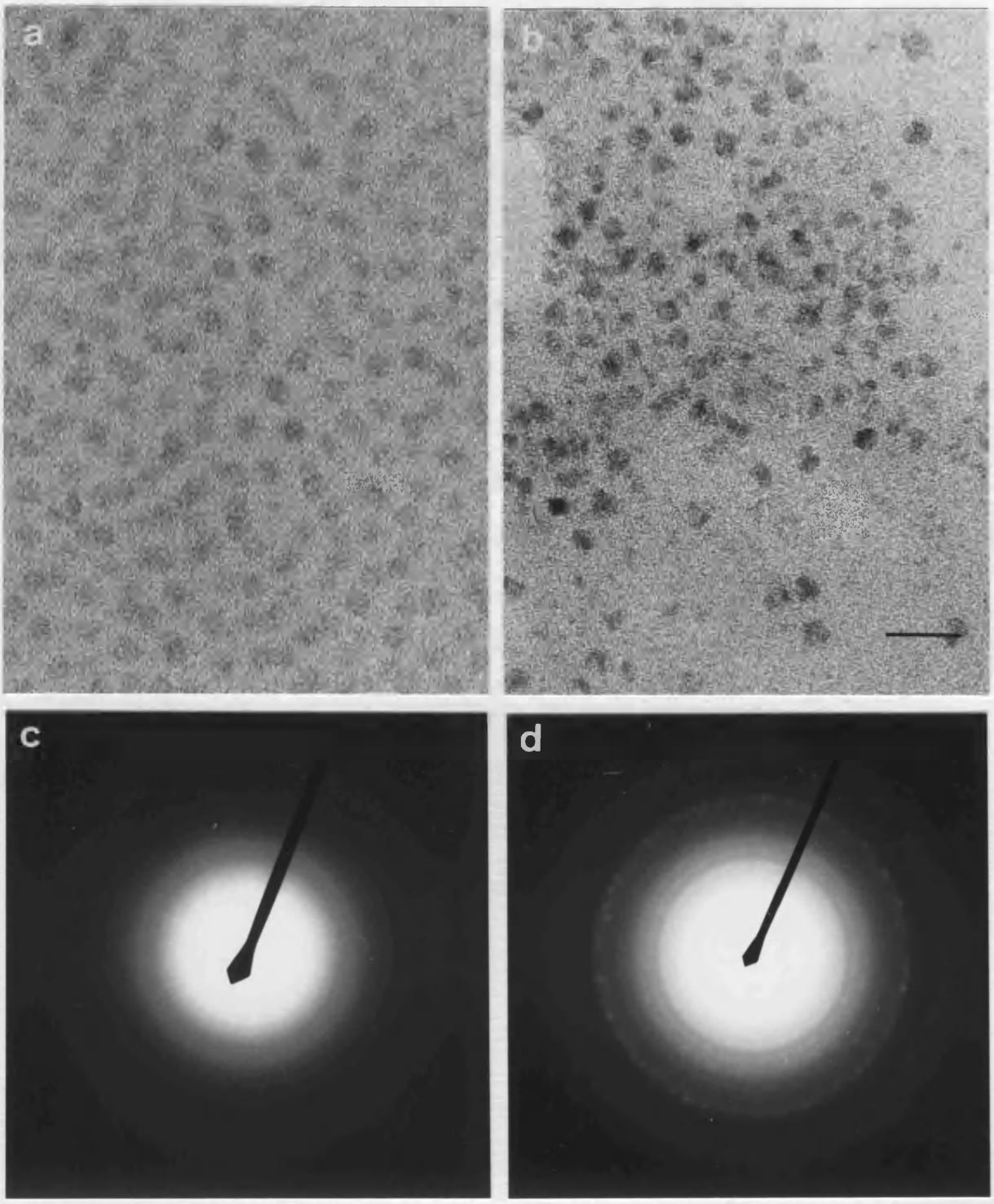

Plate 7.2 Electron micrographs and diffraction patterns of the native and reconstituted pea seed ferritins. *a & c* native ferritin, *b & d* reconstituted ferritin. Bar marker 20nm for both images, camera length 90cm for both diffraction patterns.

at 4°C. The cores in this sample were very different in appearance on the electron micrographs to those of the native sample, (plate 7.2b). They were much more well-defined with a range of regular and irregular shapes visible. Electron diffraction analysis revealed that, in contrast to the native sample, the iron cores were well crystalline ferrihydrite (see table 7.1 and plate 7.2d). The extent of aggregation varied across the electron microscopy grid, but these cores were more aggregated than those of the native sample. The mean core diameter was 5.24 nm, with a standard deviation of 0.99 nm. The particle size distribution, shown in figure 7.1d, was much broader than that of the native sample. The range of core sizes measured was 2.92 to 7.15 nm. The size distribution showed that a large number of cores had diameters above 5.5 nm which, in my experience of mammalian ferritins, is unusual for a reconstituted sample. Can this be attributed to the "different" plant protein? The plant ferritin sequence shows some similarity to the animal ferritin sequences, but no significant similarity to the bacterioferritin sequences (Dr. S. Andrews, pers. comm.).

Table 7.1. Electron diffraction data for the native human brain and reconstituted bacterial and plant ferritins.

I = intensity of line judged by eye:- S = strong, M = medium, W = weak.

Native human brain ferritin		Reconst. *E. coli* BFR		Reconst. plant ferritin	
d(Å)	I	d(Å)	I	d(Å)	I
2.49	S	2.50	S	2.50	S
2.25	S	2.27	M/S	2.31	M
1.97	M	2.00	M	1.96	M
1.72	W	1.74	W	1.72	VW
1.51	W	1.53	W	1.53	W
1.47	S	1.46	S	1.48	S

7.3 DISCUSSION

These electron microscopy studies again demonstrate the broadly similar appearance of ferritin samples isolated from diverse sources. The samples studied all exhibited discrete iron cores with mean diameters ranging between 5.24 and 5.87 nm. However, as has been shown before, the structure of the cores varies depending on the source of the ferritin (eg. Mann *et al.*, 1986 & 1987a, Treffry *et al.*, 1987 and St. Pierre *et al.*, 1989) and reconstitution of an apoferritin sample can result in the formation of more crystalline cores, than are found in the native sample, (Mann *et al.*, 1987a).

The appearance of the native human brain ferritin in the TEM fitted well into the pattern of characteristics due to a high proportion of H-subunit in the heteropolymer, which was established in chapter 4. These include a relatively small core size, rather poorly defined and irregular shaped cores and some aggregation of cores on the electron microscopy grid.

The studies of the plant ferritin were particularly interesting since the isolation of phytoferritins in quantity has proven difficult. The cores of this ferritin were amorphous in their native state; the only other reported ferritins with amorphous cores are the native forms of the bacterioferritins of *Azotobacter vinelandii* and *Pseudomonas aeruginosa* (Mann *et al.*, 1986a & 1987b). The very marked increase in the crystallinity of the cores following reconstitution of the plant ferritin was similar to the result obtained by Mann *et al.* (1987b) with the *A. vinelandii* and *P. aeruginosa* bacterioferritins. It should be noted that in both the present work and Mann *et al.* (1987b) the reconstitutions were performed in the absence of phosphate and a high phosphate to iron ratio is often associated with amorphous iron biominerals (St. Pierre *et al.*, 1989). The P:Fe ratios present in the native bacterioferritins of *A. vinelandii* and *P. aeruginosa* are between 1:1 and 1:2 (Mann *et al.*, 1987b). The lack of crystallinity in the native plant ferritin and the increase in crystallinity on reconstitution without phosphate, may have been indicative of a high phosphate content in the native sample.

It has been reported (Prof. P.M. Harrison, pers. comm.) that the native plant ferritin sample studied here had a low blocking temperature by Mössbauer spectroscopy. This could be explained by the lack of crystallinity in the iron cores, since in poorly ordered

material the energy difference between easy and hard axis magnetisations is small giving a low blocking temperature, (see appendix II and St. Pierre *et al.*, 1989). Low blocking temperatures have been found for the *P. aeruginosa* BFR (St. Pierre *et al.*, 1986a) and the haemosiderin isolated from patients with idiopathic haemochromatosis who had undergone venesection treatment (chapter 5). This observation of a low blocking temperature for pea seed ferritin is in line with the Mössbauer spectra from ^{57}Fe enriched duckweed (*Lemna gibba*) which suggested a very low mean blocking temperature for the iron complexes contained therein (believed to be >85% ferritin, Goodman & DeKock, 1982, St. Pierre *et al.*, 1989).

The transmission electron microscopy of the *E. coli* bacterioferritin was also of great interest since such studies of the purified protein have been very limited. *E. coli* BFR has a quaternary structure resembling that of horse spleen ferritin (Andrews *et al.* 1989b) and its secondary and tertiary structures are predicted to be similar also: a bundle of four antiparallel α-helices. However, it has no significant sequence homology with the mammalian ferritins (Andrews *et al.* 1989a). It has been proposed (Prof. P.M. Harrison, pers. comm.) that the *E. coli* BFR may lack the "ferroxidase" site which has been located on the H-subunit of human ferritin and thus would take up iron only relatively slowly. Should this be the case, then this bacterioferritin would be akin to human L-subunit ferritin in functional properties, though not in sequence, and the formation, upon reconstitution, of large, regular shaped cores would be expected and has been demonstrated above. It is interesting to note here, that the molecular volume of *E. coli* BFR has been estimated to be about the same as that of horse spleen apoferritin (Harrison *et al.*, 1989),

so presumably the diameter of the internal cavity would be very similar also.

In the light of electron diffraction studies of the bacterioferritins from *A. vinelandii* and *P. aeruginosa* (Mann *et al.*, 1986a & 1987) the native iron cores of *E. coli* BFR would be expected to be amorphous. Such a view is supported by Mössbauer spectroscopy studies of whole frozen *E. coli* cells and the iron storage protein isolated from iron-rich cells of *E. coli* (Bauminger *et al.*, 1980). The temperature dependent spectra obtained were very similar to those of *P. aeruginosa* and characteristic of a solid material passing from a magnetically ordered to a paramagnetic phase. A lack of crystallinity in native iron cores of *E. coli* BFR might suggest that this protein would fit into the pattern of correlation between core structure and Mössbauer spectral data proposed by St. Pierre *et al.* (1989), in that a very low magnetic ordering temperature is correlated with amorphous iron cores. It would seem likely therefore, that the crystallinity of the iron cores of the *E. coli* BFR sample described in this chapter, has been introduced by the process of reconstitution. Possibly, as with the pea seed ferritin, the absence of phosphate during reconstitution, may account for this difference.

The ferrihydrite structure of the cores in the reconstituted BFR described here has been confirmed by Mössbauer spectroscopy (Dr. J.M. Williams, pers. comm.).

Chapter 8

SUMMARY

The work presented in this thesis has been primarily concerned with the structure and properties of native and reconstituted ferritin iron cores formed under a variety of conditions. The sources of the ferritins studied have been diverse, including those isolated from organisms and tissues in their native form and ones generated by recombinant DNA techniques and site-directed mutagenesis. A further theme of the work undertaken was the study of the kinetics of *in vitro* reconstitution of horse spleen apoferritin with iron. These studies were extended to the reconstitution of this protein with manganese, instead of iron.

A summary of the principal results of the work are presented in table 8.1, along with the chapter and section where they may be found.

One of the recurring themes to emerge from these studies has been that in all except one of the ferritins studied the iron cores have been ferrihydrite. The one exception was the native pea seed ferritin in which the cores were amorphous. These results are in line with those of previously characterised ferritins (eg. Ford *et al.*, 1984, Mann *et al.*, 1986a & 1987, Treffry *et al.*, 1987 and the review by St. Pierre *et al.*, 1989). Together with the finding that the

Table 8.1 Summary of principal results

Chapter 3	
3.2.1	apoferritin catalyses iron oxidation
3.2.2	ferrihydrite structure of core established by 200 Fe atoms/molecule
3.3.1&2	Zn^{2+} inhibits iron uptake by apoferritin, main action being the inhibition of nucleation of the oxidation product, as demonstrated in the presence and absence of the protein
3.4.3b	proposed size of nucleation cluster in ferritin between 170 and 260 Fe atoms/molecule.
Chapter 4	
4.2.4& 4.3.3b	identification of residues involved in core nucleation
4.2.5& 4.3.3c	further confirmation of the identities of the residues involved at the ferroxidase centre of H-subunit
4.3.1&2	iron uptake by H-subunit homopolymers is a catalytically driven process, leading to small, irregular shaped cores, whereas that by L-subunit homopolymers is nucleation driven, resulting in larger, well formed cores
4.3.5	conclusion that primary structure of ferritin not as important as quaternary structure for fulfilling its function
Chapter 5	
5.2.	ferritin cores all have ferrihydrite structure
5.2.1&4	normal human and animal haemosiderin cores also have ferrihydrite structure
5.2.2&3	there are disease specific structures for the haemosiderin cores formed in primary and secondary iron overload

Table 8.1 continued

Chapter 6	
6.2.1	manganese can be assimilated by apoferritin in a similar way to iron, therefore ferritin not specific for iron in this respect
6.2.1	the manganese oxide cores formed were amorphous
6.2.2	apoferritin catalyses the oxidation of Mn^{2+}
Chapter 7	
7.2	similarity in appearance under the TEM of ferritins from diverse sources, ferrihydrite structure of all cores except native pea seed
7.2.2	native pea seed ferritin had amorphous iron cores

manganese oxide cores, which could be formed in horse spleen apoferritin, were amorphous, these results suggest that the ferritin protein shell may impose a constraint on the degree of crystallinity or thermodynamic stability of the product which can form inside it. How such a constraint could be achieved is not clear, but some possibilities include:

i) the limiting size of the cavity; the hexagonal unit cell of ferrihydrite is readily stabilised and ferrihydrite's normal granular morphology accommodated. Phase transformation to, for example goethite or lepidocrocite, which would require dissolution and reprecipitation, would be inhibited by the spatial restriction of the reaction volume. The ferrihydrite core would occupy most of the space in the cavity and the surface area of the core available for dissolution would be low, due to contact between the core and the protein.

ii) the kinetics of the uptake/deposition reaction; these may be too fast for the formation of lepidocrocite or goethite, due to the enhancing effects of the ferroxidase and nucleation sites.

One point that has become clear is that the protein does not provide a site which promotes the nucleation of ferrihydrite, rather than any other iron oxide, via a mechanism involving structural correspondence at the core-protein interface.

In chapters 3 and 4 several different methods of reconstitution were employed using a number of different homo- and heteropolymers. Under the various conditions, where the rate of reaction was altered by concentration, pH, addition of Zn^{2+} or the degree of catalytic activity of the protein, ferrihydrite was always formed in the ferritin cores. The ability of ferritin to perform this same reaction under somewhat varied conditions may be a reflection of its function *in vivo* where the formation of ferrihydrite cores is the only desirable product; the rate of iron loading may vary considerably under different physiological conditions and many other chemical species would be present in the intracellular compartment. The results in chapter 5 for ferritins formed *in vivo* under different conditions of iron overload uphold such a proposal.

8.1 Future work

Chapter 3

It would be interesting to try to deposit a different iron oxide in the ferritin cavity. A radical decrease in the rate of oxidation and the use of additives during reconstitution might induce such a change. For example a decrease in pH to below 6, low temperature, low oxygen tension and the addition of CO_3^{2-} might favour the formation of goethite cores. The formation of maghemite or magnetite cores by manipulation of the reconstitution conditions or *in situ* transformation of ferrihydrite cores, could have an industrial application as magnetic recording media, since the particles would be of uniform, nanometre dimensions. However, if the cavity size does impose a constraint on the stabilisation of such phases these attempts may be unsuccessful.

To further the studies in which zinc was added during reconstitution the use of a higher Fe:Zn ratio, perhaps 2:1, may provide some interesting results. At such a high ratio the zinc may be incorporated into the cores to a greater extent than was found with the ratio used in chapter 3. This may in itself prevent the formation of ferrihydrite or markedly reduce its crystallinity. In addition to selected area electron diffraction, high resolution TEM may reveal any structural imperfection in cores formed in the presence of Zn^{2+}, compared to those formed in its absence.

A kinetic and structural study of the reconstitution of H and L homopolymer ferritins in the presence of zinc may provide further insight into the role of the protein and/or the action of Zn^{2+}.

Chapter 4

In this chapter variants of human H-subunit ferritin were studied and, as such, (apart from 222 and A222,) they possessed the ferroxidase centre which largely governed their activity during the reconstitution experiments. A useful extension of this work would be to generate variants of the L-subunit, in order to study the nucleation role of the protein, in the absence of the ferroxidase centre.

Further work is required to elucidate the relative importance of the three invariant Glu residues (61,64,67, H-subunit numbering) at the proposed nucleation centre.

Chapter 5

In order to further our understanding of the nature of haemosiderin and its relationship to ferritin more data on the protein components of haemosiderins formed in different tissues and species, and under normal and pathological conditions of iron metabolism, are required.

There have been some recent reports that the iron cores of haemosiderins isolated from patients with idiopathic haemochromatosis and β-thalassemia who have not received phlebotomy and transfusion /chelation therapy, respectively, have ferrihydrite cores, (Dr. R.J. Ward, Miss F. Meldrum, pers. comm.). At present only a few samples have been examined by Mössbauer spectroscopy and electron diffraction. Many more samples need to be studied and investigation of the protein components would be valuable. However, if these initial findings are confirmed, the treatments used in both iron loading syndromes, and especially idiopathic haemochromatosis, may need to be reviewed. Current ideas about the pathways and mechanisms

of formation of the two forms of haemosiderin may also require revision.

Chapter 6

The successful reconstitution of horse spleen apoferritin with manganese suggests that ferritin/apoferritin may be useful as a reaction volume for the synthesis of other inorganic particles of nanometre dimensions. Indeed this has already been demonstrated by the *in situ* transformation of ferrihydrite to iron sulphide and the formation of a polymeric uranyl oxyhydroxide inside apoferritin (Meldrum *et al.*, 1991).

Another novel extension of this work already underway is the formation of bimetallic cores (Miss F. Meldrum, pers. comm.). Apoferritin has been loaded with iron and manganese and the presence of both metals inside the cavity has been confirmed by edXa. Only ferrihydrite electron diffraction patterns were observed when the protein had been loaded with 1000 Fe + 1000 Mn per molecule and 2000 Fe + 2000 Mn per molecule. This work provides further evidence to support the finding in chapter 6 that the manganese oxide cores formed inside apoferritin were amorphous: since there were enough cores within the selected area aperture to give the ferrihydrite pattern, but no evidence of another crystalline phase was observed.

Kinetic and structural studies of the reconstitution of H- and L-subunit homopolymers with manganese may provide some interesting and valuable results.

Chapter 7

Information on the phosphate content of the native pea seed ferritin would be most useful. If the P:Fe ratio was high, this ferritin would seem to fit into the pattern of correlation between phosphate content and crystallinity outlined by St. Pierre *et al.* (1989). An estimation of the phosphate content, and a structural study of the native form of the *Escherichia coli* bacterioferritin, would also be valuable. It will be interesting to find out the dimensions of the cavities of these two ferritins, since for the reconstituted samples, the core sizes were a little larger than those reported in this thesis for reconstituted mammalian samples.

8.2 Ferritin as a model system in Biomineralization

The deposition of ferrihydrite cores inside apoferritin is an example of biomineralization; the inorganic solid is formed under the influence of the protein shell. The protein sequesters the iron, catalyses its oxidation and directs the growth of the mineral inside the cavity. The apoferritin molecule provides a suitable surface for the partial coordination of the metal ions, while allowing further deposition to occur on the "open" side of the growing core. Ultimately the protein limits the size of the mineral particle, it also influences the structure of the oxide formed.

In apoferritin we have an ideal system for the study of biomineralization *in vitro*. Horse spleen apoferritin has long been readily available and easily prepared, its primary structure is known and its quaternary structure has been resolved to 0.26 nm resolution by X-ray diffraction. Human H- and L-subunit ferritins have also been sequenced and recently they have been cloned in *E. coli*. Recombinant

DNA techniques and site-directed mutagenesis have opened the way to probing the function of specific regions of the apoferritin molecule. In addition to this detailed knowledge of the structure of the protein, apoferritin is robust, tolerant of experimental conditions and easily reconstituted. Furthermore, the transition metal characteristics of iron enable the use of many different physical techniques by which to monitor the biomineralization process.

Our understanding of ferritin has increased rapidly since it was fist described by Schmiedeberg in 1894 and isolated from horse spleen by Laufberger in 1937, who was the first to call this *iron-rich protein* "ferritin". However, the subject is far from exhausted and the many, often interdisciplinary, research programmes currently in progress offer more challenges and will produce further insights.

APPENDIX I

Basic Theory of Transmission Electron Microscopy

Resolution

Resolution can be defined as the smallest distance by which two points on a specimen can be separated and still be distinguished as two points. The maximum theoretical resolving power of a microscope is about half the wavelength of the illuminating beam. The wavelength of the radiation is inversely proportional to its velocity. The wavelength of an electron accelerated at 100KeV is 0.037 Å and that of an electron accelerated at 200KeV is 0.0251 Å.

The basic structure of a transmission electron microscope

The image forming system of a transmission electron microscope basically consists of an evacuated column, containing, in alignment under one another; a filament, the cathode, which may be of tungsten or lanthanum hexaboride, the anode, which is a metal plate with a central aperture, magnetic lenses, a fluorescent viewing screen and a camera. See figure I.1.

Current passing through the filament causes it to heat up and emit electrons. A high negative voltage applied to the filament causes a large potential difference between the filament and the anode (which is at earth potential), this accelerates the electrons towards the anode. Some electrons pass through the aperture in the anode and travel down the column as the electron beam. The beam is focused by the first magnetic lens, the condenser lens, so that it illuminates the specimen. Most of the electrons pass through the specimen without deviation, however, some are scattered by heavy atoms in the specimen and are knocked out of the beam. This scattering of electrons forms a pattern in the emergent beam which is

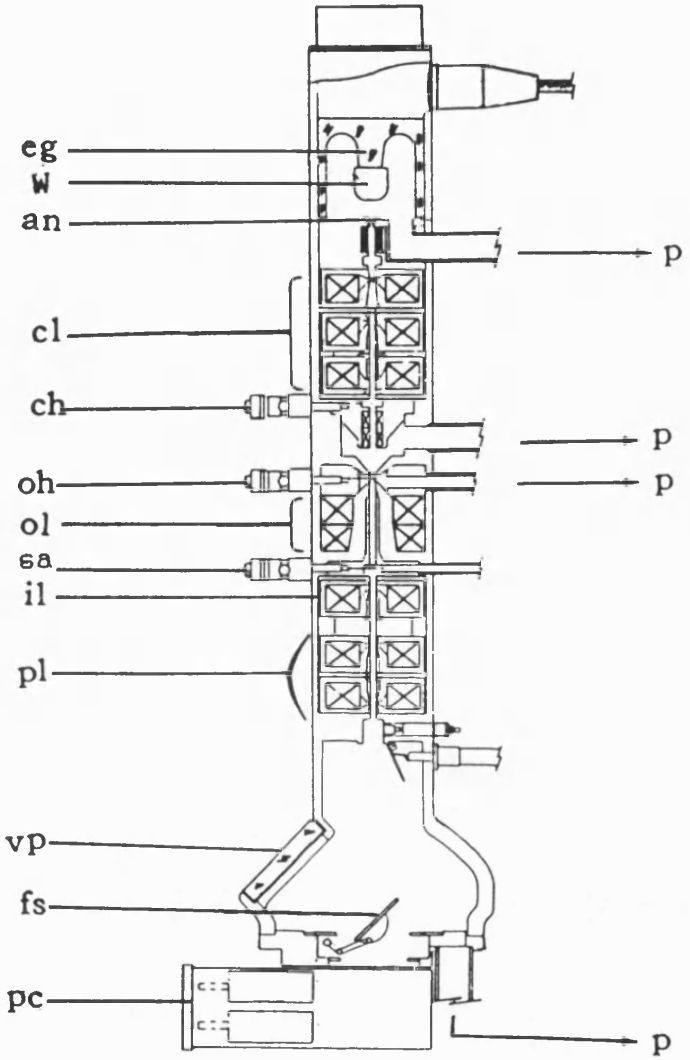

Figure I.1 Diagram of a transmission electron microscope.

eg	electron gun	*sa*	selected area aperture holder
W	Wehnelt cylinder	*p*	to pumping system
an	anode	*il*	intermediate lens
cl	condenser lens (triple)	*pl*	projector lens
ch	condenser aperture holder	*vp*	viewing port
oh	objective aperture holder	*fs*	fluorescent screen
ol	objective lens	*pc*	photographic chamber port

translated into an image when the beam is again focused. The second magnetic lens, the objective lens, focuses the emergent beam to form an enlarged image of the specimen. This image is enlarged further by the third magnetic lens, the projector lens, and is viewed on the fluorescent screen. The image can be recorded photographically by raising the fluorescent screen to allow the electrons to impinge on the photographic plate.

The electron gun

The electron gun is composed of three elements:

i) the filament, bent in the form of a V,

ii) the Wehnelt cylinder, a metal shield which surrounds the filament and contains an aperture located directly below the filament tip,

iii) the anode plate, a circular plate with a central aperture which is aligned with that of the Wehnelt cylinder.

See figure I.2.

When the filament is heated by a current, a cloud of electrons is given off (thermionic emission) which tends to be concentrated at the filament tip. The Wehnelt cylinder is maintained at a negative voltage which repels electrons leaving the filament from the inner surface of the cylinder and gathers them in the vicinity of the aperture, where they form a dense cloud. The electrons are then propelled down the column by the potential difference between the filament and the anode plate.

The magnetic lenses

These are electromagnets which are encased, apart from a small ring shaped gap, in soft iron which concentrates the magnetic field

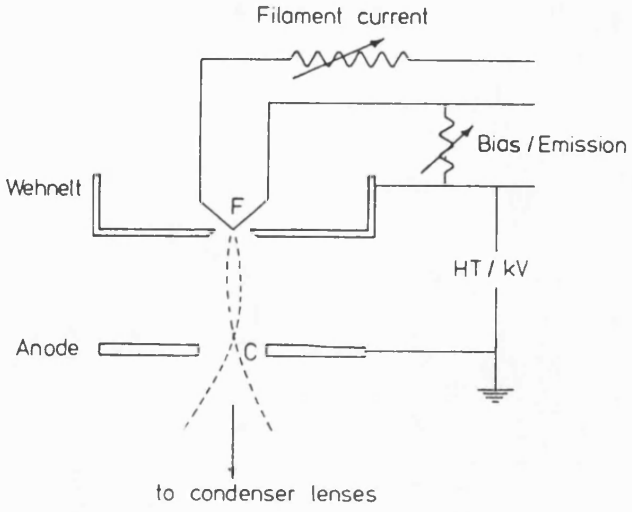

Figure I.2 The thermionic electron gun. Electrons from the filament F are accelerated through a hole in the anode. The focusing action of the gun produces a cross-over point C from which all electrons appear to come.

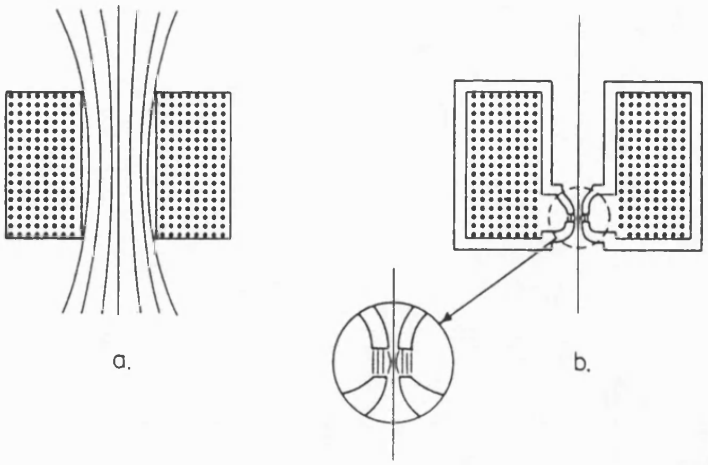

Figure I.3 *a* The field from a simple electromagnet. *b* The field is restricted to the small "lens" region by the addition of an iron yoke and pole pieces.

into the small gap. In the objective lens the field is concentrated still further by a soft iron pole piece which reduces the gap further and reduces the bore of the lens. (Figure I.3)

The current passing through the electromagnet focuses the electron beam onto a given plane. An increased current focuses the beam closer to the lens and *vice versa*. Fluctuations in either the lens current or the electron accelerating voltage will defocus the image produced by the objective lens and thereby limit the resolution of the microscope.

There are three sets of lenses:

i) the condenser lenses, these illuminate the specimen. They may be focused on the specimen to give a small intense area of illumination or focused above or below the specimen plane in order to give a larger area of less intense illumination.

ii) the objective lens. This causes the electron beam which has passed through the specimen to be focused just a few millimetres below the specimen plane. Below this focus point a magnified image of the specimen is produced.

iii) the projector lenses, these magnify the image produced by the objective lens. Increased current in the projector lenses causes the beam to come to focus higher up the column. Thus, the image will be larger since the beam will have spread more before it reaches the fluorescent screen.

The fluorescent screen

The screen on which the electron beam falls is coated with a material that fluoresces in the visible range when bombarded with electrons and therefore converts the electron image into a visible image. The resolution of the screen is limited by the grain size of

the fluorescent material and by light scattering within this material. The resolution is therefore limited to between 70 and 100 μm. Photographic plates coated with a fine grained emulsion can record all the detail inherent in the electron image.

Physical phenomena and lens defects which limit the performance of the transmission electron microscope

1. *Diffraction*

The electron beam, because of its wave nature, will be diffracted by obstacles in its path, i.e. the specimen and the objective aperture. Due to diffraction effects, a point on the specimen is never imaged as a true point but as an Airy disc pattern, comprising a central disc surrounded by a number of faint halos (diffraction, or Fresnel fringes). The radius (r) of the central disc is given by:

$$r = \frac{0.61\lambda}{n \sin \alpha}$$

where λ = wavelength

n = the refractive index of the medium between the specimen and the lens

α = the semi-aperture angle of the objective lens

(i.e. half the angle (θ) subtended by the edges of the lens or its limiting aperture at a point on the specimen, see figure I.4).

Two points on the specimen are said to be resolved if they are separated by a distance greater than or equal to, the radius of the central Airy disc which they each produce.

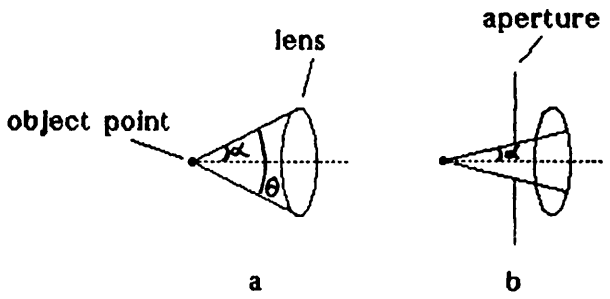

Figure I.4 The semi aperture angle (α).

a **α limited by diameter of lens,** ***b*** **α limited by an aperture.**

2. *Spherical aberration*

Rays transversing the peripheral part of a lens are focused onto a different plane from those near the optical axis. This gives rise to blurring of the image and loss of resolution. The solution is to use only the central portion of the lens field, by using very small apertures.

3. *Chromatic aberration*

Electrons of different wavelength are brought to focus on different planes which again leads to a loss of resolution. The stabilisation of the accelerating voltage has largely solved this problem. However, the wavelength of some of the electrons can also be increased by charged particles contaminating the column, lens components and apertures. Cleanliness in the microscopy room, sample preparation and loading and the use of the anti-contamination device are therefore, essential. A further source of chromatic aberration

can be the sample itself. The thicker the specimen, the more electrons will be scattered by it. Some electrons scattered by the specimen are not scattered enough to be lost from the beam, but may suffer some loss of velocity (inelastic scattering), and thus produce chromatic aberrations. This results in an increase in the diameter of the disc about image points and is known as electron noise. Chromatic aberration can be minimised by using very thin specimens or increasing the accelerating voltage used, since electrons of higher energy are scattered less by the specimen.

4. Astigmatism

One cause of astigmatism is asymmetry in the objective lens field. This results in a given point on the specimen being overfocused in one direction and underfocused in the other. Also the disc about the image point is enlarged. The distribution of Fresnel fringes around such a point cause the point to appear elongated in one direction. Resolution is thus adversely affected.

Asymmetry in the objective lens field is caused by the following:

i) inhomogeneities in the metal used for the manufacture of the objective pole piece,

ii) a less than perfectly circular bore in the pole piece,

iii) contamination of the objective aperture, specimen holder, specimen, pole piece bore, or other surfaces exposed to the beam in the vicinity of the specimen. The contamination becomes charged and affects the lens field.

The first two causes cannot be eliminated but they can be compensated for by the use of an astigmatism corrector. This device effects an equal asymmetry in the lens field, in a direction

perpendicular to the natural asymmetry. Thereby cancelling out the field asymmetry. Use of the astigmatism corrector can also compensate for some mild contamination as described in iii), but cleanliness and the routine use of an anti-contamination device are essential.

Astigmatism also occurs in the condenser lenses, but it affects the illumination rather than the resolution. Astigmatism in the condenser lenses results in the area of illumination being elongated in shape rather than round, when the beam is focused. When defocused the illumination of the specimen is not even. Such astigmatism can be corrected by the use of the condenser astigmatism corrector.

Astigmatism in the projector lenses is not a problem since it does not affect image quality to any great extent.

Electron diffraction

Crystal d-spacings are of the same order of magnitude as the wavelength of the electron. Thus, electrons are diffracted by crystal planes and an electron diffraction pattern can be obtained. The pattern obtained from a sample comprising many small, randomly oriented crystals will be a powder pattern of concentric rings. From such patterns the structure of the sample can be determined, since:

$$d = \frac{\lambda l}{r}$$

where d = crystal plane spacing, Å

λ = wavelength of electrons, Å

l = camera length, cm

r = reciprocal lattice spacing (radius of ring, cm)

A poorly crystalline material will give rise to broadened diffraction rings and an amorphous material will give very broad, diffuse rings.

In the TEM, whenever an image is formed on the viewing screen an electron diffraction pattern is present in the back focal plane of the objective lens, see figure I.5. In the back focal plane of the objective lens all parallel "rays" leaving the specimen in a specific direction pass through a point in the diffraction pattern, (three such sets of rays are shown in b of the figure). The diffraction pattern is unseen when the microscope is in imaging mode because the first projector lens is focused on the first intermediate image. The diffraction pattern can be magnified and viewed by changing the current passing through the projector lenses. It is clear from the figure that the objective aperture must be removed so that the whole diffraction pattern can be seen and that the use of a selected area aperture dictates the region of the specimen from which the pattern is formed.

Bibliography

"Practical Methods in Electron Microscopy", edited by A.M. Glauert. North Holland Publishing Co., Amsterdam. First edition 1972, third printing 1979.
vol. 1, part 2 by Beeston, B.E.P., Horne, R.W. & Markham, R.

Microscopy Handbooks 02 "The operation of the transmission electron microscope" by D. Chescoe & P.J. Goodhew. Oxford University Press, Royal Microscopical Society, 1984.

"A Beginner's Handbook in Biological Transmission Electron Microscopy" 2nd Edition by B.S. Weakley. Churchill Livingstone, London, 1981.

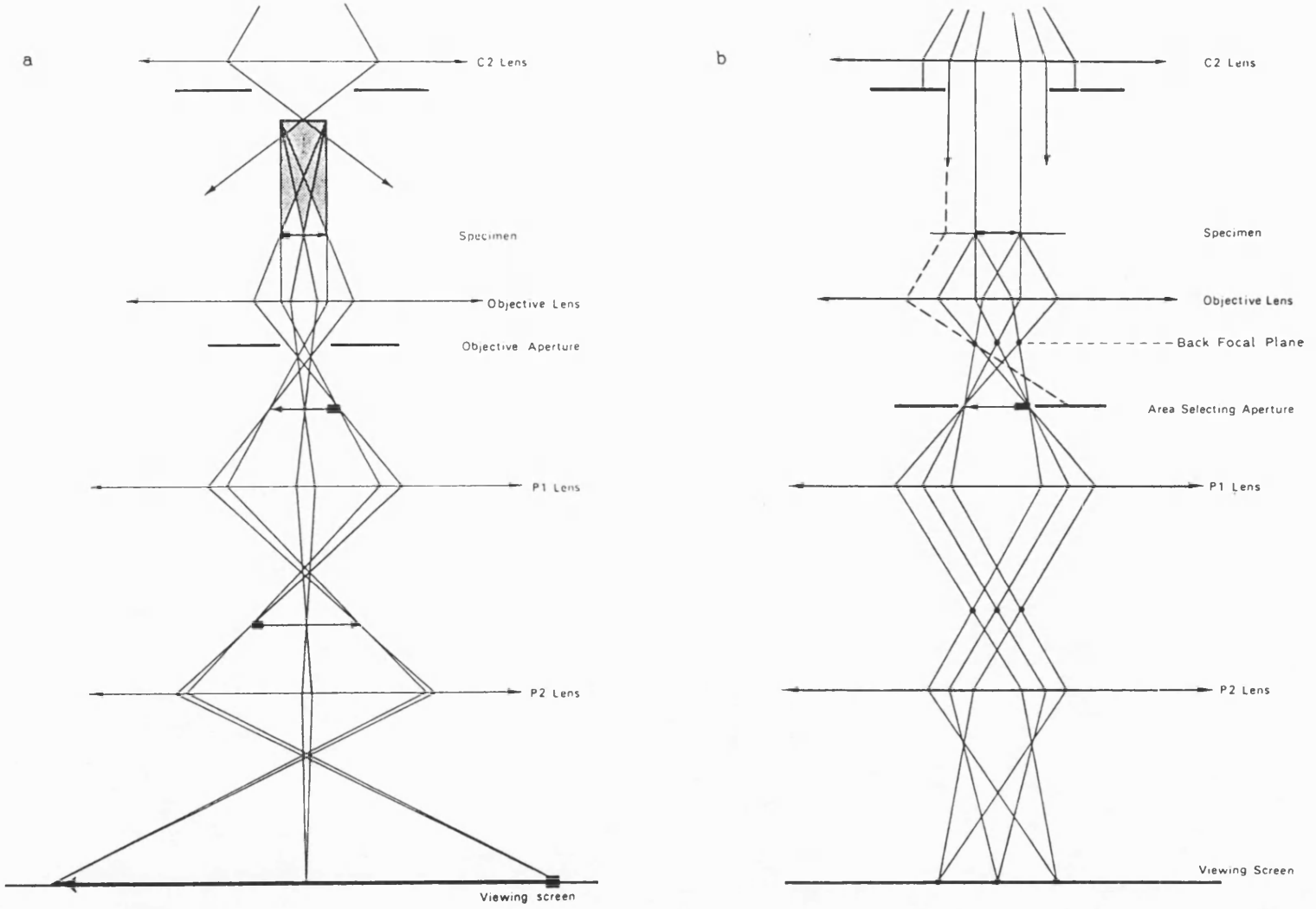

Figure I.5 Ray diagrams of *a* the imaging mode and *b* the diffraction mode of operation, in a transmission electron microscope having an objective and two projector lens imaging system.

APPENDIX II

Mössbauer Spectroscopy

Mössbauer spectroscopy is a form of absorption spectroscopy in which γ-radiation, emitted from an excited state nucleus formed as a result of radioactive decay, is resonantly absorbed. (Resonant absorption is observed for nuclei embedded in a solid, where the mass of the solid is sufficiently large that the recoil energy of the absorbing nuclei is negligible.) Since the separations between nuclear energy states are very precisely defined, resonance can only occur within a nucleus of the same type as that responsible for the emission of the radiation, thus the technique is completely specific. The naturally occurring isotope of iron, ^{57}Fe (natural abundance *ca.* 2%), is formed in an excited state by the radioactive decay of ^{57}Co by electron capture. Thus, ^{57}Co is a suitable source for ^{57}Fe Mössbauer spectroscopy.

This technique is a powerful tool for studying the magnetic and structural properties of ferritin and haemosiderin cores. ^{57}Fe Mössbauer spectroscopy is only sensitive to the iron in the sample and can thus give information about the environment of the iron atoms. The spectra obtained show the energy dependence of the resonant absorption of γ-rays by the nuclei. The precise energy at which absorption occurs is affected by the chemical environment of the nucleus. Therefore, the principle parameters obtained from a spectrum provide information on the electron density and the magnitudes of any electric field gradient and magnetic fields present at the nucleus. This is possible because the linewidths of the resonant absorptions are of the same order of magnitude as the hyperfine interactions: the interactions between the nucleus and its atomic electronic environment. This information permits the

elucidation of the structural, compositional and magnetic properties of the solid in which the nucleus is embedded.

The principle parameters of a spectrum are;

i) the electric monopole interaction, which gives rise to the chemical isomer shift, δ,

ii) the electric quadrupole interaction, giving rise to quadrupole splitting, Δ, and

iii) the magnetic dipole interaction, producing the magnetic hyperfine field.

With ^{57}Fe, the chemical isomer shift is seen as a change in the position of the centre of the spectrum, and the quadrupole splitting as the separation between the the two peaks formed as a result of the interaction between the nuclear quadrupole moment with an external electric field gradient. The magnetic dipole interaction splits the spectrum into six peaks, the separation of which allows the determination of any magnetic field present at the nucleus. Fe(II) and Fe(III) differ formally only in their number of 3d electrons, 6 and 5, respectively. Some screening of the inner s-electrons by the 3d electrons occurs, the extent of the screening being proportional to the number of 3d electrons. Thus Fe(III) appears to have a slightly greater electron density at the nucleus than Fe(II) and this results in the chemical isomer shift being appreciably smaller in Fe(III). Also, in the high spin state, Fe(III) has a symmetrical arrangement of d-electrons (1 in each orbital) and hence there is no contribution to the electric field gradient from the valence electrons, whereas high spin Fe(II) has one additional electron and hence a large electric field gradient, giving rise to large quadrupole splitting. Figure II.1 shows δ and Δ for Fe(II) in $FeSO_4$ and Fe(III) in $FeCl_3.6H_2O$ at room temperature.

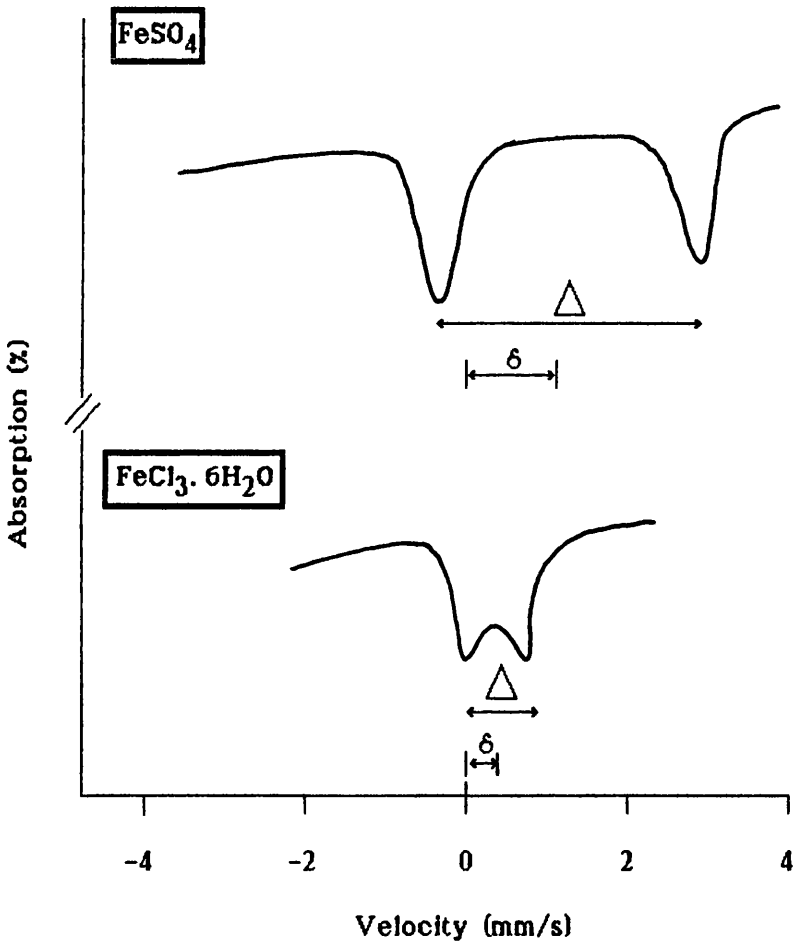

Figure II.1 Mössbauer spectra of Fe(II) and Fe(III) in simple compounds at room temperature. △ = quadrupole splitting, δ = chemical isomer shift.

Superparamagnetism

An important additional feature of the Mössbauer spectra of ferritin and haemosiderin is the phenomenon of superparamagnetism. For a material that has a density of magnetic atoms such that magnetic ordering can take place, there is a critical crystal size below which there will be a single magnetic domain in the absence of any applied magnetic field. This is because at these small dimensions (*ca.* > 20nm), the energy needed to create a domain wall exceeds the energy decrease that would be obtained by having more than one domain.

Exchange coupling between the atomic magnetic moments usually results in ferromagnetic (atomic moments parallel), ferrimagnetic (atomic moments antiparallel but with a net moment in one direction) or antiferromagnetic (atomic moments antiparallel) ordering, although the atomic spins may be "frozen" into a spin glass state. Other interactions result in certain easy and hard orientations for the spin system to lie along, with respect to the crystal lattice. Thus there is a magnetic anisotropy energy associated with the direction of the spin system. There may be more than one easy (low energy) direction for the spin system to lie along and these directions will be separated by magnetic anisotropy barriers. The magnetic anisotropy energy experienced by the spin system decreases with decreasing crystal size. Below a certain size the thermal energy may be of the same order of magnitude as the magnetic anisotropy energy barrier. Therefore fluctuations of the direction of the spin system (or magnetisation vector) may occur. Small fluctuations of the magnetisation vector around an easy direction are known as collective magnetic excitations, whereas fluctuations between easy directions, such that the magnetic anisotropy energy barriers are surmounted, are

known as superparamagnetism.

The size and nature of the iron oxide cores of ferritin and haemosiderin are such that they exhibit superparamagnetism. The Mössbauer spectra of these materials are temperature dependent; the magnetic order in the material is resolved as the temperature is lowered. This is seen as the spectrum changing from a doublet to a sextet (see figure II.2) and is due to a decrease in the rate at which the magnetisation vector switches between the various easy axes of magnetisation. The pattern of temperature dependence is characterised by the mean superparamagnetic transition temperature or blocking temperature (T_B). T_B is related to particle volume and the magnetic anisotropy constant for the material being studied by this equation:

$$T_B\, k = K\, V$$

where k = Boltzmann constant

K = magnetic anisotropy constant

V = particle volume

The range of particle sizes in ferritin and haemosiderin results in a distribution of values of T_B, so the T_B for a sample is defined as the temperature at which 50% of the spectral intensity is attributable to the doublet and 50% to the sextet.

The temperature dependent Mössbauer spectra of horse spleen haemosiderin shown in figure II.2 illustrate several points about the use of Mössbauer spectroscopy in the study of ferritin and haemosiderin. The spectrum at 77 K is a quadrupole split doublet, where Δ = 0.71 mm/s and δ = 0.48 mm/s. These values indicate that the oxidation state of the iron is Fe(III). The line widths are broadened indicating a variation in the iron site environments in the sample. The high proportion of surface sites and the semi-random structure of

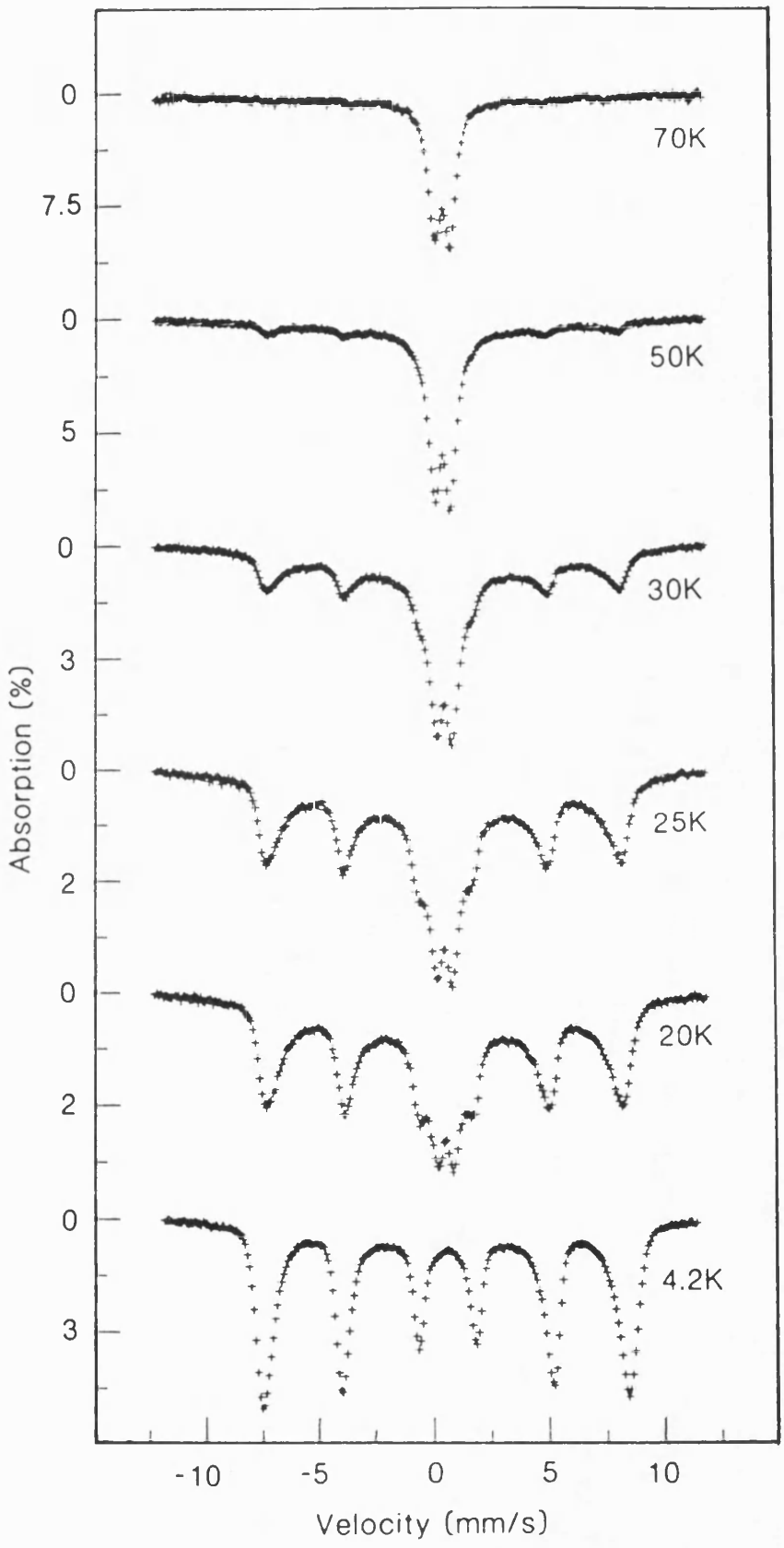

Figure II.2 Variable temperature Mössbauer spectra of horse spleen haemosiderin (from Dickson *et al.*, 1988).

ferrihydrite are consistent with broad line widths in the spectra. The variable temperature spectra show characteristic superparamagnetism and the T_B for this sample was 28 K, while the hyperfine field at 4.2 K was 49.5 *T*.

Magnetic ordering temperatures

The magnetic ordering temperature of a material is dependent on the strength of the magnetic exchange interactions between the atomic spins. The magnetic exchange interactions tend to hold the atomic spins or magnetic moments parallel or antiparallel to each other. These interactions are weakened by increasing distance between the magnetic atoms in the sample and by the replacement of oxygen bridges between the magnetic atoms with types of bridging ions, such as phosphate, which do not transmit these interactions with as much efficiency as oxygen ions.

In the Mössbauer spectroscopy of ferritins the lower magnetic ordering temperatures for the molluscan ferritins (~30 - ~37 K) compared to those of the mammalian ferritins (>50 K) can be explained by the lower iron density of the cores. This is also the case for the bacterioferritins from *Pseudomonas aeruginosa* and *Escherichia coli* where an even lower iron density is reflected in the very low magnetic ordering temperatures of ~3 K.

The magnetic ordering temperatures of these bacterioferritins is also dependent on the large amount of phosphate in the cores. At low phosphate concentrations (<2:1, iron:phosphate) the magnetic ordering temperature does not seem to be greatly affected, as the magnetic atoms are expected to be able to form exchange pathways around the phosphate ions. At higher phosphate concentrations the possible pathways become fewer in number and the magnetic ordering temperature

drops. The distribution of the phosphate ions in the cores may also be critical to the influence that they have on the magnetic ordering temperature, since phosphate located only at surface sites will disrupt magnetic exchange interactions less than phosphate ions distributed throughout the core.

Bibliography

"Physical Chemistry" by P.W. Atkins. Oxford University Press, Oxford. 1978, reprinted 1979.

"Chemical Applications of Mössbauer Spectroscopy" edited by Goldanskii, V.I. & Herber, R.H. Academic Press, London. 1968.

Bell *et al.*, 1984.

Goodman & DeKock, 1982.

St. Pierre *et al.*, 1989.

APPENDIX III

Calculation of the expected diameter of a spherical particle of ferrihydrite from its iron content

In 1967 Towe & Bradley published physical data concerning the structure of ferrihydrite based on that of haematite (αFe_2O_3). They proposed unit cell parameters of a = 5.08Å and c = 9.4Å, and from density measurements of 3.96, a cell content of near $Fe_5HO_8.4H_2O$.

From this information and given that the volume of the unit cell = 0.866 a^2cÅ^3 and the volume of a sphere = 4/3 πr^3, it was possible to calculate the expected diameter of any ferrihydrite particle if the number of iron atoms it contained was known.

In this instance the ferrihydrite particles of interest were ferritin cores for which the average number of iron atoms per molecule was known. An example calculation is given below.

For 875 iron atoms/molecule:

number of unit cells per core = 875 ÷ 5 = 175

volume of core = volume of unit cell (Å^3) × 175

= 210.07 × 175

= 36,762 Å^3

The volume of a sphere = 4/3 πr^3

$\therefore$ r^3 = 36,762 ÷ 4/3 π

= 8,776

$\therefore$ r = $\sqrt[3]{8,776}$

= 20.63 Å

$\therefore$ the expected core diameter = 41.25 Å

APPENDIX IV

Amino-acid code

Amino-acid names and code names in alphabetical order of the one letter code:

A	Ala	Alanine
B	Asx	Aspartic acid/Asparagine
C	Cys	Cysteine
D	Asp	Aspartic acid
E	Glu	Glutamic acid
F	Phe	Phenylalanine
G	Gly	Glycine
H	His	Histidine
I	Ile	Isoleucine
K	Lys	Lysine
L	Leu	Leucine
M	Met	Methionine
N	Asn	Asparagine
P	Pro	Proline
Q	Gln	Glutamine
R	Arg	Arginine
S	Ser	Serine
T	Thr	Threonine
V	Val	Valine
W	Trp	Tryptophan
Y	Tyr	Tyrosine
Z	Glx	Glutamic acid/Glutamine

APPENDIX V

X-ray Diffraction Standard Tables

From the Powder X-ray Diffraction Data File compiled by JCPDS-International Centre for Diffraction Data.

29-712 29-713

d	2.50	2.21	1.96	2.50	$5Fe_2O_3 \cdot 9H_2O$
I/I_1	100	80	80	100	Iron Oxide Hydrate (Ferrihydrite)

Rad. MoKα λ 0.7107 Filter ZrO_2 Dia.
Cut off I/I_1 Visual I/I cor.
Ref. Chukhrov, F. et al., Izv. Akad. Nauk SSSR, 23 (1975)*

Sys. Hexagonal S.G.
a_0 5.08 b_0 c_0 9.4 A C 1.9
α β γ Z 0.5 Dx 3.796
Ref. Ibid. V 210Å^3

εα nωβ εγ Sign
2V D 3.8 mp Color Yellow to dark brown
Ref. Ibid.

*Van der Giessen, J. Inorg. Nucl. Chem., 28 2155 (1966). Prepared by slow hydrolysis of ferric salts at pH>3, and below 9.5.

d A	I/I_1	hkl	d A	I/I_1	hkl
2.50	100	110			
2.21	80	200			
1.96	80	113			
1.72	50	114			
1.51	70	115			
1.48	80	106			

© JCPDS 1979

793

8-98 MAJOR CORRECTION

d	6.26	3.29	2.47	6.26	FeO(OH) 1/2($Fe_2O_3 \cdot H_2O$)
I/I_1	100	90	80	100	Iron Oxide Hydrate Lepidocrocite

Rad. CoKα λ 1.7902 Filter Fe Dia. 19cm
Cut off I/I_1 Visual
Ref. Rooksby "X-ray Identification and Crystal Structures of Clay Minerals" London, 1951, facing p. 264

Sys. Orthorhombic S.G. Amam (63)
a_0 3.88 b_0 12.54 c_0 3.07 A 0.309 C 0.245
α β γ Z 4 Dx 3.95
Ref. Ibid.

εα 1.94 nωβ 2.20 εγ 2.51 Sign -
2V 83° D 3.854 mp 250°C Color red to red brown
Ref. Posnjak and Merwin, Am. J. Sci. 47 311 (1919)

Peacock, Trans. Roy. Soc. Canada 36 IV, 117 (1942) from Siegen, Westphalia, gives a=3.87, b=12.58, c=3.07, D_x=3.97
Rm (Westphalia)
R-D values by Rooksby only

d Å	I/I_1	hkl	d Å	I/I_1	hkl
6.26	100	020	1.196	20	022,191
3.29	90	120	1.189	20	1.10.0
2.79	10R	011	1.10	20	
2.47	80	031	1.075	40	Indices by Peacock
2.36	20	111			
2.09	20	131,060			
1.937	70	051,200			
1.848	20	220			
1.732	40	151			
1.566	20	080			
1.535	20	002			
1.524	40	231			
1.496	10R	022			
1.449	10	180			
1.433	20	171			
1.418	10	260			
1.389	10	122			
1.367	30	251			
1.261	10	091,320			
1.213	10	280			

29-713 29-712

d	4.18	2.45	2.69	4.98	FeO(OH) ★
I/I_1	100	50	35	12	Iron Oxide Hydroxide Goethite

Rad. CoKα λ 1.7902 Filter Dia.
Cut off I/I_1 Diffractometer I/I cor.
Ref. Harrison, R. et al., Bull. Geol. Surv. Great Britain No. 52, 51 (1975)

Sys. Orthorhombic S.G. Pbnm (62)
a_0 4.608 b_0 9.956 c_0 3.0215 A 0.4628 C 0.3035
α β γ Z 4 Dx 4.18
Ref. Ibid. V [138.62Å^3]

εα nωβ εγ Sign
2V D 4.00 mp Color Dark brown
Ref Ibid.

Specimen from Hindlow Quarry, Derbyshire, England (E3S891). Lead nitrate internal standard (a_0 = 7.8568Å). Dx for $Fe_{3.86}Si_x(OH)_{4.31}O_{3.69}$ (x ≤ 0.012), formula from chemical analysis with impurities deducted. Chemical analysis (%): SiO_2 1.84, Fe_2O_3 86.30, H_2O (>105°C) 10.79, H_2O (<105°C) 0.86, and minor MgO, CaO, CO_2, and organic C.
To replace 17-536.

d A	I/I_1	hkl	d A	I/I_1	hkl
4.98	12	020	1.5637	10	151
4.183	100	110	1.5614	8	160
3.383	10	120	1.5091	8	002,250
2.693	35	130	1.4675	2	320
2.583	12	021	1.4541	5	061
2.527	4	101	1.4207	2	112
2.489	10	040	1.3936	3	330
2.450	50	111	1.3694	2	301
2.303	1	200	1.3590	3	170
2.253	14	121	1.3459	1	260
2.190	18	140	1.3173	3	132
2.089	1	220	1.2921	<1	042
2.011	2	131	1.2654	1	331
1.920	5	041	1.2437	1	142
1.802	6	211	1.1994	1	341
1.7728	1	141	1.1506	1	081
1.7192	20	221	1.1445	1	410
1.6906	6	240	1.1263	1	242
1.6593	3	060			
1.6037	4	231			

© JCPDS 1979

FORM M-2 B

794

24-713A

CALCULATED PATTERN – INTEGRATED C

See 24-713 24-713

4.19	2.37	2.81	100	58	40

α-MnOOH

Manganese Oxide Hydroxide Groutite

Ref. NBS Mono. 25, Sec. 11 (1973)

Sys. Orthorhombic S.G. Pbnm (62) Dx 4.171 Z 4
a_0 4.560 b_0 10.700 c_0 2.870
α β γ
Ref. Glasser and Ingram, Acta Cryst., B24 1233 (1968)

Scale factor (Integrated Intensities) 0.7057 x 10^4
λ 1.54056

d A	I/I_0	h k l	d A	I/I_0	h k l
5.35	9	020	2.529	15	021
4.19	100	110	2.429	5	101
3.470	11	120	2.369	58	111
2.809	40	130	2.307	21	140
2.675	34	040	2.280	2	200

d A	I/I_0	h k l	d A	I/I_0	h k l
2.230	2	210	1.303	1	321
2.212	8	121	1.278	6	132
2.008	6	131	1.265	5	042
1.957	3	041	1.262	2	261
1.937	5	150	1.257	3	331
1.921	1	230	1.219	3	142
1.798	4	141	1.214	1	202
1.783	2	060	1.212	3	081
1.761	13	211	1.200	5	341
1.735	9	240	1.161	1	271
1.693	38	221	1.157	2	360
1.606	26	151	1.154	3	280
1.596	9	231	1.153	1	152
1.560	5	250	1.138	1	351
1.515	13	061	1.134	4	410
1.485	2	241	1.118	1	062
1.462	6	320	1.106	3	242
1.449	7	170	1.086	1	430
1.435	9	002	1.078	1	370
1.405	2	260	1.073	2	361
1.398	4	330	1.070	1	281
1.358	6	112	1.070	1	0100
1.343	4	301	1.068	5	191
1.333	2	311	1.056	2	252
1.326	1	122	Plus 37 lines to 0.823		

FORM CI

846

24-734

24-733A

d	2.49	2.77	1.54	4.92
I/I_1	100	85	50	30

Mn_3O_4 $MnO \cdot Mn_2O_3$ ★

Manganese Oxide (Hausmannite)

Rad. $CuK\alpha_1$ λ 1.54056 Filter Mono. Dia.
Cut off I/I_1 Diffractometer $I/I_{cor.}$ =1.5
Ref. NBS Mono. 25, Sec. 10, 38 (1972)

Sys. Tetragonal S.G. $I4_1/amd$ (141)
a_0 5.7621(1) b_0 c_0 9.4696(4)Å C 1.6434
α β γ Z 4 Dx 4.834
Ref. Ibid.

εα nωβ εγ Sign
2V D mp Color Unground: Purplish black
Ref. Ibid. Ground: Dark brown

The sample was prepared by heating MnO_2 from J. T. Baker Chemical Co., Phillipsburg, N. J. to 1000°C for three days.
Pattern at 25°C.

See following card.

d A	I/I_1	hkl	d A	I/I_1	hkl
4.924	30	101	1.3487	6	305
3.089	40	112	1.3055	1	332
2.881	17	200	1.2777	10	413
2.768	85	103	1.2431	6	422
2.487	100	211	1.2305	5	404
2.463	20	202	1.2212	1	325
2.367	20	004	1.1978	5	217
2.0369	20	220	1.1935	4	316
1.8288	7	204	1.1836	4	008
1.7988	25	105	1.1439	2	431
1.7008	10	312	1.1316	4	424
1.6405	8	303	1.1245	8	415
1.5762	25	321	1.0993	2	512
1.5443	50	224	1.0826	8	503
1.5260	2	215	1.0632	3	521
1.4721	3	116	1.0325	5	327
1.4405	20	400	1.0235	3	228
1.4260	3	323	1.0185	6	440
1.3841	4	206	0.9981	1	426
1.3823	2	411	.9845	5	435

FORM M-2 B

878

18-805

d	3.41	1.68	2.41	3.41
I/I_1	100	90	80	100

γ-MnOOH

gamma-Manganese Oxide Hydrate (Manganite)

Rad. FeK λ 1.9373 Filter Mn Dia. 114.6mm
Cut off I/I_1
Ref. Bricker, Am. Min., 50 1296-1354 (1965)

Sys. Monoclinic * S.G. $B2_1/d$ (14)
a_0 8.98 b_0 5.28 c_0 5.71 A 1.701 C 1.081
α β 90° γ Z 8 Dx 4.31
Ref. From powder data, indexed by analogy with Manganite L.G.B.

εα nωβ εγ Sign
2V D mp Color
Ref.

* (pseudoorthorhombic)

d A	I/I_1	hkl	d A	I/I_1	hkl
3.41	100	210	1.099	2	
2.65	50	301,020	1.080	2	
2.52	10	012	1.015	2	
2.41	80	202	0.993	2	
2.36	2	311			
2.28	30	220			
2.20	30	212			
1.781	20	222			
1.710	6	420			
1.675	90	412			
1.637	2	230			
1.502	10	032			
1.435	16	521			
1.323	6	602			
1.262	2	240			
1.214	2				
1.182	2				
1.158	2				
1.139	2				
1.118	2				

FORM T-2 B

18-804

d	4.62	2.64	2.36	4.62
I/I_1	100	50	20	100

β-MnOOH

beta-Manganese Oxide Hydrate (Feitknechtite)

Rad. FeK λ 1.9373 Filter Ni Dia. 114.6mm
Cut off I/I_1
Ref. Bricker, Am. Min. 50 1296-1354 (1965)

Sys. Hexagonal S.G.
a_0 3.1? b_0 c_0 4.62 A C 1.490
α β γ Z 1 Dx 3.80
Ref. Ibid, a by analogy with $Mn(OH)_2$

εα nωβ εγ Sign
2V D mp Color
Ref.

Oxidation of $Mn(OH)_2$, pyrochroite yields Mn_3O_4 (hausmannite) and β-MnOOH, the mixture was formerly referred to as "hydrohausmannite".

d A	I/I_1	hkl	d A	I/I_1	hkl
4.62	100	001			
2.64	50	100			
2.36	20b	101			
1.96	10b	ni			
1.55	?	110			
1.50	?	003			

FORM T-2 B

957

GLOSSARY

Erythrocyte - mature non-nucleated red blood cell.

Erythropoiesis - formation of erythrocytes by the red marrow.

Kupffer cells - a type of phagocytic endothelial cell lining the venous sinusoids of the liver.

Parenchyma - the tissue of an organ as distinguished from supporting or connective tissue.

Reticulocyte - non-nucleated young red cell, intermediate between the nucleated normoblast and the normal red cell.

Reticuloendothelial System (RES) - a functional, rather than anatomical system of the body involved primarily in defence against infection and in disposal of the products of the breakdown of cells. It is made up of macrophages, the Kupffer cells of the liver and the reticulum cells of the lungs, bone marrow, spleen and lymph nodes.

Butterworths Medical Dictionary, 2nd Ed., 1978. M. Critchley, ed. in chief. Butterworth and Co. (Publishers) Ltd., London, Boston.

Mosby's Medical and Nursing Dictionary, 1983. Mosby, Missouri.

REFERENCES

Aisen, P. (1980). In *Iron in Biochemistry and Medicine, II* (Jacobs, A. & Worwood, M., eds), pp. 87-129, Academic Press, London.

Andrews, S.C. (1986). Studies on Ferritin and Haemosiderin from Rat Liver. PhD. Thesis, University of Sheffield; cited in Andrews, S.C., Brady, M.C., Treffry, A., Williams, J.M., Mann, S., Cleton, M.I., De Bruijn, W. & Harrison, P.M. (1988). *Biology of Metals* 1, 33-42.

Andrews, S.C., Brady, M.C., Treffry, A., Williams, J.M., Mann, S., Cleton, M.I., De Bruijn, W. & Harrison, P.M. (1988). *Biology of Metals* 1, 33-42.

Andrews, S.C., Harrison, P.M. & Guest, J.R. (1989b). *J. Bacteriology* 171, 3940-3947.

Andrews, S.C., Smith, J.M.A., Guest, J.R. & Harrison, P.M. (1989a). *Biochem. Biophys. Res. Comm.* 158, 489-496.

Andrews, S.C., Treffry, A. & Harrison, P.M. (1987a). *Biochem. J.* **245**, 439-446.

Andrews, S.C., Treffry, A. & Harrison, P.M. (1987b). *Biochem. J.* **245**, 447-453.

Arosio, P., Adelman, T.G. & Drysdale, J.W. (1978). *J. Biol. Chem.* 253, 4451-4458.

Bauminger, E.R., Cohen, S.G., Dickson, D.P.E., Levy, A., Ofer, S. & Yariv, J. (1980). *Biochim. Biophys. Acta* 623, 237-242.

Bauminger, E.R., Harrison, P.M., Nowik, I. & Treffry, A. (1989). *Biochemistry* 28, 5486-5493.

Bauminger, E.R., Iancu, T.C., Link, G., Pinson, A. & Hershko, C. (1987). *Hyperfine Interact.* 33, 249-262.

Bell, S.H., Weir, M.P., Dickson, D.P.E., Gibson, J.F., Sharp, G.A. & Peters, T.J. (1984). *Biochim. Biophys. Acta* **787**, 227-236.

Bomford, A., Conlon-Hollingshead, C. & Munro, H.N. (1981). *J. Biol. Chem.* **256**, 948-955.

Bothwell, T.H., Charlton, R.W., Cook, J.D. & Finch, C.A. (1979). *Iron Metabolism in Man* Blackwell Scientific Publications, London, UK.

Boyd, D., Vecoli, C., Belcher, D.M., Jain, S.K. & Drysdale, J.W. (1985). *J. Biol. Chem.* **260**, 11755-11761.

Brissot, P., Wright, T.L., Ma, W.L. & Weisinger, R.H. (1985). *J. Clin. Invest.* **76**, 1463-1470.

Bull, H.B. (1964). *An Introduction to Physical Biochemistry*, p. 177, F.A. Davis Company, Philadelphia, USA.

Burgess, J. (1988). *Ions in Solution: Basic Principles of Chemical Interactions*, Ellis Horwood Ltd., Chichester, UK.

Burns, R.G. & Burns, V.M. (1979). In *Marine Minerals, Vol. 6. Reviews in Mineralogy* (Burns, R.G., ed), pp. 1-46, Mineral Soc. Amer.; cited in Murray *et al.*, 1985.

Carlson, L. & Schwertmann, U. (1987). *Wat. Res.* **21**, 165-170.

Chan, B.E., Roeser, H.P., Nikles, A. & Ridgeway, K. (1985). *Anal. Biochem.* **151**, 561-565.

Chasteen, N.D. (1983). *Adv. Inorg. Biochem.* **5**, 201-233.

Chasteen, N.D. & Theil, E.C. (1982). *J. Biol. Chem.* **257**, 7672-7677.

Coffey, J.W. & de Duve, C. (1968). *J. Biol. Chem.* **243**, 3255-3263.

Coleman, C.B. & Matrone, G. (1969). *Biochim. Biophys. Acta* **177**, 106-112.

Cornell, R.M. & Schneider, W. (1989). *Polyhedron* **8**, 149-155.

Dana, E.S. (1932). *A Textbook of Mineralogy with an extended treatise on Crystallography and Physical Mineralogy* 4th ed., revised and enlarged by Ford, W.E. John Wiley & Sons, New York, USA.

Dedman, Treffry, A. & Harrison, P.M. (1990). *Inorganic Biochemistry Discussion Group* Meeting, Abstract, Spring 1990.

Dickson, D.P.E., Meagher, A., Nilssen, K.J. & Borch-Iohnsen, B. (1987). *Biochim. Biophys. Acta* **924**, 442-446.

Dickson, D.P.E., Reid, N.M.K., Mann, S., Wade, V.J., Ward, R.J. & Peters, T.J. (1988). *Biochim. Biophys. Acta* **957**, 81-90.

Egyed, A. (1982). In *The Biochemistry and Physiology of Iron* (Saltman, P. & Hegenauer, J., eds), pp. 103-119, Elsevier North Holland, Inc.

Farrant, J.L. (1954). *Biochim. Biophys. Acta* **13**, 569-576.

Finch, C.A., Ragan, H.A., Dyer, I.A. & Cook, J.D. (1978). *Proc. Soc. Exp. Biol. Med.* **159**, 335-338.

Fischbach, F.A., Gregory, D.W., Harrison, P.M., Hoy T.G. & Williams, J.M. (1971). *J. Ultrastruc. Res.*, **37**, 495-503.

Fischbach, F.A., Harrison, P.M. & Hoy, T.G. (1969). *J. Mol. Biol.* **39**, 235-238.

Flynn, C.M. (1984). *Chem. Rev.* **84**, 31-41.

Ford, G.C., Harrison, P.M., Rice, D.W., Smith, J.M.A., Treffry, A., White, J.L. & Yariv, J. (1984). *Phil. Trans. R. Soc. Lond. B*, **304**, 551-565.

Frankel, R.B., Papaefthymiou, G.C., Blakemore, R.P. O'Brien, W.D. (1983). *Biochim. Biophys. Acta* **763**, 147-159.

Gabuzda, T.G. & Pearson, J. (1968). *Nature* **220**, 1234-1235.

Giovanoli, R. (1980). In *Geology and Geochemistry of Manganese* (Varentsov, I.M. & Grasselly, G., eds) Vol. 1, pp. 159-202, E. Schweizerbart'sche Verlagsbuchhandlung, Stuttgart; cited in Murray *et al.*, 1985.

Giovanoli, R. & Leuenberger, U. (1969). *Helv. Chim. Act.*, **52**, Fasc. 8, Nr. 233, 2333-2347.

Goodman, B.A. & DeKock, P.C. (1982). *J. Plant Nutrition* **5**, 345-353.

Gorun, S.M. & Lippard, S.J. (1986). *Nature* **319**, 666-668.

Grootveld, M., Bell, J.D., Halliwell, B., Aruoma, O.I., Bomford, A. & Sadler, P.J. (1989). *J. Biol. Chem.* **264**, 4417-4422.

Haggis, G.H. (1965). *J. Mol. Biol.* **14**, 598-602.

Harris, D.C. (1978). *Biochemistry* **17**, 3071-3078.

Harrison, P.M., Andrews, S.C., Ford, G.C., Smith, J.M.A., Treffry, A., & White, J.L. (1987). In *Iron Transport in Microbes, Plants and Animals* (Winkelmann, G, vander Helm, D. & Neilands, J.B., eds), pp. 445-475, VCH Verlagsgesellschaft, Weinheim.

Harrison, P.M., Clegg, G.A. & May, K. (1980). In *Iron in Biochemistry and Medicine, II* (Jacobs, A. & Worwood, M., eds), pp. 131-171, Academic Press, London.

Harrison, P.M., Hoare, R.J., Hoy, T.G. & Macara, I.G. (1974). In *Iron in Biochemistry and Medicine* (Jacobs, A. & Worwood, M., eds), pp. 73-114, Academic Press, London.

Harrison, P.M., Artymiuk, P.J., Ford, G.C., Lawson, D.M., Smith, J.M.A., Treffry, A. & White, J.L. (1989). In *Biomineralization, Chemical and Biochemical Perspectives* (Mann, S., Webb, J. & Williams, R.J.P., eds), pp. 257-294, VCH Weinheim (FRG), New York (USA).

Hastings, D. & Emerson, S. (1986). *Geochim. et Cosmochim. Acta*, **50**, 1819-1824.

Heald, S.M., Stern, E.A., Bunker, B., Holt, E.M. & Holt, S.L. (1979). *J. Am. Chem. Soc.* **101**, 67-73.

Hem, J.D. & Lind, C.J. (1983). *Geochim. et Cosmochim. Acta*, **47**, 2037-2046.

Hershko, C., Link, G., Pinson, A., Grisaru, S., Sarel, S. & Grady, R.W. (1985). In *Proteins of Iron Storage and Transport* (Spik, G., Montreuil, J., Crichton, R.R. & Mazurier, J., eds), pp. 285-292, Elseveir Science Publications, Amsterdam.

Heusterspreute, M. & Crichton, R.R. (1981). *FEBS. Lett.* **129**, 322-327.

Hoy, T.G. & Jacobs, A. (1982). In *The Biochemistry and Physiology of Iron* (Saltman, P. & Hegenauer, J., eds), pp. 435-440, Elsevier North Holland Inc.

Jacobs, A. (1980). In *Iron in Biochemistry and Medicine, II* (Jacobs, A. & Worwood, M., eds), pp. 427-459, Academic Press, London.

Jones, J.G. (1986). In *Advances in Microbial Ecology* vol. 9 (Marshall, K.C., ed), pp. 149-185, Plenum Press, New York.

Joshi, J.G., Goodman, S., Deshpande, V.V. & Price, D.J. (1985). In *Proteins of Iron Storage and Transport* (Spik, G., Montreuil, J., Crichton, R.R. & Mazurier, J., eds), pp. 93-96, Elsevier Science Publications, Amsterdam.

Kim, K.-S., Macey, D.J., Webb, J. & Mann, S. (1989). *Proc. R. Soc. Lond. B*, **237**, 335-346.

Laufberger, M. (1937). *Bull. Soc. Chim. Biol.* **19**, 1575-1582, cited in Farrant, J.L. (1954). *Biochim. Biophys. Acta* **13**, 569-576.

Lawson, D.M., Treffry, A., Artymiuk, P.J., Harrison, P.M., Yewdall, S.J., Luzzago, A., Cesareni, G., Levi, S. & Arosio, P. (1989). *FEBS Lett.*, **254**, 207-210.

Lawson, D.M., Artymiuk, P.J., Yewdall, S.J., Smith, J.M.A., Livingstone, J.C., Treffry, A., Luzzago, A., Levi, S., Arosio, P., Cesareni, G., Thomas, C.D., Shaw, W.V. & Harrison, P.M. (1991). *Nature*, **349**, 541-544.

Lombard, M. (1990). *Inorganic Biochemistry Discussion Group* Meeting, Abstract, Spring 1990.

Lowenstam, H.A. & Weiner, S. (1989). *On Biomineralization*, Oxford University Press, New York.

Lowry, O.H., Rosebrough, N.J., Farr, A.L. & Randall, R.J. (1951). *J. Biol. Chem.* **193**, 265-275.

Macara, I.G., Hoy, T.G. & Harrison, P.M. (1972). *Biochem. J.* **126**, 151-162.

Macara, I.G., Hoy, T.G. & Harrison, P.M. (1973a). *Biochem. J.* **135**, 343-348.

Macara, I.G., Hoy, T.G. & Harrison, P.M. (1973b). *Biochem. J.* **135**, 785-789.

Macara, I.G., Hoy, T.G. & Harrison, P.M. (1973c). *Biochem. Soc. Trans.* 1, 102-104

Mackenzie, R.C., Follett, E.A.C. & Meldau, R. (1971). In *The Electron Optical Investigation of Clays* (Gard, J.A., ed), pp. 315-344, Mineralogical Society, London.

Mann, S. (1987). *Chemistry in Britain*, February, 137-140.

Mann, S. (1989). In *Origin, evolution and modern aspects of biomineralization in plants and animals* (Crick, R.E., ed), pp. 273-288, Plenum Press, New York.

Mann, S., Bannister, J.V. & Williams, R.J.P. (1986a) *J. Mol. Biol.* **188**, 225-232.

Mann, S., Perry, C.C., Webb, J., Luke, B. & Williams, R.J.P. (1986b) *Proc. R. Soc. Lond. B* **227**, 179-190.

Mann, S., Sparks, N.H.C. & Blakemore, R.P. (1987a). *Proc. R. Soc. Lond. B* **231**, 477-487.

Mann, S., Williams, J.M., Treffry, A. & Harrison, P.M. (1987b). *J. Mol. Biol.* **198**, 405-416.

Massover, W.H. (1985a). In *Proc. 43rd Ann. Meet. Electron Microscopy Soc. America* (Bailey, G.W., ed), pp. 322-323, San Francisco Press, CA, USA.

Massover, W.H. (1985b). *Biochim. Biophys. Acta* **829**, 377-386.

Massover, W.H. & Cowley, J.M. (1973). *Proc. Natl. Acad. Sci. USA* **70**, 3847-3851.

May, P.M. & Williams, D.R. (1980). In *Iron in Biochemistry and Medicine, II* (Jacobs, A. & Worwood, M., eds), pp. 1-28, Academic Press, London.

Mazur, A. & Carleton, A. (1963). *J. Biol. Chem.* **238**, 1817-1824.

Meldrum, F.C., Wade, V.J., Nimmo D.L., Heywood, B.R. & Mann, S. (1991). *Nature* **349**, 684-687.

Melikhov, I.V., Kozlovskaya, E.D., Berliner, L.B. & Prokofiev, M.A. (1987). *J. Colloid Interface Sci* **117**, 1-9.

Mengel, K. & Kirkby, E.A. (1978). *Principles of Plant Nutrition*, p. 426. International Potash Institute, Berne, Switzerland.

Moore, G.R., Mann, S. & Bannister, J.V. (1986). *J. Inorg. Biochem.* **28**, 329-336.

Morley, C.G.D., Rewers, K. & Bezkorovainy, A. (1982). In *The Biochemistry and Physiology of Iron* (Saltman, P. & Hegenauer, J., eds), pp. 171-172, Elsevier North Holland, Inc.

Mullin, J.W. (1972). *Crystallisation*, 2nd edition, chapters 5 & 6. Butterworth & Co. (Publishers) Ltd., London.

Murray, J.W., Dillard, J.G., Giovanoli, R., Moers, H. & Stumm, W. (1985). *Geochim. et Cosmochim. Acta*, **49**, 463-470.

O'Connell, M.J., Baum, H. & Peters, T.J. (1986b). *Biochem. J.* **240**, 297-300.

O'Connell, M.J., Halliwell, B., Moorhouse C.P., Aruoma, O.I., Baum, H. & Peters, T.J. (1986a). *Biochem. J.* **234**, 727-731.

O'Connell, M.J., Ward, R.J., Baum, H. & Peters, T.J. (1985). *Biochem. J.* **229**, 135-139.

O'Connell, M.J., Ward, R.J., Baum, H., Treffry, A. & Peters, T.J. (1988). *Biochem. Soc. Trans.* **16**, 828-829.

Peter, H.H. (1985). In *Proteins of Iron Storage and Transport* (Spik, G., Montreuil, J., Crichton, R.R. & Mazurier, J., eds), pp. 293-303, Elseveir Science Publications, Amsterdam.

Powell, L.W., Alpert, E., Isselbacher, K.J. & Drysdale, J.W. (1974). *Nature* **250**, 333-335.

Price, D. & Joshi, J.G. (1982). *Proc. Natl. Acad. Sci. USA* **79**, 3116-3119.

Reynolds, L.G. (1989). In *Baillière's Clinical Haematology*, vol. 2, no. 2 (Hershko, C., ed), pp. 423-433, Baillière Tindall, London.

Richter, G.W. (1982). In *The Biochemistry and Physiology of Iron* (Saltman, P. & Hegenauer, J., eds), pp. 333-344, Elsevier North Holland, Inc.

Rohrer, J.S., Joo, M-S., Dartyge, E., Sayers, D.E., Fontaine, A. & Theil, E.C. (1987). *J. Biol. Chem.* **262**, 13385-13387.

Rohrer, J.S., Frankel, R.B., Papaefthymiou, G.C. & Theil, E.C. (1989). *Inorg. Chem.* **28**, 3393-3395.

Romslo, I. (1980). In *Iron in Biochemistry and Medicine, II* (Jacobs, A. & Worwood, M., eds), pp. 325-362, Academic Press, London.

Romslo, I., Konopka, K., Husby. P. & Ulvik, R.J. (1982). In *The Biochemistry and Physiology of Iron* (Saltman, P. & Hegenauer, J., eds), pp. 315-317, Elsevier North Holland, Inc.

Sayers, D.E., Theil, E.C. & Rennick, F.J. (1983). *J. Biol. Chem.* **258**, 14076-14079.

Schneider, W. (1988). *Chimia* **42**, 9-20.

Schwertmann, U. (1964). *Z. PflErnähr. Düng. Bodenk.* **105**, 194-202; cited in Carlson, L. & Schwertmann, U. (1987). *Wat. Res.* **21**, 165-170.

Schwertmann, U. & Murad, E. (1983). *Clays and Clay Minerals* **31**, 277-284.

Schwertmann, U. & Thalmann, H. (1976). *Clay Minerals* **11**, 189- 200.

Simpson, R.J. (1990). *Inorganic Biochemistry Discussion Group* Meeting, Abstract, Spring 1990.

Smith, J.M.A., Andrews, S.C., Guest, J.R. & Harrison, P.M. (1991). In Iron Biominerals (Frankel, R.B. & Blakemore, R.P., eds), pp. 325-337, Plenum Press, New York.

St. Pierre, T.G., Bell, S.H., Dickson, D.P.E., Mann, S., Webb, J., Moore, G.R. & Williams, R.J.P. (1986a). *Biochim. Biophys. Acta* **870**, 127-134.

St. Pierre, T.G., Dickson, D.P.E., Kirkwood, J.K., Ward, R.J. & Peters, T.J. (1987). *Biochim. Biophys. Acta* **942**, 447-451.

St. Pierre, T.G., Dickson, D.P.E., Webb, J., Kim, K.-S., Macey, D.J. & Mann, S. (1986b). *Hyperfine Interactions* **29**, 1427-1430.

St. Pierre, T.G., Mann, S., Webb, J., Dickson, D.P.E., Runham, N.W. & Williams, R.J.P. (1986c). *Proc. R. Soc. Lond. B* **228**, 31-42.

St. Pierre, T.G., Pollard, R.K., Dickson, D.P.E., Ward, R.J. & Peters, T.J. (1988). *Biochim. Biophys. Acta* **952**, 158-163.

St. Pierre, T.G., Webb., J. & Mann, S. (1989). In *Biomineralization, Chemical and Biochemical Perspectives* (Mann, S., Webb, J. & Williams, R.J.P., eds), pp. 294-344, VCH Weinheim (FRG), New York (USA).

Stiefel, E.I. & Watt, G.D. (1979). *Nature*, **279**, 81-83.

Stumm, W. & Giovanoli, R. (1976). *Chimia* **30**, 423-425, cited in Murray, J.W., Dillard, J.G., Giovanoli, R., Moers, H. & Stumm, W. (1985). *Geochim. et Cosmochim. Acta*, **49**, 463-470.

Stumm, W. & Morgan, J.J. (1970). *Aquatic Chemistry An Introduction Emphasizing Chemical Equilibria in Natural Waters*, pp. 525-558, John Wiley & Sons, Inc., New York.

Taylor, R.M. & Schwertmann, U. (1978). *Clays and Clay Minerals* **26**, 373-383.

Theil, E.C. (1987). In *Ann. Rev. Biochem.* **56**, 289-315.

Theil, E.C. & Aisen, P. (1987). In *Iron Transport in Microbes, Plants and Animals* (Winkelmann, G, vander Helm, D. & Neilands, J.B., eds), pp. 491-520, VCH Verlagsgesellschaft, Weinheim.

Torrance, J.D., Gillooly, M., Mills, W., Mayet, F. & Bothwell T.H. (1982). In *The Biochemistry and Physiology of Iron* (Saltman, P. & Hegenauer, J., eds), pp.819-820, Elsevier North Holland, Inc.

Towe, K.M. & Bradley, W.F. (1967). *J. Colloid Interface Sci.* **24**, 384-392.

Treffry, A. & Harrison, P.M. (1978). *Biochem. J.* **171**, 313-320.

Treffry, A. & Harrison, P.M. (1979). *Biochem. J.* **181**, 709-716.

Treffry, A., Harrison, P.M., Cleton, M.I., de Bruijn, W.C. & Mann, S. (1987). *J. Inorg. Biochem.* **31**, 1-6.

Van Nostrand's Scientific Encyclopedia. (1968). 4th. ed. D. Van Nostrand Co. Inc., Princeton, New Jersey.

Ward, R.J., O'Connell, M.J., Dickson, D.P.E., Reid, N.M.K., Wade, V.J., Mann, S., Bomford, A. & Peters, T.J. (1989). *Biochim. Biophys. Acta* **993**, 131-133.

Wardeska, J.G., Viglione, B. & Chasteen, N.D. (1986). *J. Biol. Chem.* **261**, 6677-6683.

Watt, G.D., Frankel, R.B., Papaefthymiou, G.C., Spartalian, K. & Stiefel, E.I. (1986). *Biochemistry* **25**, 4330-4336.

Watt, G.D., Jacobs, D. & Frankel, R.B. (1988). *Proc. Natl. Acad. Sci. USA* **85**, 7457-7461.

Webb, J. & Gray, H.B. (1974). *Biochim. Biophys. Acta* **351**, 224-229.

Weir, M.P., Gibson, J.F. & Peters, T.J. (1984). *Biochem. J.* **223**, 31-38.

Williams, J.M., Andrews, S.C., Treffry, A. & Harrison, P.M. (1986). *Hyperfine Interactions* **29**, 1447-1450.

Worwood, M. (1980). In *Iron in Biochemistry and Medicine, II* (Jacobs, A. & Worwood, M., eds), pp. 203-244, Academic Press, London.

Yang, C., Meagher, A., Huynh, B-H., Sayers, D.E. & Theil, E.C. (1987). *Biochemistry* **26**, 497-503.

Yariv, J., Kalb, A.J., Sperling, R., Bauminger, E.R., Cohen, S.G. & Ofer, S. (1981). *Biochem. J.* **197**, 171-175.

Volume 234, number 1, 69–72 FEB 06003 July 1988

Structural specificity of haemosiderin iron cores in iron-overload diseases

S. Mann, V.J. Wade, D.P.E. Dickson[+], N.M.K. Reid[+], R.J. Ward*, M. O'Connell* and T.J. Peters*

School of Chemistry, University of Bath, Bath BA2 7AY, [+]Department of Physics, University of Liverpool, Liverpool L69 3BX and **Division of Clinical Cell Biology, MRC Clinical Research Centre, Harrow, Middlesex HA1 3UJ, England*

Received 26 February 1988; revised version received 27 April 1988

Haemosiderin iron cores isolated from patients with secondary haemochromatosis have a goethite-like (α-FeOOH) crystal structure whereas those from patients with primary haemochromatosis are amorphous Fe (III) oxide. Haemosiderin cores isolated from normal human spleen are crystalline ferrihydrite ($5Fe_2O_3 \cdot 9H_2O$). The disease-specific structures are significantly different from the ferrihydrite structure of associated ferritin cores. The results are important in understanding the biological processing of iron in pathological states and in the clinical treatment of iron-overload diseases.

Hemosiderin; Iron-overload; Iron-core structure

1. INTRODUCTION

The iron storage proteins, ferritin and haemosiderin, consist of a non-haem iron complex associated with multiple polypeptides. Whereas both the iron complex and the protein constituents of ferritin have been extensively studied [1,2], the chemical and structural nature of haemosiderin remains to be determined even though this protein is of fundamental importance in various iron-overload diseases [3]. We report here, for the first time, the structural identification of the haemosiderin iron cores isolated from patients with primary (PH) (idiopathic haemochromatosis) and secondary haemochromatosis (SH) due to β-thalassemia treated by multiple transfusions. Our results show that the structure of the haemosiderin iron complexes is disease-specific and different from the ferrihydrite ($5Fe_2O_3 \cdot 9H_2O$) structure of associated ferritin cores. These results are important in understanding the biochemical mechanisms of iron processing in pathological states and in the clinical treatment of these diseases.

Correspondence address: S. Mann, School of Chemistry, University of Bath, Bath BA2 7AY, England

2. EXPERIMENTAL

Haemosiderin was isolated from two patient samples of PH iron-overloaded liver and from the livers or spleens of three patients with SH using methods described [5]. Ferritin was isolated from these tissues by conventional procedures [6]. Electron microscopy and selected area electron diffraction were undertaken using a Jeol 2000FX transmission electron microscope operating at 200 keV. ^{57}Fe Mössbauer spectra were recorded on a conventional constant acceleration spectrometer using a ^{57}Co in rhodium source. Protein and iron concentrations were determined by the method of Lowry et al. [12] and by flameless atomic absorption spectroscopy, respectively. Peptide analysis was undertaken using SDS-polyacrylamide gel electrophoresis (SDS-PAGE). The solubility of the iron cores in the presence of oxalate was determined by dialysis of matched Fe concentrations (80 μmol/l) against 0.2 M ammonium oxalate/oxalic acid at pH 3.0 and 25°C. The rate of Fe dissolution was determined by assaying the iron in the dialysate after various times by electrothermal atomic absorption spectroscopy.

Published by Elsevier Science Publishers B.V. (Biomedical Division)
00145793/88/$3.50

3. RESULTS

Iron/protein wt/wt ratios in the haemosiderins were 0.43 (PH) and 0.40 (SH). Peptide analysis of the haemosiderins by SDS-PAGE showed major bands of approx. 20 kDa (PH) and 15 kDa (SH). Although the 20 kDa band was similar to that observed for the ferritin peptides, the ultrastructure of the PH-derived haemosiderin, as shown by electron microscopy of the unstained protein, was clearly different from the discrete cores of ferritin isolated from the same tissue. The haemosiderin cores were of low electron density, extensively aggregated and irregular in morphology (fig.1a). In contrast, haemosiderin cores isolated from both the liver and spleen of SH patients were well-defined angular particles (fig.1b) which were less aggregated than the PH-derived material but less discrete than the associated ferritin cores.

The structural nature of the haemosiderin and ferritin cores was determined by electron diffraction and ^{57}Fe Mössbauer spectroscopy. Ferritin cores from all the samples studied showed ferrihydrite electron diffraction patterns (PH ferritin cores were generally less crystalline). Diffraction patterns of PH-derived liver haemosiderin showed only minimal evidence for long-range order; the one distinct diffraction line at 2.49 Å and two broadened lines centred around 2.12 Å and 1.53 Å (table 1) indicated that the material was primarily amorphous Fe(III) oxide with some partial ordering based on the ferrihydrite structure. In contrast, the electron diffraction patterns of both liver and spleen SH haemosiderin showed eight or nine diffraction lines. Although many of these lines could be assigned to either ferrihydrite or goethite (α-FeOOH), the diffraction lines at ~4.2 and 2.7 Å provided unequivocal evidence for the presence of goethite. However, some of the weaker goethite lines were absent, indicating that the SH haemosiderin was not perfectly ordered stoichiometric goethite but a defect microcrystalline phase.

The ^{57}Fe Mössbauer spectra of liver PH haemosiderin showed a predominant central doublet down to 4.2 K with substantial magnetically split six-line components only occurring below this temperature. This spectral behaviour combined with the isomer shift and quadrupole splitting parameters at 0.50 and 0.67 $m \cdot ms^{-1}$, respectively, is characteristic of a magnetically disordered high spin Fe(III) material and is consistent with the electron diffraction results. The distinct difference between the Mössbauer spectra of PH- and SH-derived haemosiderins can be seen in fig.2, which shows their 4.2 K spectra. The SH haemosiderin from both liver and spleen showed only a six-line magnetically ordered high spin Fe(III) spectral component at this temperature compared with the

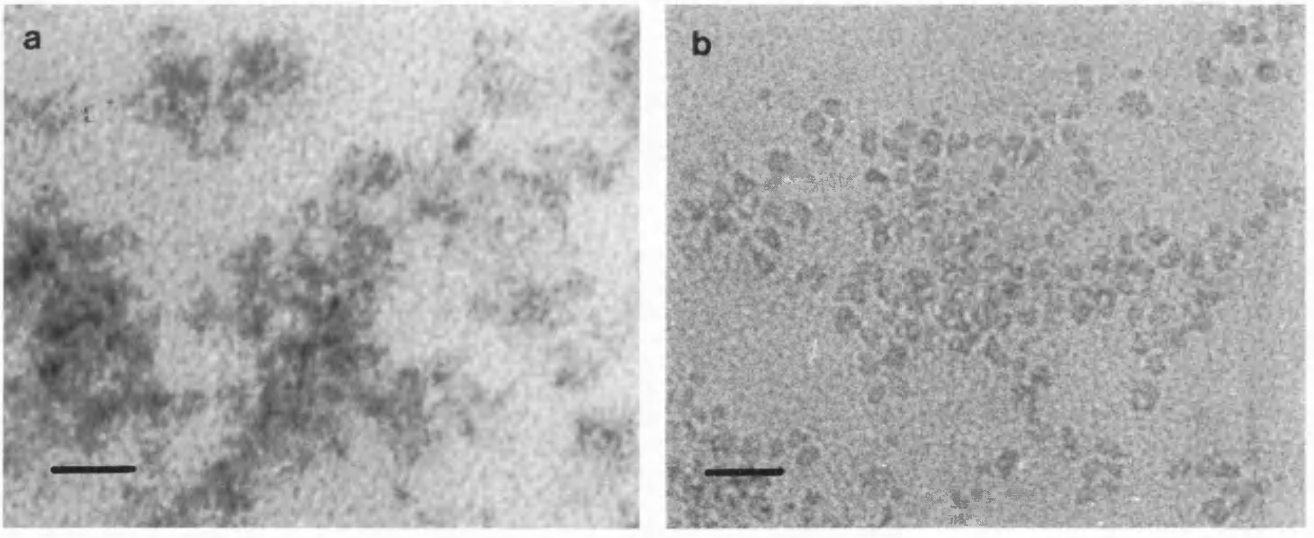

Fig.1. Transmission electron micrographs of (a) primary haemochromatosis liver haemosiderin (mean particle size = 5.8 nm; range, 5.36–6.31 nm) and (b) secondary haemochromatosis spleen haemosiderin (mean particle size = 5.6 nm; range, 4.33–6.50 nm). Scale bars = 20 nm.

Table 1

Electron diffraction data (d spacings (Å) and relative intensities) for haemosiderin isolated from iron-overloaded tissue

Primary haemochromatosis in liver	Secondary haemochromatosis			Ferritin (liver/spleen)
	Liver	Spleen		
	4.13 M	4.25 M	G	
	2.65 M	2.68 M	G	
2.49 S F	2.45 S	2.45 S	G/F	2.47 S F
	2.22 S	2.20 S	G/F	2.22 S F
2.12 B F	1.97 W	1.99 W	G/F	1.93 M F
	1.72 S	1.71 S	G/F	1.71 W F
		1.54 W	G	
1.53 B F	1.49 W	1.47 W	G/F	1.48 W F
	1.46 S	1.43 S	G	

Intensities: S, strong; M, medium; W, weak; B, broad band. Assignments made on the basis of known standard d spacings; G, goethite; F, ferrihydrite. Data for ferritin are shown for comparison

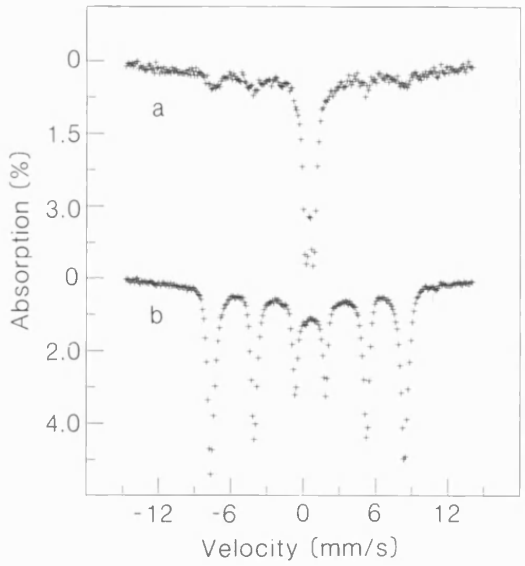

Fig.2. ^{57}Fe Mössbauer spectra recorded at 4.2 K of (a) primary haemochromatosis liver haemosiderin and (b) secondary haemochromatosis liver haemosiderin.

predominant doublet of the PH sample. The temperature dependence of the SH haemosiderin spectra (data not shown) was characteristic of a single Fe-containing phase consisting of small, magnetically ordered particles. This behaviour was qualitatively identical to that observed for the ferritin samples but the temperature at which the doublet and sextet components were equal in spectral intensity was approximately 65 K for the SH haemosiderin compared with 40 K for human ferritin [4], 28 K for horse haemosiderin [14] and 23 K for rat haemosiderin [7].

Dialysis of the protein cores against oxalate gave the following order in decreasing solubility: PH haemosiderin > PH ferritin > SH ferritin > SH haemosiderin (fig.3). Oxalate buffer was used as it is a standard analytical method for the preferential dissolution of mineralogical ferrihydrite over goethite and other iron oxides [8]. Similar results were obtained for dissolution experiments using clinically important chelators such as desferrioxamine (O'Connell, M., unpublished data).

The structural specificity of haemosiderin iron cores in PH and SH has important biochemical and biomedical implications. The general consensus in the literature is that haemosiderin is derived from ferritin by lysosomal degradation of its protein shell. For example, both horse, normal human (Dickson, D.P.E., unpublished data) [9,14] and rat [7,13] haemosiderins have structures and blocking temperatures consistent with ferrihydrite particles of smaller size than ferritin cores. However, our results indicate that this direct relationship does not apply to human haemosiderin and ferritin cores derived from iron-overloaded tissue. PH-derived liver haemosiderin arises from the uptake and storage of iron by the hepatocytes under conditions of enhanced absorption of dietary iron. The disordered nature of these cores indicates rapid intracellular iron precipitation presumably due to high local iron levels; consistent with this hypothesis is the poorly ordered ferrihydrite cores of the associated liver ferritin, and the presence of amorphous Fe(III) deposits in rat myocardial cells subjected to high iron concentrations in the growth media [10]. The major peptide band at 20 kDa and the extensive aggregation of the cores as viewed in the electron microscope suggest that although the protein is ferritin-like it is disorganised around and between the mineral particles. One possibility is that iron uptake by the hepatocytes is at such a high rate that non-specific deposition takes place external to apoferritin resulting in extensive protein-mineral aggregates.

The goethite-like structure of both liver and spleen SH haemosiderin cores is more ther-

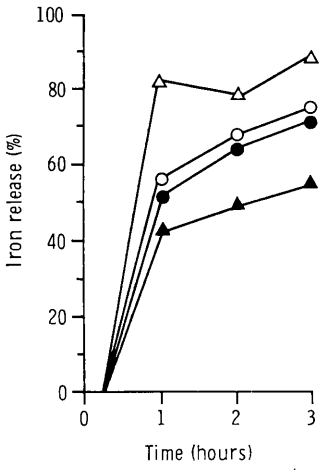

Fig.3. Dissolution of iron from iron-storage proteins. Primary haemochromatosis haemosiderin and ferritin (△,○) and secondary haemochromatosis haemosiderin and ferritin (▲,●), respectively.

modynamically stable than the ferrihydrite cores of ferritin, which suggests that the formation of these haemosiderin complexes takes place under conditions of slow crystallization, for example, from the slow oxidation of aqueous Fe(II) ions arising from low Fe(II) and O_2 concentrations, complexation, and low lysosomal pH. Alternatively, the slow degradation of Fe(III) complexes could favour goethite precipitation. Significantly, the in situ phase transformation of ferritin cores is not possible because the structures of goethite and ferrihydrite are not closely related. If ferritin is to be implicated, therefore, in the formation of SH haemosiderin it must be via chemical modification of the ferrihydrite cores. Since the source of iron in transfusional iron overload is from effete erythrocytes, the rate of processing of this iron by the reticuloendothelial (RE) system is likely to be relatively slow when compared with the dietary iron-overload of PH. Thus there is the possibility of normal ferritin uptake of iron followed by protein degradation (as shown by the 15 kDa band in SH haemosiderin) and (partial) dissolution of the ferritin cores in the lysosomes of the RE cells. The slow reprecipitation of the soluble iron within the lysosomes rather than mobilization via transferrin may reflect the saturation of this protein in the iron-overloaded system.

Finally, our results predict that the more crystalline goethite-like deposits of SH haemosiderin will be less labile than the corresponding deposits in PH and will therefore have a lower intrinsic toxicity as shown, for example, in the ability to mediate lipid peroxidation in the presence of ascorbate [11]. Also, the lower solubility of SH haemosiderin cores implies that they will be less readily removed by chelation therapy than predicted on the basis of ferrihydrite models. Furthermore, the results explain the anomalous magnetic properties of haemosiderin cores isolated from patients with SH [4].

REFERENCES

[1] Ford, G.C., Harrison, P.M., Rice, D.W., Smith, J.M.A., Treffry, A., White, J.L. and Yariv, J. (1984) Philos. Trans. R. Soc. B304, 551–565.
[2] Harrison, P.M., Andrews, S.C., Ford, G.C., Smith, J.M.A., Treffry, A. and White, J.L. (1987) in: Iron Transport in Microbes, Plants and Animals (Winkelmann, G., Van der Helm, D. and Neilands, J.B. eds) pp.445–475, VCH, Weinheim, New York.
[3] Seldon, C., Owen, M., Hopkins, J.M.P. and Peters, T.J. (1983) Br. J. Haematol. 44, 593–603.
[4] Bell, S.H., Weir, M.P., Dickson, D.P.E., Gibson, J.F., Sharp, G.A. and Peters, T.J. (1984) Biochim Biophys. Acta 787, 227–236.
[5] Weir, M.P., Gibson, J.F. and Peters, TJ. (1984) Biochem. J. 223, 31–38.
[6] Cham, B.E., Roeser, H.P., Nikles, A. and Ridgway, K. (1985) Anal. Biochem. 151, 561–565.
[7] Williams, J.M., Andrews, S.C., Treffry, A. and Harrison, P.M. (1986) Hyperfine Interactions 29, 1447–1450.
[8] Sidhu, P.S., Gilkes, R.J., Cornell, R.M., Posner, A.M. and Quirk, J.P. (1981) Clays Clay Miner. 29,269–276.
[9] Fischbach, F.A., Gregory, D.W., Harrison, P.M., Hoy, T.G. and Williams, J.M. (1971) J. Ultrastr Res. 37, 495–503.
[10] Bauminger, E.R., Iancu, T.C., Link, G., Pinsn, A. Hershko, C. (1987) Hyperfine Interactions 33 249–?
[11] O'Connell, M., Halliwell, B., Moorhouse, C. Aruoma, O.I., Baum, H. and Peters, TJ. (19 Biochem. J. 234, 727–731.
[12] Lowry, O.H., Rosebrough, W.J., Farr, A. and Ra R.J. (1951) J. Biol. Chem. 193, 265–275.
[13] Andrews, S.C., Brady, M.C., Treffry, A., W J.M., Mann, S., Cleton, M.I., De Bruijn, W. Harrison, P.M. (1988) Biol. Metals 1.
[14] Dickson, D.P.E., Pollard, R.K., Borsch-Iohns Ward, R.J. and Peters, T.J. (1988) Hy Interactions, in press.

Biochimica et Biophysica Acta, 957 (1988) 81–90
Elsevier

BBA 33227

Mössbauer spectroscopy, electron microscopy and electron diffraction studies of the iron cores in various human and animal haemosiderins

Dominic P.E. Dickson [a], Nicola M.K. Reid [a], Stephen Mann [b], Vanessa J. Wade [b], Roberta J. Ward [c] and Timothy J. Peters [c]

[a] *Department of Physics, University of Liverpool, Liverpool,* [b] *School of Chemistry, University of Bath, Bath and* [c] *Division of Clinical Cell Biology, MRC Clinical Research Centre, Harrow (U.K.)*

(Received 11 May 1988)

Key words: Haemosiderin; Iron overload; Mössbauer spectroscopy; Electron microscopy; Electron diffraction

Mössbauer spectroscopy has indicated significant differences in the iron-containing cores of various haemosiderins. In the present study, haemosiderin was isolated from a number of animal species including man. In addition, haemosiderin was isolated from patients with primary idiopathic haemochromatosis or with secondary (transfusional) iron-overload. The iron cores of the animal and normal human haemosiderin appear to be very similar by Mössbauer spectroscopy, and the electron diffraction data indicate a ferrihydrite structure similar to that of ferritin cores. The haemosiderin isolated from secondary iron-overload shows anomalous behaviour in its temperature-dependent Mössbauer spectra. This can be understood in terms of the microcrystalline goethite structure of the cores as indicated by electron diffraction. The haemosiderin cores obtained in the case of primary haemochromatosis have an amorphous Fe(III) oxide structure and show Mössbauer spectra characteristic of a magnetically disordered material, which only orders at very low temperatures.

Introduction

The iron storage proteins ferritin and haemosiderin consist of a central core of non-haem iron surrounded by a polypeptide outer shell. In haemosiderin, the outer protein shell may not form a complete envelope as in the case of ferritin. The iron-containing core and the protein shell of ferritin have been extensively studied and their composition and structure are well understood [1–2]. However, the chemical and structural nature of haemosiderin has not yet been fully determined even though this protein is of fundamental importance in iron-overload diseases [3].

Fischbach et al. [4] studied the structure of horse spleen haemosiderin and its relationship to ferritin, by X-ray diffraction, Mössbauer spectroscopy and electron microscopy. The results indicated that the structures of the cores of the two proteins were indistinguishable by X-ray diffraction or by the Mössbauer spectra at the temperatures used. However, the electron microscopy and X-ray diffraction results did indicate that the haemosiderin cores were generally smaller than those of the ferritin. In a more detailed Mössbauer spectroscopy and electron microscopy study Bell et al. [5] compared ferritin and haemosiderin extracted from iron-overloaded human spleen from

tions: SH, secondary haemochromatosis, PH, primary haemochromatosis.

dence: D.P.E. Dickson, Department of Physics, University of Liverpool, P.O. Box 147, Oliver Lodge Laboratory, Street, Liverpool L69 3BX, U.K.

β-thalassaemic patients with secondary haemochromatosis (SH). Again, the electron microscopy showed the haemosiderin cores to be somewhat smaller on average than the ferritin cores. In this study the Mössbauer spectra of the two materials were obtained at many different temperatures and showed important differences. These Mössbauer spectra showed the characteristic superparamagnetic behaviour of a magnetically ordered material in the form of small particles [6]. This leads to a temperature dependence, which is characterised by a mean superparamagnetic transition temperature or blocking temperature that is related to the product of a magnetic anisotropy constant (which depends on the nature of the particle material) and the particle volume. The haemosiderin showed a blocking temperature close to 70 K, compared with the value of around 40 K for the ferritin. As the core volumes were known to be smaller in the haemosiderin, this indicated a much higher value for the magnetic anisotropy constant for the haemosiderin and therefore significant differences in the nature of the iron-containing cores in the two cases.

In order to investigate the possible reasons for the anomalously high Mössbauer blocking temperature in SH haemosiderin, a Mössbauer study was carried out on ferritin following deproteinisation, sub-fractionation according to core size, and reconstitution of the iron core with and without phosphate [7]. None of these treatments produced any significant changes in the temperature dependence of the Mössbauer spectra, and this indicated that the high magnetic anisotropy constant of the SH haemosiderin must arise from some other significant difference in the composition or structure of the iron-containing cores.

Mössbauer studies of haemosiderin extracted from experimentally iron-overloaded rat livers [8] showed a blocking temperature of around 25 K, as might be expected for ferritin-like cores of somewhat smaller size, and this is consistent with Mössbauer data on whole livers from iron-overloaded rats [9]. Mössbauer studies of iron-overloaded tissue from other animal sources (Taractic hornbill and Spitsbergen reindeer) do not show evidence of any component with a high blocking temperature, like that of the SH human haemosiderin [9,10].

The results outlined above suggest that the haemosiderins found in different species and in different iron-overload situations may have significantly different iron cores. The aim of the present work is to investigate the iron cores of haemosiderins extracted from different species, and from human tissue under normal conditions and in various iron-overload situations. The Mössbauer spectroscopy data together with the particle size and morphology data from electron microscopy and the evidence from electron diffraction on crystallinity and structure, will provide complementary information on the structural nature of the haemosiderin cores. A preliminary report of this work and the results of a biochemical study of the different haemosiderins are presented elsewhere [11,12]. It should be noted that information on the nature of the iron cores of haemosiderin under different conditions of iron-overload may have considerable relevance for the understanding of the various iron-overload diseases and of their clinical treatment.

Experimental

Biochemical methods

Haemosiderin and ferritin were extracted from spleens and livers of horse (27y), Spitsbergen reindeer, human (76y), transfusional iron-overloaded (SH) and primary idiopathic haemochromatosis (PH) patients by conventional methods [13,14]. Additional details may be found elsewhere [12].

Mössbauer spectroscopy

^{57}Fe Mössbauer spectroscopy was carried out using a conventional constant acceleration spectrometer and a ^{57}Co in rhodium source. The samples were maintained at various low temperatures in liquid nitrogen and liquid helium bath cryostats, or in a continuous flow cryostat (Oxford Instruments). Temperatures were obtained from the vapour pressure of the cryogenic liquids or by means of a carbon-glass resistance thermometer. The spectra were calibrated using an iron metal foil at room temperature, and are plotted with the centre of the iron metal spectrum as the zero of the velocity axis.

Electron microscopy and electron diffraction

Unstained samples of ferritin and haemosiderin were prepared for transmission electron microscopy by air-drying drops of a solution of the sample onto nitrocellulose/carbon-coated copper electron microscopy grids. The ferritin samples were in 0.15 mol/l NaCl solution and the haemosiderin samples in 20 mmol/l tetramethyl ammonium hydroxide (pentahydrate, Aldrich Chemical Co.). The iron cores were examined in a Jeol 2000FX electron microscope operating at 200 keV. Electron diffraction patterns were recorded from areas of the grid which were well covered with sample, in order to obtain high diffraction intensities.

Measurements of the core diameters were made with calipers from electron micrographs (total magnification ≈ 500 k), 50 cores were measured for each histogram. The arithmetical mean diameter and standard deviation (S.D.), were calculated.

Results

Mössbauer spectroscopy

Horse and reindeer haemosiderin. Mössbauer spectra have been obtained from samples of haemosiderin extracted from the spleen and liver of horse and Spitsbergen reindeer. The variable temperature Mössbauer spectra of the horse spleen haemosiderin are shown in Fig. 1. They show the characteristic behaviour of a magnetically ordered material in the form of small particles, known as superparamagnetism [6]. The spectra show two components, a doublet and a sextet with the relative intensity of the sextet growing at the expense of the doublet as the temperature is lowered. The superparamagnetic transition temperature or blocking temperature, is defined as the temperature at which each component provides half of the total spectral intensity. The computer fits to the spectra shown in Fig. 1 give a value of approx. 28 K for the blocking temperature. Other Mössbauer parameters for these spectra are given in Table I. Spectra obtained from horse liver haemosiderin, and reindeer spleen and liver haemosiderin, showed very similar behaviour but with small variations in the blocking temperatures, which all lie between about 20 and 30 K. Mössbauer measurements on whole tissue samples were consistent

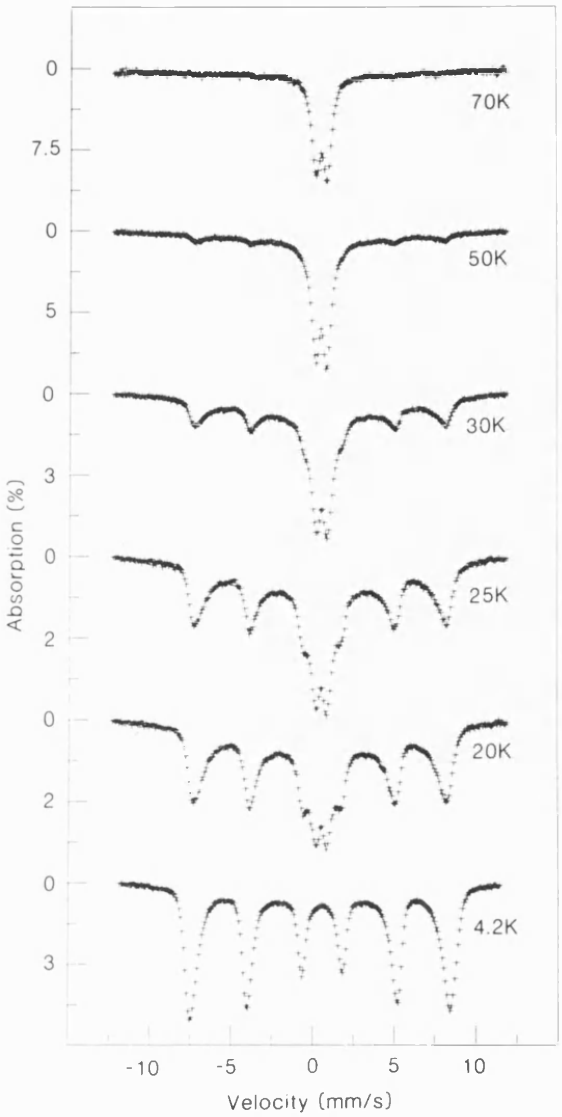

Fig. 1. Mössbauer spectra of horse spleen haemosiderin at various temperatures.

with those of the extracted haemosiderin. Further details of the Mössbauer study of these samples may be found elsewhere [15].

Normal human haemosiderin

Haemosiderin is not normally found in humans in significant quantities, except under conditions of iron-overload. However, a very small quantity of haemosiderin was obtained from a normal human spleen, from an old subject. Fig. 2 shows the Mössbauer spectra of this sample at 77, 20, 4.2 and 1.4 K. The spectra are very similar to those of the horse and reindeer haemosiderins and the

TABLE I

MÖSSBAUER HYPERFINE PARAMETERS AND BLOCKING TEMPERATURES OF THE VARIOUS HAEMOSIDERINS

Origin	Chemical shift (mm/s) at 77 K	Quadrupole splitting (mm/s) at 77 K	Hyperfine field (T) at 4.2 K	Blocking temperature (K)
Horse spleen [a]	0.48 ± 0.01	0.71 ± 0.01	49.5 ± 0.5	28
Normal human spleen	0.48 ± 0.01	0.72 ± 0.01	48.9 ± 0.5	≈ 20
SH human liver	0.48 ± 0.01	0.71 ± 0.01	49.7 ± 0.5	63
PH human liver	0.50 ± 0.01	0.67 ± 0.01	–	–

[a] Horse liver and the reindeer spleen and liver haemosiderins give values of the hyperfine parameters which are identical within the experimental errors, while the blocking temperatures all lie between 20 and 30 K.

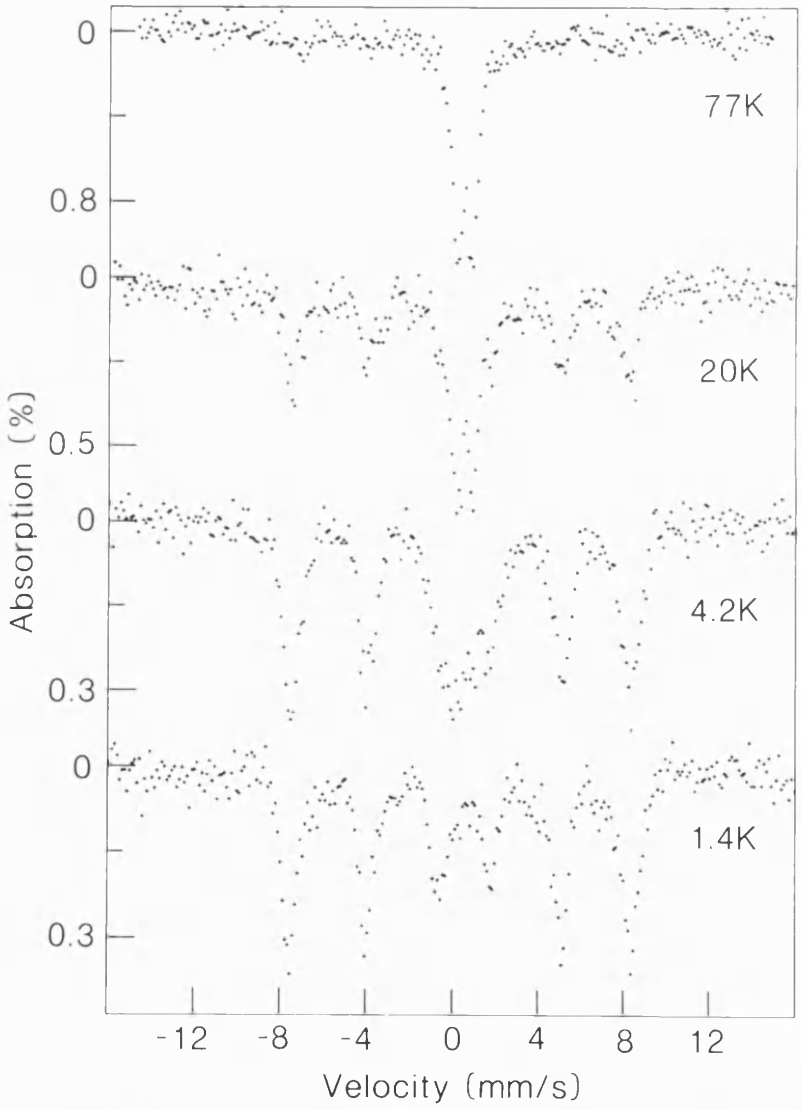

Fig. 2. Mössbauer spectra of normal human spleen haemosiderin at various temperatures.

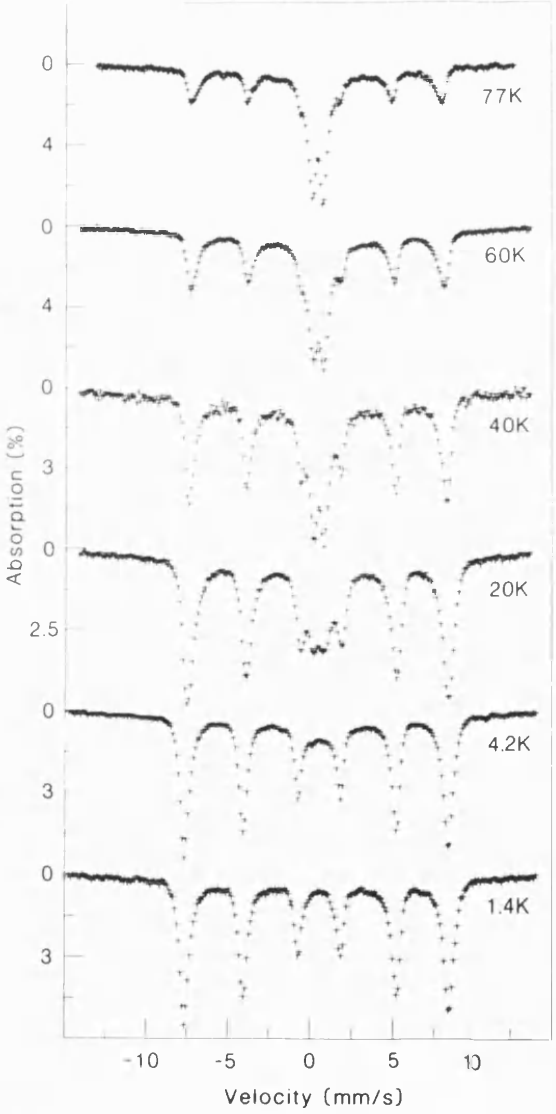

Fig. 3. Mössbauer spectra of SH liver haemosiderin at various temperatures.

computer fit to the 20 K spectrum gives a value of approx. 44% for the relative intensity of the doublet component at this temperature, indicating a blocking temperature of around 25 K. The Mössbauer hyperfine parameters, are given in Table I. Mössbauer spectra of the whole tissue were consistent with those of the extracted haemosiderin.

Secondary haemochromatosis haemosiderin

The variable temperature Mössbauer spectra of the SH haemosiderin extracted from liver are shown in Fig. 3. These are very similar to those of the spleen derived material already investigated [5]. Computer fits to give the relative intensity of the two spectral components as a function of temperature lead to a value of 63 K for the blocking temperature.

In both the previous work and in the present study, Mössbauer spectra were also obtained from samples of the whole tissue. In both cases the spectra of the whole tissue was consistent with the presence of a mixture of the haemosiderin and another material with a lower blocking temperature (presumably ferritin). These results clearly indicate that the (SH) haemosiderin with a Mössbauer blocking temperature of around 70 K is not an artifact of the extraction procedure and is found in both spleen and liver.

Primary haemochromatosis haemosiderin

The variable temperature Mössbauer spectra of a PH haemosiderin sample is shown in Fig. 4. The Mössbauer spectra are quantitatively and qualitatively very different from both those in Figs. 1 and 2, and those in Fig. 3. This can perhaps best be considered in terms of the changes that occur in the spectra between 77 and 4.2 K and the changes that occur below 4.2 K. At 77 K the spectrum consists solely of a doublet, while between 77 and 4.2 K a sextet component appears which corresponds to approx. 20% of the total spectral intensity at 4.2 K. Below 4.2 K the central doublet begins to broaden (cf. the difference between the 4.2 and 3 K spectra). At 1.4 K the intensity, that at 4.2 K was primarily associated with the central doublet, has become resolved into a broadened sextet component, which is different to the sextet component seen at 4.2 K. Thus these data suggest

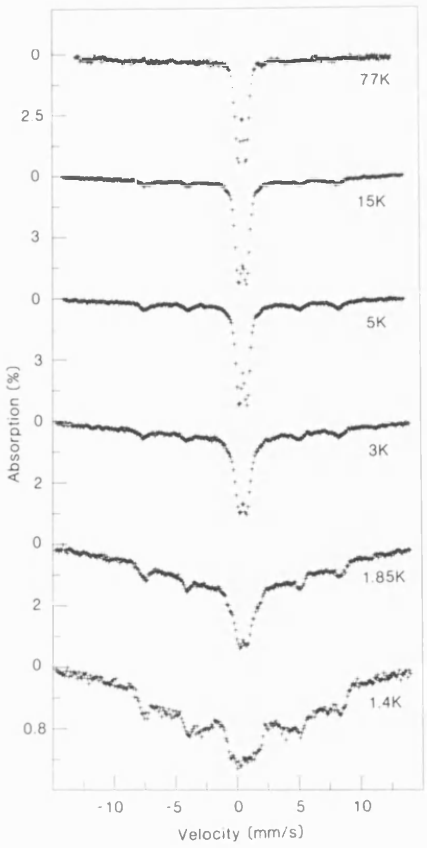

Fig. 4. Mössbauer spectra of PH liver haemosiderin at various temperatures.

the presence of two iron-containing species in this haemosiderin. One of these, corresponding to about 20% of the total iron present, appears to be rather similar to the animal and normal human haemosiderins discussed above, with a blocking temperature of around 15 to 20 K. The other, major component, does not show resolved magnetic splitting in the Mössbauer spectra until well below 4.2 K and the spectral behaviour is qualitatively different to superparamagnetism. This compound is similar in its Mössbauer behaviour to the bacterial ferritins from *Escherichia coli* [16] and *Pseudomonas aeruginosa* [17] and also to the iron-containing materials found in iron-overloaded heart cell cultures [18].

Mössbauer spectra obtained from a haemosiderin sample extracted from the liver of a different PH patient, showed precisely the same behaviour as the major component of the spectra shown in Fig. 4, but without the minor component which has been related above to the animal and

normal human haemosiderin. This confirms the importance of the magnetically disordered (except at very low temperatures) majority component as the predominant form of iron in primary haemochromatosis haemosiderin.

As in all the previous cases the consistency of the Mössbauer spectra of whole tissue samples with those of the extracted haemosiderin, confirmed that the extraction procedure did not produce any significant changes in the iron-containing cores. Mössbauer spectra of the ferritin extracted from the PH liver were consistent with the normal superparamagnetic behaviour of ferritin.

Electron microscopy and electron diffraction

Horse and reindeer haemosiderin. Electron micrographs of the horse and reindeer spleen haemosiderin showed discrete cores of irregular shape which were partially aggregated on the E.M. grid. Mean particle sizes were 6.12 nm (S.D. 0.51 nm) for the horse sample (Fig. 5a) and 5.88 nm (S.D. 0.81 nm) for the reindeer sample. Associated ferritin cores from horse spleen were discrete and spherical and of mean core diameter 7.22 nm (S.D. 0.44 nm).

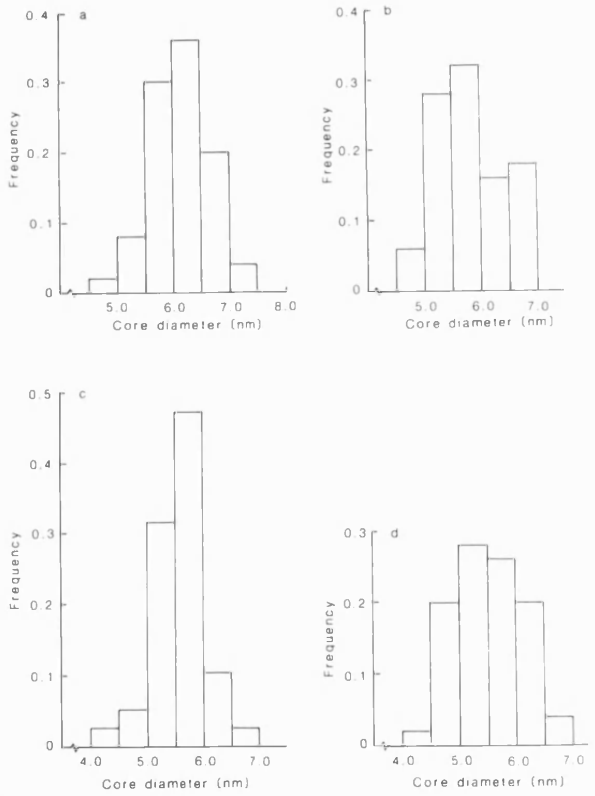

Fig. 5. Particle size distributions for: (a) horse spleen haemosiderin; (b) normal human spleen haemosiderin; (c) SH spleen haemosiderin; and (d) SH liver haemosiderin.

TABLE II

ELECTRON DIFFRACTION DATA

d-Spacings (nm) and relative intensities. Intensities; S, strong; M, medium; W, weak; B, broad band. Assignments made on the basis of known standard *d*-spacings; G = goethite, F = ferrihydrite.

Horse haemosiderin [a] spleen	PH haemosiderin liver	SH haemosiderin		SH ferritin
		spleen	liver	
		0.424 M	0.413 M G	
		0.268 M	0.265 M G	
0.250 S F	0.249 S F	0.245 S	0.245 S G/F	0.247 S F
0.224 S F		0.220 S	0.222 S G/F	0.222 S F
0.199 M F	0.212 B F	0.199 W	0.197 W F	0.196 M F
0.171 W F		0.171 S	0.172 S G/F	0.171 W F
		0.154 W	G	
0.151 W F	0.153 B F	0.147 W	0.149 W F	0.148 W F
0.146 S F		0.143 S	0.146 S F	0.144 S F

[a] Reindeer and normal human spleen haemosiderin gave only ferrihydrite *d*-spacings.

Electron diffraction patterns of both haemosiderin and ferritin isolated from horse spleen and reindeer spleen haemosiderin gave lines corresponding to well-ordered ferrihydrite ($5Fe_2O_3 \cdot 9H_2O$), (Table II).

Normal human haemosiderin. Electron microscopy of the normal human spleen haemosiderin showed its cores to be discrete, rather irregular in shape and partially aggregated on the E.M. grid (Fig. 6). The cores were less discrete than those of the SH spleen haemosiderin and more discrete than those of the SH liver haemosiderin. The mean particle size was 5.81 nm (S.D. 0.59 nm), see Fig. 5b.

Electron diffraction patterns gave *d*-spacings corresponding to well-ordered ferryhydrite (Table II).

Secondary haemochromatosis haemosiderin. Electron micrographs of the spleen and liver samples of SH haemosiderin showed the presence of discrete but aggregated iron cores (Fig. 7). In general the liver haemosiderin cores were less discrete and more rounded in shape than the spleen

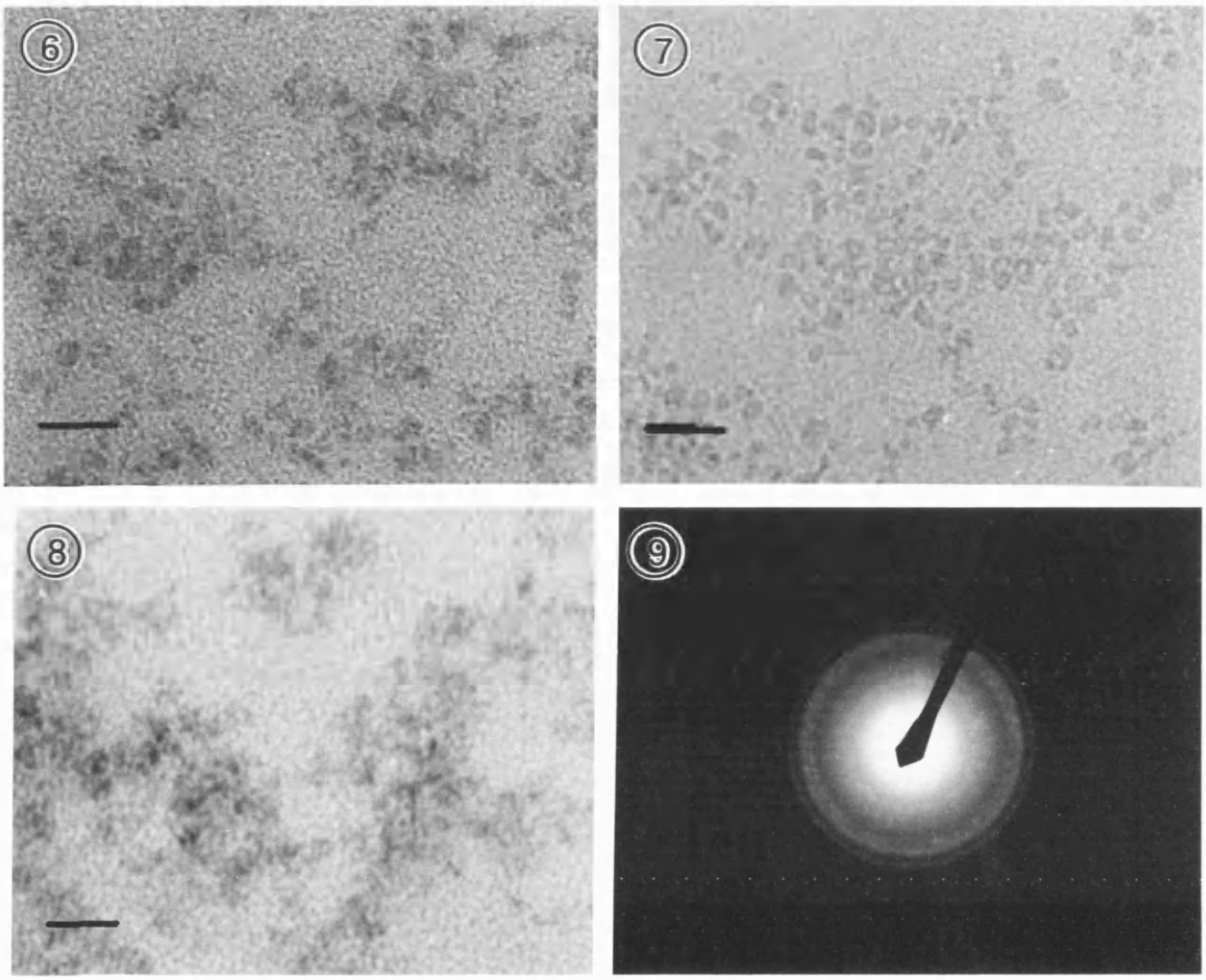

Figs. 6–9. (6) Electron micrograph of unstained normal human spleen haemosiderin. Scale bar = 20 nm. (7) Electron micrograph of unstained SH spleen haemosiderin. Scale bar = 20 nm. (8) Electron micrograph of unstained PH liver haemosiderin. Scale bar = 20 nm. (9) Electron diffraction pattern for SH spleen haemosiderin cores showing powder rings corresponding to a goethite (α-FeOOH) like crystal structure.

haemosiderin cores; the latter being more angular than the ferritin cores from the same tissue. The mean haemosiderin core diameters were 5.57 nm (S.D. 0.48 nm) and 6.14 nm (S.D. 0.43 nm) for the two spleen samples studied and 5.49 nm (S.D. 0.55) for the liver sample (Fig. 5c and d); the associated spleen and liver ferritin mean core diameters were 6.83 nm (S.D. 0.36 nm) and 6.39 nm (S.D. 0.48 nm), respectively.

Electron diffraction patterns from the SH haemosiderin cores were markedly different from the corresponding ferritin patterns, which all showed the ferrihydrite structure. The haemosiderin patterns had 6–9 diffraction lines with *d*-spacings and intensities different from the ferritin patterns (Fig. 9, Table II). For example, the 0.25 nm line of ferrihydrite was absent, possibly being split into the 0.268 and 0.245 nm lines; these lines are indicative of a goethite (α-FeOOH) phase. Also an increase in intensity of the ferrihydrite line at 0.170 nm was marked; α-FeOOH has a medium strong line at this *d*-spacing. Similarly the weak line at 0.420 nm, which is absent in the ferritin pattern, can be attributed to α-FeOOH.

Primary (idiopathic) haemochromatosis haemosiderin. Electron micrographs of PH haemosiderin (Fig. 8) revealed a very different material compared with the other samples studied. The iron cores were of low electron density, had a poorly defined irregular shape and were extensively aggregated on the E.M. grid. A few isolated particles were visible on the micrographs and had diameters ranging between 5.36 and 6.31 nm. The mean core size for the associated ferritin was 6.02 nm (S.D. 0.45 nm).

Electron diffraction analysis of this material showed the iron cores to be essentially amorphous. The electron diffraction patterns showed one line at 0.249 nm and two broad bands centred at 0.212 and 0.153 nm, suggesting the presence of a largely amorphous Fe(III) oxide with partial ordering based on the ferrihydrite structure. However, electron diffraction analysis of a second sample of PH haemosiderin showed no diffraction lines. These results are consistent with the Mössbauer data. The haemosiderin cores which showed weak ferrihydrite diffraction lines gave the spectra shown in Fig. 4, whereas the totally amorphous sample gave Mössbauer spectra with no evidence for the minor superparamagnetic phase.

Significantly, the ferritin isolated from the liver of the first PH patient comprised poorly ordered ferrihydrite (the electron diffraction pattern revealed only three lines at 0.245, 0.168 and 0.147 nm and a broad-band centred at 0.213 nm), in comparison with the well-ordered ferrihydrite structure of the SH liver ferritin.

Discussion

The Mössbauer spectroscopy, electron microscopy and electron diffraction data presented above give clear evidence for the existence of three different types of haemosiderin, which are distinguishable as a result of significant differences in their iron-containing cores.

Animal and normal human haemosiderin

The Mössbauer spectra of these samples are similar to those of ferritin at 77 and 4.2 K but show a different temperature dependence between these temperatures, with blocking temperatures in the region of around 20 to 30 K. This is what would be expected if the cores were structurally similar to those of ferritin but smaller, giving a lower average value of KV, the product of the magnetic anisotropy constant and the particle volume, and hence a lower blocking temperature. This is confirmed by the electron microscopy data, which clearly shows smaller particle sizes than in the case of ferritin. The electron diffraction data show diffraction patterns corresponding to a well-ordered ferrihydrite ($5Fe_2O_3 \cdot 9H_2O$) structure similar to that observed for ferritin.

Secondary haemochromatosis haemosiderin

The Mössbauer spectra show a much higher blocking temperature than for both ferritin, and animal and normal human haemosiderins. This cannot be explained in terms of particle size effects as the electron microscopy shows that the particles are on average smaller than those of ferritin and comparable with those of the other haemosiderins. There is a small particle-size effect, as the electron microscopy data show that the SH spleen haemosiderin has a slightly higher mean core size and a somewhat narrower size distribution for its iron-containing cores than the SH haemosiderin obtained from liver, and these differences are reflected in the Mössbauer data. However, the Mössbauer data indicate that there must be another much more significant difference in the iron containing cores of SH haemosiderin, leading to a much larger magnetic anisotropy constant.

This difference can be clearly seen in the electron diffraction data, with the SH haemosiderin giving diffraction rings similar to those of goethite (α-FeOOH). The diffraction pattern is, however, not identical to that of a well-crystallised mineral form of goethite and this indicates that the cores are essentially micro-crystalline with significant defects.

These data provide a clear explanation of the difference in the Mössbauer blocking temperatures, in that the more highly ordered goethite-like structure of SH haemosiderin cores leads to a higher value of the magnetic anisotropy constant. The magnetic anisotropy constant is related to magnetic differences between the crystal axes and could be expected to be greater in a more well-ordered system. Indeed there is clear evidence

from experiments involving spin reorientation by applied magnetic fields that goethite has a high magnetic anisotropy constant [19]. Thus the problem of the anomalously high blocking temperature in the Mössbauer spectra of SH haemosiderin is resolved.

Primary haemochromatosis haemosiderin

The Mössbauer spectra of PH haemosiderin (Fig. 4) are clearly very different from those of the other haemosiderins. These spectra indicate the presence of two iron species. One of these, the minority component, corresponding to about 20% of the total spectral intensity, is consistent with the spectra obtained from the normal human and animal haemosiderins. The other, majority component, only shows resolved magnetic ordering in its Mössbauer spectra at much lower temperatures below 2 K. This spectral behaviour is different from the normal superparamagnetic situation and is consistent with that observed both in certain bacterial ferritins and iron-loaded heart cell cultures. In heart cell cultures the Mössbauer spectra obtained are particularly similar to those presented here, with two components being apparent in the spectral behaviour as a function of temperature.

The electron diffraction data on one of the PH haemosiderin samples indicate that the iron-containing cores have a structure corresponding to poorly crystallised ferrihydrite and that they are therefore similar (except in degree of order) to those of the normal human and animal haemosiderins and also ferritin. This appears at first sight to be at variance with the Mössbauer data. However, there need be no conflict between the results of the two techniques if consideration is given to the way in which the various iron-containing species contribute to the data. In the case of Mössbauer spectroscopy, the spectrum is a summation of sub-spectra for every different type of iron atom present in the sample and, at low temperatures, to a very good approximation, the relative intensities of the different sub-components in the spectra are equal to the relative abundance of iron atoms in each type of chemical or physical environment. This is indeed one of the great strengths of Mössbauer spectroscopy compared with other techniques in that all forms of the Mössbauer active element contribute to the spectrum. However, in the case of electron diffraction, only ordered material will contribute to the diffraction pattern. Thus, while the electron diffraction data clearly show the presence of ferrihydrite-like material in the PH haemosiderin sample, this does not preclude the presence of additional amorphous iron-containing material which is electron diffraction 'silent' but which shows up in the Mössbauer spectra.

The above interpretation was confirmed by the data from a second PH haemosiderin sample which showed only one Mössbauer component, like that of bacterial ferritin, and correspondingly no electron diffraction lines, indicating that the haemosiderin iron cores are essentially amorphous.

Acknowledgements

The financial support of the Science and Engineering Research Council and the Medical Research Council is gratefully acknowledged.

References

1 Ford, G.C., Harrison, P.M., Rice, D.W., Smith, J.M.A., Treffry, A., White, J.L. and Yariv, J. (1984) Phil. Trans. R. Soc. Lond. B304, 551–565.
2 Harrison, P.M., Andrews, S.C., Ford, G.C., Smith, J.M.A., Treffry, A. and White, J.L. (1987) in Iron Transport in Microbes, Plants and Animals (Winkelmann, G., Van der Helm, D. and Neilands, J.B., eds.), pp. 445–475 VCH, Weinheim and New York.
3 Selden, C., Owen, M., Hopkins, J.M.P. and Peters, T.J. (1980) Br. J. Haematol. 44, 593–603.
4 Fischbach, F.A., Gregory, D.W., Harrison, P.M., Hoy, T.G. and Williams, J.M. (1971) J. Ultrastruct. Res. 37, 495–503.
5 Bell, S.H., Weir, M.P., Dickson, D.P.E., Gibson, J.F., Sharp, G.A. and Peters, T.J. (1984) Biochim. Biophys. Acta 787, 227–236.
6 Mørup, S., Dumesic, J.A. and Topsøe, H. (1980) in Applications of Mossbauer Spectroscopy, Vol. II (Cohen, R.L., ed.), pp. 1–53, Academic Press, New York.
7 St. Pierre, T.G., Pollard, R.K., Dickson, D.P.E., Ward, R.J. and Peters, T.J. (1988) Biochim. Biophys. Acta 952, 158–163.
8 Williams, J.M., Andrews, S.C., Treffry, A. and Harrison, P.M. (1986) Hyperfine Interactions 29, 1447–1450.
9 St. Pierre, T.G., Dickson, D.P.E., Kirkwood, J.K., Ward, R.J. and Peters, T.J. (1987) Biochim. Biophys. Acta 924, 447–451.
10 Dickson, D.P.E., Meagher, A., Nilssen, K.J. and Borch-Iohnsen, B. (1987) Biochim. Biophys. Acta 924, 442–446.

11 Mann, S., Wade, V.J., Dickson, D.P.E., Reid, N.M.K., Ward, R.J. and Peters, T.J. (1988) FEBS Lett. 234, 69–74.
12 Ward, R.J., O'Connell, M.J., Dickson, D.P.E., Reid, N.M.K., Wade V.J., Mann, S., Bomford, A. and Peters, T.J. (1988) Biochim. Biophys. Acta, in press.
13 Weir, M.P., Gibson, J.F. and Peters, T.J. (1984) Biochem. J. 223, 31–38.
14 Chan, B.E., Roeser, H.P., Nikles, A. and Ridgway, K. (1985) Anal. Biochem. 151, 561–565.
15 Dickson, D.P.E., Pollard, R.K., Borch-Iohnsen, B., Ward, R.J. and Peters, T.J. (1988) Hyperfine Interactions 41, 889–892.
16 Bauminger, E.R., Cohen, S.G., Dickson, D.P.E., Levy, A., Ofer, S. and Yariv, J. (1980) Biochim. Biophys. Acta 623, 237–242.
17 St. Pierre, T.G., Bell, S.H., Dickson, D.P.E., Mann, S., Webb, J., Moore, G.R. and Williams, R.J.P. (1986) Biochim. Biophys. Acta 870, 127–134.
18 Bauminger, E.R., Iancu, T.C., Link, G., Pinson, A. and Hershko, C. (1987) Hyperfine Interact. 33, 249–262.
19 Meagher, A., Pankhurst, Q.A. and Dickson, D.P.E. (1986) Hyperfine Interact. 28, 533–536.

Reprinted from Nature, Vol. 349, No. 6311, pp. 684–687, 21st February, 1991

Synthesis of inorganic nanophase materials in supramolecular protein cages

Fiona C. Meldrum, Vanessa J. Wade, Duncan L. Nimmo, Brigid R. Heywood & Stephen Mann*

School of Chemistry, University of Bath, Bath BA2 7AY, UK

THERE is currently great interest in the synthesis of inorganic materials of nanometre dimensions. The small size of these particles endows them with unusual structural and optical properties that may find application in catalysis and electro-optical devices. Such materials may also prove valuable as precursor phases to strong ceramics. Many approaches to the synthesis of these materials have focused on constraining the reaction environment through the use of surface-bound organic groups[1], polymers[2,3], porous glasses[4,5], zeolites[6], phospholipid vesicles[7,8] and reverse micelles[9]. Nanometre-sized particles may also be produced *in vivo* by microorganisms[10]. Here we describe a novel synthetic route based on the use of a supramolecular protein structure as a reaction cage in which to form inorganic phases. We show that the iron-storage protein ferritin can be used to generate nanometre-sized iron sulphide particles by *in situ* reaction of the iron oxide core of the native ferritin. Discrete nanoscale particles of manganese and uranium oxo-species can also be formed in the protein cavity. Our results highlight the potential of adapting natural biomineralization processes to problems in materials science, and suggest that the use of biological molecules and their synthetic analogues in mediating solid-state reactions constitutes a promising approach to nanophase engineering.

Ferritin is a robust iron-storage protein that can withstand high temperatures (85 °C) and pH (8.5–9) for limited periods without significant disruption of its quaternary structure of 24 polypeptide subunits. These subunits are assembled into a hollow sphere of 8–9 nm internal diameter[11] which contains an iron oxide core of structure similar to that of the mineral ferrihydrite ($5Fe_2O_3 \cdot 9H_2O$). Hydrophilic and hydrophobic channels penetrate the protein shell and provide the means by which iron atoms can be accumulated within or removed from the molecules. *In vitro* reconstitution of iron (III) oxide cores can be readily achieved by room-temperature incubation of the intact empty protein (apoferritin) protein with Fe(II) solutions at moderate pH[12].

Figure 1 illustrates the general reaction schemes adopted in this work. Three approaches were undertaken: (*a*) *in situ* chemical reaction of native iron oxide cores with molecules and ions capable of penetrating into the internal cavity; (*b*) redox-driven reactions involving metal-ion uptake and deposition in apoferritin molecules; and (*c*) ion binding and hydrolytic polymerization of metal ions within apoferritin.

Following approach (*a*), iron sulphide particles were generated within ferritin by reaction of de-aerated solutions of the native protein (Cd-free, Boehringer Horse Spleen Ferritin) in 0.1 M AMPSO buffer (3-[(1,1-dimethyl-2-hydroxyethyl)amino]-2-hydroxypropanesulphonic acid), at pH 8.5 with H_2S. A black solution was formed within 20 s. A similar discolouration was observed for the reaction with Na_2S at pH 8.0, except that the formation of iron sulphide was significantly slower. In both cases, no bulk precipitation was observed, indicating that iron sulphide had been produced within the ferritin cavity by reaction of the native iron oxide cores. In comparison, analogous reactions involving synthetically prepared ferrihydrite suspensions resulted in an immediate black discolouration, followed within minutes by a black precipitate. Samples from the ferritin reaction were mounted onto carbon- and formvar-coated-nickel electron

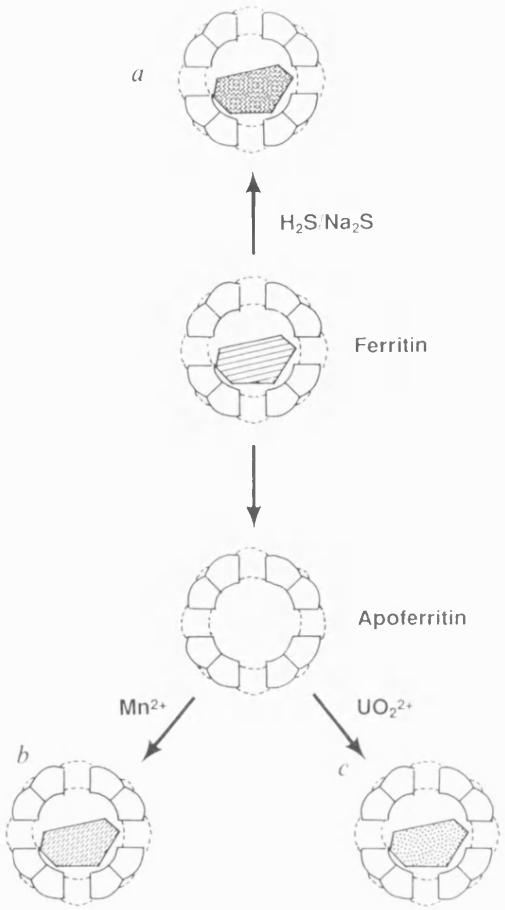

FIG. 1 Schematic representation of the use of ferritin in the synthesis of nanophase materials. *a*, Iron sulphide formation by *in situ* reaction of native iron oxide cores. *b*, Manganese oxide reconstitution by redox-driven reactions within apoferritin. *c*, Uranyl oxyhydroxide deposition by ion-binding and hydrolytic polymerization.

microscope grids and were studied immediately to minimize reoxidation reactions. Analysis was carried out by transmission electron microscopy (TEM), electron diffraction (ED) and energy-dispersive X-ray analysis (EDXA). Whereas the control experiments described above produced gel-like aggregates of amorphous iron sulphide, the protein samples showed discrete electron-dense cores (Fig. 2*a*) containing iron and sulphur (Fig. 2*b*). The particles formed in the H_2S preparation were irregular in shape, whereas those formed in the presence of Na_2S were generally spherical. The mean particle size and standard deviation were 6.8 nm and 1.2 nm, and 7.8 nm and 1.1 nm, for the H_2S and Na_2S samples respectively. Before reaction, the ferritin cores were spherical with a mean core diameter of 7.8 nm and standard deviation of 0.6 nm. This suggests that some iron may have been lost from the core on reaction with H_2S. EDXA analysis showed that the Fe/S ratio was close to unity for the H_2S product but was much greater for the Na_2S-derived particles, suggesting only partial reaction in the latter system. This is consistent with the electron diffraction patterns, which showed that some residual well crystallized ferrihydrite (six diffraction lines), characteristic of the original native ferritin core, was present in the iron sulphide cores formed by reaction with Na_2S. In contrast, the electron-dense cores prepared by addition of H_2S gave only three weak, broad ferrihydrite lines, demonstrating considerable loss in crystallinity on reaction. No diffraction lines corresponding to crystalline iron sulphides were observed.

These results indicate that *in situ* transformation of ferritin iron oxide cores to discrete nanometre-sized iron sulphide particles can be readily achieved. Reaction with gaseous H_2S occurs

* To whom correspondence should be addressed.

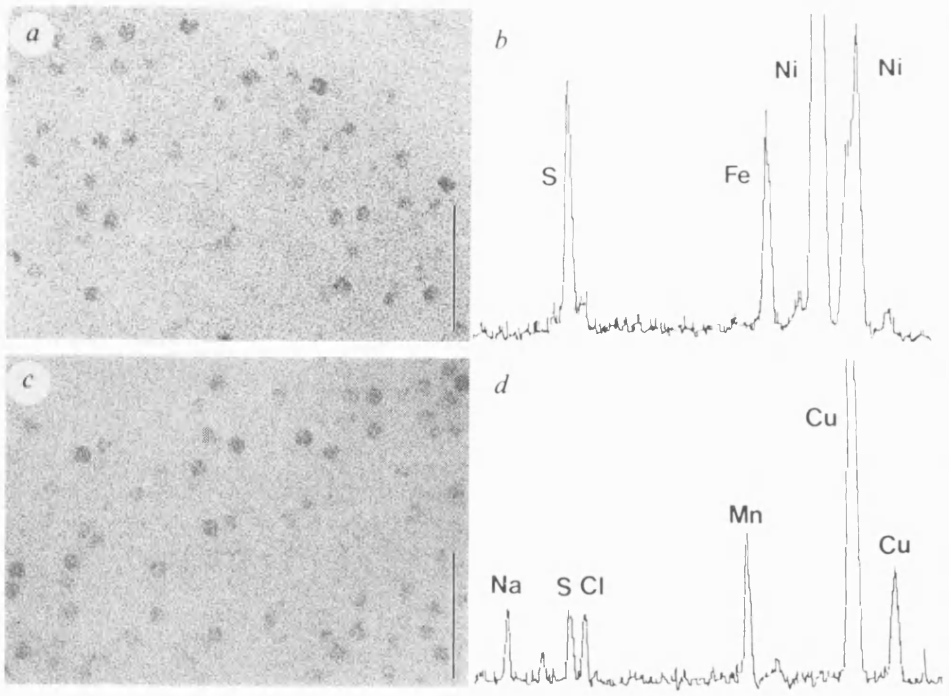

FIG. 2 TEM micrographs and corresponding EDXA spectra of iron sulphide cores (*a*, *b*) and manganese oxide cores (*c*, *d*) of ferritin. Scale bars in *a* and *c*, 50 nm. Ni and Cu peaks arise from the electron microscope grids; Na, Cl and S are background peaks from salt and buffer solutions.

more readily than with Na_2S, the latter giving mixed iron oxide and sulphide cores. This is probably due to more rapid penetration of the protein shell by the neutral H_2S molecules compared with charged HS^-/S^{2-} species.

Approach (*b*) was based on the reconstitution of apoferritin molecules with redox-active metal ions such as Mn(II). Apoferritin was prepared by repeated dialysis of ferritin solutions against a 0.5% solution of thioglycollic acid in 0.1 M sodium acetate buffer (pH 4.5), followed by dialysis against 0.15 M NaCl solution. Reconstitution of the protein to a theoretical value of 4,000 Mn ions per molecule was undertaken by combining buffered apoferritin solutions with $MnCl_2 \cdot 4H_2O$ solutions at pH values of 8.0–9.2. At pH 9, a fine-grained dark brown precipitate was observed in the protein-free control experiment after 4 h whereas the protein solution was a clear light brown colour, indicating specific deposition of manganeses oxides within the protein cavity. Experiments at lower pH were left for longer periods (up to two weeks). All reconstitutions showed evidence of some non-specific precipitation outside the protein cage.

Samples for TEM were either centrifuged and dialysed against 0.15 M NaCl or passed down a Sephadex G-25 chromatography column followed by reconcentration using an ultrafiltration cell. Discrete electron-dense particles of regular morphology, with mean size and standard deviation of 7.14 nm and 0.46 nm respectively, were imaged (Fig. 2*c*). EDXA spectra showed that the cores contained manganese (Fig. 2*d*). Electron diffraction patterns suggested that the manganese oxide cores were amorphous. By contrast, the non-specific product precipitated outside the protein cavities was identified as a mixture of the crystalline oxides groutite (α-MnOOH) and hausmannite (Mn_3O_4).

Bimetallic cores were prepared by similar experiments involving the successive addition of Fe(II) and Mn(II) solutions to apoferritin at pH 6.5 and pH 8.5 respectively. The resulting cores were discrete nanometre-size particles that contained both iron and manganese (data not shown). Electron diffraction patterns indicated that the Fe and Mn phases of individual cores were present as crystalline ferrihydrite and an amorphous oxide respectively. The influence of manganese on the magnetic properties of the ferrihydrite phase is currently under investigation.

These results indicate that apoferritin molecules can be reconstituted specifically with Mn(II) in a way similar to that commonly used for Fe(II)[12]. Mn(II) is known to bind to apoferritin

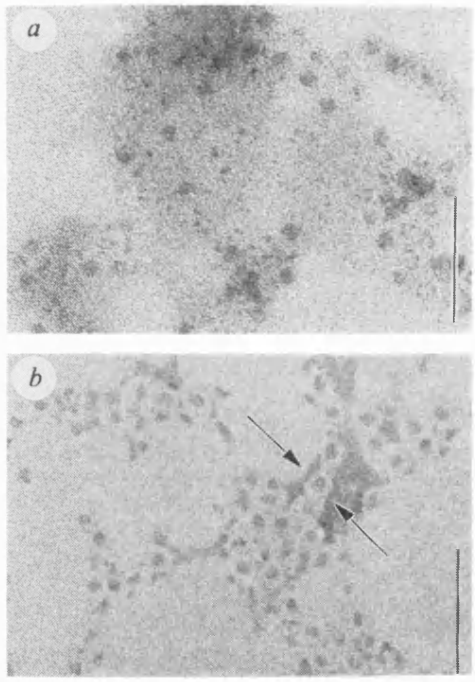

FIG. 3 *a*, TEM micrograph of apoferritin reconstituted with uranyl acetate, showing discrete cores of uranyl oxyhydroxide. *b*, As for *a*, but also showing evidence of negative staining of the external surface of the protein shell (arrows). Scale bars, 50 nm.

with a stoichiometry of 8 ions per molecule[13], suggesting an initial binding site in the threefold channel. This site is presumably not involved in oxide deposition, which must involve migration of the manganese cations into the central cavity.

We have conducted similar experiments with other redox-active metal ions such as Ti(III), Co(II) and Cr(II). The results were less conclusive than those for the Mn(II) experiments. TEM analysis showed some evidence of reconstitution with Ti(III) and Cr(II), but the cores were very small and poorly defined. Effective reconstitution of the apoferritin molecules

may depend on establishing the appropriate balance between many kinetic processes involving ion uptake, oxidation and polymerization, and factors such as ion concentrations, pH and redox potential may have to be carefully controlled in these reactions.

Finally, we have explored the possibility of using hydrolytic polymerization reactions as a basis for inorganic precipitation within the apoferritin cavity (Fig. 1*c*). The uranyl cation, UO_2^{2+}, is known to bind to apoferritin with a stoichiometry of 12 ions per molecule[14], possibly suggesting binding at the subunit dimer interface on the internal surface of the protein. A solution of $UO_2(O_2CCH_3)_2$ was added to apoferritin in 0.8 M TES (N-tris[hydroxymethyl]methyl-2-aminoethanesulphonic acid) at pH 8 in the dark to give a theoretical loading of 4,000 U atoms per apoferritin molecule. A yellow gel was formed after 24 h in both the protein and protein-free experiments. Analysis of the protein sample by TEM showed discrete electron-dense cores of mean diameter 6 nm (Fig. 3*a*), whereas similar analysis of the control experiment showed no discrete particles. Some cores showed associated staining of their surrounding protein coats by external UO_2^{2+} binding (Fig. 3*b*). No evidence of crystallinity in the polymerized uranyl oxyhydroxide was obtained.

Thus, supramolecular protein cages have the potential to act as constrained reaction environments in the synthesis of inorganic materials of nanometre dimension. The recent success in expressing human H-chain mutant ferritins[15] provides a possible route to the chemical tailoring of the inner surface of the protein cavity. We plan to investigate the use of such proteins in the oriented nucleation of spatially confined, crystallographically specific nanophase materials. □

Received 13 December 1990; accepted 17 January 1991.

1. Steigerwald, M. *et al. J. Am. chem. Soc.* **110,** 3046–3050 (1988).
2. Rossetti, R., Ellison, J. L., Gibson, J. M. & Brus, L. E. *J. chem. Phys.* **80,** 4464–4469 (1984).
3. Wang, Y., Liu, H. & Jiang, Y. *J. chem. Soc. chem. Commun.* 1878–1879 (1989).
4. Ekimov, A. I., Efros, Al. L. & Onushchenko, A. A. *Solid St. Commun.* **56,** 921–924 (1985).
5. Borrelli, N. F. *et al. J. appl. Phys.* **61,** 5399–5409 (1987).
6. Herron, N. *et al. J Am. chem. Soc.* **111,** 530–540 (1989).
7. Mann, S., Hannington, J. P. & Williams, R. J. P. *Nature* **324,** 565–567 (1986).
8. Heywood, B. R., Fendler, J. H. & Mann, S. *J. Colloid Interface Sci.* **138,** 295–298 (1990).
9. Inouye, K. *et al. J. phys. Chem.* **86,** 1465–1469 (1982).
10. Dameron, C. T. *et al. Nature* **338,** 596–597 (1989).
11. Ford, G. C. *et al. Phil. Trans. R. Soc. Lond.* B **304,** 551–565 (1984).
12. Macara, I. G., Hoy, T. G. & Harrison, P. M. *Biochem. J.* **126,** 151–162 (1972).
13. Wardeska, J. G., Viglione, B. & Chasteen, N. D. *J. biol. Chem.* **261,** 6677–6683 (1986).
14. Harrison, P. M. *et al.* in *Iron Transport in Microbes, Plants and Animals* (eds Winkelman, G., Van der Her, D. & Neilands, J. B.) 445–475 (VCH Publishers, New York, 1987).
15. Levi, L. *et al. J. biol. Chem.* **263,** 18086–18092 (1988).

Reprinted from *J. Mol. Biol.* (1991) **221**, 1443–1452

Influence of Site-directed Modifications on the Formation of Iron Cores in Ferritin

Vanessa J. Wade, Sonia Levi, Paolo Arosio, Amyra Treffry, Pauline M. Harrison and Stephen Mann

J. Mol. Biol. (1991) **221**, 1443–1452

Influence of Site-directed Modifications on the Formation of Iron Cores in Ferritin

Vanessa J. Wade[1], Sonia Levi[2], Paolo Arosio[2], Amyra Treffry[3] Pauline M. Harrison[3] and Stephen Mann[1]†

[1]*School of Chemistry, University of Bath Bath BA2 7AY, U.K.*

[2]*Department of Biomedical Science and Technology, University of Milano San Raffaele Hospital, Milano, Italy*

[3]*Department of Molecular Biology and Biotechnology University of Sheffield Sheffield S10 2TN, U.K.*

(Received 7 March 1991; accepted 27 June 1991)

The structure and crystal chemical properties of iron cores of reconstituted recombinant human ferritins and their site-directed variants have been studied by transmission electron microscopy and electron diffraction. The kinetics of Fe uptake have been compared spectrophotometrically. Recombinant L and H-chain ferritins, and recombinant H-chain variants incorporating modifications in the threefold (Asp131 → His or Glu134 → Ala) and fourfold (Leu169 → Arg) channels, at the partially buried ferroxidase sites (Glu62,His65 → Lys,Gly), a putative nucleation site on the inner surface (Glu61,Glu64,Glu67 → Ala), and both the ferroxidase and nucleation sites (Glu62,His65 → Lys,Gly and Glu61,Glu64,Glu67 → Ala), were investigated. An additional H-chain variant, incorporating substitution of the last ten C-terminal residues for those of the L-chain protein, was also studied. Most of the proteins assimilated iron to give discrete electron-dense cores of the Fe(III) hydrated oxide, ferrihydrite ($Fe_2O_3.nH_2O$). No differences were observed for variants modified in the three- or fourfold channels compared with the unmodified H-chain ferritin. The recombinant L-chain ferritin and H-chain variant depleted of the ferroxidase site, however, showed markedly reduced uptake kinetics and comprised cores of increased diameter and regularity. Depletion of the inner surface Glu residues, whilst maintaining the ferroxidase site, resulted in a partially reduced rate of Fe uptake and iron cores of wider particle size distribution. Modification of both ferroxidase and inner surface Glu residues resulted in complete inhibition of iron uptake and deposition. No cores were observed by electron microscopy although negative staining showed that the protein shell was intact. The general requirement of an appropriate spatial charge density across the cavity surface rather than specific amino acid residues could explain how, in spite of an almost complete lack of identity between the amino acid sequences of bacterioferritin and mammalian ferritins, ferrihydrite is deposited within the cavity of both proteins under similar reconstitution conditions.

Keywords: ferritin; iron storage proteins; iron biomineralization

1. Introduction

The iron storage protein, ferritin, comprises a spherical shell of 24 polypeptide subunits surrounding an inorganic core of hydrous iron (III) oxide (Ford *et al.*, 1984; Thomas *et al.*, 1988). The functional specificity of the protein is considered to be due to several factors. These include selective transport of reactants into the protein shell *via* molecular channels, site-specific catalytic oxidation of Fe(II) and nucleation of the Fe(III) oxide on the cavity surface (Harrison *et al.*, 1989). Most of the earlier studies, however, used horse-spleen ferritin which, like most ferritins, is a heteropolymer of two types of polypeptide chain, designated H and L (Arosio *et al.*, 1977). As these types show only 55%

† Author to whom all correspondence should be addressed.

0022-2836/91/201443-10 $03.00/0

identity in amino acid sequences (Boyd *et al.*, 1985) it has been difficult to assess in detail the structure/function properties of the molecule.

Recent successes in expressing recombinant human H-chain (rHF†: Levi *et al.*, 1987, 1988) and recombinant human L-chain (rLF: Levi *et al.*, 1989*b*; Thomas *et al.*, 1988) homopolymer ferritins in *Escherichia coli*, combined with structural studies (Lawson *et al.*, 1989, 1991), have resulted in significant advances in our understanding of the functional differences in these subunit types. Although both homopolymers had the capacity to incorporate iron, rHF exhibited iron uptake and ferroxidase kinetics severalfold faster than rLF (Levi *et al.*, 1988, 1989*b*). Lawson *et al.* (1989, 1991) have identified the ferroxidase centre ligands as Glu27, Glu62 and His65 which are embedded within each of the four-helix bundles comprising the subunits. Together with several neighbouring residues, these amino acids are present in all known H-chains but absent in ferritin L-chains. Site-directed modifications, namely Glu62 → Lys and His65 → Gly (H to L subunit changes), resulted in complete loss of ferroxidase activity in the rHF protein although core formation did occur, albeit slowly, at pH 7·0.

Engineering of rHF ferritins at sites other than the ferroxidase centre has been undertaken (Levi *et al.*, 1989*a*; Treffry *et al.*, 1989). Interestingly, modifications in the H and L-chain conserved hydrophilic threefold channel (Asp131, Glu134 → His) resulted in a 70% reduction in the rate of core formation (Treffry *et al.*, 1989) whilst a change in the hydrophobic fourfold channel (His173 → Leu: H to L subunit change) had minimal effect on Fe uptake (Levi *et al.*, 1989*a*).

The studies on recombinant ferritins suggest that one possible mechanism of selective Fe uptake lies with the specific H-chain ferroxidase activity (Levi *et al.*, 1989*b*, Lawson *et al.*, 1989, 1991). The proposed Fe(II) oxidation site is approximately seven to ten Å (1 Å = 0·1 nm) from the internal surface and communication with the external and internal environments may be possible by means of narrow channels through the interior of the subunits; this channel is blocked in L-chain ferritins (Lawson *et al.*, 1991). However, it is significant that iron cores can be reconstituted *in vitro* under relatively high Fe/protein ratios in ferritins lacking ferroxidase centres (Levi *et al.*, 1989*b*; Lawson *et al.*, 1989). This suggests that the inner surface of the cavity has a nucleation capacity higher than that in bulk solution since non-specific hydrolytic polymerization is not generally observed. Although a specific nucleation centre has not been identified, carboxylate ligands have been implicated in several studies (Chasteen & Theil, 1982; Levi *et al.*, 1989*a*; Treffry *et al.*, 1977; Wetz & Crichton, 1976; Yang *et al.*, 1987). One possibility is that a cluster of carboxylate residues on the inner surface serves as a domain for the stabilization of incipient nuclei (Ford *et al.*, 1984; Mann *et al.*, 1986). A potential candidate for such a nucleation centre is the inner surface grouping of residues Glu61,Glu64,Glu67 which are conserved in both H and L-chains and are known to serve as ligands for metal binding (Harrison *et al.*, 1987, 1989; Lawson *et al.*, 1991).

In the work presented here we have investigated the influence of homopolymer types and site-directed modifications in recombinant ferritins on the reconstitution of iron cores *in vitro*. We describe the crystal chemical properties of the reconstituted cores and their corresponding kinetics of iron uptake. We have determined the structure, size and shape of cores deposited in rLF, rHF and rHF variants altered in threefold or fourfold channel sites, depleted in ferroxidase activity and/or modified in respect to the putative nucleation site described above. The results indicate that extensive modifications need to be made to the protein shell in order to prevent core formation. The amino acid modifications studied did not influence the structure of the iron biomineral although the absence of the ferroxidase centre ligands resulted in a small, but significant, increase in core diameter. The effect of these modifications on the kinetics of a multi-step pathway to core formation is discussed.

2. Materials and Methods

(a) *Ferritins and variants*

Human rHF and rLF were expressed and isolated as previously described (Levi *et al.*, 1988, 1989*b*; Treffry *et al.*, 1989). Rat rLF was obtained according to Thomas *et al.* (1988). Human liver ferritin (HLF: Levi *et al.* 1988) and human brain ferritin (HBF: Dedman, Treffry & Harrison, unpublished results) were prepared by standard methods. Human rHF variants were obtained, purified and treated for iron removal according to methods described (Luzzago & Cesareni, 1989; Levi *et al.* 1987, 1988, 1989*a*).

(b) *Reconstitution procedures*

Apoferritins were reconstituted by addition of ferrous ammonium sulphate solutions under controlled conditions to give calculated loadings of 2000 Fe atoms/molecule (Macara *et al.*, 1972). Where possible, variants and controls were reconstituted on the same day using the same batch solutions. In all, 3 methods were used

(i) *Method 1*

Reconstitution of apoferritins (0·5 to 1 mg/ml) in 0·1 M-Hepes (pH 7·0) was achieved by the addition of 5 increments of 1·0 to 2·0 mM-$(NH_4)_2Fe(SO_4)_2$ solution, 20 min apart, at room temperature. The protein solutions were kept at 4°C for 18 h and then dialysed against 1 mM-desferrioxamine to remove any non-specific oxidation products followed by dialysis against 50 mM-Hepes (pH 7·0). A similar procedure but using apoferritins (0·2 mg/ml) in 0·1 M-MOPS (pH 7·0) and without desferrioxamine treatment was also used.

(ii) *Method 2*

As for method 1 except that the increments were added 1 week apart.

† Abbreviations used: rHF, recombinant H-chain ferritin; rLF, recombinant L-chain ferritin; HLF, human liver ferritin; HBF, human brain ferritin.

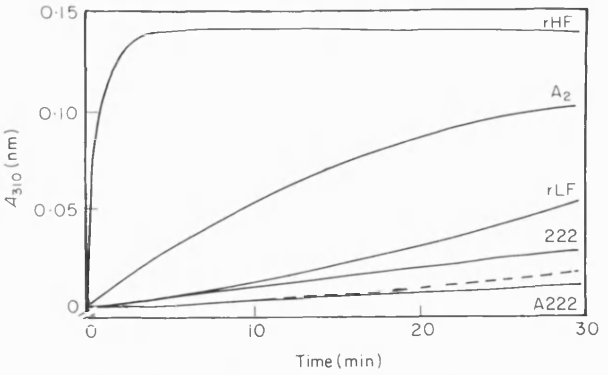

Figure 1. Iron uptake plots for recombinant homopolymer and human H-chain variant ferritins. A2, modifications on cavity surface (Glu61,Gly64,Glu67 → Ala); 222, ferroxidase site (Glu62,His65 → Lys,Gly); A222, cavity surface and ferroxidase centre (Glu61,Glu64,Glu67 → Ala + Glu62,His65 → Lys,Gly). Broken line is the control without ferritin.

(iii) *Method 3*

Reconstitution of apoferritins (0·5 mg/ml) in 0·05 M-MES (pH 6·45) was achieved by the addition of 20 increments of 0·1 mM $(NH_4)_2Fe(SO_4)_2$ solution, 15 min apart at room temperature.

In all 3 methods the kinetics of Fe uptake were determined spectrophotometrically at 310 nm as described by Levi *et al.* (1988).

(c) *Electron Microscopy*

Unstained samples of reconstituted proteins were prepared for electron microscopy by air-drying small drops of a solution of the sample onto nitrocellulose/carbon-coated copper electron microscopy grids. These were examined in a Jeol 2000FX transmission electron microscope operating at 100 keV. Electron diffraction patterns were recorded from selected areas well-covered with ferritin cores in order to obtain high diffraction intensities. A calibrated camera length of 80 cm was used. Measurements of core diameters were made with callipers from enlarged electron micrographs. Particle size distributions were made by measurement of 50 protein iron-cores.

Stained images of protein molecules were obtained by incubating electron microscopy grids containing air-dried samples with 1·5% (w/v) sodium silicotungstate solution for 1 min at room temperature followed by washing with distilled water.

3. Results

(a) *Recombinant H and L-chain ferritins and heteropolymer ferritins*

The kinetics of Fe uptake were significantly faster for rHF than rLF (Fig. 1) as described elsewhere (Levi *et al.*, 1988, 1989*b*). However, in both cases, the corresponding electron micrographs of unstained ferritins showed discrete electron-dense cores (Fig. 2) indicating specific reconstitution.

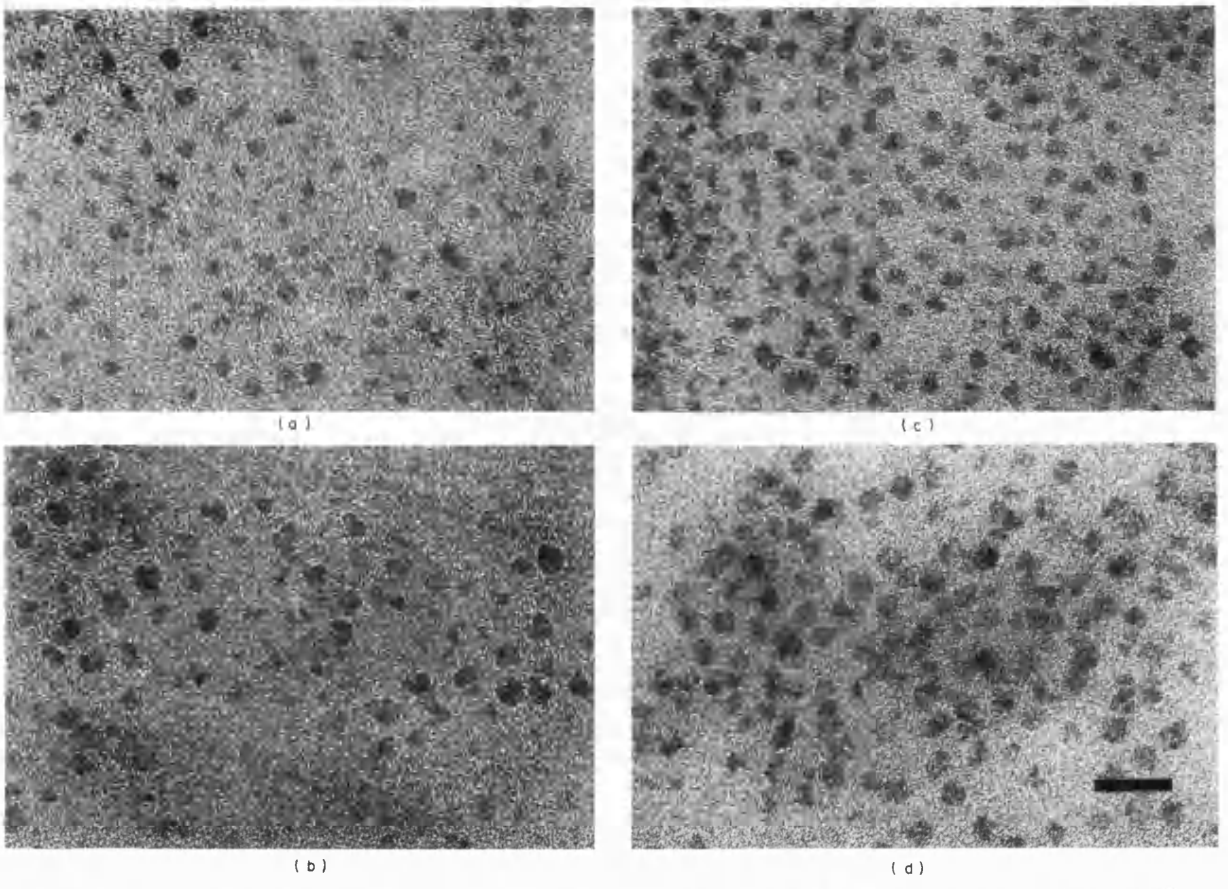

Figure 2. Transmission electron micrographs of unstained iron cores of reconstituted human ferritins. (a) rHF, (b) rLF, (c) HBF, (d) HLF. Scale bar represents 20 nm in all micrographs.

Table 1

Particle size data for reconstituted recombinant homopolymer ferritins and heteropolymer proteins

Method	Protein	Mean†	Range†
1	rHF	4·79	2·80–6·72
	rLF	5·36	3·30–7·19
	HLF	4·57	2·63–6·67
2	rat-rLF	5·78	3·82–7·06
3	rHF	4·48	2·68–6·20
	HBF	4·84	2·68–6·61
	HLF	5·40	3·49–7·02

rHF, Recombinant H-chain ferritin; rLF, recombinant L-chain ferritin; HBF, human brain ferritin (60% H: 40% L); HLF, human liver ferritin (10% H: 90% L).

†Values in nm.

Electron diffraction patterns from both samples were similar, consisting of four or five lines at *d* spacings, 0·25 nm, 0·228 nm, 0·204 nm and 0·15 nm. Reconstitution by method 3 compared with method 1 gave better-resolved lines indicative of increased crystallinity. However, in all cases the structure of the iron cores was consistent with the mineral, ferrihydrite ($9Fe_2O_3 \cdot 5H_2O$) (Towe & Bradley, 1967).

There were some significant differences in shape and size of the iron cores independent of the method of reconstitution. Human rHF cores were smaller in mean diameter (Table 1) than the rLF cores and were generally irregular in morphology. By contrast, there was a distinct population of large cores in reconstituted rLF that were spherical in shape. The particle size distribution of rLF was shifted to higher core diameters than for rHF and there was evidence of a slightly bimodal distribution in the former (Fig. 3). The iron cores of rat rLF (Fig. 3, Table 1) mirrored those of human rLF but with an even larger mean diameter possibly due to the change in reconstitution procedure.

Comparison of recombinant homopolymers with reconstituted native proteins of variable H/L ratio were in general agreement with the observation that an increased percentage of the L-chain resulted in larger, well-defined iron cores. For example, using reconstitution method 3, rHF, HBF and HLF gave discrete electron-dense cores (Fig. 2) with the mean core diameters increasing in the sequence rHF < HBF < HLF (Table 1, Fig. 3). Furthermore, HLF, unlike rHF and HBF, exhibited a bimodal distribution similar to rLF. These differences were not so apparent, however, for reconstitution method 1 (Table 1).

(b) *rHF variants*

Table 2 lists the recombinant human rHF variants used in this study. They include a crystallization variant involving a modification (Lys86 → Gln: Treffry *et al.*, 1989, Lawson *et al.*, 1989) which was further modified in the threefold channels (Asp131 → His or Glu134 → Ala) (Treffry *et al.*, 1989), depleted of the ferroxidase centre (Glu62,His65 → Lys,Gly: Lawson *et al.*, 1989), or depleted in both the ferroxidase and putative nucleation sites (Glu61,Glu64,Glu67 → Ala + Glu62,His65 → Lys,Gly: Arosio, unpublished results). Modifications to the rHF protein included changes in the fourfold channel (Leu169 → Arg or His173 → Leu) (Luzzago & Cesareni, 1989; Levi *et al.*, 1989*a*) and depletion of the putative nucleation site (Glu61,Glu64,Glu67 → Ala: Arosio, unpublished results).

Table 2

List of recombinant human H-chain variant ferritins

Site	Mutation
Loop	Lys86 → Gln†
Channel	
3-fold‡	Asp131 → His
	Glu134 → Ala
4-fold	Leu169 → Arg
	His173 → Leu§
Ferroxidase‡	Glu62 → Lys + His65 → Gly
Nucleation	Glu61,Glu64,Glu67 → Ala
Ferroxidase and nucleation‡	Glu62 → Lys + His65 → Gly + Glu61,Glu64,Glu67 → Ala

†This substitution, which does not effect iron uptake, was introduced to enable crystallization.

‡Modifications made on the crystallization variant (Lys86 → Gln).

§Last 10 residues of the carboxy terminus were substituted for the L-chain residues.

Previous iron uptake data (Levi *et al.*, 1989*a*, Treffry *et al.*, 1989) have shown that the crystallization and fourfold channel variants exhibit kinetic properties similar to those of rHF, and modifications in the threefold channel appear partially to reduce the rate of Fe uptake. A significant reduction was observed for the variant depleted of three inner surface glutamate residues (Fig. 1). By contrast, markedly reduced kinetics were observed for the variant lacking ferroxidase activity (Fig. 1) although core formation did appear to take place. However, the variant modified in both the ferroxi-

Table 3

Particle size data for reconstituted recombinant H-chain ferritin variants

Method	Protein	Mean†	Range†
1	rHF	4·48	3·04–6·70
	Leu169 → Arg	4·84	2·70–6·68
	His173 → Leu	4·55	2·87–6·24
	rHF	4·30	2·77–5·74
	Glu61,Glu64,Glu67 → Ala	4·19	2·08–5·91
	Lys86 → Gln	4·65	2·84–6·27
	Asp131 → His	4·35	2·40–5·98
	Glu134 → Ala	4·18	2·25–6·06
1	rHF	4·31	3·01–6·20
	Lys86 → Gln	4·13	2·79–5·63
	Glu62 → Lys,His65 → Gly	4·85	2·62–6·85
	(rLF)	(4·80)	(2·63–6·57)
2	Lys86 → Gln	3·63	2·40–6·10
	Glu62 → Lys,His65 → Gly	4·76	2·71–6·46

Data are grouped according to individual sets of experiments.

†Values in nm.

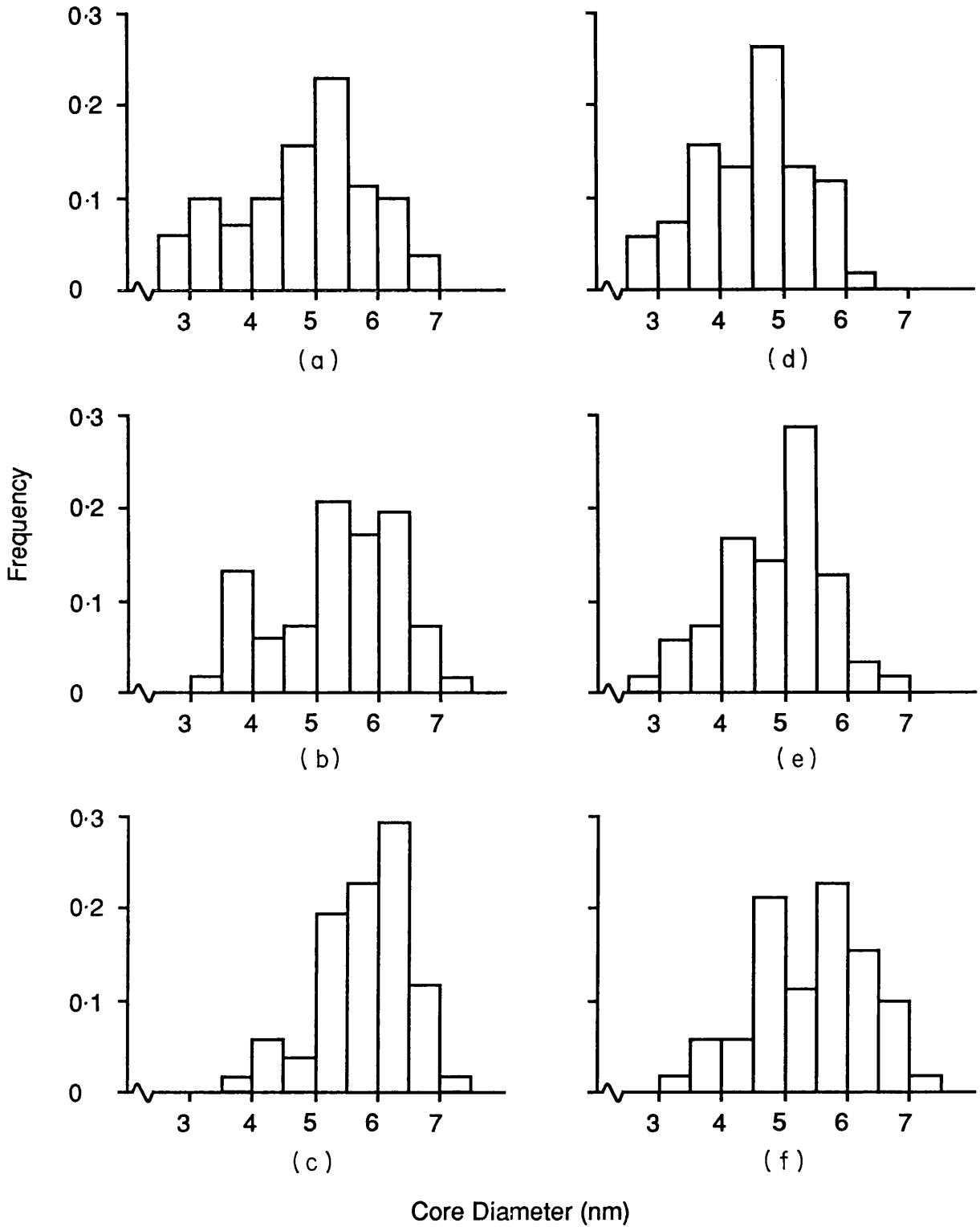

Figure 3. Particle size distributions for, (a) rHF (method 1), (b) rLF (method 1), (c) rat rLF (method 2), (d) rHF (method 3), (e) HBF (method 3), (f) HLF (method 3).

dase and inner surface glutamate sites showed negligible Fe uptake (Fig. 1) and the reconstitution was associated with extensive precipitation of iron oxide in bulk solution.

Electron micrographs of reconstituted (method 1) ferritins modified in the fourfold channel or inner surface glutamate residues were compared with those of a rHF sample (control). In each case, discrete electron-dense cores were imaged (Fig. 4) which gave diffraction patterns corresponding to poorly crystalline ferrihydrite. No differences in mineral structure were determined. Mean diameters and particle size ranges (Table 3) were similar for each sample. The modification, Glu61,Glu64,

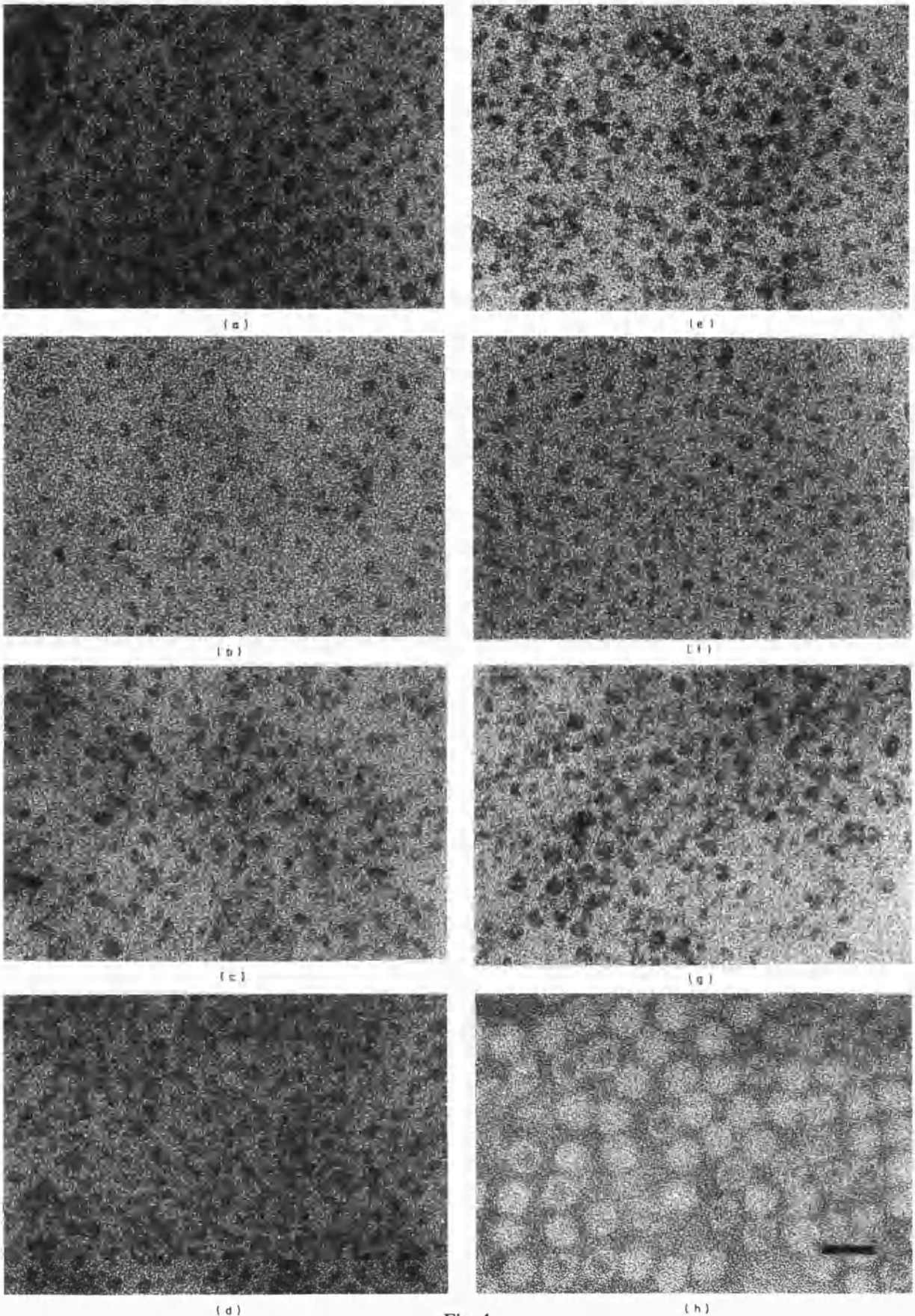

Fig. 4.

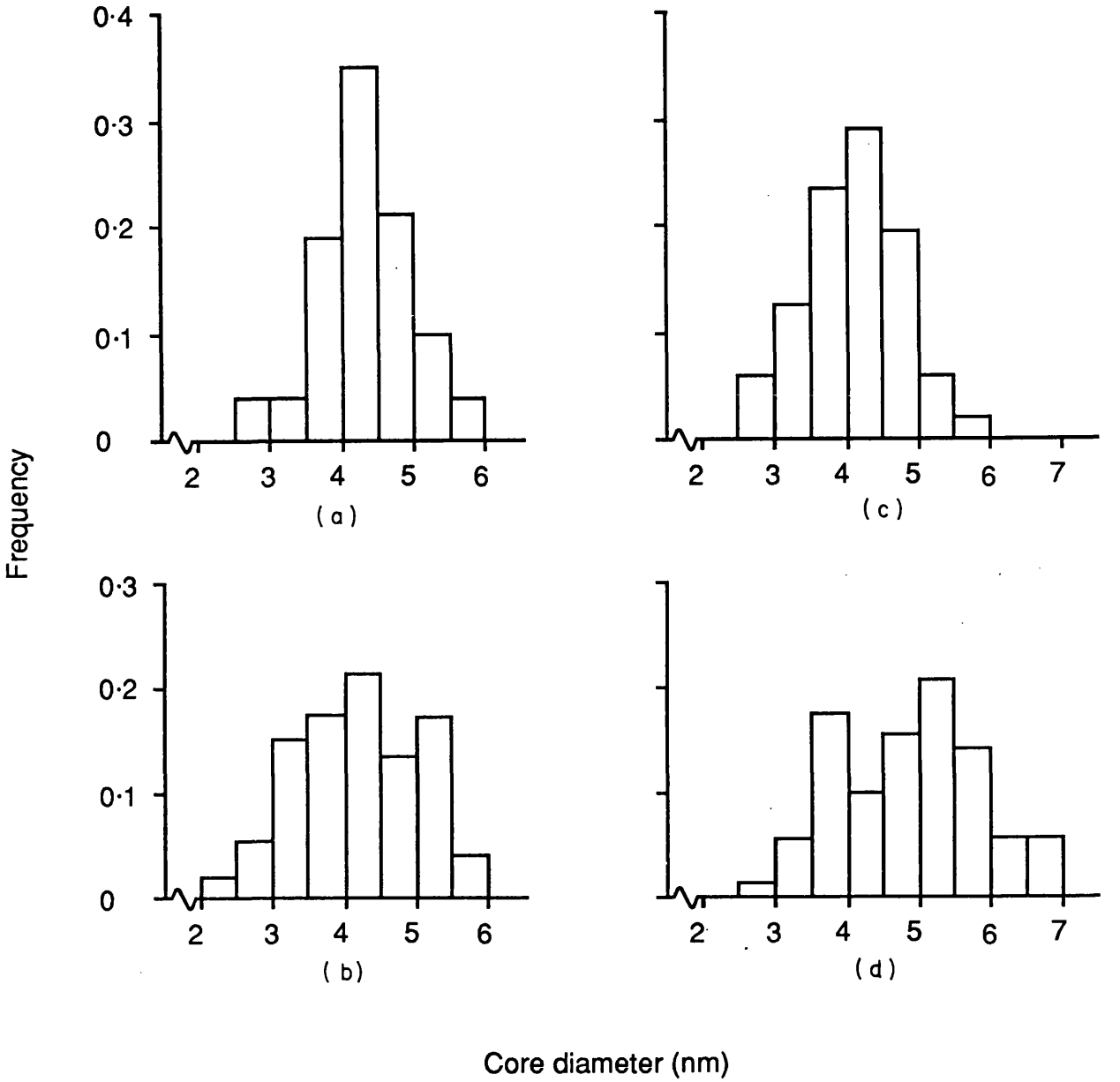

Figure 5. Particle size distributions for, (a) rHF, (b) variant Glu61,Glu64,Glu67 → Ala, (c) variant Lys86 → Gln and (d) variant Glu62,His65 → Lys,Gly. All proteins were reconstituted by method 1.

Glu67 → Ala, however, resulted in a broadening of the core size distribution due to an increased number of cores with diameters less than 3·5 nm (Fig. 5). Thus, although modification of the inner surface glutamate residues results in significant kinetic reduction of iron uptake, the variant remains functional presumably through its retained ferroxidase centre.

Mutations superimposed on the loop (crystallization) modification resulted in discrete electron-dense cores when imaged in the electron microscope (Fig. 4). No structural differences were observed for different variants and the electron diffraction data were identical to the ferrihydrite patterns obtained for the rHF-derived proteins. Mean core sizes and particle size ranges are shown in Table 3. There was some variability in the absolute values of these data from samples reconstituted by different methods or

Figure 4. Transmission electron micrographs of iron cores of reconstituted rHF variants. Modifications include, (a) 4-fold channels, Leu169 → Arg, (b) 4-fold channels, His173 → Leu, (c) cavity surface, Glu61,Glu64,Glu67 → Ala, (d) loop, Lys86 → Gln, (e) 3-fold channels, Asp131 → His, (f) 3-fold channels, Glu134 → Ala, (g) ferroxidase site, Glu62, His65 → Lys,Gly, (h) ferroxidase and cavity surface, Glu61,Glu64,Glu67 → Ala + Glu62,His65 → Lys,Gly. All samples except for (h) are unstained. The occasional dark centres observed in (h) are due to staining artefacts; no iron cores were seen in the corresponding unstained protein. Scale bar represents 20 nm in all micrographs.

even by the same method but on different days. However, the same relative trends were observed.

Changes in the threefold channels gave a marginal reduction in the mean core size and shifted the size distribution to lower values compared with the control sample (crystallization variant: Table 3). Experiments with the ferroxidase-depleted variant resulted in a significant increase in the mean core dimension compared with the control samples (Table 3). There was a distinct population of cores above six nm in diameter and the particle size distribution was bimodal (Fig. 5). Interestingly, a sample of rLF reconstituted in these experiments had almost identical mean core size and distribution to that of the ferroxidase-depleted variant (Table 3) indicating a close similarity between these two proteins.

Reconstitution of the variant modified at both the ferroxidase and inner surface glutamate sites resulted in non-specific bulk oxidation and precipitation. Examination of the protein by electron microscopy failed to identify reconstituted cores. However, counter-staining of the grids with sodium silicotungstate showed the presence of intact, unloaded apoferritin molecules (Fig. 4). Gel electrophoresis of this variant was consistent with these results (data not shown). The results indicate that these extensive modifications give rise to protein with conserved quaternary structure but depleted in functional activity.

4. Discussion

The results presented here indicate that site-directed modifications in the threefold and fourfold channels, ferroxidase centre and inner surface residues of recombinant H-chain ferritin can be accomplished without loss of functional potential. Although alterations in these regions can have varying, often minor, effects, a remarkable number of changes can be tolerated. Thus amino acid substitutions within the fourfolds channels have no significant effect on rates of iron uptake, mean core size or structure. Changes within the threefold channels produce only a modest decrease in iron incorporation rates and clearly do not alter the ability to nucleate ferrihydrite cores. Alterations in the ferroxidase centre ligands or, to a lesser extent, the inner surface glutamate residues, do diminish Fe uptake kinetics, but cores of normal ferrihydrite structure still form and it is only when changes in both regions are combined that the protein fails to take up iron.

The ability of ferritin to compete effectively with bulk precipitation is a kinetic effect dependent on oxidation and/or nucleation processes (Fig. 6). Clearly, when the ferroxidase centres are intact, Fe(II) is rapidly oxidized and the increased localized supersaturation leads to rapid ferrihydrite deposition within the cavity. Provided that this process is not limited by diffusion or nucleation processes, iron oxide precipitation will be specific to the protein. Furthermore, in homopolymer molecules which contain the same number of ferroxidase centres, most of the added Fe(II) will be distributed essentially equally amongst all the molecules. In the absence of the ferroxidase centres, deposition within the cavity can only be competitive with bulk precipitation if Fe(II) is preferentially sequestered by the protein and/or stabilization of the Fe(III) nuclei is enhanced. In both cases, the presence of carboxylate ligands such as the conserved Glu61, Glu64,Glu67 residues may be important, either as metal ion binding sites or as negatively charged domains that lower the activation energy of cluster formation. Under such conditions, ferrihydrite formation will be relatively slow compared with the ferroxidase mechanism as shown by the marked kinetic differences of iron uptake in rHF and rLF proteins. Moreover, a slower nucleation-driven process in rLF can lead to discrimination between molecules because statistically some molecules will contain nuclei prior to others and these will develop at the expense of molecules without nuclei by autocatalytic growth processes. Thus some molecules may remain empty whilst others attain a relatively large particle size.

These observations are in agreement with previous findings that the population of naturally occurring human ferritins of low iron content contained mainly L-chain polypeptides (Arosio *et al.*, 1977). Presumably, in heteropolymer ferritins of variable H/L ratio, both oxidation and nucleation processes are operative at rates depending on the relative percentage of H and L-chains. The tailoring of core formation to the concentrations of Fe in

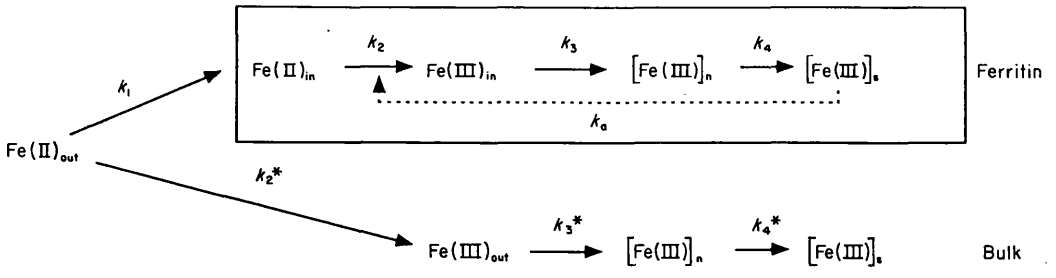

Figure 6. Scheme showing possible mechanistic steps involved in iron oxide formation in ferritin and bulk solution. Rate constants, k_1, diffusion *via* intersubunit channels; k_2, oxidation; k_3, nucleation; k_4, growth; k_a, autocatalysis; n, nuclei; s, solid. At least 2 steps may be rate determining; an oxidative step, k_2, in ferroxidase-containing, H-chain ferritins, and a nucleation-driven process, k_3, in L-chain ferritins.

diffifferent biological environments is thus feasible thnrough selection of different subunit compositions.

]Modification of the ferroxidase ligands, Glu62 and Hisis65, results in a variant analogous to the rLF honmopolymer in its low rate of Fe uptake and sonmewhat increased mean particle size. Although thee cavity surfaces of rLF and rHF are very diffifferent with respect to their amino acid compositioon (only 56% of these residues are identical in huuman ferritins) both molecules contain the three gluutamate residues, Glu61,Glu64,Glu67, as does the ferrroxidase-depleted variant. This seems to argue forr the general importance of these residues in catalyssing iron oxide deposition over that in bulk solutioon. The L-chains have, in addition to the conserved Glu61,Glu64,Glu67 residues, two additioonal carboxylate groups, Glu57,Glu60, (H-chain nuumbering) close to the cavity surface which might auugment cation sequestration and nuclei formation in the absence of the ferroxidase centre.

] Depletion of the Glu61,Glu64,Glu67 residues, hoowever, does not result in a functionally inactive prrotein. The rate of iron uptake in this variant is appproximately 20% of that for rHF suggesting that thee glutamate residues may play a role in the oxidatioon process at the ferroxidase centres. It is possible thaat in rHF the glutamate ligands are involved in maoving Fe(III) from the ferroxidase centre into the cavvity. Whether the Glu61,Glu64,Glu67 residues act inddependently or co-operatively remains to be deetermined. However, some preliminary results apppear to highlight Glu61 as being the key residue. Foor example, an invertebrate ferritin containing Gluu61 and not Glu64,Glu67 has recently been cloned annd overexpressed and found to rapidly take up iron (Hirzmann, Dietzel, Preis, Symmons, Kunz, Treffry & Harrison, unpublished results) and a recent huuman H-chain variant containing only one substitutution, Glu61 → Ala, is similar to the variant Gluu61,Glu64,Glu67 → Ala in its rate of iron uptake (Levi & Arosio, unpublished results). Details of the conre structure of these proteins as well as the effect of changing Glu61 along with the ferroxidase liggands are at present unknown.

] In conclusion, we have shown that residues close to or on the cavity surface of various types of ferrritin are involved in oxidation or nucleation-driiven processes that effectively compete with the buulk deposition of ferrihydrite. The protein only beecomes functionally inactive when both processes arre curtailed by a combination of site-directed maodifications. The finding that many amino acid suubstitutions maintain the ability to deposit iron as ferrrihydrite specifically within the cavity suggests thaat the size and architecture of the internal cavity, ratther than the precise sequence of residues, may be a ddominant influence in iron core formation. In this regard it is notable not only that H-chain and L-chain ferritins are isomorphous (Lawson *et al.*, 19991) but that the bacterioferritin of *E. coli*, which is able to deposit iron as ferrihydrite (Mann *et al.*, 19987), has a generally similar size and molecular construction to that of ferritin although its amino acid sequence shows little similarity (Andrews *et al.*, 1989). Thus the regulation of biomineralization in ferritin may be dependent primarily on the matching of electrostatic fields rather than structural correspondence at the mineral–protein interface. Indeed, no preferred orientation of the ferrihydrite cores with respect to the protein shell has been observed by X-ray diffraction in either ferritin (Fischbach *et al.*, 1969) or a reconstituted bacterioferritin (Smith *et al.*, 1991).

We thank Drs A. Luzzago and G. Cesareni for assistance with mutant constructions and F. C. Meldrum for help with electron microscopy. We acknowledge the Wellcome Foundation, SERC, European Community grants BAP-0246 and 0253 and the CNR Targeted Project in Biotechnology and Bioinstrumentation for financial assistance.

References

Andrews, S. C., Smith, J. M. A., Guest, J. R. & Harrison, P. M. (1989). Amino acid sequence of the bacterioferritin of *Escherichia coli*-K12 (cytochrome b_1) *Biochem. Biophys. Res. Commun.* **158**, 489–496.

Arosio, P., Yokota, M. & Drysdale, J. W. (1977). Characterisation of serum ferritin in iron overload: possible identity to natural apoferritin. *Brit. J. Haematol.* **36**, 199–207.

Boyd, D., Vecoli, C., Belcher, D. M., Jain, S. K. & Drysdale, J. W. (1985). Structural and functional relationships of human ferritin H and L chains deduced from cDNA clones *J. Biol. Chem.* **260**, 11755–11761.

Chasteen, N. D. & Theil, E. C. (1982). Iron binding by horse spleen apoferritin. A vanadyl(IV) EPR spin probe study. *J. Biol. Chem.* **257**, 7672–7677.

Fischbach, F. A., Harrison, P. M. & Hoy, T. G. (1969). The structural relationship between ferritin protein and its mineral core. *J. Mol. Biol.* **39**, 235–238.

Ford, G. C., Harrison, P. M., Rice, D. W., Smith, J. M. A., Treffry, A., White, J. L. & Jariv, J. (1984). Ferritin: design and formation of an iron-storage molecule. *Phil. Trans. Roy. Soc. London,* **B304**, 551–565.

Harrison, P. M., Andrews, S. C., Ford, G. C., Smith, J. M. A., Treffry, A. & White, J. L. (1987). Ferritin and bacterioferritin: iron sequestering molecules from man to microbe, In *Iron Transport in Microbes, Plants and Animals* (Winkelmann, G., van der Helm, D. & Neilands, J. B., eds), pp. 445–475, VCH Verlagsgesellschaft, Weinheim.

Harrison, P. M., Artymiuk, P. J., Ford, G. C., Lawson, P. M., Smith, J. M. A., Treffry, A. & White, J. L. (1989). Ferritin: function and structural design of an iron-storage protein. In *Biomineralisation: Chemical and Biochemical Perspectives* (Mann, S., Webb, J., Williams, R. J. P., eds), pp. 257–294, VCH Verlagsgesellschaft, Weinheim.

Lawson, D. M., Treffry, A., Artymiuk, P. J., Harrison, P. M., Yewdall, S. J., Luzzago, A., Cesareni, G., Levi, S. & Arosio, P. (1989). Identification of the ferroxidase centre in ferritin. *FEBS Letters,* **254**, 207–210.

Lawson, D. M., Artymiuk, P. J., Yewdall, S. J., Smith, J. M. A., Livingstone, J. C., Treffry, A., Luzzago, A., Levi, S., Arosio, P., Cesareni, G., Thomas, C. D.,

Shaw, W. V. & Harrison, P. M. (1991). Solving the structure of human H ferritin by genetically engineering intermolecular crystal contacts. *Nature (London)*, **349**, 541–544.

Levi, S., Cesareni, G., Arosio, P., Lorenzetti, R., Soria, M., Sollazzo, M., Albertini, A. & Cortese, R. (1987). Characterization of human ferritin H-chain synthesized in *Escherichia coli*. *Gene*. **51**, 269–274.

Levi, L., Luzzago, A., Cesareni, G., Cozzi, A., Franceschinelli, F., Albertini, A. & Arosio, P. (1988). Mechanism of ferritin iron uptake: activity of the H-chain and deletion mapping of the ferro-oxidase site. *J. Biol. Chem.* **163**, 18086–18092.

Levi, S., Luzzago, A., Franceschinelli, F., Santambrogio, P., Cesareni, G. & Arosio, P. (1989*a*). Mutational analysis of the channel and loop sequences of human ferritin H-chain. *Biochem. J.* **264**, 381–388.

Levi, S., Salfeld, J., Franceschinelli, F., Cozzi, A., Dorner, M. & Arosio, P. (1989*b*). Expression and structural and functional properties of human ferritin L-chain from *Escherichia coli*. *Biochemistry*, **28**, 5179–5184.

Luzzago, A. & Cesareni, G. (1989). Isolation of point mutations that effect the folding of the H-chain of human ferritin in *E. coli*. *EMBO J.* **8**, 569–576.

Macara, I. G., Hoy, G. & Harrison, P. M. (1972). The formation of ferritin from apoferritin. *Biochem. J.* **126**, 151–162.

Mann, S., Bannister, J. V. & Williams, R. J. P. (1986). Structure and composition of ferritin cores isolated from human spleen, limpet (*Patella vulgata*) hemolymph and bacterial (*Pseudomonas aeruginosa*) cells. *J. Mol. Biol.* **188**, 225–232.

Mann, S., Williams, J. M., Treffry, A. & Harrison, P. M. (1987). Reconstituted and native iron-cores of bacterioferritin and ferritin. *J. Mol. Biol.* **198**, 405–416.

Smith, J. M. A., Andrews, S. C., Guest, J. R. & Harrison, P. M. (1991). Bacterioferritin: a microbial iron-storage protein? *Iron Biominerals* (Frankel, R. B. & Blakemore, R. P., eds), pp. 325–337, Plenum, New York.

Thomas, C. D., Shaw, W. V., Lawson, D. M., Treffry, A., Artymiuk, P. J. & Harrison, P. M. (1988). Expression and purification of the rat liver ferritin light chain after cloning in *Escherichia coli*. *Biochem. Soc. Trans.* **16**, 838–839.

Towe, K. M. & Bradley, W. P. (1967). Mineralogical constitution of colloidal "hydrous ferric oxides". *J. Colloid. Interface Sci.* **24**, 384–392.

Treffry, A., Banyard, S. H., Hoare, R. J. & Harrison, P. M. (1977). Structure and ion-binding properties of ferritin and apoferritin. In *Proteins of Iron Metabolism* (Brown E. B., ed.), pp. 3–11, Grune & Stratton Inc., New York.

Treffry, A., Harrison, P. M., Luzzago, A. & Cesareni, G. (1989). Recombinant H-chain ferritins: effects of change in the 3-fold channels. *FEBS Letters*, **247**, 268–272.

Wetz, K. & Crichton, R. R. (1976). Chemical modification as a probe of the topography and reactivity of horse spleen apoferritin. *Eur. J. Biochem.* **61**, 545–550.

Yang, C. Y., Meagher, A., Huynh, B. H., Sayers, D. E. & Theil, E. C. (1987). Iron(III) clusters bound to horse spleen apoferritin: an X-ray absorption and Mössbauer spectroscopy study that shows that iron nuclei can form on the protein. *Biochemistry*, **26**, 497–503.

Edited by A. R. Fersht